



A University of Sussex PhD thesis

Available online via Sussex Research Online:

<http://sro.sussex.ac.uk/>

This thesis is protected by copyright which belongs to the author.

This thesis cannot be reproduced or quoted extensively from without first obtaining permission in writing from the Author

The content must not be changed in any way or sold commercially in any format or medium without the formal permission of the Author

When referring to this work, full bibliographic details including the author, title, awarding institution and date of the thesis must be given

Please visit Sussex Research Online for more information and further details

Structure-based drug discovery approaches to identify
modulators of the Nrf2 pathway and glutamate receptors
AMPA GluA2 and Kainate GluK1 and GluK2

Thalia Lizbeth Carreno Velazquez

DPhil

University of Sussex

September 2017

I hereby declare that this thesis has not been and will not be, submitted in whole or in part to another University for the award of any other degree.

Signature: _____

UNIVERSITY OF SUSSEX

THALIA LIZBETH CARRENO VELAZQUEZ

PHD IN BIOCHEMISTRY

“STRUCTURE-BASED DRUG DISCOVERY APPROACHES TO IDENTIFY MODULATORS OF THE NRF2 PATHWAY AND GLUTAMATE RECEPTORS AMPA GLUA2 AND KAINATE GLUK1 AND GLUK2”

SUMMARY

Nrf2 project

The protein nuclear factor erythroid 2-related factor 2 (Nrf2) is a transcription factor that provides protection against oxidative stress and the dysfunction of this pathway has been suggested to be implicated in many neurodegenerative diseases. The aim of this thesis was to identify novel Nrf2 activators that disrupt the protein-protein interaction between Nrf2 and Keap1 and thereby induce increased expression of antioxidant enzymes and protective genes. The crystal structure of the Keap1-Nrf2 interface was used to perform a virtual screen and compounds from the screen were assayed using a cellular nuclear complementation assay that measures the nuclear translocation of Nrf2 from the cytosol. Although two novel compounds were found to increase the Nrf2 nuclear translocation, they had low activity and further characterisation did not provide sufficient evidence of a Nrf2-Keap1 robust interaction.

iGluRs project

AMPA and kainate receptors are ionotropic glutamate receptors (iGluRs) that are important for excitatory transmission and synaptic plasticity and are linked to several neurological disorders such as epilepsy, schizophrenia and autism. This project aimed to find novel allosteric modulators binding in the ligand-binding domain (LBD) of the GluA2 and GluK1 and GluK2 subtypes of AMPA and kainate receptors, respectively, using protein purification and X-ray crystallography methodologies. Fragment screening for GluA2 identified eight novel fragments, five of which were located at the dimer interface and three located in a novel site near the glycine-threonine dipeptide linker. As regards kainate receptors, structural information on the GluK1 and GluK2 LBD was obtained, both proteins were soaked with in-house fragments with one compound displaying 20% occupancy in the GluK2 dimer interface. These data form the basis of future studies in the search for novel drugs for the treatment of epilepsy and schizophrenia.

ACKNOWLEDGEMENTS

First, I would like to express my respect and gratitude to my supervisor Prof. John Atack for giving me the opportunity to undertake a research thesis in the Sussex Drug Discovery Centre group, and for the continuous guidance and support during these years of my research. In addition, I would like to extend my gratitude to Prof. Simon Ward, Prof. Martin Gosling and Dr. Majid Hafezparast for the advice and contributions towards my research.

I would also like to thank all the research team (students and staff) in the SDDC, with special gratitude to Gareth Williams, Sarah Walker, Paul Beswick, Lewis Pennicott, Ben Wahab, Marco Derudas, Iain Barret and Raj Gill.

Special thanks to Dr. Mark Roe and Dr. Antony Oliver for the great help, instruction and advice they provided.

With gratitude to my scholarship sponsor CONACYT from Mexico government to grant me a PhD research grade funding.

To my family, my parents Rosario and David, to my lovely sister Sinai, my grandparents Luvia and Salustio for the wonderful support during my life and my studies, for always encouraging me to become a better person. “Gracias familia por darme todo su cariño y amor, y por enseñarme a ser una mejor persona, sin ustedes no hubiera podido lograr esto”

Finally, to my soulmate Andy, I could not have done it without your love and support.

THANK YOU!!

Contents

Section	Title	Page
	List of figures	1-4
	List of tables	5
	Abbreviations	6-8
CHAPTER ONE – General Introduction to drug discovery		
1.1	Overview of the drug discovery process	9
1.2	Hit identification	13
1.2.1	High-throughput screening (HTS)	14
1.2.2	Structure-based drug discovery	14
1.2.2.1	X-ray crystallography	14
1.2.2.2	NMR structure determination	17
1.2.2.3	Virtual screening	18
CHAPTER TWO – Nuclear factor (erythroid-derived 2)-like 2 (Nrf2)		
2.1	Abstract	20
2.2	Introduction	
2.2.1	The Nrf2-ARE system	21
2.2.2	Nrf2 phosphorylation	23
2.2.3	Nrf2 functions	26
2.2.4	Nrf2 multi-organ protector against disease	27
2.2.4.1	Lungs	28
2.2.4.2	Liver and gastrointestinal tract	28
2.2.4.3	Skin	29
2.2.4.4	Heart	30
2.2.4.5	Brain and nervous system	30
2.2.5	Nrf2 in neurodegenerative diseases	30
2.2.6	Modulators of the Nrf2/ARE pathway	31
2.3	Aims	39
2.4	Materials and methods	
2.4.1	Materials	40
2.4.2	Methods	40
2.4.2.1	Virtual screening strategy	40
2.4.2.2	Nrf2 enzyme fragment complementation assay	46
2.4.2.2.1	Assay development	47
	Sulforaphane, DMSO tolerance and incubation conditions	48
2.4.2.2.2	Assay validation (literature compounds)	48
2.4.2.2.3	Compound screening	49
2.4.2.3	Viability assay	50
2.4.2.4	Detection of reactive oxygen species (ROS)	51
2.4.2.5	Compound characterisation	52
2.4.2.5.1	Cell culture	52
2.4.2.5.2	Cell fractionation	52
2.4.2.5.3	Western blotting	53

2.5	Results	
2.5.1	Nrf2 enzyme fragment complementation assay	54
2.5.1.1	Assay development	54
	Sulforaphane, DMSO tolerance and incubation conditions	55
2.5.1.2	Assay validation (literature compounds)	58
2.5.1.3	Compound screening	59
2.5.2	Viability assay	62
2.5.3	Detection of reactive oxygen species (ROS)	63
2.5.3	Western blot	65
2.5.3.1	Nrf2 detection in wild type U2OS cell line	65
2.5.3.2	Nrf2 detection in U2OS-Nrf2 cell line (DiscoverX)	68
2.5.3.3	Nrf2 detection in HEK-293 cell line	71
2.6	Discussion	73
 CHAPTER THREE – Introduction to glutamate receptors		
3.1	Glutamate neurotransmission	77
3.2	Glutamate neurotransmission in disease	79
3.3	Glutamate receptors gene families	83
3.3.1	mGluRs	83
3.3.2	iGluRs (NMDA, AMPA and Kainate)	87
3.4	iGluRs structure	
3.4.1	General features	88
3.4.2	AMPA receptors	92
3.4.2.1	Alternative splicing (flip/flop) and RNA editing site (Q/R)	96
3.4.2.2	Activation and inactivation of ion channels (gating)	98
3.4.2.3	AMPA auxiliary proteins	99
3.4.2.4	Agonist binding	100
3.4.2.5	AMPA antagonist	103
3.4.3	Kainate receptors	104
3.4.3.1	Kainate receptor structure	104
3.4.3.2	Ligand binding domain	107
3.4.3.3	Kainate agonists	111
3.4.4	NMDA receptors	114
3.5	iGluR function and pharmacology	
3.5.1	AMPA Receptors	118
3.5.1.1	Function and distribution	118
3.5.1.2	Antagonists and pharmacology	120
3.5.2	Kainate Receptors	126
3.5.2.1	Function and distribution	126
3.5.2.2	Antagonist and pharmacology	129
3.5.3	NMDA Receptors	134
3.5.3.1	Function and distribution	134
3.5.3.2	Antagonist and pharmacology	137

CHAPTER FOUR – AMPA project

4.1 Abstract	140
4.2 Aims	142
4.3 Materials and methods	143
4.3.1 Cloning and plasmid vector	143
4.3.2 Competent cells	145
4.3.3 Bacterial transformation	146
4.3.4 Protein expression	146
4.3.5 Protein purification	147
4.3.5.1 Immobilized metal affinity chromatography (IMAC)	147
4.3.5.2 Size Exclusion Chromatography (SEC)	149
4.3.6 Crystallography	151
4.3.7 Fragment screening-XChem	153
4.4 Results	
4.4.1 IMAC purification	156
4.4.2 SEC purification	158
4.4.3 Crystallography	161
4.4.4 Fragment screening-XChem	166
4.5 Discussion	181

CHAPTER FIVE – KAINATE project

5.1 Abstract	183
5.2 Aims	184
GLUK1	185
5.3 Materials and methods	186
5.3.1 Cloning and plasmid vector	186
5.3.2 Competent cells	188
5.3.3 Bacteria transformation	188
5.3.4 Protein expression	189
5.3.5 Protein purification	190
5.3.5.1 Immobilized metal affinity chromatography (IMAC)	190
5.3.5.2 Size Exclusion Chromatography (SEC)	191
5.3.6 Crystallography	192
5.3.7 Fragment screening (soaking)	193
5.3.8 Kainate calcium assay	195
5.4 Results	
5.4.1 Protein expression and purification of human GluK1 LBD	197
5.4.2 IMAC purification	198
5.4.3 SEC purification	200
5.4.4 Crystallography	203
5.4.5 Fragment screening (soaking)	209
5.4.6 Kainate calcium assay	210
5.5 Discussion	214

GLUK2	
5.6 Materials and methods	218
5.6.1 Cloning and plasmid vector	218
5.6.2 Competent cells	220
5.6.3 Bacteria transformation	220
5.6.4 Protein expression	220
5.6.5 Protein purification	220
5.6.5.1 Immobilized metal affinity chromatography (IMAC)	220
5.6.5.2 Size Exclusion Chromatography (SEC)	221
5.6.6 Crystallography	221
5.6.7 Fragment screening (soaking)	223
5.6.8 Kainate calcium assay	224
5.7 Results	226
5.7.1 IMAC purification	226
5.7.2 SEC purification	228
5.7.3 Crystallography	231
5.7.4 Fragment screening (soaking)	239
5.7.5 Kainate calcium assay	240
5.8 Discussion	243
CHAPTER SIX – Conclusions and future work	
6.1 Nrf2 project	246
6.2 AMPA project	247
6.3 Kainate project	248
7.0 BIBLIOGRAPHY	250
APPENDIX I	284
APPENDIX II	287

LIST OF FIGURES

Figure 1.1. Drug discovery process

Figure 1.2. Different screening strategies used in the hit identification process

Figure 1.3. X-ray crystallography procedure

Figure 1.4. Structure determination by NMR spectroscopy

Figure 1.5. Structure-based virtual screening approach

Figure 2.1. Summary of Nrf2 structure

Figure 2.2. Keap1 protein structure and sequence

Figure 2.3. Summary of the Nrf2-ARE cellular protection pathway

Figure 2.4. Diagram of the “Hinge and Latch” model of Nrf2 releases from Keap1

Figure 2.5. Nrf2 has a protective effect in a variety of different tissues and organs

Figure 2.6. The protective role of Nrf2 expression in liver disease

Figure 2.7. Keap1 cysteine residues involved in chemical inducers

Figure 2.8. Sulforaphane-induced activation of the Nrf2 pathway

Figure 2.9. Nrf2 plays a role in 3-NP-mediated neurotoxicity

Figure 2.10. Nrf2-Keap1 protein-protein interface

Figure 2.11. Summary of the virtual screening strategy

Figure 2.12. PathHunter Nrf2 nuclear translocation assay mechanism

Figure 2.13. Summary strategy followed for compound characterisation methodology

Figure 2.14. General procedure of the PathHunter kit for assay development and screening compound

Figure 2.15. CellTiter-Glo® luminescent cell viability assay principle

Figure 2.16. Ros-Glo H₂O₂ assay reaction

Figure 2.17. Effect of DL-Sulforaphane on Nrf2 nuclear translocation in the U2OS Nrf2 assay

Figure 2.18. DMSO tolerance curve

Figure 2.19. Comparison of incubation times at 37°C vs RT at 6 hours with sulforaphane

Figure 2.20. Chemical structure of literature compounds

Figure 2.21. Activity of testing compounds by Nrf2 cellular assay

Figure 2.22. Compounds with a possible Keap1-Nrf2 activity

Figure 2.23. Chemical structure of the hit compounds for Nrf2 activity

Figure 2.24. U2OS viability assay with test compounds

Figure 2.25. ROS induction in U2OS-Nrf2 cultured cells

Figure 2.26. Wild type U2OS cells vs U2OS with sulforaphane treatment

Figure 2.27. Densitometry analysis of Western Blot from U2OS cells with or without sulforaphane treatment

Figure 2.28. Nrf2 nuclear accumulation in U2OS-Nrf2 cells

Figure 2.29. Nrf2 densitometry analysis of Western Blots from U2OS-Nrf2 cell line with test compounds

Figure 2.30. Effect of compounds on Nrf2 levels in HEK-293

Figure 2.31. Densitometry analysis of Western Blot HEK-293 cell line with compounds

Figure 3.1. Excitatory glutamate synapse

Figure 3.2. Representation of a typical mGluR structure

Figure 3.3. Metabotropic Glutamate Receptor

Figure 3.4. Classification of mGluRs families

Figure 3.5. The ionotropic receptor gene family

Figure 3.6. Ionotropic glutamate receptor domains

Figure 3.7. Gluk1 LBD S1S2 clamshell-like structure

Figure 3.8. iGluR tetramer assembly representation

Figure 3.9. Construct of the LBD (S1S2) design

Figure 3.10. AMPA agonists and antagonist

Figure 3.11. Structural architecture and symmetry of rGluA2

Figure 3.12. Tetrameric distinct conformations

Figure 3.13. Schematic representation of the location and sequence comparison of the Flip/Flop AMPA subunit variations

Figure 3.14. Gating steps in glutamate receptors

Figure 3.15. GluA2-LBD in complex with glutamate

Figure 3.16. Glutamate, kainate and AMPA binding interactions

Figure 3.17. Competitive and Non-competitive antagonist

Figure 3.18. Electron microscopy structure of full-length GluK2

Figure 3.19. Conformational changes in the GluK2 gating process

Figure 3.20. LBD binding pocket Gluk1 and GluK2 in complex with glutamate

Figure 3.21. GluK2 structure in complex with glutamate and kainate

Figure 3.22. Glutamate binding site pocket for kainate receptors GluK1, GluK2 and GluK3

Figure 3.23. Structures of kainate receptor agonists

Figure 3.24. RNA alternative splicing in NMDA receptor subunit

Figure 3.25. Comparison of the heterotetrameric GluN1-GluN2B receptor and the homotetrameric GluA2 receptor

Figure 3.26. Schematic representation of the proposed mechanism of NMDA receptor inhibition and activation

Figure 3.27. Mechanism of long-term potentiation (LTP)

Figure 3.28. AMPA non-competitive antagonist binding site

Figure 3.29. Putative model of the mechanism of the non-competitive inhibitor in AMPA receptors

Figure 3.30. Synaptic transmission and pre-synaptic LTP regulation by kainate receptors in the cingulate cortex

Figure 3.31. Chemical structure of kainate receptors allosteric antagonists

Figure 3.32. Chemical structures of BPAM344, BPAM521 and BPAM121

Figure 3.33. Binding interactions of BPAM344, BPAM521 and BPAM121 with LBD-GluK1

Figure 3.34. GluK1-LBD in complex with BPAM344 and kainate

Figure 3.35. Diagram of the topology of activated NMDA receptors

Figure 3.36. NMDA dependent long-term potentiation (LTP) and long-term depression (LTD)

Figure 3.37. Chemical structures of several NMDA antagonists

Figure 4.1. AMPA overall project plan

Figure 4.2. Cartoon showing the strategy for the GluA2 ligand-binding domain construct design

Figure 4.3. rGluA2 LBD sequence construct for protein expression and purification

Figure 4.4. Plasmid map of the inserted rat GluA2 LBD gene, of which 5µg of lyophilised plasmid was obtained by Invitrogen

Figure 4.5. Talon resin loaded with NTA-Co²⁺ for protein purification

Figure 4.6. SEC principle

Figure 4.7. Crystallisation phase diagram

Figure 4.8. ECHO acoustic droplet ejection

Figure 4.9. SDS-PAGE gel of IMAC purification of the rGluA2 LBD protein

Figure 4.10. SDS-PAGE gel of 3C protease activity

Figure 4.11. Size exclusion chromatography of the rGluA2 LBD after 3C proteolytic removal of the 6xHis-SUMO tag

Figure 4.12. Final purity of the protein rGluA2

Figure 4.13. Rectangular orthorhombic crystals of the LBD of rGluA2

Figure 4.14. Monomer of the LBD of rGluA2 in complex with glutamate

Figure 4.15. Glutamate binding interactions with LBD rGluA2

Figure 4.16. Identified sites in the LBD of rGluA2

Figure 4.17. Summary of LBD of rGluA2 in complex with fragment hits obtained after XChem fragment screen

Figure 4.18. Compounds 1, 2 and 6 in the LBD of rGluA2

Figure 4.19. Compounds 3, 4 and 7 in the LBD of rGluA2

Figure 4.20. Compounds 5 and 8 in the LBD of rGluA2

Figure 4.21. Comparison of the possible binding mode of compounds 1 and 3 in the binding site 1a

Figure 4.22. Comparison of the possible binding mode of compounds 6, 7 and 8 in the binding site 1b

Figure 4.23. Comparison of the possible binding mode of compounds binding site 2

Figure 4.24. Transduction domain of rGluA2 in complex with antagonist CP 465,022 and Compound 2

Figure 4.25. Hypothetical ligand "X" formed by two fragments.

Figure 4.26. Ligand X in the dimer interface of rGluA2.

Figure 5.1. Scheme of overall strategy and screening cascade

Figure 5.2. LBD rGluK1 sequence design for protein expression and purification

Figure 5.3. Plasmid map of the inserted synthetic rat gene GluK1 LBD, of which 5µg of lyophilised plasmid was obtained by Invitrogen.

Figure 5.4. Expression test and purification of the hGluK1 LBD

Figure 5.5. SDS-PAGE gel of IMAC purification

Figure 5.6. SDS-PAGE gel of 3C protease activity

Figure 5.7. Size exclusion chromatography for rGluK1

Figure 5.8. SDS-PAGE gel verification of pure rGluK1 protein

Figure 5.9. rGluK1 tetragonal crystals

Figure 5.10. LBD rGluK1 structures obtained with X-ray crystallography

Figure 5.11. Ligand binding domain of rGluK1 in complex with kainic acid

Figure 5.12. Structure alignment between rGluK1 LBD and GluA2 LBD

Figure 5.13. Sequence alignment of the LBD of rGluA2 and rGluK1

Figure 5.14. Kainate binding interaction diagram for rGluK1 LBD

Figure 5.15. Chemical structures of kainate, domoate and CNQX

Figure 5.16. GluK1 kainate/domoate agonist dose response curves

Figure 5.17. GluK1-CNQX antagonist dose response curve

Figure 5.18. LBD rGluK2 sequence design for protein expression and purification

Figure 5.19. Plasmid map of the inserted recombinant rat gene GluK2 LBD

Figure 5.20. Layout plate of the microseeding experiments performed for crystals optimisation

Figure 5.21. SDS-PAGE gel of IMAC purification

Figure 5.22. SDS-PAGE gel of 3C protease activity

Figure 5.23. Size exclusion chromatography for rGluK2 protein

Figure 5.24. SDS-PAGE gel purity verification of rGluK2 protein

Figure 5.25. Light microscopy images of crystal hits from crystallography commercial screening kits

Figure 5.26. Light microscopic images of rGluK2 orthorhombic crystals

Figure 5.27. LBD rGluK2 dimer structure obtained with X-ray crystallography

Figure 5.28. Alignment of rGluK2 dimer structures

Figure 5.29. Dimer comparison between in-house crystal structures of rGluK1 and rGluK2

Figure 5.30. Glutamic acid binding interaction diagram for rGluK2 LBD

Figure 5.31. Glutamate binding pocket in LBD of rGluK2

Figure 5.32. Compound UOS-15592 at 1mM appeared to bind in the dimer interface of rGluK2 structure

Figure 5.33. GluK2 kainate/domoate agonist concentration response curves

Figure 5.34. In-house compound UOS-30693

Figure 5.35. GluK2 antagonist concentration response curve

LIST OF TABLES

Table 1.1	Phasing methods used in structural solution
Table 2.1	Summary of Nrf2 activators and their therapeutic utility
Table 2.2.	Keap1/Nrf2 crystal structures used for modelling
Table 2.3.	Compounds with Nrf2 activity
Table 3.1.	Crystal structures of the LBD in complex with different ligands
Table 3.2.	Agonist affinities to AMPA, kainate and NMDA receptors
Table 3.3.	Cryo-EM structures of GluN1/GluN2B NMDA receptor
Table 3.4.	Summary of AMPA antagonist drugs.
Table 4.1.	Commercial crystallisation screens used for primary crystallography experiments.
Table 4.2.	Conditions of well B1 of commercial Morpheus® screen
Table 4.3.	Different batches of purified protein obtained after purification experiments
Table 4.4.	Morpheus® HT-96 crystal hits conditions
Table 4.5.	Crystallographic statistics for the rGluA2 LBD in complex with glutamate
Table 4.6.	Compound hits found in XChem fragment screening library
Table 4.7.	Crystallographic statistics for the rGluA2 LBD crystals in complex with compound fragments
Table 5.1.	Commercial crystallisation screens used for preliminary experiments
Table 5.2.	Fragments structures used for soaking experiments, compounds synthesized in-house
Table 5.3.	Compound selection criteria for soaking experiments with protein crystals
Table 5.4.	Different batches of purified protein obtained after purification experiments
Table 5.5.	Crystallographic Statistics of rGluK1 LBD
Table 5.6.	Parameters tested for 96-well plate for human GluK1/GluK2 Ca ²⁺ assay development
Table 5.7.	Commercial crystallisation screens used for preliminary crystallography experiments
Table 5.8.	Different batches of pure protein obtained after purification experiments
Table 5.9.	Conditions of the crystal hits obtained after crystallography screening
Table 5.10.	Crystallographic statistics of rGluK2 LBD

ABBREVIATIONS

2-Me-Tet-AMPA	2-methyl-tetrazolyl-[2-amino-3-(3-hydroxy-5-methyl-4-isoxazolyl)propanoic acid
3-NP	3-nitropropionic acid
4-HNE	4-hydroxynonenal
8-OHdG	8-Oxo-2'-deoxyguanosine
Ab	Antibody
AD	Alzheimer disease
AEDs	Anti-epileptic drugs
ALS	Amyotrophic lateral sclerosis
Amp	Ampicillin
AMP397	Becampanel
AMPA	α -amino-3-hydroxy-5-methyl-4-isoxazolepropionic acid
ARE	Antioxidant response element
ASP	Amnesic shellfish poisoning
ATF4	Activation transcription factor 4
ATP	Adenosine triphosphate
ATPA	(S)-2-amino-3-(3-hydroxy-5-ter-butylisoxazol-4-yl) propionic acid
AUBAs	2-arylureidobenzoic acids
BDNF	Brain derived neurotrophic factor
BHT	Butylated hydroxytoluene
BIS-TRIS	2,2-Bis(hydroxymethyl)-2,2',2''-nitrilotriethanol
BMA	Beta-D-mannose
Br-HIBO	(2S)-2-amino-3-(4-bromo-3-oxo-1,2-oxazol-5-yl)propanoic acid
bZIP	Basic leucine zipper
CBP	CREB-binding protein
CDDO-Me	Bardoxolone methyl
CNC	Cap "n" collar
CNQX	6-cyano-7nitroquinoxaline-2,3-dione
CNS	Central nervous system
Con-A	Concanavalin A
COOT	Crystallography object-oriented toolkit
COPD	Chronic obstructive pulmonary disease
CPDT	5,6-dihydrocyclopenta-1,2dithiole-3-thione
CPN-9	N-(4-(2-pyridyl)(1,3-thiazol-2-yl))-2-(2,4,6-trimethylphenoxy) acetamide
CPP4	Collaborative Computational Project No.4
D3T	3H-1,2,-dithiole-3-thione
DMEM	Dulbecco's modified eagle medium
DMF	Dimethyl fumarate
DMSO	Dimethyl sulfoxide
DNQX	6,7-dinitroquinoxaline-2,3-dione
<i>E. coli</i>	<i>Escherichia coli</i>
ECL	Enhanced chemiluminescence
EDTA	Ethylenediaminetetraacetic acid
EM	Electron microscopy

EMBL	European Molecular Biology Laboratory
EMSA	Electrophoresis mobility shift assay
ERK	Extracellular signal-regulated kinase
FBS	Fetal bovine serum
FPLC	Fast protein liquid chromatography
GABA	Gamma-Aminobutyric acid
GAPDH	Glyceraldehyde 3-phosphate dehydrogenase
GCL	Glutamate cysteine ligase
GPCR	G-protein coupled receptor
HEK293	Human embryonic kidney cells 293
HEPES	4-(2-hydroxyethyl)-1-piperazineethanesulfonic acid
HO-1	Heme oxygenase-1
HRP	Horseradish peroxidase
HRV3C	Human Rhinovirus 3C protease
HSPs	Heat shock proteins
iGluRs	Ionotropic glutamate receptors
IMAC	Immobilized metal affinity chromatography
iPSCs	Induced pluripotent stem cells
IPTG	Isopropyl β -D-1-thiogalactopyranoside
JAE	Juvenile absence epilepsy
JNK	c-Jun N-terminal kinase
Keap1	Kelch-like ECH-associated protein 1
LDH	Lactate dehydrogenase
LTP	Long-term potentiation
MAD	Multi-wavelength anomalous diffraction
MAF	Musculoaponeurotic fibrosarcoma
MES	2-(N-morpholino)ethanesulfonic acid
mGluRs	Metabotropic glutamate receptors
MIR	Multiple isomorphous replacement
MME	Methyl ether
MOE	Molecular operating environment
MOLS	Mutually orthogonal latin squares
MPQX	Fanapanel / ZK200775
MPTP	1-methyl-4-phenyl-1,2,3,6-tetrahydropyridine
MR	Molecular Replacement
mRNA	Messenger RNA
MWCO	Molecular weight cut-off
NAG	N-acetyl-D-glucosamine
NAM	Negative allosteric modulator
NBQX	2,3-dihydroxy-6-nitro-7-sulfamoyl-benzo[f]quinoxaline-2,3-dione
Neh	Nrf2-embedded contact homology
NFE2L2	Nuclear factor erythroid 2-related factor 2 gene
NF-kB	Nuclear factor kappa-light-chain-enhancer of activated B cells
NGX-242	Tezampanel or LY293-558

NICER	National individual anonymised data transmitted by the cantonal cancer registries
NMDA	N-methyl-D-aspartatic acid
NMR	Nuclear magnetic resonance
NPS	Nitrate phosphate sulfate
NQO1	NAD(P)H quinone oxidoreductase 1
Nrf-1	Nuclear respiratory factor 1
Nrf2	Nuclear factor erythroid 2-related factor 2
NTA	Nitrilotriacetic acid
Oxr1	Oxidation resistance 1 protein
PAM	Positive-allosteric modulator
PBS	Phosphate-buffered saline
PCP	Phencyclidine
PDB	Protein data bank
PEG	Polyethylene glycol
PERK	RNA-like endoplasmic reticulum kinase
PES	Polyethersulfone
PGTCS	Primary generalized tonic-clinic seizures
PHENIX	Python-based Hierarchical Environment for Integrated Xtallography
PI3K	Phosphatidylinositol 3-kinase
PS	Penicillin-Streptomycin
RFU	Relative fluorescence units
RLU	Relative luminescence units
ROS	Reactive oxygen species
RSE	Refractory status epilepticus
RT-PCR	Reverse transcription polymerase chain reaction
SAD	Single-wavelength anomalous diffraction
SAH	Subarachnoid haemorrhage
SDS-PAGE	Sodium dodecyl sulfate polyacrylamide gel electrophoresis
SEC	Size exclusion chromatography
SFN	Sulforaphane
sMAF	Small musculoaponeurotic fibrosarcoma
SOC	Super optimal broth with catabolite repression
SOD1	Superoxide dismutase 1
tBHQ	tert-butylhydroquinone
TCEP	Tris(2-carboxyethyl)phosphine
TLE	Temporal lobe epilepsy
U2OS	Human bone osteosarcoma epithelial cell line
UGT	UDP-glucuronosyltransferase
UniProt	Universal Protein Resource
UOS	University of Sussex
WB	Western blot
XChem	Diamond fragment screening
β-gal	Beta galactosidase

CHAPTER 1

GENERAL INTRODUCTION TO DRUG DISCOVERY

1.1 OVERVIEW OF THE DRUG DISCOVERY PROCESS

Developing a new drug from initial research to a commercial final product is a long and complex process that can take around 12 to 15 years or more and costs around \$2.6 billion (Hughes et al. 2011; Mullin 2014). Usually a target is a protein and/or pathway involved in pathology, so the modification of the target will result in a beneficial therapeutic effect. The idea for a target identification can originate from academic or industrial research, usually both work in collaboration to build enough supporting evidence for a desired target (target validation). Once a target is chosen, academia and/or industry design a variety of early processes to identify molecules that are able to satisfy the characteristics of a suitable drug. Some of those early stages are target validation, assay development, high throughput screening, hit identification and lead optimisation, which conclude in preclinical and clinical stages (Fig. 1.1).

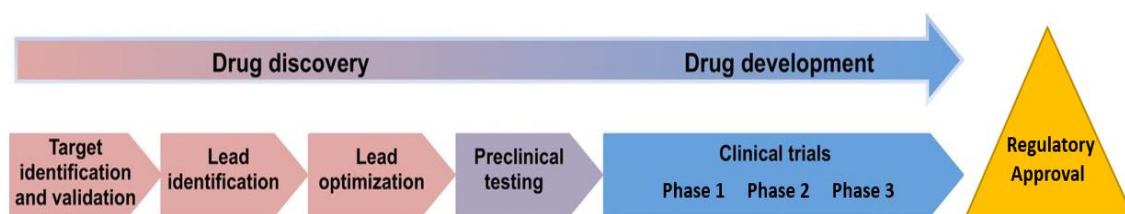


Figure 1.1. Drug Discovery process. Drug discovery comprises the initial stages of target identification and validation to clinical trials for regulatory approval (Adapted from Gopinathan et al. 2015).

Target identification and validation

The first step of a drug discovery process is the target identification, which means identifying a molecular target for a drug molecule. A molecular target is usually a molecule involved in biological processes, usually a protein in isolation or in complex, is associated with a disease. A drug molecule or a small compound binding to the molecular target (i.e. protein) can have therapeutic effects in the disease related to the molecular target. This stage itself is focused on identifying the correct drug targets for a specific disease, which usually does not have treatment or is in some way insufficient. Some methods used for target identification are chemoproteomics, phenotypic screening and gene association studies (Hughes et al. 2011). The most common molecular drugs are small molecules which bind in specific proteins, however, other approaches for new drugs have been investigated. For example, the development of lipid drugs such as Vascepa, approved by the FDA in 2012. This drug targets the modulation of cholesterol levels and prevents cardiovascular disease and pancreatitis (Hiatt & Smith 2014). Another example is the development of small molecule drugs (glycomimetics) that mimic the function of carbohydrates involved in disease-protein interactions (Ernst & Magnani 2009). More recently mRNA-based drugs have been developed by Moderna Therapeutics and AstraZeneca, the most recent is AZD8601 which has possible regenerative and healing properties in heart failure, diabetic wound and ischaemic vascular diseases. AZD8601 is a mRNA modified drug that is currently under phase I clinical trial in patients with type II diabetes mellitus (Mullard, 2016 & NCT02935712, clinicaltrials.gov).

A potential target must undergo a validation process, which is focused on demonstrating the effect of a target disruption on disease-related relevant pathology. Transgenic animals and gene knockout experiments allow the observation of phenotypic changes as a result of gene manipulation. These techniques are established approaches for target validation *in vivo* in animal models (Hughes et al. 2011). However, some animal models are difficult to compare to human processes. Proteomics is a technique for the study of proteins expressed in cells, this technique is also used for target validation by identifying novel proteins required for biological processes. These proteins might act as a potential drug target in a specific-related disease (Kopeck et al., 2005). Other well-established techniques includes antisense technology and RNA interference (RNAi) that help disrupting the expression of a particular gene (Hughes et al. 2011). If a drug target fails in the target identification and validation steps it suggests that the drug will not work for a molecular target involved in disease or might not be safe to use in humans (Hughes et al. 2011).

Lead identification

When a drug target is identified and validated, research will focus on lead discovery (hit identification and screening assays). In this stage high-throughput screening is commonly used to identify potential candidates for a lead generation (hit-to-lead). Hit-to-lead phase is focused in refining each hit to produce a more potent and selective compound to be studied in *in-vivo* models (Hughes et al. 2011).

Lead Optimisation

This stage is focused on the search for optimal efficacy, in which compounds are modified to improve potency, selectivity, pharmacodynamics and pharmacokinetics properties. Toxicological properties are tested in this stage, such as *in vitro* genotoxicity measured by the Ames test and *in vivo* toxicity model using the Irwin observation test that measures physiological and behavioural functions for new substances (Hughes et al. 2011). After lead optimisation compounds are ready for final characterisation before preclinical studies (Hughes et al. 2011).

Preclinical testing and clinical trials

Preclinical studies are required before the initiation of clinical studies to establish if a drug is safe in humans; studies are focused on finding out potential toxicity. According to the U.S. Food & Drug Administration (FDA) guidelines, preclinical research must provide detailed information on dosing and toxicity levels using good laboratory practices (GLP).

The aim of clinical studies is to test if the candidate drug is safe and well-tolerated and has efficacy in human volunteers. FDA has human guidelines for drug testing that include characterisation of absorption, metabolism, excretion, toxicity and undesired side effects. Clinical trials are defined by three to four phases according to the FDA.

Phase 0, a reduced dose of the drug is given to a small group of volunteers to observe the expected drug behaviour in humans. This dose is too small to observe a full therapeutic effect but gives important preliminary information. The main objective of this phase is to accelerate the development and approval of new drugs.

Phase I, studies to evaluate safety, side effects and dosage range in terminally ill volunteers.

Phase II, testing drug in patients with a disease or condition and comparison of the drug to a placebo. Safety and short-term adverse events are also monitored.

Phase III, similar to phase II studies safety and adverse events in a larger patient population, different dosages and in combination with other available treatments (drugs).

Phase IV, studies after FDA has approved market release of a drug. Final studies to obtain any additional information about safety, efficacy and optimal use.

(clinicaltrials.gov and FDA guidelines)

1.2 HIT IDENTIFICATION

Hit identification is the process of identifying a small molecule “compound” with activity against the desired target (i.e., protein). The obtained compounds will be identified by a screening approach such as high-throughput screening or structure-based drug design. There are additional different screening approaches used for compound identification (Fig. 1.2). For example, fragment screening, in which compound solutions are soaked and incubated with protein crystals to obtain structural information of the binding mode by fragments. Virtual screen is another method use for screening virtual compounds in the well-known structure binding sites. Other screening approaches are; focused screen, physiological screen and NMR screen.

Screen	Description	Comments
High throughput	Large numbers of compounds analysed in a assay generally designed to run in plates of 384 wells and above	Large compound collections often run by big pharma but smaller compound banks can also be run in either pharma or academia which can help reduce costs. Companies also now trying to provide coverage across a wide chemical space using computer assisted analysis to reduce the numbers of compounds screened.
Focused screen	Compounds previously identified as hitting specific classes of targets (e.g. kinases) and compounds with similar structures	Can provide a cheaper avenue to finding a hit molecule but completely novel structures may not be discovered and there may be difficulties obtaining a patent position in a well-covered IP area
Fragment screen	Soak small compounds into crystals to obtain compounds with low mM activity which can then be used as building blocks for larger molecules	Can join selected fragments together to fit into the chemical space to increase potency. Requires a crystal structure to be available
Structural aided drug design	Use of crystal structures to help design molecules	Often used as an adjunct to other screening strategies within big pharma. In this case usually have docked a compound into the crystal and use this to help predict where modifications could be added to provide increased potency or selectivity
Virtual screen	Docking models: interrogation of a virtual compound library with the X-ray structure of the protein or, if have a known ligand, as a base to develop further compounds on	Can provide the starting structures for a focused screen without the need to use expensive large library screens. Can also be used to look for novel patent space around existing compound structures
Physiological screen	A tissue-based approach for determination of the effects of a drug at the tissue rather than the cellular or subcellular level, for example, muscle contractility	Bespoke screens of lower throughput. Aim to more closely mimic the complexity of tissue rather than just looking at single readouts. May appeal to academic experts in disease area to screen smaller number of compounds to give a more disease relevant readout
NMR screen	Screen small compounds (fragments) by soaking into protein targets of known crystal or NMR structure to look for hits with low mM activity which can then be used as building blocks for larger molecules	Use of NMR as a structure determining tool

NMR, nuclear magnetic resonance.

Figure 1.2. Different screening strategies used in the hit identification process (Hughes et al. 2011).

1.2.1 HIGH-THROUGHPUT SCREENING (HTS)

High-throughput screening (HTS) is currently a standard method for drug discovery research. HTS is a method of screening and assaying a large amount of compound libraries against the specific drug target (Szymański et al. 2012). The main purpose of this large screening is to identify novel lead compounds active against a molecular drug target by using robotic technologies such as liquid handling and robotic automation, multi-platform plate readers, high content imaging tools, sensitive detectors and data processing software (Target discovery institute-Nuffield department of Medicine; 2017). The main advantage of HTS compared to other screening approaches is the ability to screen large-scale libraries in a quick and low cost process. Commonly, HTS assays are performed in microtiter plates ranging from 96-, 384- or 1536-well formats. A number of active hits will be obtained after screening compound libraries, these hits will be further interrogated through hit validation studies. The ability to screen a large range of compounds can give important information on the interaction of compounds into biological processes in a quick automated manner. For that reason, HTS is an important currently used method in drug discovery research; it is estimated that HTS has provided economic savings of 130 million dollars over the development of a new drug (Szymański et al. 2012).

1.2.2 STRUCTURE-BASED DRUG DISCOVERY

Structure-based drug discovery is the design and development of a compound as a drug candidate and is based on the determination of the three-dimensional structure of the protein by X-ray crystallography or nuclear magnetic resonance (NMR) spectroscopy. Homology models and virtual screening can be used when the structure of the target is not available, using well-known structures of a related protein. The use of structure-based methods are increasing rapidly and playing an important role in the research of drug discovery and frequently can be used as a complementary method with HTS.

1.2.2.1 X-RAY CRYSTALLOGRAPHY

X-ray crystallography is the technique used in structure-based drug discovery to obtain 3D-structural molecular information from a crystallized protein. The recombinant gene of the target is cloned into a vector to express into a host (usually bacteria strains) and produce the protein target. The protein obtained needs to be as pure as possible, homogenous and correctly folded in solution. The pure protein sample is prepared at high concentration in controlled dehydration

experiments (crystallisation) to force the protein to form crystals. Crystallisation occurs when the concentration of the protein reaches the precipitation (supersaturation or metastable) zone. Crystallisation experiments usually examine and test a wide range of variables, such as pH, temperature, protein, buffer, salt and precipitant concentrations, plate format (hanging drop, sitting drop and under oil), solution volumes and drop ratio (Merz et al. 2010).

When crystallisation experiments result in adequate quality crystalline solid form (larger size and singular form), these are exposed to an X-ray beam to obtain diffraction patterns. The processing of the diffraction data is mathematically complex, however, there are many software packages such as MOSFLM, HKL-3000R and XDS and computational programs such as CCP4 with established algorithms to facilitate the data processing (Otwinowski & Minor 1997; Smyth & Martin 2000). The collected X-ray diffraction data records the measurement of the intensity of the electromagnetic waves. Each reflection of the diffraction pattern correlates to a wave containing an amplitude and a phase value. The amplitude is obtained by using the intensity data, however the phase information is lost during the data collection, this is known as the “phase problem” (Taylor 2010). The diffraction data will be transformed into structural information by solving the phase problem.

There are different approaches to solve the phase problem, the most popular method is molecular replacement (MR) which utilizes the existence of a previously known structure of a similar protein homologous to the structure to be solved (Büttner et al. 2015). Other methods less commonly used for solving the phase problem are; single-wavelength anomalous diffraction (SAD), multi-wavelength anomalous diffraction (MAD), single-isomorphous replacement (SIR) and multiple isomorphous replacement (MIR; Hendrickson & Ogata 1997; Smyth & Martin 2000; Taylor 2010). Isomorphous replacement and anomalous replacement methods require previous information of the heavy atoms and anomalous scattering atoms of the substructure respectively (Table 1.1).

Once the phase problem is solved an electron density map is generated for structural refinement to obtain the final molecular structure model. Optimised crystals are usually soaked with fragments to collect information about a protein structure in complex with ligands, these ligands will need further chemistry optimisation to improve drug-like properties. Ligands that are able to bind in the protein structure will be further tested in an *in vitro* assay to study the relationship between binding and function.

Table 1.1. Phasing methods used in structural solution (Adated from Taylor, 2010).

Method	Previous knowledge	Comments
Molecular replacement (MR)	Homology model available	Homology model sharing at least 30% of sequence identity
Isomorphous replacement (SIR/MIR)	Heavy-atom substructure	Soak crystals with heavy atoms solution
Anomalous replacement (SAD/MAD)	Anomalous-atom substructure	SAD reduces potential radiation damage compared to MAD when collecting

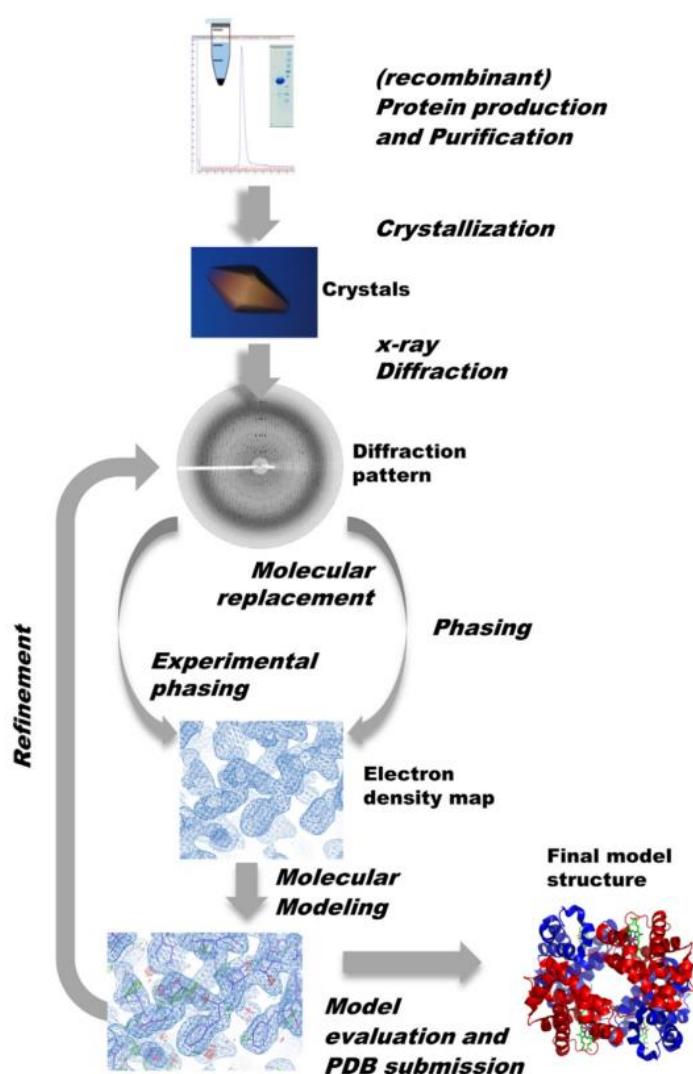


Figure 1.3. X-ray crystallography procedure. Target protein is expressed and purified to obtain diffracting crystals, diffraction data is used for phase determination and calculation of electron density map. The electron density map obtained is used for molecular model building and structural refinement where phases and electro density maps are improved (Büttner et al. 2015).

1.2.2.2 NMR STRUCTURE DETERMINATION

Nuclear magnetic resonance (NMR) spectroscopy is an analytical technique used for the determination of physical and chemical properties of atoms in molecules using the magnetic properties of atomic nuclei (Berg et al. 2002). This technique is an indirect method that uses computer calculations parametrized empirically for characterizing the 3D-conformation of proteins. Similar to X-ray crystallography the protein sample has to be in solution for protein expression and purification experiments. For structure determination, the collection of different 2D and 3D NMR spectra is necessary for the generation of a resonance spectrum measurement. Advantages of this technique are; the information of molecular parameters (chemical shifts, angles and distances), coupling constants and chemical kinetics, and the potential to study the solvent influence in the protein sample (Rzepa 1996). Some disadvantages of this technique for structure determination are the difficulty in identifying which NMR peak corresponds to which nuclei in the spectrum, the re-assignment of the spectrum for each ligand in complex with the protein and most analysis are limited to protein below 30 kDa (Hubbard 2011).

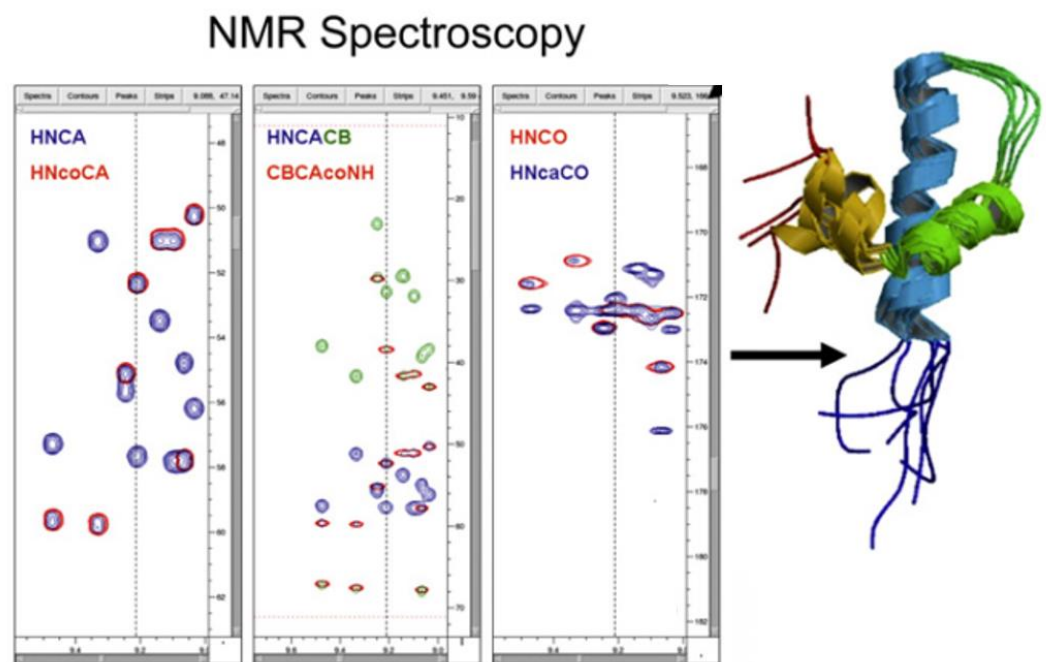


Figure 1.4. Structure determination by NMR spectroscopy. Example of the different 3D spectra using multiple-isotopes ^{13}C , ^{15}N and ^1H for generation of protein structure (Adapted from Hubbard 2011).

1.2.2.3 VIRTUAL SCREENING

Virtual screening (Fig. 1.5) is a technique used for structure-based drug discovery in which large libraries of small molecules are computationally screened against a target structure (i.e. a protein-protein binding pocket). In order to perform a virtual screen it is necessary to have deposited known structures of the target in the protein data bank (PDB; Lionta et al. 2014). The libraries are drug-like compounds that have been previously synthesised as commercial compounds. The general process starts with identifying the binding site of the target and selecting a specific compound database (library). The database used usually corresponds to a collection of physically available compounds; each drug discovery research group has a preferred database according to the target of study. The next step is performing molecular docking of each compound into the binding site of the target. Docking studies predict the orientation of the compound into the target site to form a stable complex by sampling the coordinate space of the binding site and ranking each possible compound pose. There is a wide range of docking software such as; molecular operating environment (MOE), mutually orthogonal latin squares (MOLS), SwissDock, GOLD and DOCK. These software packages use sampling algorithms to generate a score system which measures different parameters of the predicted binding mode, for example, the free energy of the binding, surface of the dynamics, ligand flexibility and the clashing or impact of the pocket (Lyne 2002; Lionta et al. 2014). MOE is a fully integrated drug discovery software package with a wide range of applications such as structure- and fragment-based design, pharmacophore discovery, medicinal chemistry and biologics applications, protein and antibody modelling, molecular simulations, cheminformatics and quantitative structure-activity relationships (QSAR) models. MOLS is a software program specialised for peptide modelling and protein-ligand docking (Paul & Gautham 2016). An advantage of SwissDock is that it uses a web server to predict the possible interactions between a target protein and a small molecule, it is accessible through a web browser and results can be viewed online (Grosdidier et al. 2011). GOLD is software used for binding mode predictions that utilizes the Chemscore scoring function for predicting ligand binding (Verdonk et al. 2003). Finally, the DOCK software uses a geometric matching algorithm to superimpose the ligand into the binding pocket to obtain receptor flexibility and force-field based scoring analysis.

The compounds filtered by molecular docking and scoring go through several post-analysis tools to filter the compounds that are suitable for further analysis. Some common post-analysis filter steps include medicinal chemistry studies, toxicity, chemical reactivity and drug-like similarity. After the compounds are selected, they will be tested in a biological *in vitro* or *in vivo* assay format. Some advantages of virtual screening are the rapid and low cost of screening a large

amount of compound libraries, large amount of virtual screen and docking computational programs and the ability to predict binding mode of a specific target. Some disadvantages are the requirement to know the three-dimensional information deposited in the PDB, the need for further filtered parameters and it cannot substitute a biological assay screen such as high-throughput screening (HTS). However, both methods can complement each other for the selection of novel compounds. Usually virtual screening is performed first and then compounds hits are tested with HTS.

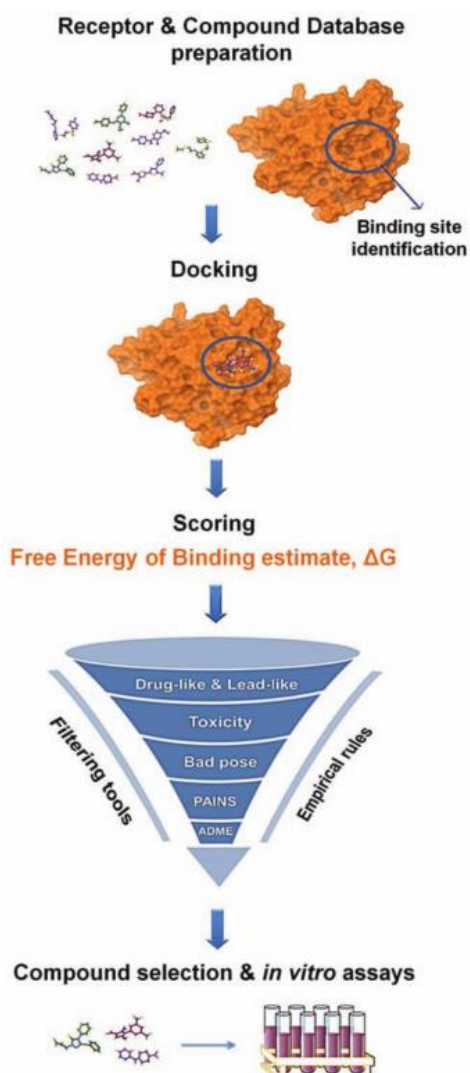


Figure 1.5. Structure-based virtual screening approach. The starting point is identifying the binding site of the target in previously known structures and the selection of an adequate compound database. Molecular docking and scoring will then be performed using computational software to further post-analyse to selected compounds using filtering tools such as, pan-assay interference compounds (PAINS) and absorption, distribution, metabolism and excretion (ADME) properties filters and finally test selected compounds *in vitro* assays (Lionta et al. 2014).

CHAPTER 2

NUCLEAR FACTOR ERYTHROID 2-RELATED FACTOR 2 (NRF2)

2.1 ABSTRACT

The normal function of the antioxidant defence pathways are essential for cell survival. Dysfunction and up-regulation of the oxidative stress pathways are implicated with the pathogenesis of many neurodegenerative diseases, including Alzheimer disease, Parkinson's disease and Amyotrophic lateral sclerosis. The protein nuclear factor erythroid 2-related factor 2 (Nrf2) is an important transcription factor that functions to regulate the redox balance against oxidative and electrophilic stresses. The Nrf2-Kelch-like ECH-associated protein 1 (Keap1) pathway acts as a sensor in response to oxidative/electrophilic stress. The Nrf2-Keap1 dissociates in response to oxidative stress and Nrf2 translocates to the nucleus to increase the expression of protective genes and antioxidant enzymes such as the phase II detoxifying enzymes glutathione S-transferase (GST), quinone reductase (QR), heme oxygenase-1 (HO-1) and NAD(P)H quinone oxidoreductase 1 (NQO1). Accordingly, Nrf2 is an attractive cellular pathway for drug discovery. In order to identify a novel Nrf2 activator that disrupts the Nrf2-Keap1 protein-protein interaction, a virtual screen was performed based upon the known structure of the protein-protein interface between Nrf2-Keap1 and evaluated compounds in a DiscoverX nuclear complementation assay that measures the translocation of Nrf2 from the cytoplasm to the nucleus. In this assay, sulforaphane was used as a positive control and had an EC_{50} of 400 ± 55 nM. In silico screening of a library of over 3 million compounds identified a number of virtual screening "hits" of which 122 were purchased and evaluated further. Of these compounds, five produced an activation ranging from 15-100% relative to the sulforaphane control (which was defined as 100% activity). However, the use of a ROS-Glo assay showed that three of these five compounds were activating the pathway non-specifically by themselves producing free radicals rather than disrupting the protein-protein interaction. Two novel compounds appeared to increase Nrf2 nuclear translocation in a Keap1-Nrf2 cell-based assay. However, both compounds displayed relative low activity and there was insufficient evidence of Nrf2-Keap1 robust interaction and so a no-go decision of the project was made.

2.2 INTRODUCTION

2.2.1 THE NRF2-ARE SYSTEM

The *NFE2L2* gene encodes for a 68 kDa protein, the nuclear factor erythroid 2-related factor 2 (Nrf2), which belongs to a family of proteins characterised by their cap 'n' collar (CNC) protein structure. These CNC proteins are basic leucine zipper (bZIP) transcription factors that are characterised by the presence of a conserved 43 amino acid CNC domain in the C-terminal region which acts as a DNA binding domain, CNC domain is located in Neh1 region of Nrf2 (Fig. 2.1). In the nucleus, bZIP proteins heterodimerize with other proteins (musculoaponeurotic fibrosarcoma oncogene homolog, small MAF or c-JUN) which are then be able to bind to specific DNA sites called anti-oxidant response elements (ARE; Nguyen et al. 2009). Nrf2 is the major transcription factor that binds with members of the small musculoaponeurotic fibrosarcoma (MAF) family and consequently it binds to ARE sites which are able to regulate the transcription of hundreds of cytoprotective genes (including antioxidants) and thereby protect cells from environmental stresses and enhance cell survival (Katsuoka et al. 2005; Blank 2008). Accordingly Nrf2 is essential for the cellular response pathways against different types of stress (Kensler et al. 2007; Kumagai et al. 2013; Sandberg et al. 2014).

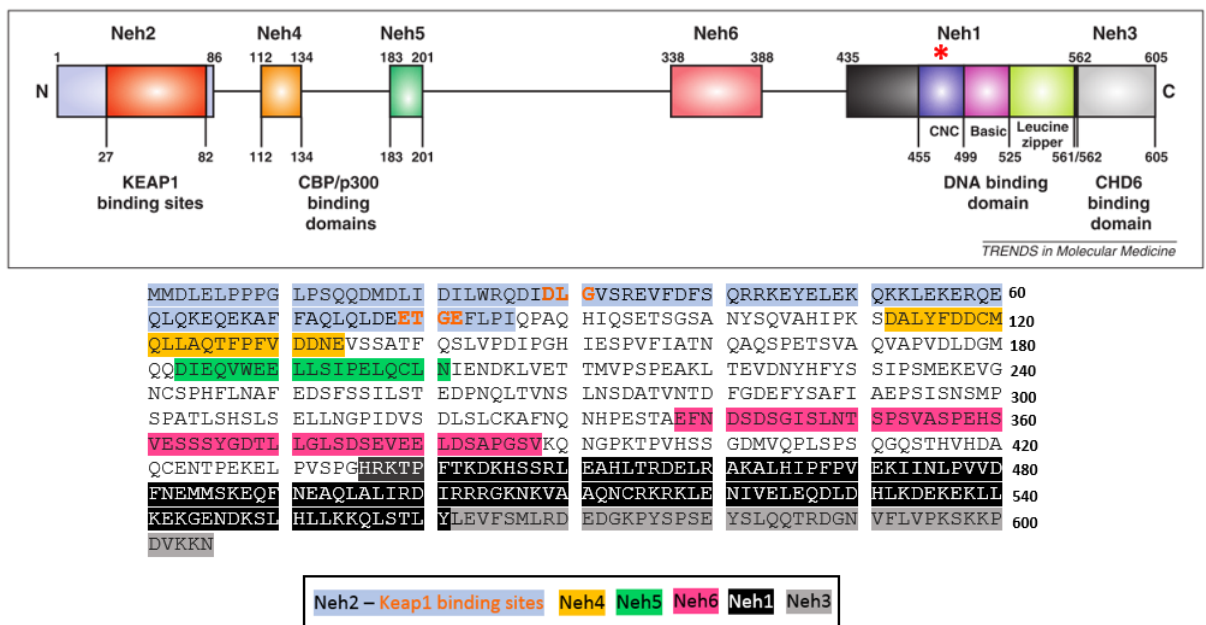


Figure 2.1. Summary of Nrf2 structure. Nrf2 protein contains 605 amino acids and six Nrf2-embedded contact homology (Neh) domains (Neh1-6). The CNC-bZIP located in the Neh1 region, CNC shown with a red asterisk. Within the C-terminal region, the Neh1, Neh3 and Neh6 domains are responsible for DNA binding, transcriptional activity and degradation signal respectively. Cromodomain-helicase-DNA-binding protein 6 (CHD6) in Neh3 is a chromatin-remodelling protein that plays an important role in transcription regulation. The N-terminal region contains

the Neh2, Neh4 and Neh5 domains which are important for binding with Keap1, regulation of Nrf2 target gene expression and interaction with CREB-binding protein (CBP) and p300 proteins respectively (Boutten et al. 2011). The linear sequence of the protein Q16236-1 UniProtKB is also shown, displaying the different domains of the protein.

Nrf2 contains six Nrf2-Erythroid-derived CNC homology (Neh) domains (Neh1-6; Fig. 2.1). The Neh2 domain is important for binding with the cytosolic repressor protein Kelch-like erythroid cell embedded contact homology (ECH)-associated protein (Keap1). Under normal conditions Nrf2 binds to Keap1 under which conditions Nrf2 is inactive and the Nrf2-Keap1 complex is directed towards Nrf2 ubiquitination and subsequent proteasomal degradation using the CUL-3 E3 ubiquitin ligase complex (Fig. 2.3; Motohashi & Yamamoto 2004; Kensler et al. 2007). Keap1 has been demonstrated to regulate Nrf2 protein levels either by enhancing its rate of degradation or altering its cellular localisation. The process of Nrf2 degradation is relatively rapid, with the normal half-life of Nrf2 being 18.5 minutes, suggesting that turnover of Nrf2 is an important process in normal cells (Itoh et al. 2003).

Keap1 (Fig. 2.2 & 2.3) is a 69-kDa rich in cysteine residues protein, which act as a sensor of stress signals. Modification of these cysteine residues (i.e. oxidation to form disulphide bonds) results in conformational changes in Keap1 which then releases Nrf2. One proposed model of Nrf2 dissociation is the “hinge and latch” mechanism, in which Keap1 homodimer binds with two sites of the Neh2 domain of Nrf2 (29-DLG and 79-ETGE). Conformational changes of Keap1 by cysteine modifications cause disruption of the low affinity site with Nrf2 DLG (the latch) causing Nrf2 accumulation, dissociation and prevention of the proteasome ubiquitination process (Fig. 2.4; Suzuki et al. 2013).

Once released from Keap1, Nrf2 is phosphorylated by cytosolic kinases which activate Nrf2 resulting in the protein translocating into the nucleus where it can heterodimerize with sMAF or c-JUN proteins. These complexes then bind to antioxidant response elements (ARE) and induce the expression of several ARE-responsive genes, including phase II detoxifying enzymes and antioxidants (Fig. 2.3). This adaptive response will enhance cell survival to several types of stress mediated by electrophiles and free radicals (Kensler et al. 2007).

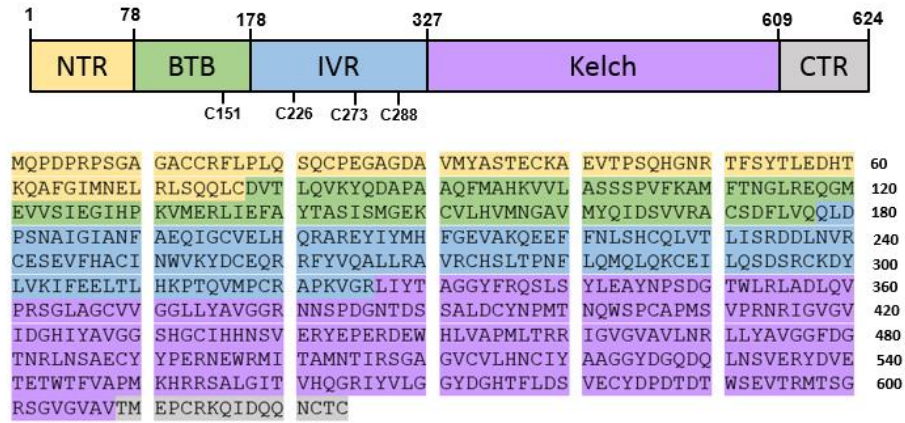


Figure 2.2. Keap1 protein structure and sequence. Protein is formed by five domains; the N-terminal region (NTR), the bric-a-brac, tram-track, broad complex domain (BTB), the intervening region (IVR) and the C-terminal region (CTR; Coople 2012; Baird et al. 2014). Sequence Q14145-1, UniProtKB; the colours correspond to the different domains of the protein structure. (Adapted from Baird et al. 2014).

2.2.2 Nrf2 phosphorylation

The Nrf2-Keap1 interaction is not the only factor regulating stability and cellular localisation of Nrf2. A number of kinases are reported to directly phosphorylate Nrf2. For example, p38 mitogen-activated protein kinases (MAPKs) can phosphorylate multiple serine residues (Ser-215, 408 and 577) of Nrf2 promoting its association with Keap1 and blocking its nuclear translocation (Keum et al. 2006; Sun et al. 2009; Bryan et al. 2013). p38 MAPKS are the only kinases that have been shown to reduce the Nrf2 nuclear translocation, however the exact interaction has not been confirmed. In contrast, protein kinase C (PKC) has an important role in promoting nuclear translocation of Nrf2 and facilitating the release from Keap1 by directly phosphorylating Nrf2 at serine 40 (Huang et al., 2002). Similarly the phosphatidylinositol 3-kinase (PI3K) is important in regulating the Nrf2 pathway, however the specific mechanism is yet not clear (Wang et al. 2008). The c-Jun N-terminal kinase (JNK), and the extracellular signal-regulated kinase (ERK) have an important part in activation of Nrf2, since both kinases have been shown to accelerate the release from Keap1 and stimulate the nuclear translocation of Nrf2 (Xu et al. 2006). In addition, the tyrosine kinase Fyn phosphorylates the Nrf2 tyrosine 568 to induce the nuclear export and proteasome degradation, regulating the Nrf2-ARE system (Sandberg et al. 2014). In recent studies the protein kinase RNA-like endoplasmic reticulum kinase (PERK) also showed some interaction with Nrf2, however the site of phosphorylation is still unclear (Nakaso et al., 2003, Cullinan et al., 2003, Xu et al., 2006 & Bryan et al. 2013).

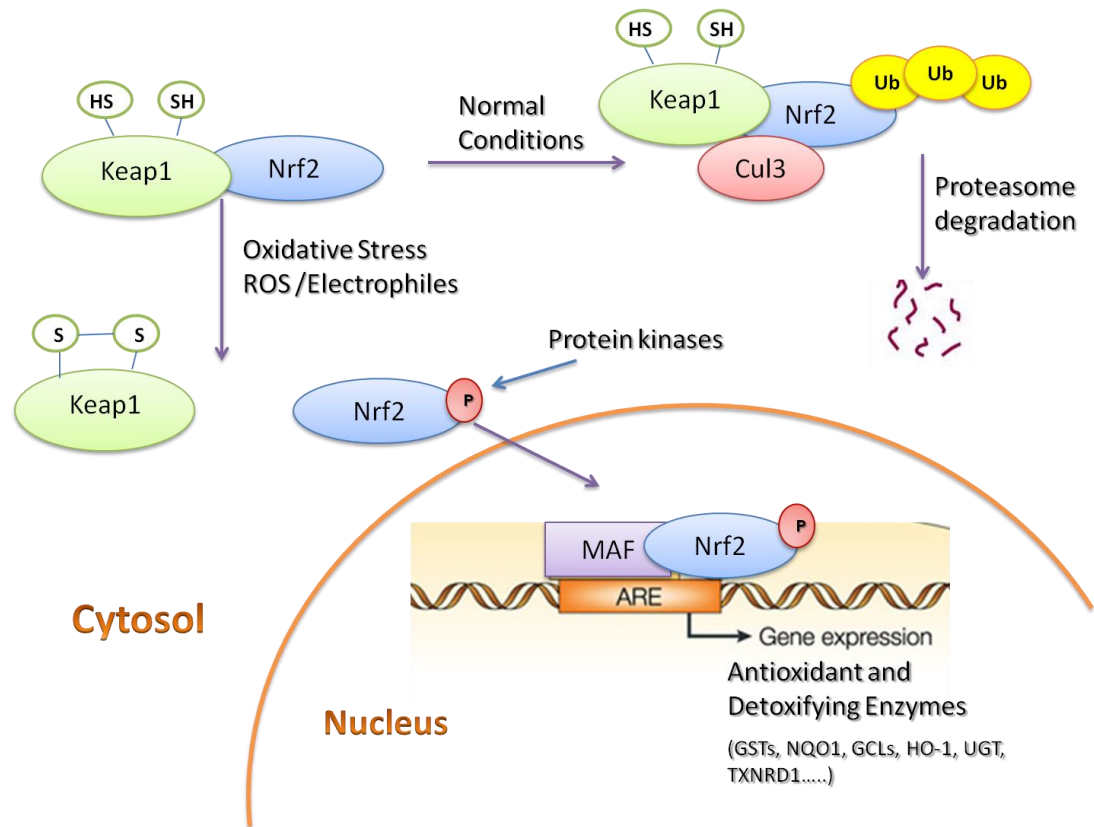


Figure 2.3. Summary of the Nrf2-ARE cellular protection pathway. Under basal conditions, Nrf2 is targeted to ubiquitin degradation by the Keap1/Cul3 E3 ubiquitin ligase complex. Under conditions of oxidative stress, cysteine-rich Keap1 is oxidised and the resulting conformational change releases Nrf2 which is then phosphorylated and undergoes translocation into the nucleus where it associates with small MAF and then promotes the expression of ARE-driven genes (Adapted from Lee et al. 2005). GSTs, Glutathione S-transferases; NQO1, NAD(P)H:quinone oxidoreductase 1; GCLs, Glutamate cysteine ligase subunit; HO-1, Heme oxygenase 1; UGT, UDP-glucuronosyltransferase and TXNRD1, thioredoxin reductase 1.

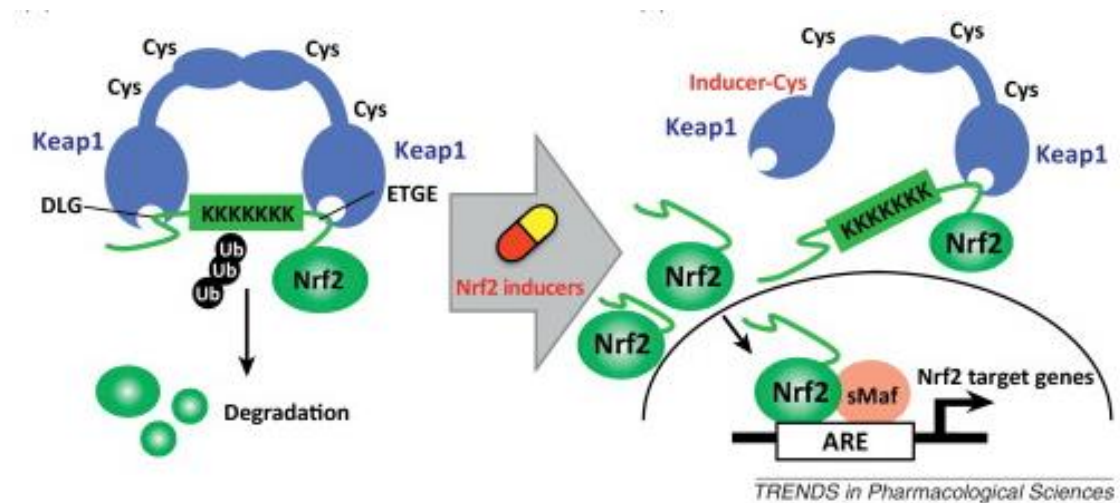


Figure 2.4. Diagram of the “Hinge and Latch” model of Nrf2 releases from Keap1. The protein Keap1 is present in the cytosol as a homodimer in a cherry-bob conformation, in which the homodimer binds to the Nrf2 protein sequence in two sites inside the Neh2 domain located at the N-terminal of the protein, one in high affinity ETGE the “hinge” and the lower affinity DLG the “latch”. DLG corresponding to aspartic acid, leucine and glycine and ETGE to glutamic acid, threonine, glycine and glutamic acid according to the one letter amino acid code. Both binding sites of Keap1 with DLG and ETGE facilitate the proteasomal degradation of Nrf2 by allowing the ubiquitination in the seven lysine (K) residues in the protein sequence. However, cysteine modification of Keap1 leads to a conformational change of Keap1, destabilizing the DLG binding (latch) and results in the accumulation and stabilisation of Nrf2, several kinases might also activate Nrf2 for complete dissociation from Keap1 (Suzuki et al. 2013).

2.2.3 NRF2 FUNCTIONS

Nrf2 is considered the key controller of the redox homeostatic gene regulatory network and is therefore one of the important systems protecting against oxidant and electrophile-induced damage in the cells (Ishii 2000; Sandberg et al. 2014). Other systems involved in protection against oxidative stress are the pentose phosphate pathway (Kuehne et al. 2015), mitochondrial antioxidant pathways such as peroxiredoxin (Prx) and cAMP response element-binding protein/cAMP response element (CREB/CRE) transcriptional pathway (Lee et al. 2009; Perkins et al. 2015). Over the last few years it has been demonstrated that Nrf2 regulates the expression of a wide range of detoxification, antioxidant and conjugating enzymes, as well as proteins that enhance the export of xenobiotics and enzymes important in protection of inflammation induced damage. These protective enzymes and proteins include, for example, glutathione S-transferases (GSTs; Chanas et al. 2002), NAD(P)H:quinone oxidoreductase 1 (NQO1; Hong et al. 2010), brain derived neurotrophic factor (BDNF; Sakata et al. 2012), anti-apoptotic B-cell lymphoma 2 (BCL-2; Niture & Jaiswal 2012), anti-inflammatory interleukin IL-10 (Boyle et al. 2011), the mitochondrial transcription co-factor NRF-1 (Piantadosi et al. 2011) and heme oxygenase 1 (HO-1; Hong et al. 2010).

The importance of this protective system is demonstrated by the fact that Nrf2 knockout mice demonstrate a deficiency in the production of phase II detoxification antioxidant enzymes that are indispensable against oxidative and xenobiotic stress (Sandberg et al. 2014). Phase II detoxification enzymes are responsible for the conjugation reactions of xenobiotics in the biotransformation metabolism, usually these enzymes are transferases that transfer a functional group from one molecule to another to facilitate the elimination of drugs in the metabolism (Jancova et al. 2010). These mice with deficiency of phase II detoxification enzymes are also more sensitive to toxic electrophiles, leading to elevated neurotoxicity and resulting in acute and severe pathological effects in brain (more severe damage in stroke and traumatic brain injury), liver (cancer and liver toxicity), lungs (hyperoxic lung injury) and intestine (intestinal ischemia reperfusion; Ishii 2000; Motohashi & Yamamoto 2004; Sandberg et al. 2014).

2.2.4 NRF2 AS A MULTI-ORGAN PROTECTOR AGAINST DISEASE

A relationship between the activation of Nrf2-ARE pathway with anti-inflammatory effects has been suggested, one hypothesis is an interaction with the nuclear factor kappa-light-chain-enhancer of activated B cells (NF- κ B), a protein complex important for the transcription control of DNA, cytokines and cell survival. This relationship is not yet understood but NF- κ B binding sites in the Nrf2 gene have been identified suggesting a similar role for inflammatory processes (Nair et al. 2008; Sandberg et al. 2014). Antioxidant response studies in animal models demonstrate that genetic disruption (gene silencing or gene deletion) of Nrf2 increased brain, liver, and pulmonary injury due to the decreased levels of ARE-driven cellular protection systems and overexpression of Nrf2 can protect these organs from induced toxicity response (Fig.2.5; Lee et al. 2005). Below are some examples of diseases related to Nrf2 dysfunction in different organs.

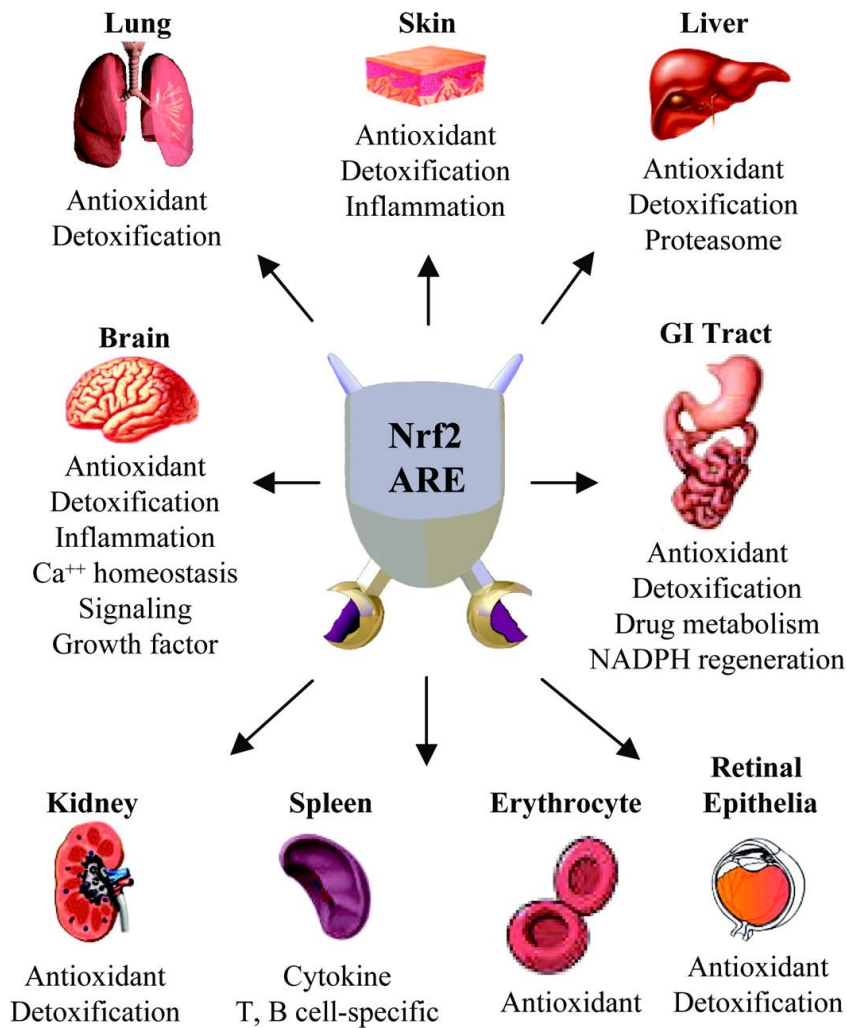


Figure 2.5. Nrf2 has a protective effect in a variety of different tissues and organs. Nrf2 increases the expression of ARE-driven detoxification and antioxidants genes (Lee et al. 2005).

2.2.4.1 LUNGS

Nrf2 is highly expressed in lungs and it is associated with protection against inflammatory agents and oxidants (Chan & Kan 1999). Nrf2 knockout (KO) mice displayed acute respiratory distress syndrome with the administration of toxic butylated hydroxytoluene (BHT) compared with wild type, suggesting an important role of Nrf2 in the defence against oxidants in the lungs (Chan & Kan 1999). Oral administration of BHT is used for the induction of lung damage and alveolar epithelial cells destruction (Chan & Kan 1999). Nrf2 protects lungs against hyperoxic injury in mice, macrophage inflammation and epithelial injury were increased by 47% and 43% in Nrf2 deficient compared to wild type mice after 72 hours of hyperoxia exposure (Cho et al. 2002). Also, in a Nrf2 KO experiment showed that wild type Nrf2 mice displayed protection from lung injury and fibrosis induced by bleomycin administration in a pulmonary fibrosis animal model (Cho et al. 2004).

Chronic obstructive pulmonary disease (COPD), a progressive condition characterised by lung damage, emphysema and breathing disorders, is associated with cigarette smoking. Cigarette smoke-induced emphysema studies showed greater bronchoalveolar inflammation and apoptotic alveolar cells in Nrf2 KO compared with the wild type mice (Rangasamy et al. 2004; Iizuka et al. 2005; Ishii et al. 2005). The Nrf2-ARE driven genes have an important role in protection in pulmonary emphysema by regulating the oxidant/anti-oxidant balance, inflammation and protease/anti-protease balance in alveolar macrophages (Ishii et al. 2005; Boutten et al. 2011).

2.2.4.2 LIVER AND GASTROINTESTINAL TRACT

The liver plays an important role in metabolizing xenobiotics, such as, chemicals, drugs and toxins. It performs the break down and elimination of chemical compounds with the help of phase I (oxidation, reduction and hydrolysis reactions) and phase II (conjugation reactions) metabolism. Hence, the liver is vulnerable to oxidative stress and liver diseases related with oxidants are hepatitis, fibrosis, cirrhosis and hepatocellular carcinoma (Fig. 2.6). Nrf2 is known to activate the phase II antioxidant enzymes that help balance the redox homeostasis and therefore Nrf2 has an important role in preventing liver and gastrointestinal tract disease (Shin et al. 2013). Studies in mice have showed that Nrf2 gene deletion increases the sensitivity to xenobiotics. For example, it has been shown that Nrf2 knockout mice have an increased sensitivity to acetaminophen toxicity relative to wild type animals (Enomoto et al. 2001). Similarly, treatment of carcinogen benzo(a)pyrene showed more severe damage (gastric

neoplasia and liver toxicity) in mice with Nrf2-deficient compared to wild type animals (Ramos-Gomez et al. 2001). These studies indicate that Nrf2 is important in regulating drug metabolizing enzymes and antioxidant genes in the liver and gastrointestinal tract (Aleksunes et al., 2007 & Klaassen & Reisman 2010).

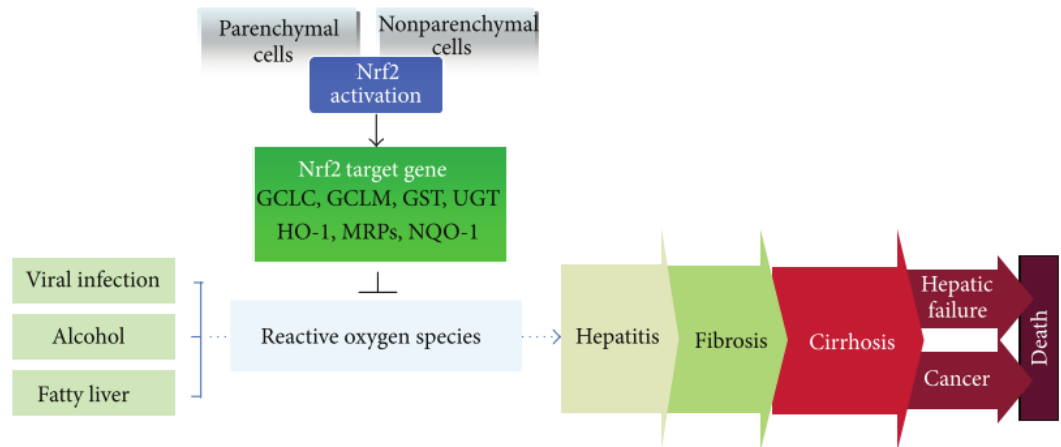


Figure 2.6. The protective role of Nrf2 expression in liver disease. The schematic representation of the Nrf2 activation to help prevent liver diseases by controlling the reactive oxygen species levels in cells (Shin et al. 2013). GCLC, glutamate-cysteine ligase catalytic subunit; GCLM, glutamate-cysteine ligase modifier subunit; GST, glutathione s-transferase; UGT, uridine 5'-diphospho-glucuronosyltransferase; HO-1, heme oxygenase; MRPs, multidrug resistance proteins and NQO-1, NAD(P)H quinone dehydrogenase 1.

2.2.4.3 SKIN

Studies in mice have also shown that Nrf2 has an important role in the protection of skin against UV rays. Hence, compared to wild type mice, UVB-irradiated Nrf2 knockout animals showed increased skin ageing, deeper coarse wrinkle formation, skin flexibility diminution, epidermal thickening and higher skin reactivity; the same mice demonstrated lower levels of glutathione levels in the skin (Hirota et al. 2011; Saw et al. 2011). In a fibroblast study, primary human skin fibroblasts displayed better resistance to ionizing radiation when treated with antioxidant and Nrf2-activator sulforaphane, however this resistance was dependent on Nrf2 activation, nuclear translocation and induction of antioxidant enzymes (Mathew et al. 2014).

2.2.4.4 HEART

Recent studies suggest that Nrf2 deficiency increases the earlier onset of cardiac dysfunction and the development of heart failure (Wang et al. 2014a; Sandberg et al. 2014). In Nrf2 knockout mice treated with the anticancer drug doxorubicin (Dox), the absence of Nrf2 amplified the adverse effects associated with Dox, such as cardiomyocyte necrosis, protein aggregation and cardiac dysfunction relative to wild type animals. In the same study the overexpression of Nrf2 in cultured rat neonatal wild type cardiomyocytes suppressed Dox cytotoxicity, suggesting that Nrf2 ameliorates Dox-induced damage by triggering expression of antioxidants (Li et al. 2014a).

2.2.4.5 BRAIN AND NERVOUS SYSTEM

Subarachnoid haemorrhage (SAH) is caused by the rupture of a cerebral aneurysm and is characterised by bleeding in the space between the brain and the tissues that cover the brain (pia mater). In animal models, Nrf2 over-expression has been shown to reduce the secondary complications of SAH, such as vasospasm and neuronal injury. A SAH mouse model has been developed by injecting blood into the prechiasmatic cistern in the brain, this model has shown to cause cerebral vasospasm in the mouse. Deletion of Nrf2 in knockout mice resulted in more severe brain injury with increased brain edema, blood-brain barrier disruption and neural apoptosis after injection of blood into the prechiasmatic cistern (Li et al. 2014b). Induced activation and over-expression of Nrf2 protects neurons against stressors and insults and consequently the Nrf2-ARE pathway is an important potential target for neurodegenerative diseases and CNS disorders (Calkins et al. 2009).

2.2.5 NRF2 IN NEURODEGENERATIVE DISEASES

The pathogenesis of various neurodegenerative diseases such as Parkinson's disease, amyotrophic lateral sclerosis, and Alzheimer's disease have all been linked with oxidative stress and mitochondrial dysfunction (Perry et al. 2002; Jenner 2003; Barber et al. 2006).

It has been shown, for example, that free radicals and reactive oxygen species (ROS) accumulation from redox imbalance leads to neuronal death and possible neurodegeneration (Dawson & Dawson 1996; Abramov et al. 2007). Astrocytes have several functions for the correct maintenance of neurons, it has been suggested that astrocytes can perform nervous system repair due to their relative high amount of key proteins and antioxidants (such as glutathione)

involved in neutralizing damaging free radicals (Aschner 2000; Kimelberg & Nedergaard 2010). Data from studies in animal models suggests that Nrf2 can rescue neurons and astrocytes from glutamate toxicity, ischemic insults and mitochondrial complex II inhibition (Kraft et al. 2004; Lee et al. 2005; Ramsey et al. 2008). Furthermore, overexpression of Nrf2 in astrocytes reduces chemical-mediated neurotoxicity in Parkinson's and Huntington's diseases and increases motor neuron survival in mouse models (Chen et al. 2009; Calkins et al. 2010; Gan et al. 2012). Malonate is used in animal models to induce neuron degeneration simulating Huntington's disease. For example, a genetic model of astrocyte-specific Nrf2 overexpression showed greater neuroprotection against malonate toxicity in mice in comparison to wild type mice (Calkins et al. 2010). Similarly, a study in mice in which 1-methy-4-phenyl-1,2,3,6-tetrahydropyridine (MPTP) was used to produce neurotoxicity of neurons in the substantia nigra, and consequently Parkinson's disease-like symptoms, showed that Nrf2 overexpression eliminates MPTP toxicity and help prevent neuronal death (Chen et al. 2009). In an amyotrophic lateral sclerosis (ALS) animal model using transgenic mice with mutation in Cu/Zn-superoxide dismutase (SOD1), overexpressing Nrf2 resulted in delayed disease development, increased overall survival and lower glial reactivity (Vargas et al. 2008). If the Nrf2-ARE pathway is able to rescue cells against these insults and oxidative stressors, then the Nrf2 pathway might have an important role in neuroprotection as many studies have shown (Kraft et al. 2004; Vargas et al. 2008; Calkins et al. 2009; Chen et al. 2009; Gan et al. 2012).

2.2.6 MODULATORS OF THE NRF2/ARE PATHWAY

There are several compounds or substances such as; sulforaphane, quercetin, tert-butylhydroquinone (tBHQ) and 5,6-dihydrocyclopenta-1,2dithiole-3-thione (CPDT) that can induce and activate the Nrf2-ARE pathway (Gharavi et al. 2007; Kimura et al. 2009; Li et al. 2012). This activation has been measured by different approaches, including measurement of Nrf2 nuclear translocation and induction of downstream antioxidant genes (i.e. NAD(P)H, GST and HO-1).

As discussed previously, Keap1 is a cysteine rich protein, the cysteine residues are highly reactive and have the potential to sense modulators of Nrf2 forming disulphide adducts with them. These modulators activate the Nrf2/ARE pathway indirectly by directly modifying the sulfhydryl groups of Keap1 cysteines by oxidation, reduction, or alkylation, thereby avoiding the further ubiquitination of Nrf2 and releasing it from Keap1. Cysteine residues of Keap1 involved in Keap1-Nrf2 degradation are Cys-151, Cys-273 and Cys-288 and small molecules that mimic ROS

(electrophiles) interact with these cysteine residues to change the conformation of Keap1, resulting in dissociation of Nrf2 from Keap1 and thereby inhibits Nrf2 ubiquitination and degradation (Fig. 2.7; Hong et al. 2005; Kobayashi et al. 2006; 2009).

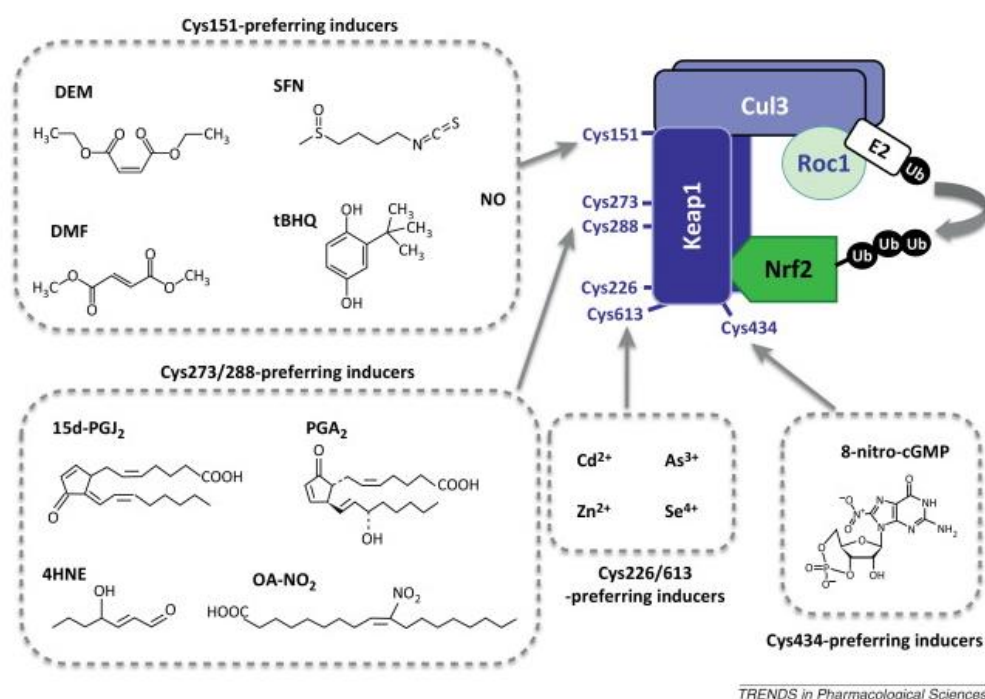


Figure 2.7. Keap1 cysteine residues involved in chemical inducers. Some electrophiles and heavy metals are able to modify the cysteine residues of Keap1, consequently this redox cysteine modifications induce conformational changes in Keap1 resulting in dissociation from Cul3, thereby inhibiting Nrf2 degradation. tBHQ, tert-butylhydroquinone; SFN, sulforaphane; DEM, diethyl maleate; DMF, dimethylformamide; 15d-PJ₂, 5-deoxy-Delta(12,14)-prostaglandin J₂; PGA₂, prostaglandin A₂; 4HNE, 4-hydroxynonenal; OA-NO₂, nitro-oleic acid and 8-nitro-cGMP, 8-nitroguanosine 3',5'-cyclic monophosphate (Suzuki et al. 2013).

One of the most studied Nrf2/ARE modulators is tert-butylhydroquinone (tBHQ), a hydroquinone derivative that protects neuroblastoma cells from glutamate toxicity and hydrogen peroxide (H₂O₂)-induced apoptosis (Lee et al. 2005) by binding with the cysteine residue Cys-151 of Keap1, followed by Keap1 change conformation to Nrf2 release, escaping ubiquitination and degradation (Zhang 2006). tBHQ induces the Nrf2-ARE pathway by indirectly stimulating the dissociation of Nrf2 from Keap1 and Nrf2 then can be translocate to the nucleus and activate ARE gene expression. Additional studies used tBHQ and sulforaphane to induce

Nrf2-ARE pathway cellular protection by translating antioxidants proteins against oxidative insults such as dopamine, hydrogen peroxide and glutamate (Murphy et al. 1991; Li & Johnson 2002; Houghton et al. 2016). In a mouse primary cortical neuronal culture study, overexpression of Nrf2 via adenovirus infection in Nrf2-deficient neurons restored ARE genes expression and conferred neuroprotection from H₂O₂ and glutamate (Kraft et al. 2004). Further, in astrocytes, the overexpression of Nrf2-sMAF made neurons more resistant to glutamate toxicity (Lee et al. 2005). A microarray analysis showed the increase in expression of 97 genes and decrease of 37 genes in astrocytes by tBHQ treatment, many of which included detoxifying genes involved in the Nrf2/ARE pathway (Calkins et al. 2009). However, there are concerns about the safety and toxicity of long-term administration of tBHQ with studies suggesting that long-term exposure might induce carcinogenicity in mice. For example, administration of tBHQ for several days to rodents was shown to induce more neoplastic lesions in the stomach, kidney and urinary bladder. However the specific mechanism, whether or not these effects are specifically related to the Nrf2 mechanism of this toxicity is not well understood, some alternatives are the indirect formation of reactive GSH-conjugates, activation of caspase and apoptosis, and the formation of reactive species (Li et al. 2002; Gharavi et al. 2007).

Sulforaphane, a compound extracted from broccoli, has been shown to activate Nrf2 by modifying the Cys-151 of Keap1 protein (Kobayashi et al. 2009). This compound has been shown to induce the activation of the Nrf2/ARE pathway in animal models of intracerebral haemorrhage and traumatic brain injury (Fig. 2.8). Accordingly, Nrf2 pathway activation after oxidative stress could help to restore or protect cells against toxicity, moreover Nrf2-deficient animals showed more severe damage against oxidative insults (Zhao et al. 2007a; Zhao et al. 2007b). For example, primary neurons from Nrf2-deficient embryos and *in vivo* Nrf2-knockout mice increased toxicity after exposure to a mycotoxin 3-nitropropionic acid (3-NP); a neurotoxin which induces brain mitochondrial dysfunction (selective loss of striatal neurons), simulating Huntington's disease pathology (Fig. 2.9; Calkins et al. 2009). Similarly, experiments in animals of traumatic brain injury using the controlled impact surgery model showed that Nrf2 knockout mice displayed higher levels of oxidative markers such as, 4-hydroxynonenal (4-HNE) and the 8-Oxo-2'-deoxyguanosine (8-OHdG) in brain after injury compared with the wild type mice, suggesting Nrf2 as a key role in oxidative stress response against brain injury (Hong et al. 2010). These same authors also treated mice with sulforaphane and it reduced contusion, neurological dysfunction and neuronal death after traumatic brain injury (Hong et al. 2010).

Sulforaphane is under clinical evaluation for schizophrenia, autism disorders and cancer; there are 52 different clinical studies for sulforaphane, which 28 are terminated or completed, 9 recruiting, 2 enrolling, 8 not yet recruiting and 5 suspended or unknown (www.clinicaltrials.gov). An open study in ten patients with schizophrenia suggests sulforaphane as a potential therapeutic drug in improving cognitive functions in schizophrenia; trial number NCT01716858 (Shiina et al. 2015). Two other clinical trials in phase II and III are currently enrolling to investigate if sulforaphane can improve clinical symptoms and cognitive functions in schizophrenia patients; trials NCT02880462 and NCT02810964.

A randomised, double-blind, placebo-controlled phase II single-site trial of sulforaphane-rich broccoli sprout extract in autism patients showed that sulforaphane significantly improved social interaction, abnormal behaviour and verbal communication; however more further studies need to be perform to investigate the specific mechanism of action in autism disorder; trial number NCT01474993 (Singh et al. 2014). However, the toxicity and reactivity of the molecule might cause the termination of clinical trials and research investigations. Consequently, Evgen Pharma developed Sulforadex (SFX-01), an orally stable powder composed by sulforaphane encapsulated within α -cyclodextrin. Sulforaphane is normally an unstable oily liquid but in complex with α -cyclodextrin can be stabilized by encapsulating it in the hydrophobic interior of the core structure and making it available for pharmaceutical delivery for possible therapeutic effects. Two clinical trials to investigate the safety and tolerability of single and multiple doses of SFX-01 in healthy males have concluded but results have not been released (NCT01948362 & NCT02055716). Currently, another two clinical trials are recruiting for the study of safety, tolerability and efficacy of SFX-01 in breast neoplasm and spontaneous subarachnoid haemorrhage (NCT02970682 & NCT02614742, respectively).

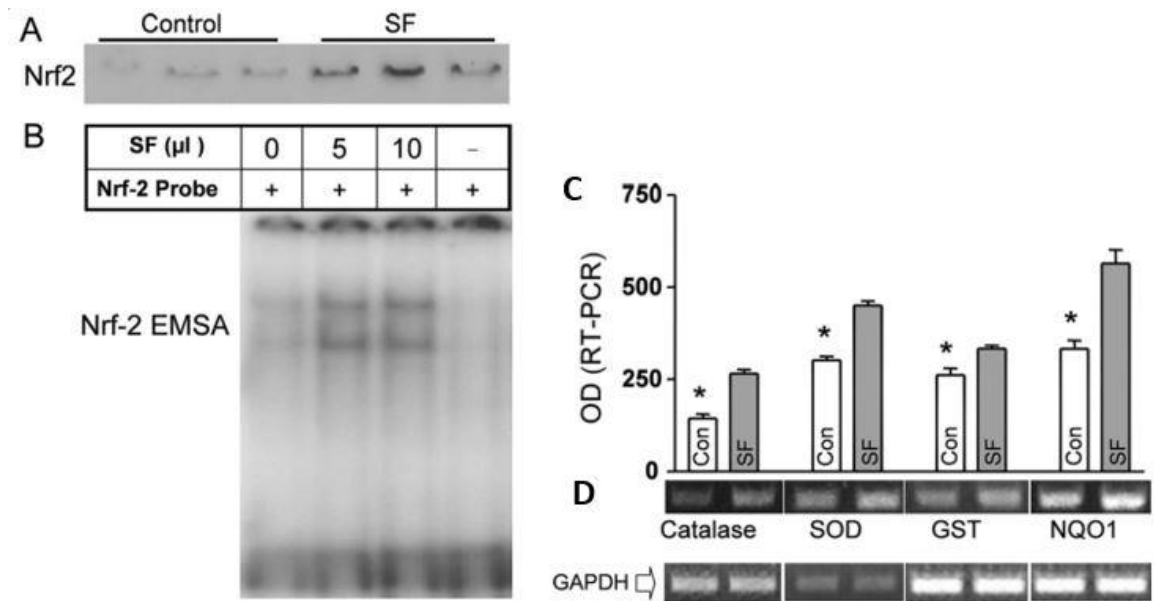


Figure 2.8. Sulforaphane-induced activation of the Nrf2 pathway. **A**, Detection of Nrf2 protein by Western blot in nuclear fractions of hematoma-affected striata 24 hours after induction of intracerebral haemorrhage. Sulforaphane treatment increased Nrf2 in the nuclear fraction, consistent with a hematoma-induced translocation of Nrf2 from the cytoplasm to the nucleus. **B**, Study of the Nrf2 DNA binding activity to the antioxidant response elements (ARE). For the electrophoresis mobility shift assay (EMSA) experiments Nrf2 nuclear protein was incubated with ^{32}P -labeled, double stranded oligonucleotides. Intraperitoneal injection of sulforaphane (5 and 10 mg/kg) increased Nrf2 ARE DNA binding activity. 10 mg of nuclear protein extracts were run from 0, 5 and 10 mg/kg of sulforaphane treatment in animals. **C**, The expression of Nrf2 antioxidant genes (measured by RT-PCR) in rodent brain following intracerebral haemorrhage and the administration of either vehicle or sulforaphane (5 mg/kg). Data clearly shows a SF-induced increase in the expression of catalase, superoxide dismutase (SOD), glutathione S-transferase (GST) and NAD(P)H:quinone oxidoreductase 1 (NQO1). **D**, Image of the data quantified in panel C showing the RT-PCR products of the downstream genes (catalase, SOD, GST, NQO1) of Nrf2/ARE pathway with GAPDH used as a loading control. Figure and legend adapted from Zhao et al. 2007b.

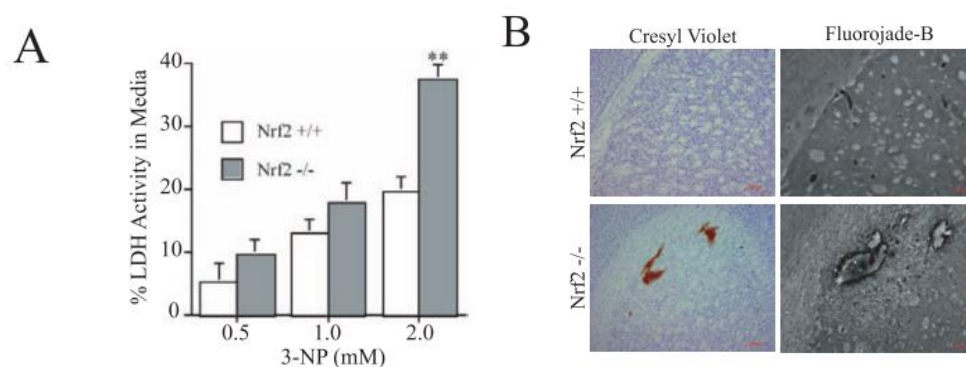


Figure 2.9. Nrf2 plays a role in 3-NP-mediated neurotoxicity. **A**, There was an increase in the toxicity of 3-NP in primary neurons (2 days of culture in 0.5, 1.0 and 2.0 mM 3-NP) from Nrf2 knockout compared to wild type mice as measured using lactate dehydrogenase (LDH) activity in the media as an index of neurotoxicity. **B**, Striatum lesion volume was quantified in coronal sections of the brain and stained with cresyl violet and with fluorojade-B for detection of degeneration in neurons (Figure and legend adapted from Calkins et al. 2009).

In mice the administration of the Nrf2 activator 3H-1,2,-dithiole-3-thione (D3T) prior to the injection of MPTP protected glial cells from neurotoxicity whereas this protective effect of D3T was lacking in Nrf2 knockout mice (Burton et al. 2006), consistent with D3T have a neuroprotective effect that is mediated via the Nrf2 pathway, possibly as a consequence of D3T binding with the cysteine reactive residues of the Keap1 protein and thereby producing Nrf2 activation (Kwak et al. 2003).

Other small molecules that are claimed to be Nrf2 activators include; curcumin, spirulina, some planar aromatic compounds, β -naphthoflavone, 3-methylcholanthrene, triterpenoids, some flavonoids, isothiocyanates, organosulfur, indoles and diterpenes (Boutten et al. 2011; Sandberg et al., 2014). Moreover, small molecules that have a predisposition to react with sulfhydryl groups can interact with the Keap1 protein and activate Nrf2-ARE pathway. For example, curcumin induces oxidation or alkylation of the cysteine residues in Keap1 and releases Nrf2 which translocates to the nucleus and produces a consequent increase in the expression of antioxidant enzymes (González-Reyes et al. 2013). However, the mechanism of action by which these molecules activates the Nrf2 pathway is not yet clear but most of them are hypothesised to modify cysteine reactive residues of Keap1.

Bardoxolone methyl (CDDO-Me) is a synthetic triterpenoid antioxidant inflammation modulator that activates the Keap1-Nrf2 pathway by binding with Keap1 cysteine residues (Wang et al. 2014b). In a kidney injury model, the administration of CDDO-Me increases renal Nrf2 and heme oxygenase-1 (HO-1) mRNA expression and protein levels (Wu et al. 2011). Additionally, knockout mice demonstrated acute kidney defects caused by increased inflammation and oxidative stress (Pergola et al. 2011). For example, a study shown that CDDO-Me treatment in wild type mice prevents the increased concentration of urea nitrogen in blood characteristic in acute kidney injury (Wu et al. 2011).

In a phase 2, double blind, randomized trial with chronic kidney disease associated with type 2 diabetes patients, the administration of CDDO-Me significantly improved kidney functions relative to placebo-treated patients (Pergola et al. 2011). However, the phase III clinical trial in the late state of disease, patients developed severe renal dysfunction or cardiovascular failure in a higher rate with CDDO-Me treatment than with placebo; therefore the trial was terminated due to safety concerns (Pergola et al. 2011; de Zeeuw et al. 2013; Sandberg et al. 2014). Cardiovascular adverse events related with CDDO-Me were investigated and were suggested to have off-target effects in modulating the endothelin pathway by promoting acute sodium and volume retention and increasing blood pressure in patients with severe chronic kidney disease (Chin et al. 2014).

There are some clinically used drugs that appear to activate the Nrf2 pathway, such as melatonin and valproate. Melatonin, which is used in sleep disorders in children, suppresses the degradation of Nrf2 by inhibiting the proteasome activity (Vriend & Reiter 2015). Valproate, which is used clinically as an anticonvulsant in epilepsy, as well as in anxiety disorders, migraine and bipolar disorders, has been demonstrated to increase cellular levels of reactive oxygen species (ROS) and activate the Nrf2/ARE pathway indirectly. In cellular and animal experiments the treatment of valproate increased the association of transcription factors, such as Nrf2 and nuclear factor- κ B (NF- κ B), as well as the levels of heme oxygenase-1 and human NAD(P)H:quinone oxidoreductase 1 genes (Kawai & Arinze 2006; Sandberg et al. 2014; Liao et al. 2016). However, the full mechanism of action is not well understood.

Table 2.1 Summary of Nrf2 activators and their therapeutic utility.

Activator	Pre-clinical/Clinical significance	Comments	Reference
Sulforaphane	Antioxidant, schizophrenia, autism, aging, asthma, cystic fibrosis and cancer	Toxic, reactive and unstable. 48 clinical trials to investigate specific mechanism of actions.	www.clinicaltrials.gov (Singh et al. 2014; Alumkal et al. 2015; Shiina et al. 2015; Singh & Zimmerman 2016)
CDDO-Me	Chronic kidney disease & type 2 diabetes	Serious adverse effects (heart failure, muscle spasms, etc)	(Pergola et al. 2011; de Zeeuw et al. 2013)
tBHQ	Late-life Depression	Dietary supplement (fish oil) High doses or chronic exposure link to carcinogenesis	(Gharavi & El-Kadi 2005)
Quercetin	Antioxidant and anti-inflammatory properties.	Obtained from plants (flavonols), used as a dietary supplement and additive in food products	(Harwood et al. 2007; Boots et al. 2008; Jin et al. 2010)
D3T	Chemopreventive and anti-inflammatory properties	Cytotoxicity is not well understood	(Kuo et al. 2016; Li et al. 2016)
Curcumin	Antioxidant and anti-inflammatory properties	Dietary supplement. Current clinical trials to study the effect and safety in the treatment of neurological diseases such as schizophrenia, Alzheimer's disease, epilepsy and depression.	(Kulkarni & Dhir 2010) www.clinicaltrials.gov
Spirulina	Source of vitamins, minerals and phytonutrients Glucose metabolism in Diabetes.	Dietary supplement (green algae). If contaminated can be unsafe for use (toxins and heavy metals). More research is needed for establish therapeutics benefits.	(Gilroy et al. 2000; Gershwin & Belay 2008; Marcel et al. 2011)
DMF	Psoriasis, necrobiosis lipoidica, granuloma annulare, sarcoidosis and multiple sclerosis	Drugs containing DMF have adverse side effects, such as gastrointestinal disorders and progressive multifocal leukoencephalopathy.	(Nowack et al. 2002; Kreuter et al. 2005; Roll et al. 2007; Weber et al. 2009; Bovenschen et al. 2010; Fox et al. 2012; Gold et al. 2012)

Bardoxolone methyl (CDDO-ME), tert-butyhydroquinone (tBHQ), 3H-1,2,-dithiole-3-thione (D3T) and Dimethyl fumarate (DMF)

2.3 AIMS

As described in the preceding sections, Nrf2 is an important transcription factor for redox homeostasis in cells and has a therapeutic potential in disorders associated with oxidative stress such as cancer and neurodegenerative disorders. Recently, several groups have reported a variety of small molecule Nrf2 activators that can enhance the function of the Nrf2/ARE pathway. However, these molecules, for example sulforaphane, valproate and others, are relatively unselective, which not only makes the interpretation of their effects within the central nervous system difficult but also can result in off-target side effects (i.e., non-Nrf2-related).

The aim of this work is to identify novel and specific small activators of this pathway which will be expected to have an improved selectivity and safety profile relative to existing activators. The approach is to exploit X-ray crystallographic structural information regarding the Nrf2-Keap1 protein-protein interaction to conduct a virtual screen of molecules that might interrupt the protein-protein interface and thereby cause Nrf2 to dissociate from or prevent the association with Keap1, resulting in an increase in free cytosolic protein that is then available to translocate to the nucleus. Compounds selected from the virtual screen will then be purchased and evaluated in a DiscoverX PathHunter enzyme fragment complementation cellular assay designed to measure the translocation of Nrf2 from the cytoplasm into the nucleus.

2.4 MATERIALS AND METHODS

2.4.1 MATERIALS

Description	Use for	Supplier and Catalogue Number
Select U2OS cell culture kit	Cell culture	DiscoverX (92-0018GL3)
Cell plating 0 reagent	Cell plating	DiscoverX (93-0563R0A)
Revive U2OS medium	Cell thawing	DiscoverX (92-0016RM5S)
Preserve U2OS freezing reagent	Cell freezing	DiscoverX (92-0017FR3S)
Cell detachment reagent	Cell detachment	DiscoverX (92-0009)
Hydrogen peroxide solution	Cell oxidant reagent	Fluka (Sigma Aldrich, 88597)
DL-Sulforaphane	Cell oxidant reagent	Sigma Aldrich (S4441)
PBS	Assay buffer	Sigma Aldrich (79382)
DMSO	Assay buffer	Fisher chemical (10080110)
Corning® 384 Well flat clear bottom white polystyrene TC-treated microplates	Cell seeding for assay	Corning (3707)
96-V well microplate translucent polypropylene	Source dilution plate	MIC9050, Scientific Laboratory Supplies

2.4.2 METHODS

2.4.2.1 VIRTUAL SCREENING STRATEGY

In the protein data bank (PDB) there are eighteen crystal structures relating to Keap1-Nrf2 binding interface, some structures display the *apo* state of the protein (with no ligand) and others are in the *holo* state (with ligand). The SDDC's computational chemist, Dr. Ben Wahab, performed the structural superpose and alignment of sixteen crystal structures from the PDB (Table 2.2) resulting in a root-mean-square deviation (RMSD) of 0.451 Å over 285 residues (alignment results shown in Appendix I). The RMSD value was used to study the similarity between structures, the low RMSD obtained demonstrated a similar conformation between the PDB structures of Keap1 (given that the structures were both *holo* and *apo*, it indicates a reasonably rigid protein). The alignment and super-positioning results were used for the investigation of interactions between the sixteen structures and the ones displaying the Keap1-Nrf2 interactions were used as a guide for pocket analysis and pharmacophore design.

PDB 1X2R displays Keap1 as a forked-stem dimer structure in a large globular conformation (known as a multiple tryptophan-aspartic acid (WD)-40 β -propeller structure) in which the Neh2 ETGE sequence region of Nrf2 binds with high affinity in the homodimer. The structures of Keap1 with Nrf2 or similar peptides were used as a reference for the modelling and virtual screening experiments (Fig.2.10).

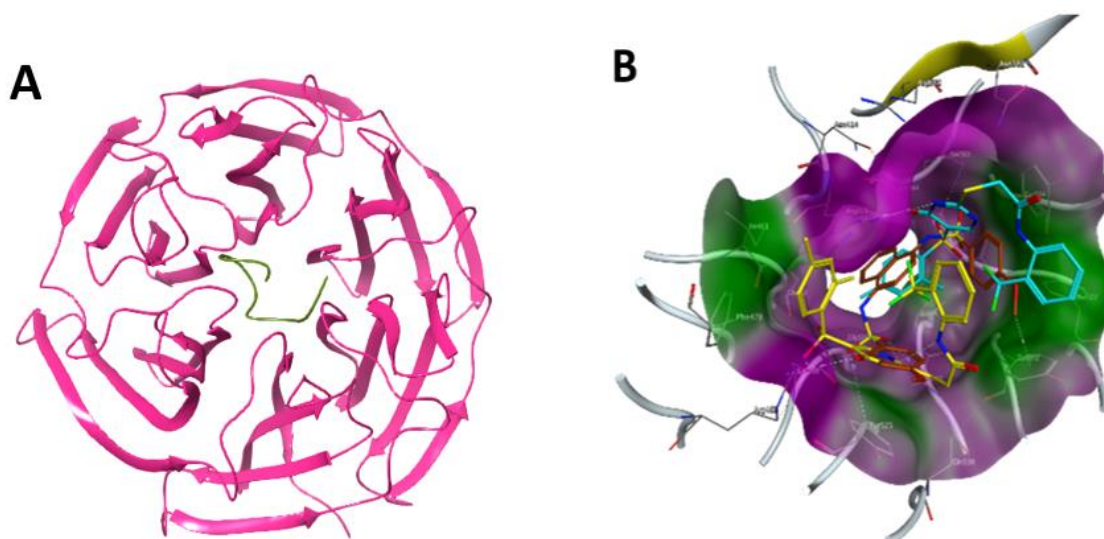
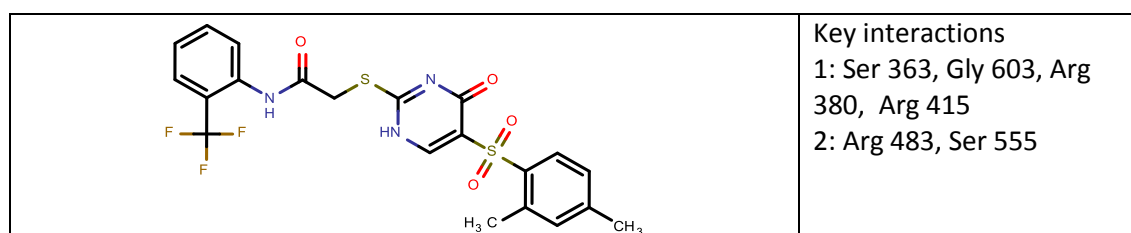


Figure 2.10. Nrf2-Keap1 protein-protein interface. A. Nrf2 peptide LDEETGEFL from the Neh2 region in green and Keap1 protein in pink from 1X2R structure. B. Keap1-Nrf2 binding pocket with surface with Nrf2 like-loop of known structures Cpd15 (yellow and cyan) and Cpd16 (red) from PBD 4IN4 and 4IQK. Surface in green is hydrophobic, purple is hydrophilic and white/grey is neither. Structures generated by Maestro Schrödinger 11.1 (Maestro, Schrödinger, LLC, New York, NY, 2017).

Table 2.2. Keap1/Nrf2 crystal structures used for modelling.

PDB ID	Resolution (Å)	Comments	Reference
1U6D	1.85	<i>Apo</i> of human Keap1	(Li X. et al. 2004)
1ZGK	1.35	<i>Apo</i> of human Keap1	(Beamer et al. 2005)
1X2J	1.60	<i>Apo</i> of mouse Keap1	(Padmanabhan et al. 2006)
1X2R	1.70	Mouse Keap1 with Neh2-ETGE peptide	(Padmanabhan et al. 2006)
2DYH	1.90	Mouse Keap1 with Neh2-DLG peptide	(Tong et al. 2007)
2Z32	2.00	Mouse Keap1 in complex with ProTalpha	(Padmanabhan et al., 2008)
3ADE	2.80	Mouse Keap1 with Sequestosome-1	(Komatsu et al. 2010)
3VNG	2.10	Human <i>holo</i> Keap1 with small molecule	(Satoh et al. 2015)
3VNH	2.10	Human <i>holo</i> Keap1 with small molecule	(Satoh et al. 2015)
3ZGD	1.98	<i>Apo</i> of human Keap1	(Hörrer et al. 2013)
4IN4	2.59	Human Keap1 in complex with Cpd 15	(Marcotte <i>et al.</i> , 2013)
4IQK	1.97	Human Keap1 in complex with Cpd 16	(Marcotte <i>et al.</i> , 2013)
3WDZ	2.60	Mouse Keap1 in complex with p62	(Ichimura et al. 2013)
4IFL	1.80	<i>Apo</i> of human Keap1	(Pan et al. 2012)
4IFN	2.40	Human <i>holo</i> Keap1 with peptide	(Pan et al. 2012)
3WN7	1.57	Mouse Keap1 with Nrf2-DLG region	(Fukutomi et al. 2014)

Sixteen structures were used for modelling. 3ZGC (Hörrer et al. 2013) structure was not used due to mutations with the crystal contacts with Nrf2 for blocking binding interactions. 2FLU (Lo et al. 2006) structure was not used because there were already enough crystals structures for virtual screening.



4IFN: Keap1 in complex with compound (Pan et al. 2012).

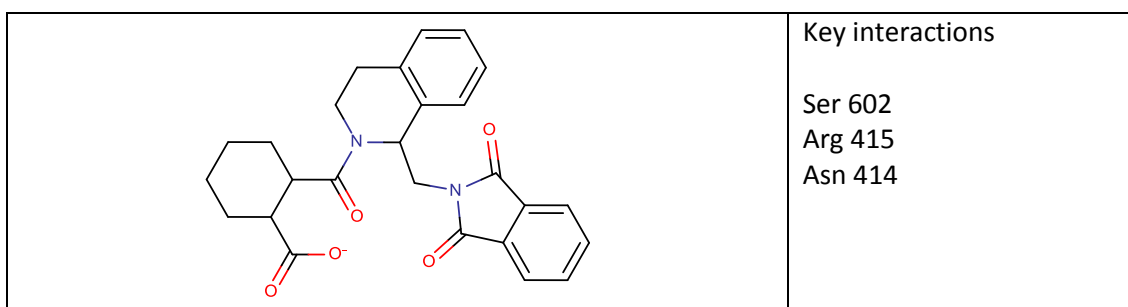


Diagram and results generated by Dr. Ben Wahab and modified for the purposes this thesis.

Part of the pocket analysis was to study the conserved water molecules involved in the binding pocket, with a total of fifteen conserved molecules around the binding space and four under the pocket (Appendix I). Conserved water molecules are believed to be important for binding interactions between both proteins. A set of 22 pharmacophores were designed around the known interactions from the documented binders with each pharmacophore having at least three features of the binding pocket (pharmacophore list in detail generated by Dr. Ben Wahab in Appendix I).

1.8 million compounds from the SUNScreen internal database were pre-screened with the designed pharmacophores using the Molecular Operating Environment (MOE) software. This pre-screening identified 1901 unique hits, from which 1,000 were docked into the 1X2R structure using MOE. The compounds were filtered by structural and physicochemical criteria and 250 compounds were analysed for medicinal chemistry appraisal. A total of 122 compounds were purchased from preferred suppliers for testing (Fig. 2.11).

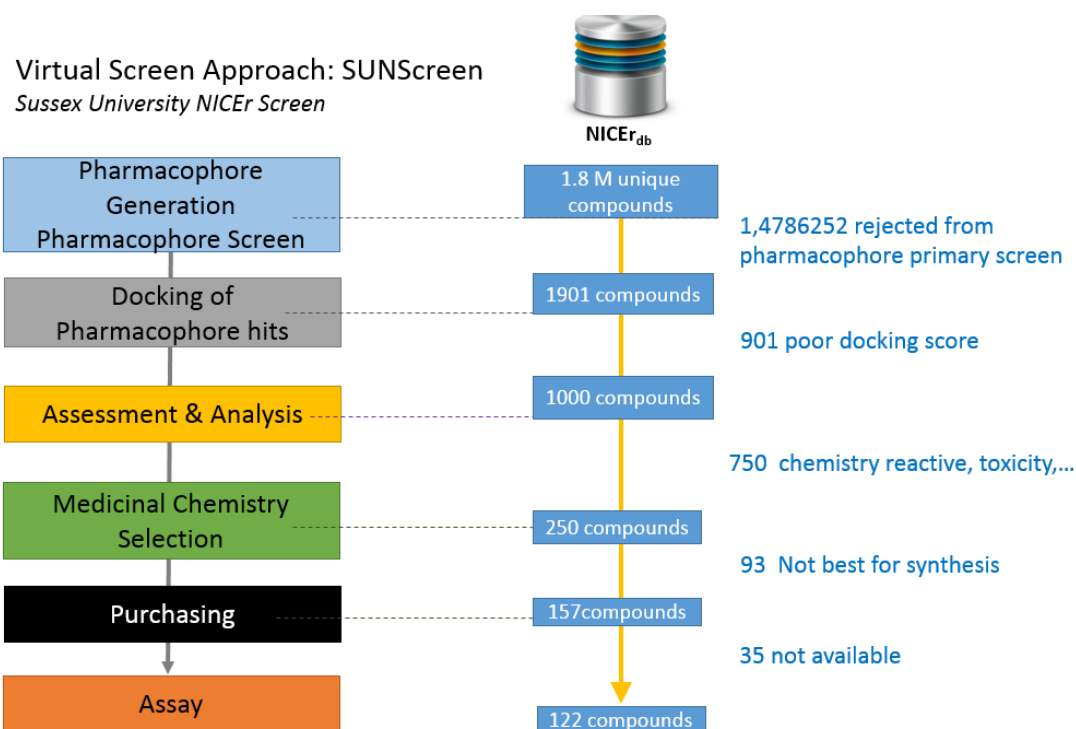


Figure 2.11. Summary of the virtual screening strategy. SUNScreen is the Sussex University NICEr database of materials from reliable preferred suppliers, filtered by structural and physicochemical criteria. 1.8 million compounds were subjected to pharmacophore screening, resulting in 1901 unique hits that were subjected to docking analysis based on a score system that measured the energy of the binding, surface dynamic, impact of the pocket, etc. Next steps included assessment and analysis to filter compounds by structural and physicochemical criteria. The medicinal chemistry appraisal was used to select the compounds with best features for design and synthesis of compounds. Finally 122 compounds were purchased for screening assay (35 compounds were not available).

2.4.2.2 NRF2 ENZYME FRAGMENT COMPLEMENTATION ASSAY

The assay is based on enzyme fragment complementation technology (from DiscoverX, PathHunter). In this approach, the complementing fragments of β -galactosidase are expressed in different compartments of stably transfected U2OS cells (Fig. 2.12). Upon nuclear translocation of the Nrf2 from the cytosol within the cells, the two β -gal fragments complement forming a functional enzyme that hydrolyses substrate and generate a chemiluminescent signal.

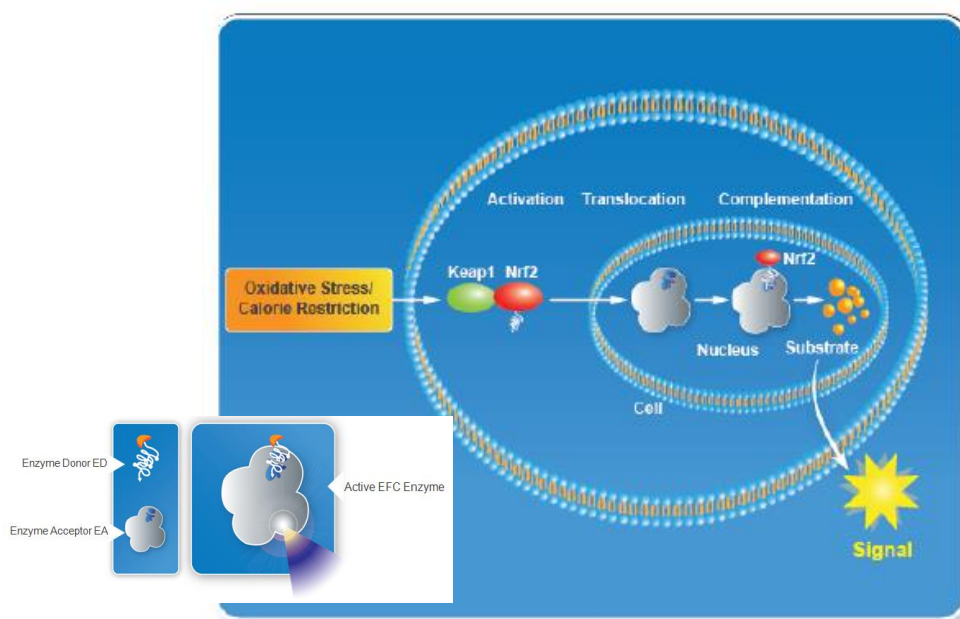


Figure 2.12. PathHunter Nrf2 nuclear translocation assay mechanism. A small inactive fragment of β -gal (enzyme donor, ED) was fused into the Nrf2 protein in U2OS cells. Another inactive fragment termed enzyme acceptor (EA) is located in the nucleus. Nrf2 dissociation from Keap1 results in Nrf2 nuclear translocation and complementation of both β -gal fragments (ED+EA), forming a functional enzyme. Enzyme activity is then quantitatively detected as chemiluminescent signal (active substrate).



Figure 2.13. Summary strategy followed for compound characterisation methodology. Single point assay compound hits were followed up by measuring EC_{50} in a biological assay, then verification of cellular viability and ROS generation to finally characterise the Nrf2 nuclear expression by western blotting.

2.4.2.2.1 ASSAY DEVELOPMENT

U2OS cells were harvested from a T75 flask and seeded into a 384-well microplate (final concentration of 5,000 cells per well) and incubated overnight at 37°C in 5% CO₂. Next day a series of ten 3-fold serial dilutions of sulforaphane in dimethyl sulfoxide (DMSO) were prepared, final top concentration of 5 µM in a 96-well plate. The concentration of each dilution was prepared at 5X the final screening concentration (5 µl compound + 20 µl of cells). The same procedure was followed for control wells PBS/DMSO. 5 µl of sulforaphane (5X) was transferred into the 384-well microplate (cells) and incubated for 90 minutes at 37°C in 5% CO₂, following the addition of detection reagent (12 µl) to each well, for a final well volume of 37µl. Plates were then incubated at room temperature in the dark for 1 hour after which luminescence was read using the plate reader Pherastar FS from BMG Labtech (Optic module LUM plus, Gain 3600 and optic used measurements from top).

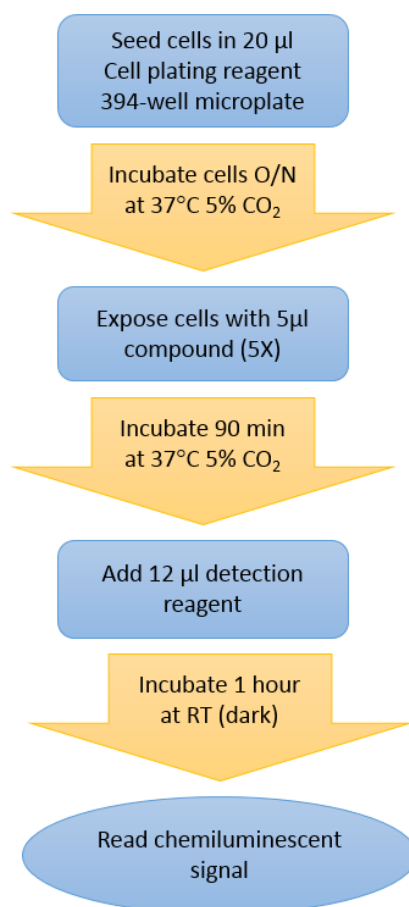


Figure 2.14. General procedure of the PathHunter kit for assay development and screening compound.

DMSO Tolerance

Dimethyl sulfoxide (DMSO) is used as a solvent to solubilise and dilute compounds that are difficult to dissolve in water or other assay buffers. Solvents can affect the assay performance, thus a DMSO tolerance curve was performed to ensure cell tolerance to DMSO. The cellular assay was tested at different concentrations of DMSO: 0.03%, 0.1%, 0.3%, 0.7%, 1.0% and 2.0%.

Incubation Conditions

To validate the assay different incubation conditions were tested. The incubation of cells exposed with compounds was tested at two different temperatures: room temperature and 37°C. In order to observe the optimal incubation time the luminescence signal was read every hour up to 6 hours. A control of DMSO/PBS was performed to observe the basal values.

2.4.2.2.2 ASSAY VALIDATION (LITERATURE COMPOUNDS)

U2OS cells were harvested from a T75 flask and seeded into a 384-well microplate (final concentration of 5,000 cells per well) and incubated overnight at 37°C in 5% CO₂. The next day a 96-well plate with compounds and controls was prepared, the compounds were tested in a final maximal concentration of 30 µM (for single point experiments) and 88 µM (for assay experiments, EC₅₀ determination, compound concentration was determined by the maximum of DMSO allowed in the assay) diluted in DMSO, final DMSO concentration 0.3% and 1% respectively. Sulforaphane was included in each plate as a positive control. 5 µl of testing compound (5X) was transferred into the 384-well microplate (cells) and incubated for 90 minutes at 37°C in 5% CO₂, following which detection reagent (12 µl) was added to each well. Plates were then incubated at room temperature in the dark for 1 hour after which luminescence was read using a BMG Pherastar FS reader.

2.4.2.2.3 COMPOUND SCREENING

A library of 122 compounds were screened for activity on Nrf2 nuclear translocation, using the PathHunter Keap1-Nrf2 assay (DiscoverX). The compounds were prepared in stocks of 10 mM with DMSO. From the compound library, the compounds were screened for single point detection at 30 μ M final concentration (0.3% DMSO). Sulforaphane at 5 μ M and DMSO/PBS at 0.3% were used as positive and negative controls respectively.

After the detection of hit compounds from single point assay, an EC₅₀ assay was performed using a FluidX Xpp-721 robot for compound addition. The compounds were tested with a series of ten 1:3 serial dilutions in DMSO, top concentration of 88 μ M this maintained the DMSO percentage in 1%, as recommended by the assay supplier.

384-well assay plate map format for FluidX Xpp-721 robot:

	1	2	3	4	5	6	7	8	9	10	11	12	13	14	15	16	17	18	19	20	21	22	23	24
A	Control - DMSO																							Control + Sulfora- phane
B			1	2	1	2	1	2	1	2	1	2	1	2	1	2	1	2	1	2	1	2		
C																								
D			3	4	3	4	3	4	3	4	3	4	3	4	3	4	3	4	3	4	3	4		
E			5	6	5	6	5	6	5	6	5	6	5	6	5	6	5	6	5	6	5	6		
F																								Control - DMSO
G																								
H			7	8	7	8	7	8	7	8	7	8	7	8	7	8	7	8	7	8	7	8		
I																								
J			9	10	9	10	9	10	9	10	9	10	9	10	9	10	9	10	9	10	9	10		
K																								Control + Sulfora- phane
L			11	12	11	12	11	12	11	12	11	12	11	12	11	12	11	12	11	12	11	12		
M																								
N			13	14	13	14	13	14	13	14	13	14	13	14	13	14	13	14	13	14	13	14		
O																								
P			15	16	15	16	15	16	15	16	15	16	15	16	15	16	15	16	15	16	15	16		

Numbers indicate each different compound, for example all wells in number 1 corresponding to the same compound in different serial dilutions.

2.4.2.3 VIABILITY ASSAY

Compounds that were active in the EC₅₀ assay were assayed to ensure they were not toxic in cells. To confirm the toxicity of the compounds, an ATP viability assay (CellTiter-Glo® Luminescent cell viability assay, Promega) was performed. The assay measures the viable cells in culture based on the quantitation of the ATP in the cells by adding a single reagent that causes the formation of oxyluciferin and a luminescent signal (luciferase reaction) in the presence of ATP from viable cells (Fig. 2.15).

U2OS Nrf2 cells were seeded into a 384-well plate, compounds at 88 µM were added and incubated for 2 hours at 37°C, 5% CO₂. The cells were then equilibrated at room temperature for 30 min. CellTiter-Glo reagent was added (25 µl) and incubated for 10 minutes at room temperature. The ATP concentration was detected as relative light units (RLU) using a luminometer reader.

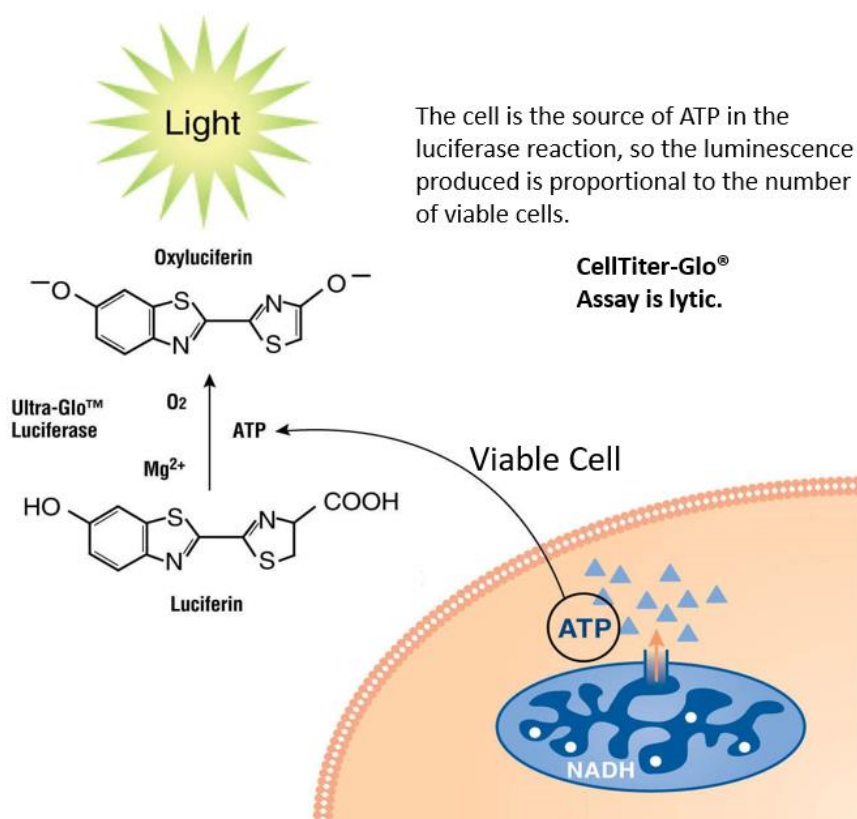


Figure 2.15. CellTiter-Glo® luminescent cell viability assay principle. Viable cells generated ATP, upon lysis of cells, mono-oxygenation reaction of luciferin is catalysed by luciferase recombinant reagent with the help of ATP, Mg²⁺ and O₂. (Figure adapted from <https://www.promega.co.uk/-/media/images/resources/figures/9100-9199/9155ma-mod.jpg>).

2.4.2.4 DETECTION OF REACTIVE OXYGEN SPECIES (ROS)

In order to confirm if the compounds were non-specifically disrupting the protein-protein interaction the production of free radicals was measured. If compounds are highly reactive and react with the cysteine residues of Keap1 it will produce a large amount of free radicals, suggesting that the activation of Nrf2 pathway is non-specific. Consequently, the ROS-Glo™ H₂O₂ Assay from Promega was used to measure the levels of H₂O₂ directly in U2OS cell culture.

5,000 U2OS Nrf2 cells in 20 µl were seeded into 384-well plates. The compounds, sulforaphane and Menadione (a free radical generator that induced cell death was recommended by supplier Cat. No. M5625, Sigma Aldrich) controls in combination with the H₂O₂ substrate solution (20 µl) were added and incubated for 2 hours at 37°C, 5% CO₂. A volume of 40 µl of ROS-Glo detection solution was then added and left at room temperature for 20 minutes to equilibrate the plate. The luminescence signal was then detected using a BMG Pherastar FS reader.

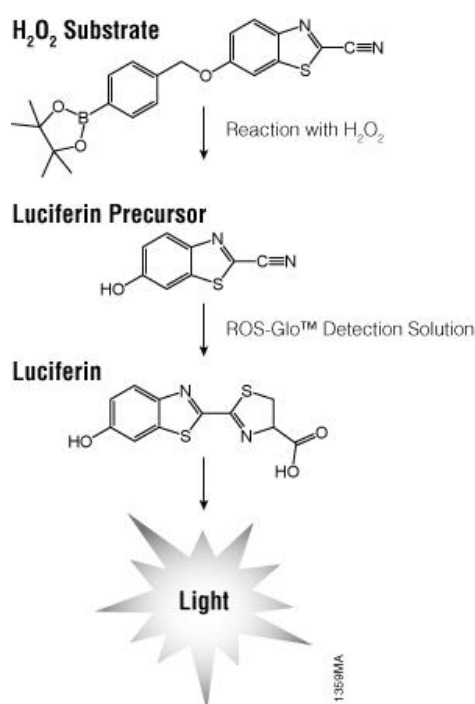


Figure 2.16. Ros-Glo H₂O₂ assay reaction. Luciferin H₂O₂ substrate incubated with sample reacts directly with H₂O₂ to generate a luciferin precursor. After the addition of a second reagent with recombinant luciferase, ATP and D-cysteine, the precursor is converted to luciferin to produce a light signal. The signal is proportional to the levels of H₂O₂ in the sample.

2.4.2.5 COMPOUND CHARACTERISATION

2.4.2.5.1 CELL CULTURE

U2OS-Nrf2, U2OS WT and HEK293 cells were cultured as a monolayer using Dulbecco's modified eagle medium (Life Technologies, Gibco™) supplemented with 10% fetal bovine serum (Life Technologies, Gibco™) and 5% penicillin-streptomycin (Life Technologies, Gibco™) at 37°C and 5% CO₂.

2.4.2.5.2 CELL FRACTIONATION

The cells were cultured for 3 days in T75 flasks, then washed with PBS and harvested with trypsin. Cells were pelleted by centrifugation (500g for 3 min) and the pellet was washed 3x with PBS, and then resuspended in 300µl of lysis buffer (20 mM Tris-HCl, 101 mM NaCl, 1 mM EDTA, 0.5% Triton X-100, protease and phosphatase inhibitor cocktail, Roche). After incubation on ice for 15 min, with vortexing every five minutes, cells were centrifuged at 1,000g for 10 min. Supernatants (cytosolic extract) were collected and nuclear pellet was washed 3x with PBS and resuspended in 50µl of lysis buffer. The nuclear fraction was sonicated for 30s (Sonics, Vibra cell sonicator). The protein levels in both fractions were quantified using the Bicinchoninic acid protein (BCA) assay kit from Sigma-Aldrich. Both the supernatant (cytosol) and pellet (membrane and nuclei) fractions were used for Western blot analysis to measure the levels of Nrf2 protein expression.

2.4.2.5.3 WESTERN BLOTTING

The cellular fractions were diluted with 10 µl of SDS sample buffer. 30-60 µg of protein content were separated using SDS-PAGE gel (NUPAGE 4-12%, 140V for 1 hour) and transferred onto a PVDF membrane (Amersham Hybond™-P 0.45, Cat. No.10600023, GE). The membrane was blocked overnight with 5% non-fat dry milk in PBST at 4°C. The membrane was then probed with primary antibodies* overnight at 4°C. The next day the membrane was washed 1x15 minutes and 3x5 minutes with PBST and then incubated with HRP secondary antibody for 45 minutes at room temperature. Blots were washed 1x15 minutes and 3x5 minutes with PBST, and then developed using a Pierce ECL detection reagent and exposed to X-ray film (CL-Xposure film, Cat. No. 34089 Thermo Scientific).

The Nrf2 protein has a predicted molecular weight of 68 kDa; the Nrf2 antibody was validated from supplier Abcam to detect a band of approximately 110 kDa in western blot experiments (<http://www.abcam.com/nrf2-antibody-ab137550.html>). The antibody had been used for detecting Nrf2 protein in western blot experiments in published literature (Yamashita et al. 2014; Grootaert et al. 2015; Yamada et al. 2016 & Sun et al. 2017).

*The following antibodies were used:

Primary antibodies

Antibody	Type	Dilution	Supplier	Cat. No.
Nrf2	Rabbit polyclonal	1:1000	Abcam	ab137550
GAPDH	Mouse monoclonal	0.5µg/ml	Novus biological	NB600-502SS
H2B	Rabbit polyclonal	1:10,000	Abcam	ab1790

Secondary antibodies

Antibody	Type	Dilution	Supplier	Cat. No.
HRP-Ab	Anti-rabbit IgG	1:30,000	GE Healthcare Life Sciences	NA934
HRP-Ab	Anti-mouse IgG	1:10,000	Dako	P0260

2.5 RESULTS

2.5.1 NRF2 ENZYME FRAGMENT COMPLEMENTATION ASSAY

2.5.1.1 ASSAY DEVELOPMENT

In the Nrf2 cellular assay sulforaphane was used as a control because it is well known that sulforaphane induces the nuclear translocation of Nrf2 by reacting with the cysteine residues of Keap1. The general methodology recommended by the supplier was performed. Hence, sulforaphane was added into cells at 5 μ M (3-fold serial concentrations) with 0.3% of DMSO. As shown in Fig. 2.17, increase of sulforaphane concentration results in a proportional increase of chemiluminescent signal, indicating the nuclear translocation of Nrf2 by this compound. EC₅₀ of 400 nM was obtained, similar to the manufacturer's value of 506 nM (from supplier validation results, DiscoverRx). Control wells with PBS/DMSO gave a baseline in the graph.

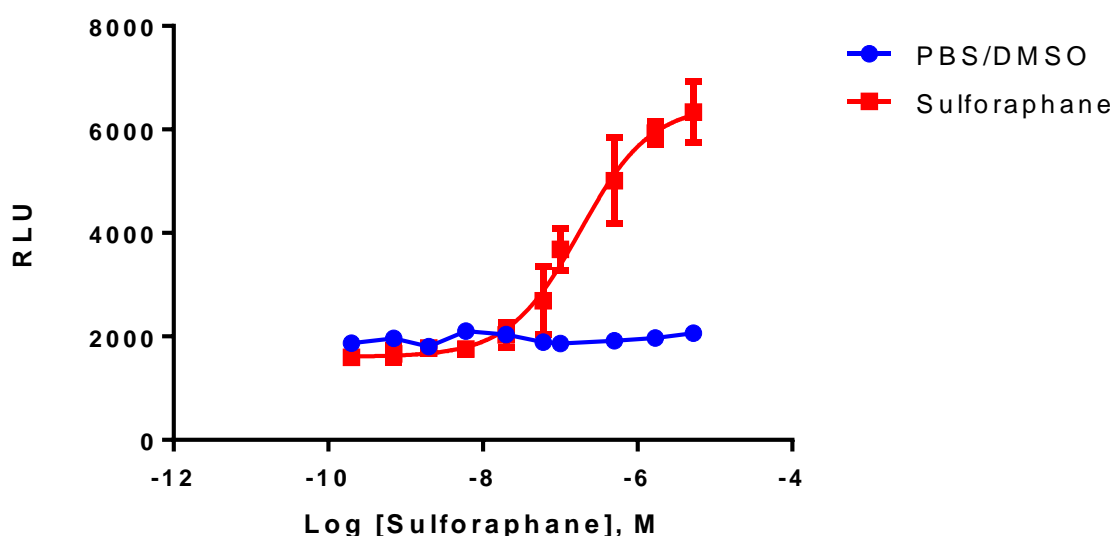


Figure 2.17. Effect of DL-Sulforaphane on Nrf2 nuclear translocation in the U2OS Nrf2 assay. Sulforaphane tested at a maximal concentration of 5 μ M gave an EC₅₀ of 400 nM. Error bars represent the mean \pm SD of n=3 individual experiments performed within one week. Signal-to-noise ratio S/N = 3.28, in which S is the average of the higher values and N is the average of the control values (PBS/DMSO). Experiments performed at 37°C for 90 minutes and DMSO final concentration of 0.3%. Y-axis in relative luminescence units (RLU) and X-axis is the concentration of compound in molar units.

DMSO Tolerance

Different percentages of DMSO in the assay were tested, the results are the following:

DMSO %	Average EC_{50} (nM)	S/N
0.03 %	570.5	4.0
0.1 %	385.6	4.4
0.3 %	450.6	3.9
0.7 %	415.5	3.8
1.0 %	376.6	4.0
2.0 %	596.8	4.3

The EC_{50} values and signal-to-noise ratios were similar at different DMSO percentages. The assay demonstrated good tolerance up to 2.0 % of DMSO, indicating that compounds can be dispensed at 2% DMSO with a final assay concentration of 200 μ M. Percentage of DMSO is the final concentration in the assay. The potency of sulforaphane was slightly higher with 1.0% this could be for the better solubility of the compound in the solvent.

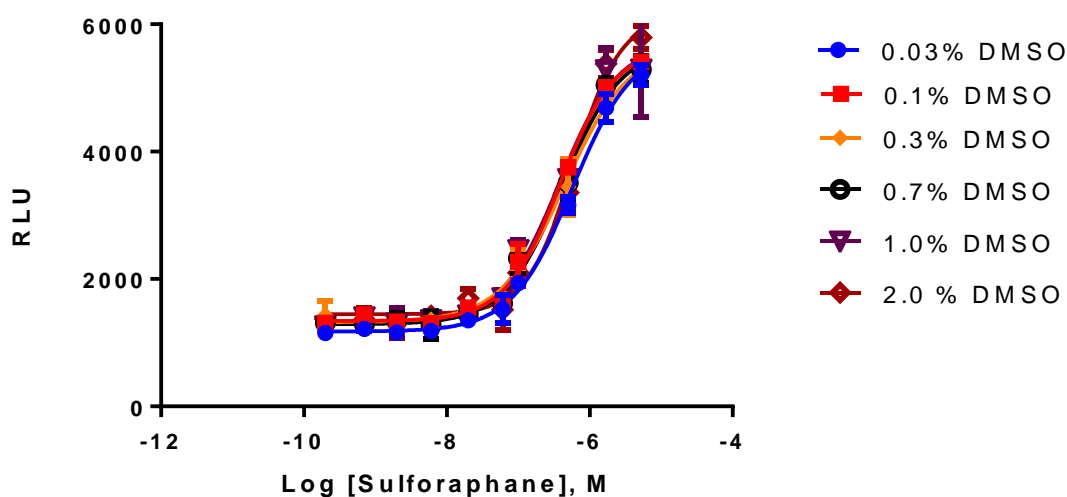
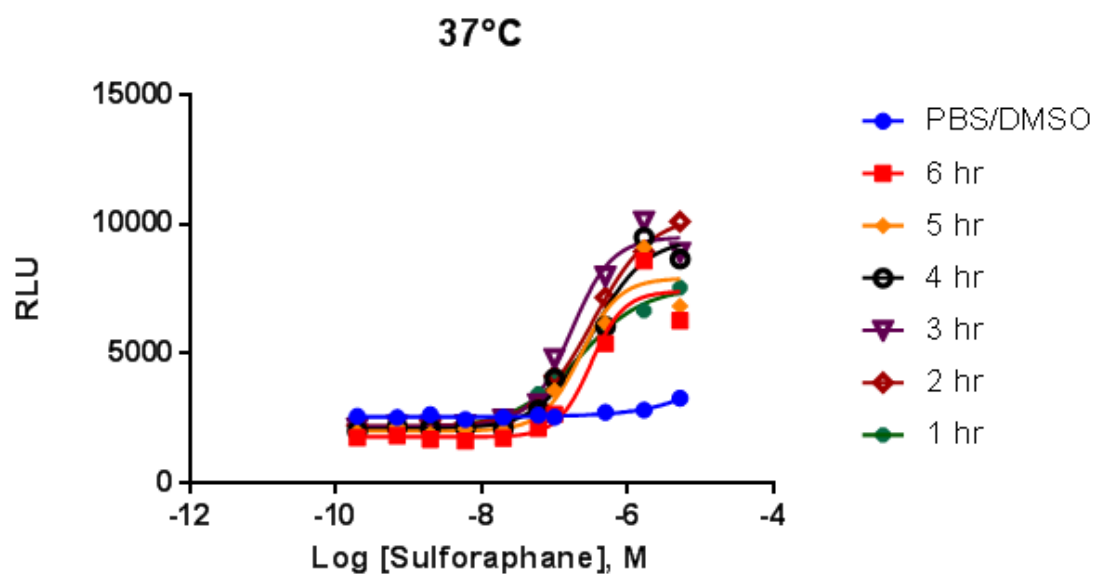


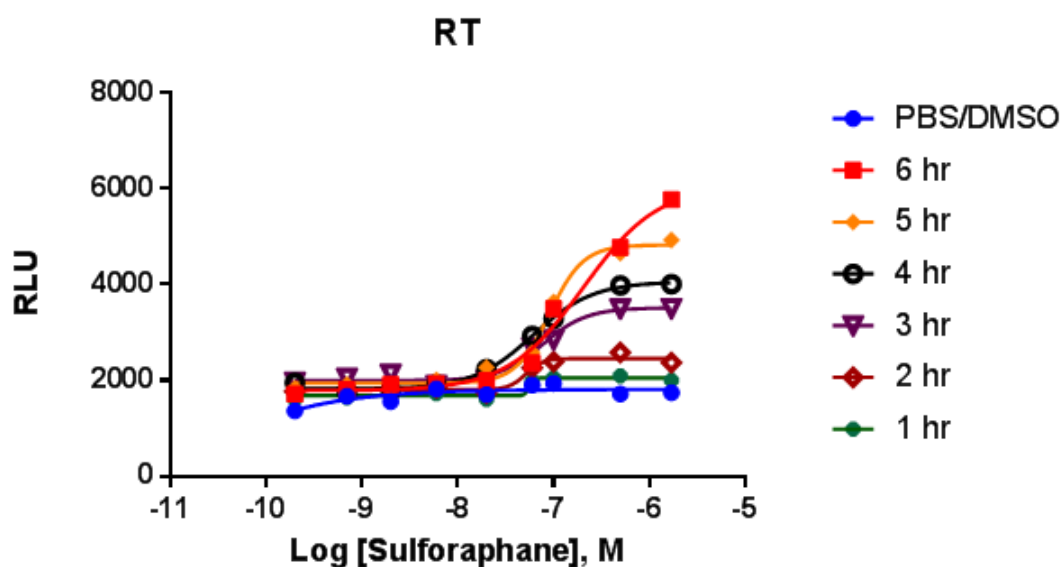
Figure 2.18. DMSO tolerance curve. Sulforaphane tested at different concentrations of DMSO. Error bars (SD) represent the mean \pm SD of $n=3$ individual experiments. S/N was calculated with the average of the higher and lower values. Experiments performed at 37°C for 2 hours to test the maximal incubation time of 90 minutes. Y-axis in relative luminescence units (RLU) and X-axis is the concentration of compound in molar units.

Incubation Conditions

In order to obtain the optimal incubation time and temperature conditions for the test compounds, the signal and S/N from the control compound sulforaphane were compared at room temperature (RT) and 37°C. The plate was read every hour for 6 hours (Fig. 2.19). The optimal incubation time was 2 hours at 37°C, reaching the highest intensity with sulforaphane control and highest S/N value of 3.9. To summarize, the optimal conditions for the assay test with sulforaphane was to incubate plates at 37°C for 2 hours, followed by further incubation with the detection reagent for 1 hour at room temperature in the dark. With a range of final DMSO concentrating in the assay from 0.03% to 2.0%. These conditions will be used for the compound screening single point and EC₅₀.



Time (hr)	1	2	3	4	5	6
S/N	2.9	3.9	3.4	3.3	2.6	2.4



Time (hr)	1	2	3	4	5	6
S/N	1.1	1.3	2.0	2.3	2.9	3.4

Figure 2.19. Comparison of incubation times at 37°C vs RT at 6 hours with sulforaphane compound. Sulforaphane optimal EC_{50} value at room temperature was at 6 hours with 204.1 nM. The EC_{50} values at 37°C incubation for 6, 2 and 1 hour were 314.7 nM, 341.7 nM and 216.7 nM respectively. The S/N values are displayed in the table below the graphs. Y-axis in relative luminescence units (RLU) and X-axis is the concentration of compound in molar units, $n = 1$ experiment.

2.5.1.2 ASSAY VALIDATION (LITERATURE COMPOUNDS)

Previous studies (Kanno et al., 2012; Marcotte et al., 2013) using virtual screening and confirmed with luciferase cell assay, suggest that these novel small molecules disturb the protein-protein interaction between Keap1-Nrf2. Three such compounds were synthesised in-house and tested with the Nrf2 assay: N-(4-(2-pyridyl)(1,3-thiazol-2-yl))-2-(2,4,6-trimethylphenoxy) acetamide (CPN-9) (Kanno et al., 2012), and two benzene-disulfonamide compounds (Marcotte et al., 2013) named in-house as compound 13545 and 13546.

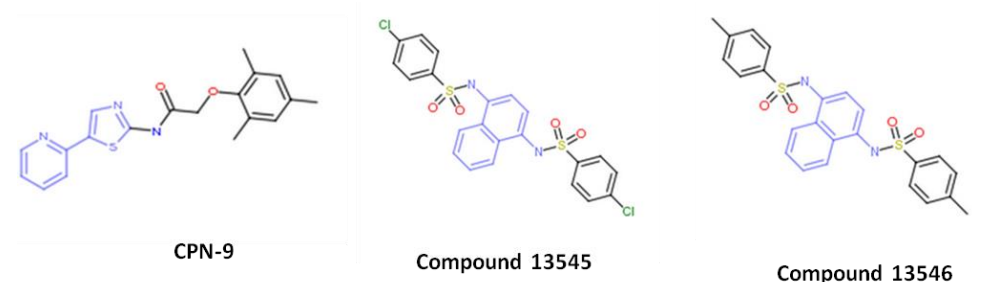


Figure 2.20. Chemical structure of literature compounds. Novel Nrf2 activators CPN-9 (Kanno et al. 2012), compounds 13545 and 13546 (Marcotte et al. 2013). These compounds have been shown to protect cells against oxidative stress and cell death *in vitro* experiments.

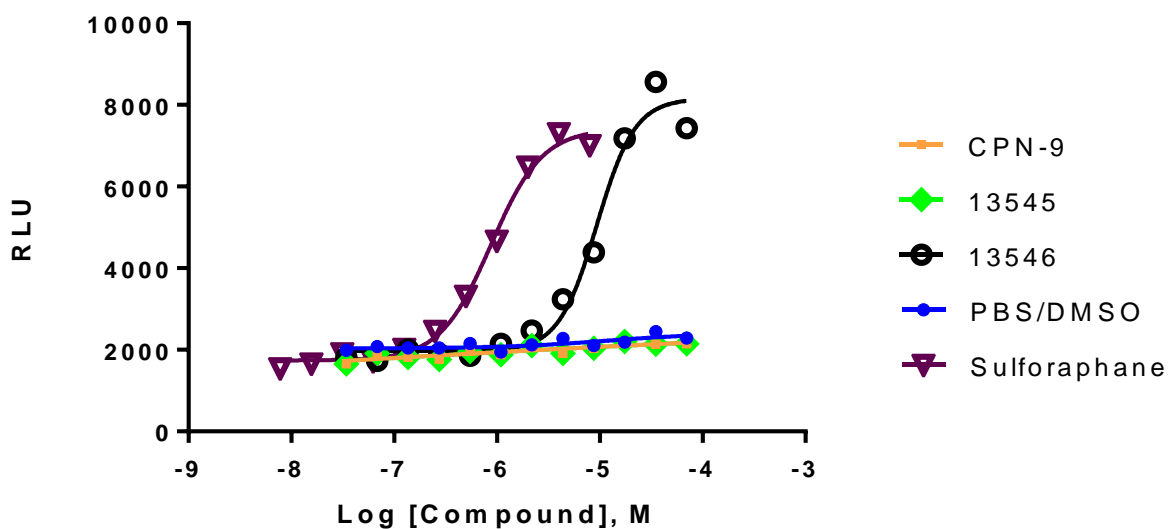


Figure 2.21. Activity of testing compounds by Nrf2 cellular assay. Cells U2OS were tested with each compound at maximum concentration of 70 μ M and sulforaphane at 8 μ M. Y-axis in relative luminescence units (RLU) and X-axis the concentration of compound in molar units, $n = 1$ experiment.

It was expected that the three compounds would give a high signal of Nrf2 induction. Only the compound 13546 produced Nrf2 translocation into the nucleus with an EC₅₀ of 9.4 µM (literature EC₅₀ of 2.7 µM) and the sulforaphane control of EC₅₀ 0.87 µM (Fig. 2.21).

2.5.1.3 COMPOUND SCREENING

122 compounds were screened in a single point assay of which 11 hit compounds were detected with at least 15% activity normalized relative to the sulforaphane control. EC₅₀ values were obtained to confirm the Nrf2 activity. From the 11 compounds only 5 compounds showed activity in the Nrf2 assay (Table 2.3, Fig. 2.23).

Table 2.3. Compounds with Nrf2 activity. Compounds that showed activity in the Nrf2 translocation assay, % normalised with sulforaphane control at 5 µM.

Compound	% activity
UOS-00014231-001	25 %
UOS-00014239-001	20 %
UOS-00014262-001	>100 %
UOS-00014265-001	15 %
UOS-00014266-001	40 %

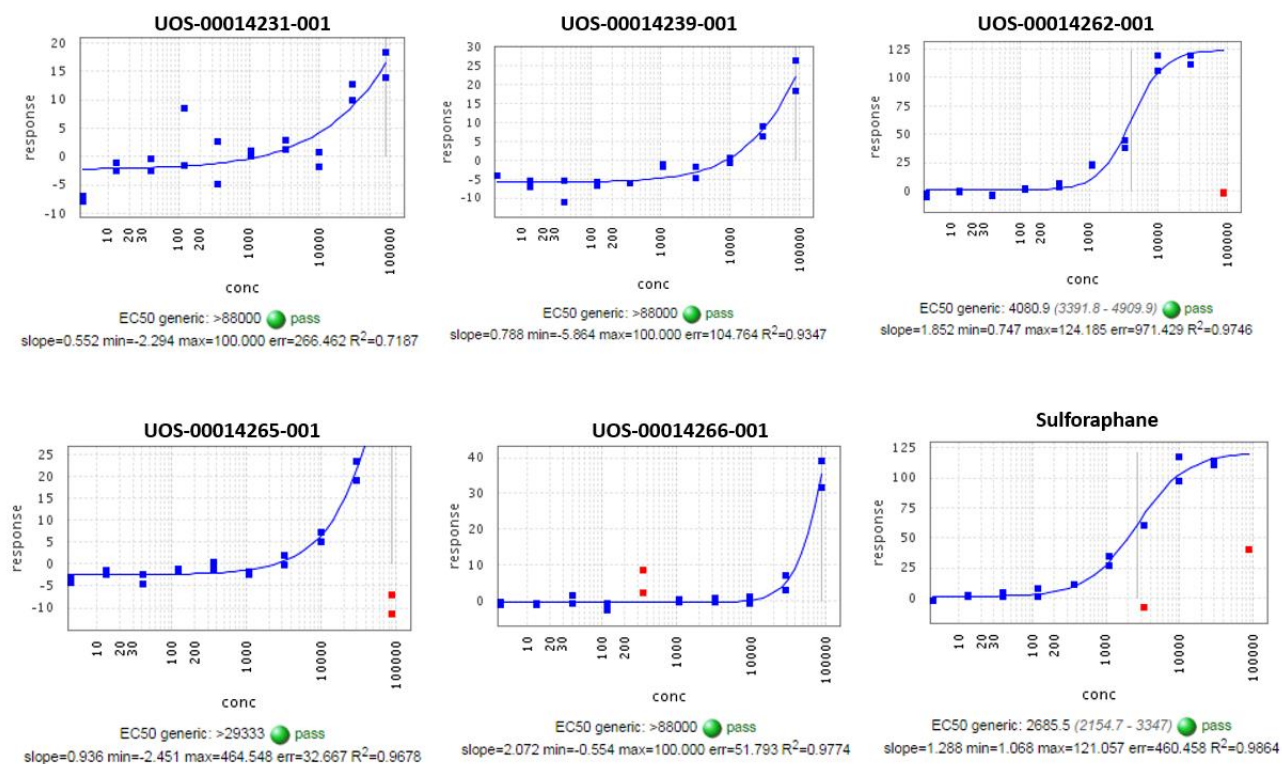


Figure 2.22. Compounds with a possible Keap1-Nrf2 activity. The compounds were tested with a final concentration of 88 μ M, using a sulforaphane control of 5 μ M. Data and graphs analysed with the Domatics Studies Notebook analysis package. Red dots are automatically excluded data points that are distant from the mean (error points, away from the standard deviation) generated by Domatics Studies. Y-axis is % of response normalized with control and X-axis is the concentration of compound in nanomolar, n = 2 experiments.

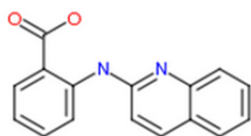
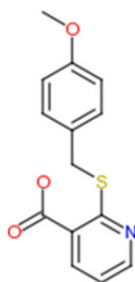
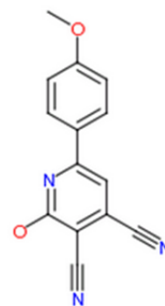
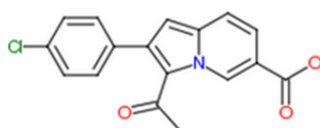
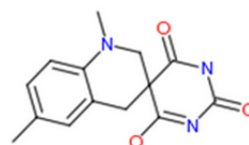
UOS-00014231-001**UOS-00014239-001****UOS-00014262-001****UOS-00014265-001****UOS-00014266-001**

Figure 2.23. Chemical structure of the hit compounds for Nrf2 activity.

2.5.2 VIABILITY ASSAY

The five novel compounds, plus the literature compound 13546 were not toxic to U2OS cells during a 2 hour exposure time. After 2 hours the cell viability decreases by only ~5% in all compounds and the control sulforaphane. This shows that the compounds are not toxic and do not cause cell death when incubated for 2 hours. Hydrogen peroxide (H_2O_2) is well known to induce cell death (Whittemore et al. 1995), for that reason it was used as a control in the viability assay. It was observed that higher concentration of H_2O_2 decrease significantly the concentration of ATP (Fig. 2.24) in cells indicating cell death and toxicity, the levels of ATP are directly proportional to the number of viable cells present in the well. The low concentrations of H_2O_2 displayed higher levels of RLU, the possible reason for this is that the dose-curve of H_2O_2 was performed in a different plate from the compounds, the number of cells might vary from plate to plate increasing the RLU detection.

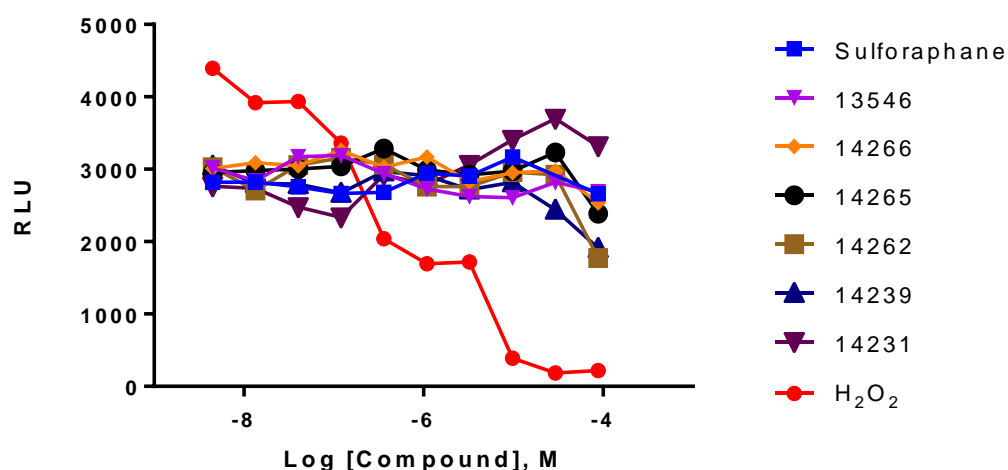


Figure 2.24. U2OS viability assay with test compounds. Compounds and control hydrogen peroxide were tested at 88 μM , 1:3 serial dilutions, $n = 1$ experiments. Plate incubated at 37°C for 2 hours. RLU is proportional to the concentration of ATP from cells, only hydrogen peroxide displayed a significant decrease of ATP in cells suggesting cell death.

2.5.3 DETECTION OF REACTIVE OXYGEN SPECIES (ROS)

As previously discussed, compounds with Nrf2 assay activity can either interact by specifically disrupting the protein-protein interaction or non-specifically by causing ROS, which results in a change in Keap1 conformation as a result of interacting with cysteine residues of Keap1 protein. The purpose of this experiment was to measure the generation of ROS by test compounds. If compounds increase ROS levels it suggests interaction with Keap1 cysteine residues.

The ROS-Glo H₂O₂ assay was used to measure the increase of ROS generated in cells, after 2 hours exposure of test compounds. Menadione was used as a control, since it is well known to induce reactive oxygen species and sulforaphane is well known to interact with Keap1 cysteine residues.

As can be seen in Fig. 2.25, the majority of the compounds induced reactive oxidant reagents as indicated by an increase in the luminescence signal. These results suggested that the compounds affect the Keap1-Nrf2 protein interaction by indirectly causing stress or reacting with the cysteine residues of Keap1, but not interacting at the protein-protein interface pocket. The compounds UOS-00014231 and UOS-00014239 showed a decrease in ROS, suggesting a possible Nrf2-Keap1 direct interaction. The decreasing level of ROS can be due to the production of antioxidants by the nuclear translocation of Nrf2. The next step was to observe the translocation activity of the compounds by western blot analysis.

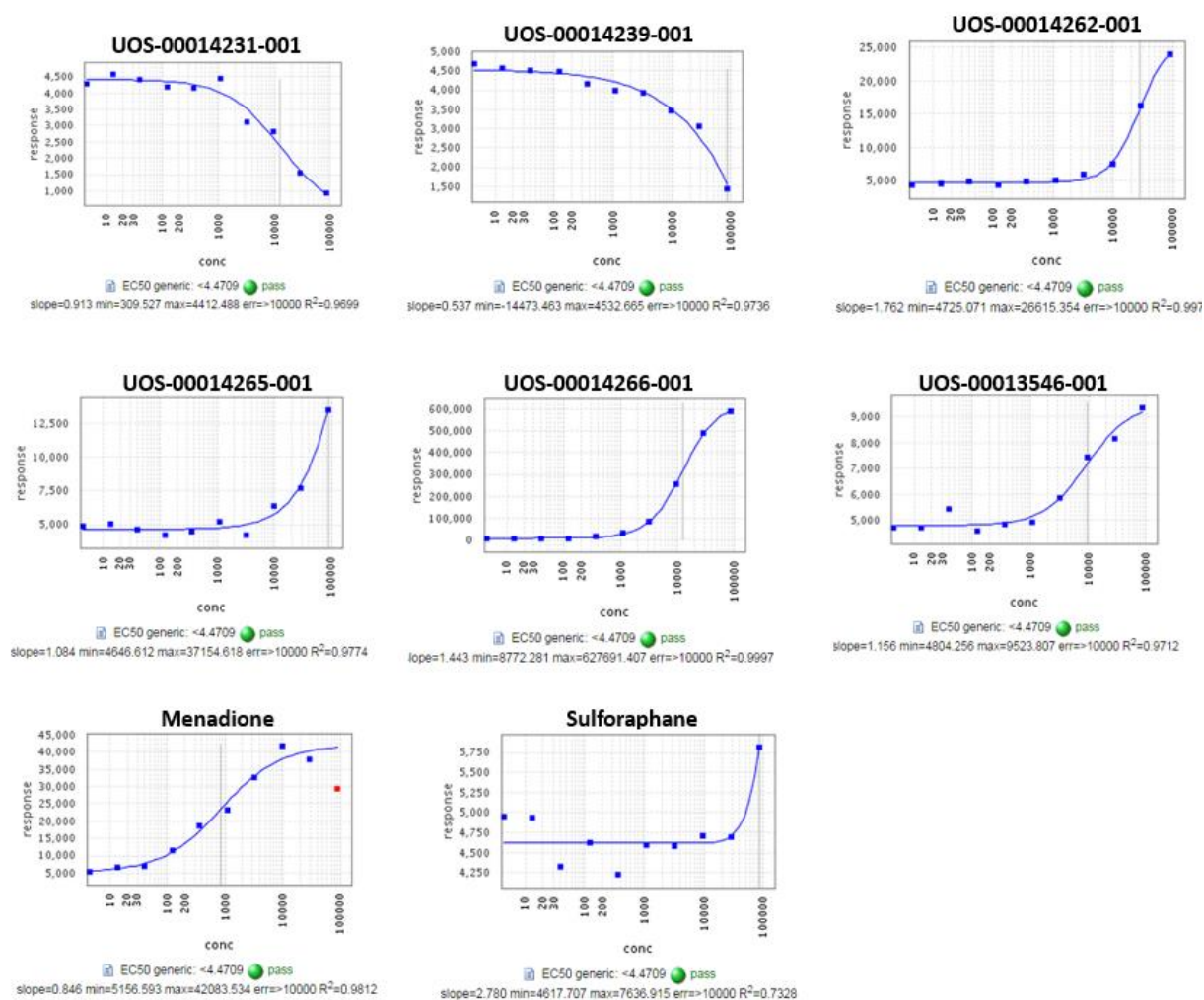


Figure 2.25. ROS induction in U2OS-Nrf2 cultured cells. The cells were treated with increasing concentrations of compounds with a maximum concentration of 88 μM . Controls: Menadione and Sulforaphane. The response values in the Y-axis correspond to the relative luminescence units (RLU) and X-axis correspond to the concentration of compound in nanomolar, $n=1$ experiments, red dots in the graph are being excluded automatically by the program. Data and graphs analysed with the Domatics Studies Notebook analysis package. The compounds displayed an increase in ROS generation, except compounds 14231 and 14239 that showed a reduction in ROS generation suggesting a regulated balance induced by Nrf2-ARE pathway activation.

2.5.3 WESTERN BLOT

2.5.3.1 NRF2 DETECTION IN WILD TYPE U2OS CELL LINE

In order to observe nuclear translocation of Nrf2, the effects of oxidative stress were studied in wild type (WT) U2OS cells. Sulforaphane has been shown to activate the Nrf2-Keap1 pathway and induce the phase II antioxidant genes (i.e. GSTs, NQO1, HO-1 and TXNRD1) by reacting with the cysteine residues of Keap1 protein (Bryan et al. 2013; Baird et al. 2014). Accordingly, sulforaphane was chosen as a positive control in U2OS for inducing the nuclear translocation of Nrf2. Sulforaphane has been tested in the literature at different concentration from 5-50 μ M in different cell lines such as, HEK-293, HeLA, COS1, MDA-MB-231 and CaCO2 (Traka et al. 2005; Juge et al. 2007; Kanematsu et al. 2010; Lau et al. 2013; Kemmerer et al. 2015; Ullah 2015). From the different concentrations tested in the literature it was decided to exposed U2OS cells with a high concentration of sulforaphane (40 μ M) to be able to observe an Nrf2 nuclear translocation induction. Nrf2 is predicted to display a band of ~65 kDa, however the antibody supplier (Abcam) and the literature had found evidence that the biological relevant species of Nrf2 migrates at ~110 kDa in a denaturing gel (SDS-PAGE) (Lau et al. 2013 & Grootaert et al. 2015). It had been suggested that in the nucleus Nrf2 is bound to ubiquitin so the molecular weight would be higher than cytoplasm, other suggested reasons are; post-translational modifications, splice variants and the relative charge of the composition of amino acids. Additionally, different commercially available antibodies were able to only detect a band of Nrf2 ~100 kDa, such as; NovusBio (NBP1-32822), Cell signaling technology (12721), Abcam (ab62352) and R&D systems (AF3925 & MAB3925). A comparison of commercially available Nrf2 antibodies in a 7.5% SDS-PAGE with sulforaphane treatment displays a band at ~100 and 72 kDa (Lau et al. 2013). In these experiments the Nrf2 protein band was also detected at ~100 kDa in the nuclear fractions.

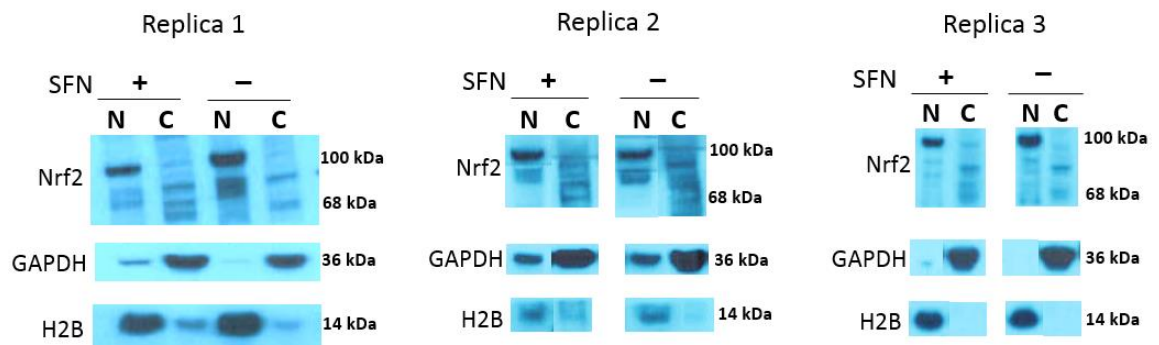


Figure 2.26. Wild type U2OS cells vs U2OS with sulforaphane treatment. U2OS cells were incubated with 40 μ M of sulforaphane (SFN) or 0.4% DMSO in PBS for 2 hours. Cell fractions were subjected to western blot analysis. The controls for the cytosolic and nuclear fractions were GAPDH and H2B respectively and were used to verify the differential centrifugation experiments. GAPDH is an enzyme that catalyses several steps of glycolysis in the cytosol of cells and is highly expressed in all cells; H2B is a histone involved in the chromatin production and is localised only in nuclear cells.

The differential centrifugation fractionation protocol worked since GAPDH and H2B were preferentially enriched in the correct cellular fractions (cytosolic and nuclear respectively). Increased translocation of Nrf2 from the cytoplasm to the nucleus was not observed in cells treated with sulforaphane, cytoplasmic Nrf2 was observed in relative low levels in the control conditions, indicating none or low levels of Nrf2 to translocate. This could be due to U2OS cells being a cancer cell line (osteosarcoma) and as a consequence alternative defence pathways against oxidative stress are highly upregulated. For example including those using oxidation resistance 1 protein (Oxr1; Oliver et al., 2011), heat shock proteins (Hsps; Jolly et al. 2000) or activating transcription factor 4 (ATF4; Lange et al., 2008) instead of activation of the Nrf2 pathway as evidenced by the similar Nrf2 nuclear protein levels in the treated and untreated cells (Fig. 2.26 & 2.27). The cytosolic fraction of Nrf2 was detectable but not in a higher intensity, therefore it was not possible to make a cytosolic quantification. These results indicate that untreated cells have slightly higher Nrf2 protein in the nucleus measured by densitometry relative to H2B control, however this is not significant compared to cells treated with sulforaphane (Fig. 2.27). Due to the cytosolic fraction not being completely detectable it was not possible to establish a measurement of the nuclear translocation of Nrf2.

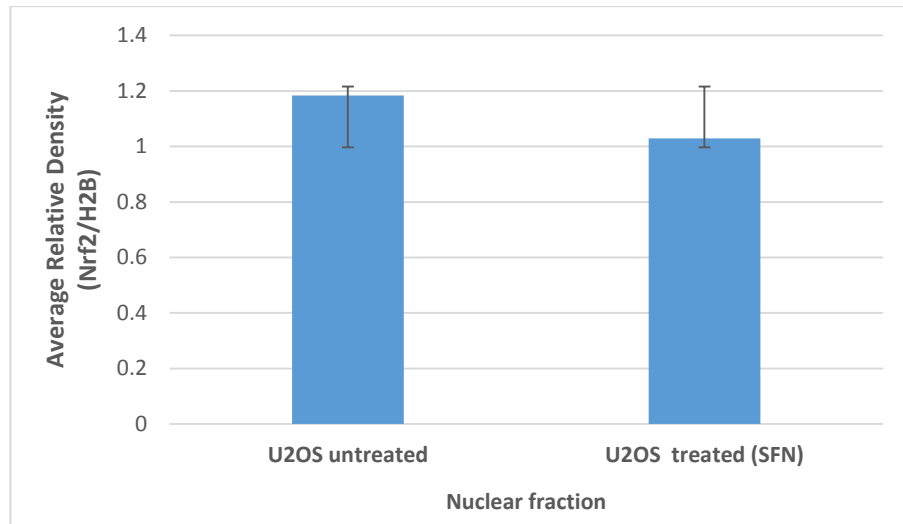


Figure 2.27. Densitometry analysis of Western Blot from U2OS cells with and without sulforaphane treatment. Cells were treated with sulforaphane or with control PBS/DMSO for two hours. Nrf2 levels were normalised against histone H2B antibody and quantified by densitometry with ImageJ. Three different gels were used for western blot and for densitometry analysis, the relative density was calculated using the H2B band relative to each sample to eliminate the effects of the different exposure times. Values are the mean \pm SD of three independent experiments.

2.5.3.2 NRF2 DETECTION IN U2OS-NRF2 CELL LINE (DISCOVERX)

The commercial kit PathHunter® U2OS Keap1-Nrf2 was used to analyse the Nrf2 nuclear translocation with 122 compounds from virtual screening (as described in compound screening section 2.4.2.2.3). The commercial cell line U2OS-Nrf2 was used to test selective compounds for western blot analysis. This cell line is engineered to co-express two enzyme fragments of β -galactosidase that in the presence of Nrf2 nuclear translocation will produce a detectable chemiluminescent signal. Therefore, it was important to examine Nrf2 protein in nuclear and cytosolic fractions when it is incubated with test compounds by western blotting.

The compounds tested for Nrf2 nuclear translocation for western blot, chemical structures in shown in Fig. 2.20 & 2.23:

- UOS-00014239-001
- UOS-00014231-001
- UOS-00013634-001 (CPN-9)
- UOS-00013546-001
- Sulforaphane (positive control)
- DMSO/PBS (control negative)

In this experiment it was decided to increase the concentration of sulforaphane from 40 μ M to 90 μ M to observe a more significant induction of Nrf2 expression as a control and exposure time in cells from 2 to 4 hours, incubation times similar to the literature (Sakao & Singh 2012; Zhuang et al. 2014). The purpose was to find compounds that disrupt Keap1-Nrf2 protein interaction and induce the nuclear translocation of Nrf2. Compounds 14239 and 14231 were selected based upon their respective EC_{50} values of ~ 0.469 M and $\sim 3.491 \times 10^{-5}$ M, viability assays and ROS-GLO assay. Compound 13634 is a novel small molecule (CPN-9) which has been reported to upregulate the Nrf2 pathway and increase the expression of antioxidants and phase II detoxification enzymes by inducing Nrf2 nuclear translocation (Kanno et al. 2012). Compound 13546 is a small compound closely related to a tested compound N,N'-1,4-naphthalenediylbis 4-methoxybenzenesulfonamide (named as compound Cpd16 in the literature), which was shown to interact with the cysteine residues in Keap1 and stimulates Nrf2 nuclear translocation (Marcotte et al. 2013). Sulforaphane was used as a positive control for Nrf2 nuclear translocation.

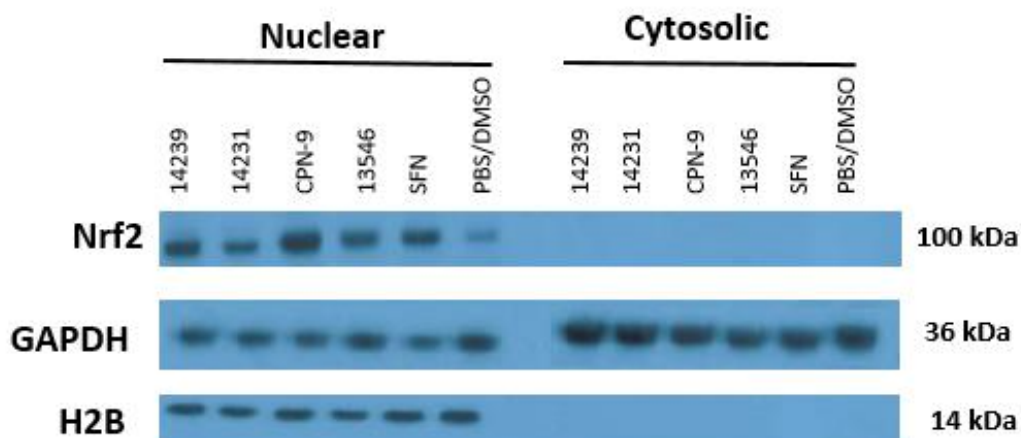


Figure 2.28. Nrf2 nuclear accumulation in U2OS-Nrf2 cells. Cells were treated with 90 μ M of test compounds for 4 hours. Nuclear and cytosolic fractions were subjected to western blot analysis. GAPDH and H2B antibodies were used as loading control and to verify the differential centrifugation experiments.

These results indicate that some compounds increase the levels of Nrf2 in the nuclear fraction compared to the control (Fig. 2.28), however Nrf2 protein was not observed in any of the cytosolic fractions. Nrf2 protein levels were enhanced with compounds 14239, CPN-9, 13546 and sulforaphane. It appears from these results that compound CPN-9 has a more pronounced effect on Nrf2 expression in the nuclear fraction. However, CPN-9 compound did not show nuclear translocation in the PathHunter Keap1-Nrf2 assay (Fig. 2.21), suggesting that CPN-9 might indirectly activate Nrf2 pathway, instead of interacting with Nrf2 and Keap1. For example, CPN-9 might induce the activation of Nrf2 by increasing kinases activity, however the mechanism of action between CPN-9 and Keap1-Nrf2 pathway is not known.

Nrf2 expression in cytosolic fraction could not be detected by this method. This might be due to a reduced level of protein expression in cytosolic fraction, making it more difficult to detect by western blot analysis. Similarly, studies in gastric cancer cell lines have showed only detectable levels of Nrf2 in the nucleus, suggesting that some cell lines express higher levels of Nrf2 in the nucleus depending on their antioxidant rate activity as part of a cancer cell line behaviour (Kawasaki et al. 2015).

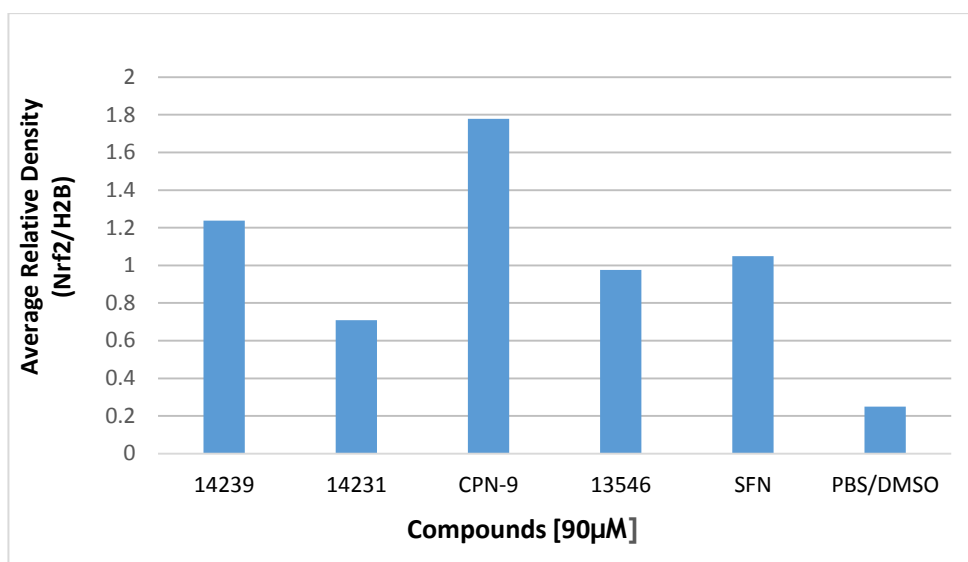


Figure 2.29. Nrf2 densitometry analysis of Western Blots from U2OS-Nrf2 cell line with test compounds. Nrf2 levels were normalised against histone H2B antibody and quantified by densitometry with ImageJ. For densitometry the relative density was calculated using the H2B band relative to each sample to eliminate the effects of the different exposure times. Values are the mean of two different cellular samples treated in separate individual experiments*.

*This cell line is part of a commercial kit assay, the use of which was limited to a specific period of time, there was not enough cells for a third repeat due to license expiration.

The densitometry analysis (Fig. 2.29) showed that CPN-9 compound has the most effect on nuclear expression of Nrf2, followed by 14239 and sulforaphane, however these results are not significant due to only having two replicas of the experiments. Therefore, these results suggest a higher Nrf2 expression on the nuclear fraction by compound CPN-9. Compound 14239 increased the expression of Nrf2 in the nuclear fraction compared to compound 14231, consequently, the next experiments were decided to be focused on the study of compound 14239 as a potential target for Nrf2 signalling.

2.5.3.3 NRF2 DETECTION IN HEK-293 CELL LINE

Since the results displayed no significant effect in the U2OS cells, it was sought to examine whether the compounds had an effect on Nrf2 nuclear translocation in an alternative cell line, HEK-293 again using sulforaphane, CPN-9, compound 14239, hydrogen peroxide and PBS/DMSO as control with western blot analysis. Human embryonic kidney (HEK)-293 cells were chosen because they are easy to grow and widely used for biology research. A study in this cell line using immunohistochemistry demonstrated Nrf2 expression and nuclear translocation with 5 μ M of sulforaphane treatment (Wen. et al. 2014). It was decided to verify the nuclear translocation of Nrf2 protein triggered by compound 14239. These results showed that test compounds failed to demonstrate an increased induction of Nrf2 nuclear translocation (Fig. 2.30). One possibility is the high viscosity of nuclear fractions for HEK-293 cells, this was reduced with sonication but it was still difficult to maintain equal protein content into the gel, H2B control was used as a loading control for this matter. The results using this cell line are more variable than U2OS cell lines. Therefore, the possibility of compound 14239 as a potential inducer of Nrf2 nuclear translocation cannot be dismissed. Cytosolic Nrf2 expression was not detectable in HEK-293 cells, consistent with previous experiments with the wild type U2OS and U2OS-Nrf2 (DiscoverRx) cell lines.

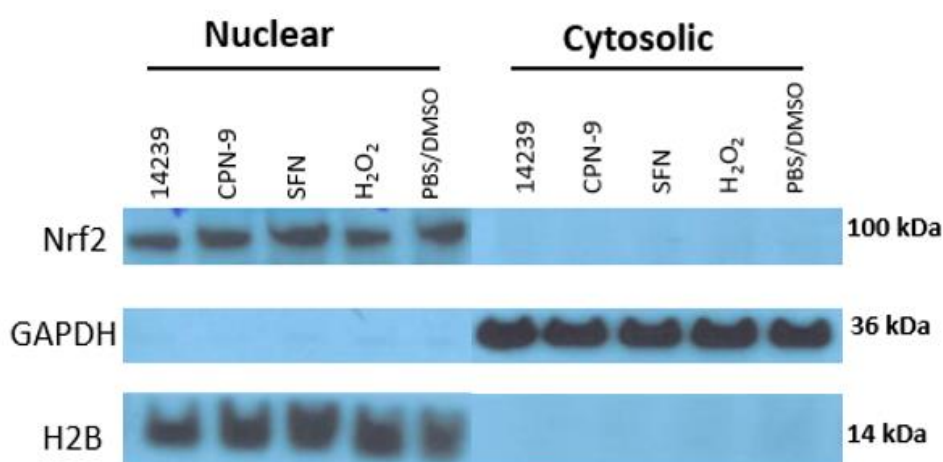


Figure 2.30. Effect of compounds on Nrf2 levels in HEK-293. Cells were treated with 90 μ M of compounds for 4 hours. Nuclear and cytosolic fractions were subjected to western blot analysis. GAPDH and H2B were used as loading and differential centrifugation controls.

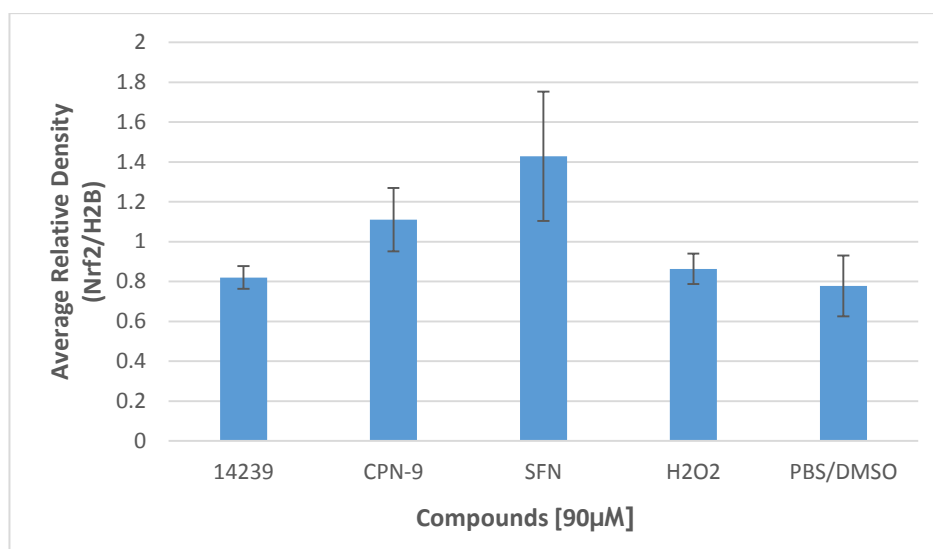


Figure 2.31. Densitometry analysis of Western Blot HEK-293 cell line with compounds. Nrf2 levels were normalised against histone H2B antibody and quantified by densitometry with ImageJ. Three different gels were used for western blot and for densitometry analysis the relative density was calculated using the H2B band relative to each sample to eliminate the effects of the different exposure times. Values are the mean \pm SD of 3 independent experiments.

Densitometry analysis of the western blot experiments (Fig.2.31) showed that sulforaphane slightly increased the Nrf2 in the nuclear fraction, however the control of PBS/DMSO showed similar levels of expression to H₂O₂ treatment. In conclusion, HEK-293 cell line western blot experiments failed to demonstrate an effect on Nrf2 by test compounds.

2.6 DISCUSSION

Structure-based virtual screening was used to identify compounds that disrupt the interaction of Keap1-Nrf2. The strategy was to use 16 of the 18 crystal structures of the protein data bank (PDB) that show the Keap-Nrf2 interaction interface, resolution of crystal structures from 1.35 Å to 2.80 Å. The other two structures 3ZGC (Hörrer et al. 2013) and 2FLU (Lo et al. 2006) were not used due to having mutations in the binding pocket and already having enough crystals structures for the virtual screening. From the crystal structures selected a pocket analysis was performed of Keap1 in complex with the N-terminal region of Nrf2 and other ligands (i.e., Cpd15, ProTalpha and p62; Table 2.2). Pharmacophore design was used with at least three features of the binding pocket for further docking analysis based on score system using MOE and medical chemical appraisal selection. The interface between the two proteins is relatively small, which is a challenge for compounds that can bind and disrupt the protein-protein interaction. The virtual screen (VS) approach was similar to other literature studies for identifying novel small inhibitors of the Keap1-Nrf2 protein-protein interaction (Kanno et al. 2012; Marcotte et al. 2013; Zhuang et al. 2014). Three compounds (CPN-9, Cpd16 and analogue) were tested in the Nrf2 translocation assay in which only compound Cpd16 (internally named 13546) displayed activity for Nrf2 nuclear translocation. One of the VS approaches found in the literature was a structured-based virtual screening followed by docking studies using 1X2R as a reference of the protein-protein interaction, similar to the virtual screen approach performed in this thesis (Marcotte et al. 2013). A second approach by Zhuang et al. used the same structure-based VS integrated with hit-based substructure search for finding compounds with similar structure for clustering analysis (Zhuang et al. 2014). In contrast, a ligand-based VS using a quantitative structure-activity relationship (QSAR) technique for predicting the biological activity of compounds was published (Kanno et al. 2012).

In order to study the activation of Nrf2, the *in vitro* cell-based Keap1-Nrf2 pathHunter® assay from DiscoverRx was used. The advantage of an *in vitro* assay is that it can be automatized for high-throughput screening in a simpler and more convenient way than *in vivo* experiments. The majority of publications have utilized *in vitro* cellular assays to study the activation of the Nrf2-Keap1 pathway followed by further studies using *in vivo* models. Another way to study Nrf2 activation in neurons is by using neuronal models derived from induced pluripotent stem cells (iPSCs), this *in vitro* method has been used in Nrf2 signalling activation in drug discovery and cell therapy research (Pistollato et al. 2016). Neurons derived from iPSCs can generate specific disease models, patient specific cells can be used for the generation of an *in vitro* assay. This technology has been used with various models of neurodegeneration such as Parkinson's

disease (PS), Alzheimer's disease (AZ) and Amyotrophic lateral sclerosis (ALS). The main advantage of this method is that the cells generated can be used for cell-based assay and drug screens (Borger et al. 2017).

In these studies sulforaphane was demonstrated to induce the nuclear translocation of Nrf2 according to literature, our EC₅₀ values ranging from 0.37 μ M to 0.87 μ M are similar to supplier value of 0.50 μ M (DiscoverX); another literature value of sulforaphane EC₅₀ is 33 μ M obtained from a ARE luciferase reported assay measured with Steady-Glo (Promega) incubated in AREc32 cells for 24 hours (Wu et al. 2014). The significant differences between EC₅₀ values can be due to the difference of both methods, they used a cell line with copies of the GST ARE promoter linked to a luciferase gene to quantify the ARE induction by luciferase activity. In contrast, this research used a commercial assay method based on β -galactosidase enzyme fragment-complementation to measure the Nrf2 nuclear translocation in U2OS-Nrf2 cells. The same Nrf2 nuclear translocation assay was used to identify (3S)-1-[4-[(2,3,5,6-tetramethylphenyl) sulfonylamino]-1-naphthyl]pyrrolidine-3-carboxylic acid (RA839), a small compound that shown to bound to the Keap1 protein and disrupted the interaction with Nrf2 (Winkel et al. 2015). Reference compounds recommended by manufacturer for Nrf2 nuclear translocation assay were sulforaphane (EC₅₀ 0.50 μ M), bardoxolone methyl (CDDO-Methyl; EC₅₀ 0.16 μ M), quercetin (EC₅₀ 4.3 μ M), iodoacetamide (EC₅₀ 2.3 μ M) and tert-butylhydroquinone (tBHQ; EC₅₀ 71.1 μ M), values obtained from DiscoverX assay validation experiments. The preferred reference compounds were sulforaphane and CDDO-Methyl based on the EC₅₀ values, hence sulforaphane was chosen due to price and availability from supplier (Sigma Aldrich). In the cellular assay sulforaphane increased Nrf2 nuclear translocation in a concentration-dependent manner, it was also used as a control in the cellular assay and western blot experiments.

Literature Nrf2 activators such as sulforaphane (Ullah 2015), CPN-9 (Kanno et al. 2012) and Cpd16 (Marcotte et al. 2013) were tested in the Nrf2 pathHunter nuclear translocation assay. Compound CPN-9 and compound 13545 (analogue to Cpd16) did not display Nrf2 activity in the assay, in contrast with sulforaphane and Cpd16 (compound 13546) that displayed an EC₅₀ of 0.37 to 0.87 μ M and Cpd16 EC₅₀ of 9.4 μ M (literature value of 2.7 μ M). Published data of CPN-9 measured the Nrf2 activation by the upregulation of ARE downstream genes but there is no evidence of the direct interaction with the protein-protein interface. Interestingly, ARE-driven luciferase reporter assays were performed in the literature to confirm the activity on Nrf2 activation and results showed that only Cpd16 displayed dose-response activity in Nrf2-ARE genes (Marcotte et al. 2013).

According to the virtual screening and cellular screening results, there are compounds that appeared to induce the Nrf2-ARE pathway, however further studies showed that most compounds induce the Nrf2 translocation by inducing high ROS levels and reacting with the Keap1 cysteine residues. Only two compounds were not interacting by inducing this oxidative stress mechanism. After testing the compounds 14239 and 14231 with western blotting the results suggest that compound 14239 increases Nrf2 levels in the nucleus in U2OS-Nrf2 cell line, the suggested mechanism of action is by disrupting the protein-protein interaction of Nrf2-Keap1, however this was not confirmed in the western blot experiments or any other technique. One way to study this theory is by fluorescent polarisation binding assay (Hancock et al. 2012), the purified fluorescein-labelled peptides display a fluorescence polarization response when bound to Keap1 protein.

Nonetheless, these results are not conclusive; the sulforaphane treatment in U2OS wild type cells did not show an increase of Nrf2 levels in the nuclear fraction. It was decided to test sulforaphane, compounds 14239, 14231, CPN-9 and compound 13546 in the U2OS-Nrf2 cell line and interestingly the results suggest some overexpression of Nrf2 in the nucleus by CPN-9, compound 14239 and sulforaphane against the PBS/DMSO control treatment. This result suggests that the lack of Nrf2 expression in the cytosolic might be due to a higher rate of oxidative response in the nucleus for a cancer cell line or the rapid degradation of cytosolic protein by Keap1 protease complex. The results obtained with HEK-293 indicate a similar mechanism to the U2OS cell line (altered pathways). HEK-293 cells are immortalized by sheared human adenovirus type 5 DNA and these resulted in an altered and dysregulated p53 and retinoblastoma protein (pRB) that are important for stress response, DNA replication, tumour suppression, cell division and cell cycle control (Harris & Levine 2005; Giacinti & Giordano 2006; Kavsan et al. 2011).

Importantly Nrf2 protein needs other proteins to bind the DNA, suggesting that even when the Nrf2 is overexpressed other proteins stayed at basal levels. This could prevent Nrf2 to induce any response in the nucleus and possibly the free protein could be exported naturally to the cytosol to trigger the Keap1-ubiquitination and degradation processes. For example, the normal basal levels of sMAF proteins might not be enough for the over induced levels of Nrf2 in the nucleus, nevertheless there is no evidence and this is just a hypothesis. However, further experiments need to be performed to confirm this data. Compounds were then tested with a general cell line HEK-293 in which a slight increase of nuclear Nrf2 levels with sulforaphane and CPN-9 was observed, however the controls were invalid, being the same levels as hydrogen

peroxide, making the results inconclusive and invalid. In addition, the nuclear samples were not completely soluble and this could make the data difficult to interpret.

In contrast to the Keap1-Nrf2 strategy, sMAF proteins play a critical role in the inducible expression of ARE-driven genes becoming a potential modulator of Nrf2-ARE pathway. Nuclear levels of MAF proteins are essential for the heterodimerization with Nrf2 protein, however this approach requires Nrf2 being localized in the nucleus and previously dissociated from Keap1 protein. There is no current research publications using MAF proteins to modulate Nrf2-ARE pathway, but future work can be a potential mechanism of study.

Both compounds found to activate Nrf2 activity in the nuclear translocation assay displayed relatively low activity and there was insufficient evidence of Nrf2-Keap1 robust interaction, it was therefore decided not to continue further experiments. The necessity to find other methods to confirm the Nrf2 nuclear translocation by test compounds is essential, such as, immunofluorescence, mRNA expression of downstream genes, etc. It has been decided to conclude this project, due to unclear and inconclusive results. In research discovery groups it is important to be able to distinguish when to terminate research when results are not significant to continue. However, Nrf2 protein is still relevant for future research in neurodegenerative diseases and in oxidative stress injury.

CHAPTER 3

INTRODUCTION OF GLUTAMATE RECEPTORS

3.1 GLUTAMATE NEUROTRANSMISSION

L-Glutamate is the principal excitatory neurotransmitter in all vertebrate mammalian central nervous systems (CNS). Glutamate is synthesised in the brain and plays an important role in information processing, memory and neuronal plasticity (McEntee & Crook 1993; Huber et al. 1998; Riedel et al. 2003).

The glutamate neurotransmission is an excitatory synapse process that involves a range of different glutamate receptors in neurons. Glutamate is able to bind to different ionotropic (Kainate, AMPA and NMDA) or metabotropic receptors. In glial cells, glutamate is broken down to glutamine by glutamine synthetase and is exported extracellularly (Niciu et al. 2012); the extracellular concentration of glutamate is normally low $\sim 1 \mu\text{M}$ (Anderson & Swanson 2000; Platt 2007). The sodium-coupled neutral amino acid transporter 7 (SNAT7) takes the extracellular glutamine into neurons (presynaptic axon; Fig.3.1). Inside the presynaptic neuron glutamine is converted into Glutamate by glutaminase enzyme, another source of glutamate inside neurons comes from glucose in the Krebs cycle that converted α -ketoglutarate to glutamate by glutamate dehydrogenase (GLDH; Newsholme et al. 2003). The vesicular glutamate transporter (VGluT) proteins encapsulate glutamate into synaptic vesicles from the cytoplasm. An action potential in the presynaptic axon activates calcium channels in a voltage-dependent manner, glutamate is then released into the synaptic cleft (Niciu et al. 2012). The soluble N-ethylmaleimide-sensitive factor activating protein receptor (SNARE) are proteins that help the fusion of the vesicle into the membrane for glutamate release. Glutamate then binds to different transmembrane receptors, such as G-protein coupled metabotropic receptors (mGluRs) or ionotropic glutamate receptors (iGluRs) to induce the depolarization of the neuron. Glutamate receptors can be found on glial cells, presynaptic and postsynaptic neurons. The released glutamate can be recycled from the synaptic cleft into glial cells and neurons by excitatory amino acid transporters (EAAT; Niciu et al. 2012). In addition, the cystine-glutamate antiporter called system Xc⁻ exchanges extracellular cysteine for intracellular glutamate in a 1:1 ratio to regulate the extracellular levels of glutamate. This antiporter is critical in the formation of the antioxidant glutathione for oxidative protection (Bridges et al. 2012; Niciu et al. 2012).

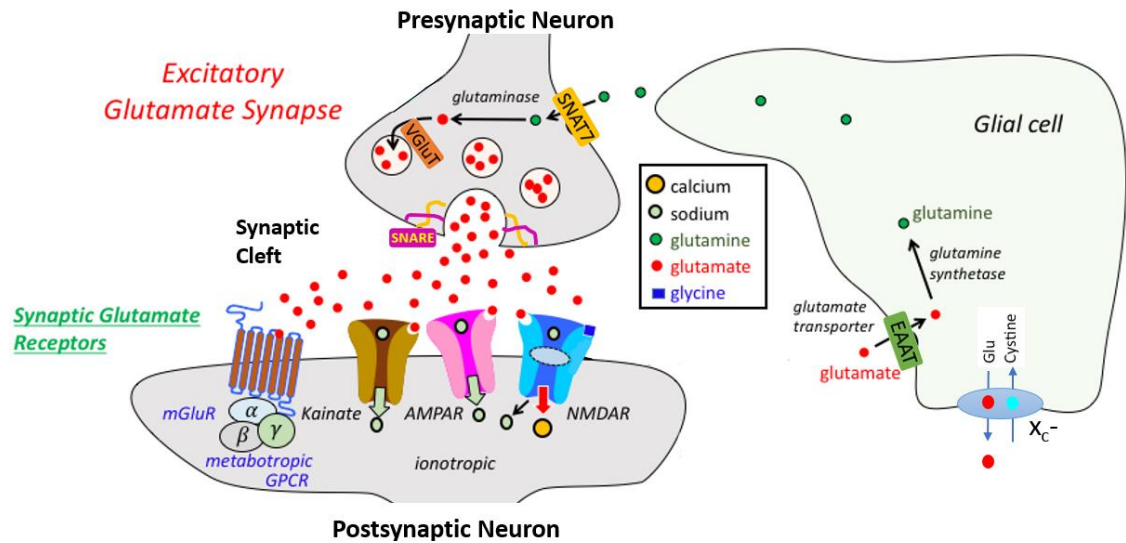


Figure 3.1. Excitatory glutamate synapse. The release of glutamate from the presynaptic neuron into the synaptic cleft activates several glutamate receptors mGluRs and iGluRs. The glutamate from the synaptic cleft is transported into glial cells by glutamate transporters (EAAT), glutamine synthetase converts glutamate into glutamine inside glial cells. Glutamine is further released into the extracellular space to be transported into the presynaptic neuron by SNAT7. Glutaminase converts glutamine into glutamate and VGLUT package glutamate into synaptic vesicles. Vesicles are further fused into the membrane by SNARE proteins to release neurotransmitter into the synaptic cleft to initiate synapsis. The antiporter X_c^- regulates the levels of extracellular glutamate by exchanging extracellular cystine for intracellular glutamate. Ionotropic glutamate receptors Kainate, AMPA and NMDA in brown, pink and blue respectively. Metabotropic glutamate receptor in blue with red. EAAT- Excitatory amino acid transporter; SNAT7 – Sodium-coupled neutral amino acid transporter 7; VGLUT – Vesicular Glutamate transporter; SNARE – Soluble N-ethylmaleimide-sensitive factor activating protein receptor; GPCR – G-protein-couple receptors (Adapted from Tulane University, Medical Pharmacology TMedWeb.

http://tmedweb.tulane.edu/pharmwiki/doku.php/overview_of_cns_neurotransmitters).

3.2 GLUTAMATE NEUROTRANSMISSION IN DISEASE

Glutamate is the principal excitatory neurotransmitter however high concentrations of glutamate could be toxic for neurons and cause cell death (Lau & Tymianski 2010). Glutamate activates two types of receptors; the ligand gated ion channels (ionotropic) and G-protein coupled (metabotropic) receptors (Traynelis et al. 2010). These receptors are distributed in several areas of the brain and CNS and therefore important for normal development and correct function of the nervous system. In general dysregulation and dysfunction of glutamate receptors is linked to several neurological disorders and degenerative diseases such as Parkinson's (mGluRs such as mGluR5), Schizophrenia (NMDA receptors), Alzheimer's disease (Kainate, AMPA and NMDA receptors), epilepsy (kainate receptors), stroke, brain damage and many more (Serafimoska & Johansen 2011; Matute 2011; Fritsch et al. 2014; Anggono et al. 2016).

Intellectual disability (ID) is a neurodevelopmental disorder characterised by limitations in the intellectual functioning and adaptive behaviour such as, learning, reasoning, problem solving, social and practical skills. The symptoms originate before the age of 18 and ID patients often have additional abnormalities such as epilepsy, autism and dysmorphic features (Volk et al. 2015). The ID affects 1% to 3% of the general population in North America (Volk et al. 2015; The Arc 2016). More than 450 genes that are linked to ID and autism have been identified (van Bokhoven 2011), a large number of these genes had association with the glutamate neurotransmission (van Bokhoven 2011; Soto et al. 2014; Bonnet-Brilhault et al. 2016). Gene mutations in iGluRs AMPA (GRIA2 and GRIA3) and NMDA (GRIN1 and GRIN2A) have been linked to ID, epilepsy and neurodevelopmental phenotypes (van Bokhoven 2011; Soto et al. 2014).

Down syndrome (DS), is a genetic condition characterised for having three copies of the chromosome 21 instead of the normal two and displays symptoms of ID, weak muscle tone (hypotonia) and dysmorphic facial features in infancy. Post-mortem brain tissues of DS patients showed endosome abnormalities suggesting an altered endocytic pathway in DS pathology affecting glutamate receptors endocytosis (Cataldo et al. 2000). More specifically, the synaptic endosomal protein sorting nexin 27 (SNX27) involved in endocytosis, trafficking and degradation of membrane receptors such as AMPA and NMDA was significantly reduced in DS patients (Wang et al. 2013). Deletion of SNX27 gene (mice knockout) showed reduction in glutamate synaptic transmission, increasing the degradation of AMPA and NMDA receptors and avoiding the recruitment of glutamate receptors in long-term potentiation (LTP) and synaptic plasticity suggesting a deficiency in learning and memory processes (Wang et al. 2013; Hussain et al. 2014; Volk et al. 2015). Restoring SNX27 gene in Ts65Dn mice completely rescued synaptic dysfunction

and cognitive deficits, suggesting an important role in glutamate synapsis in DS (Wang et al. 2013).

22q11 deletion syndrome (22q11DS) is a genetic disorder caused by the deletion of a small piece of chromosome 22, this syndrome has a wide range of symptoms including heart abnormalities, cleft palate, immune system deficiency and higher risk of developing psychiatric disorders and schizophrenia (Evers et al. 2015). 22q11DS displays abnormalities in glutamate metabolism, it is suggested that patients with this syndrome lack or have reduced levels of proline dehydrogenase (PRODH), the enzyme that converts proline to glutamate. Patients with 22q11DS display high levels of proline and reduced levels of PRODH, however more studies need to be conducted in order to understand the specific mechanism with glutamate neurotransmission (Goodman et al. 2000; Evers et al. 2015).

The fragile X syndrome (FXS) is a genetic condition characterised by the mutation of *FMR1* gene, the loss of *FMR1* causes a lack of expression of the fragile X mental retardation protein (FMRP). FXS affects more males than females, the symptoms include; learning disabilities, cognitive impairment, anxiety and hyperactive behaviour. One in three patients with the syndrome develop autism spectrum disorders (ASD) defined as a neurodevelopmental set of disorders characterised by impairment in social interactions, communication, interests and behaviours (Volk et al. 2015). FMRP is a RNA-binding protein that regulates protein production in cells, it has an important role in development of synapses in neurons and is required for normal glutamate synapse control. More specifically FMRP have shown to bind and interact with glutamate receptors mGluR5 and NMDA (subunits NR1, 2A, 2B and 3A); currently there is no cure for this syndrome however new approaches for targeting mGluR5 are promising for a novel treatment (Darnell & Klann 2013; Pop et al. 2014; Scharf et al. 2015).

Previous research has suggested glutamate neurotransmission involved in the pathophysiology of ASD. A group of sixty patients with ASD were studied to confirm significant elevated levels of glutamate in blood plasma, a smaller study of fourteen autistic children was reproduced using high-performance liquid chromatography (HPLC) to confirm the same results, glutamic acid levels were higher compared to control subjects (Moreno et al. 1992; Moreno-Fuenmayor et al. 1996). Similarly, elevated glutamate levels in plasma have been found in patients with Asperger's syndrome a disorder included in ASD and their families (Aldred et al. 2003; Cai et al. 2016). A study with adults, eighteen male patients with autism and nineteen healthy male subjects found higher glutamate serum levels in autism patients 82.2 μM versus 61.1 μM in healthy controls using HPLC (Shinohe et al. 2006).

Hassan et al. studied glutamate levels in blood plasma and four regions of the brain in ten children with autism versus ten healthy patients using HPLC and proton magnetic resonance spectroscopy ($^1\text{HMRS}$) respectively. The results were similar to others, levels of glutamate were significantly higher than control subjects in blood serum and the four brain regions tested: bilateral anterior cingulate, left striatum, left cerebellar hemisphere and left frontal lobe (Hassan et al. 2013). In a similar way, a small pilot study using magnetic resonance spectroscopy found that seven adolescent males with autistic disorders displayed a significantly higher level of glutamate in the anterior cingulate cortex, a part of the brain located in the medial surface of the cerebral cortex and important for learning, processing, emotion formation and memory compared to the control group (Joshi et al. 2013). Similarly, patients with ASD displayed significantly higher concentration of glutamate and glutamine in the brain region amygdala-hippocampal involved in processing, behaviour, learning and memory using *in vivo* $^1\text{HMRS}$ (Page et al. 2006).

Higher levels of glutamate/glutamine were found in obsessive-compulsive disorder (OCD) patients using proton magnetic resonance spectroscopy ($^1\text{HMRS}$) in the orbitofrontal cortex (OFC) which is part of cognitive processing in decision-making (Whiteside et al. 2006). Ten patients diagnosed with social anxiety displayed higher glutamate levels relative to creatinine in the anterior cingulate complex, these glutamate levels are positively correlated with the intensity of social anxiety symptoms (Phan et al. 2005). Whereas, a NMR brain scanning in major depressive disorder (MDD) patients showed that depressed patients had reduced levels of glutamate/glutamine and γ -aminobutyric acid (GABA) in prefrontal brain regions (Hasler et al. 2007). There is strong evidence demonstrating that glutamate neurotransmission plays an important role in autism, OCD, depression, anxiety disorders and decision making, however, the exact mechanism of dysregulation of glutamate levels in serum and brain are not yet established.

In schizophrenia, the “glutamate hypothesis” correlates glutamate receptors with mental conditions by detecting reduced levels of glutamate, glutamine and n-acetylaspartate in the dorsolateral prefrontal cortex suggesting a dysfunction in the glutamate neurotransmission in the brain (Ohrmann et al. 2005; Stone 2011). More specifically, it is believed that schizophrenia is caused by hypofunctional glutamate NMDA receptors in view of the fact that antagonists ketamine and phencyclidine (PCP or angel dust) are used for pharmacological models of schizophrenia. Both antagonists gave conditions that mimic the positive (hallucinations and delusions), cognitive (memory problems), negative (apathy and lack of emotion) and affective (anxiety and depression) symptoms of schizophrenia (Lahti et al. 2001; Konradi & Heckers 2003; Morris et al. 2005; Morrisette & Stahl 2011).

There are a few studies suggesting an important role of kainate receptors in psychiatric disorders. For example, GluK1 and GluK2 expression were reduced in limbic cortices of post-mortem brains from bipolar and schizophrenia patients using *in-situ* hybridization histochemistry (Beneyto et al. 2007). More interestingly, PCP chronic treatment was found to decrease GluK1 and GluK2 expression in rat prefrontal cortex (Barbon et al. 2007; Woo et al. 2007). In Schizophrenia patients, a GRIK3 polymorphism study found an association between GluK3 receptor polymorphism (T928G) and the mental disorder (Begni et al. 2002). A chromosomal analysis study found a link between polymorphism on the GRIK4 gene (KA-1) in Schizophrenia and bipolar disorder (Pickard et al. 2006). In contrast, a study in Japanese population found that GRIK1 single nucleotide polymorphisms do not play a role in schizophrenia pathology (Shibata et al. 2001). The research suggests a link between glutamate receptors NMDA and kainate with Schizophrenia and bipolar disorder, more research needs to be conducted to elucidate the exact mechanism of these receptors with the pathology.

Alzheimer's disease (AD), the most common cause of dementia, is a chronic neurodegenerative disease that is estimated to affect 850,000 people in the UK (NHS). In past years, various autoradiography studies have shown that AMPA, kainate and NMDA receptors are reduced in severe Alzheimer disease (AD) in areas of neuronal cell loss suggesting a dysregulation of glutamate receptors in AD (Jansen et al. 1989; Chalmers et al. 1990; Penney et al. 1990; Dewar et al. 1991; Carlson et al. 1993).

Excitatory glutamate neurotransmission plays a role in the initiation and spread of seizure activity. In epilepsy the seizure episodes are caused by the sudden and disorderly discharges of neurons in the brain, these neurons are activated at the same time causing major excitatory signals. The long lasting activation of glutamate receptors such as NMDA and kainate are associated with epilepsy. For example, brain tissues from patients with temporal lobe epilepsy (TLE) showed high levels of expression of GluK1 receptors (Sperk et al. 1983; Olney et al. 1986; Matute 2011). Also, a tetranucleotide repeat polymorphism of the GluK1 gene (chromosome 21q22.1) have been linked to juvenile absence epilepsy (JAE; Sander et al. 1997). There is strong evidence linking kainate and NMDA receptors with epilepsy and seizure pathology, targeting these receptors can provide a new potential for novel antiepileptic treatments.

Finally, kainate receptors have also been linked to pain processing in the brain and some selective GluK1 antagonists have been shown to reduce chronic pain (Li et al. 1999; Guo et al. 2002; Palecek et al. 2004; Zhuo 2017b). For example GluK1 antagonist LY-382884 reduces pain responses measured by electrophysiology in spinothalamic tract (STT) neurons in response to

mechanical and thermal stimuli in a peripheral neuropathy model in primates (Palecek et al. 2004). In addition, a mouse model showed that responses to capsaicin or inflammatory pain were notably reduced in GluK1-deficient mice compared to GluK2 receptors (Ko et al. 2005). All these findings can provide important information for the study of pain therapy. Glutamate neurotransmission is important for correct excitatory synapses, any dysregulation can cause a wide range of neurological disorders, their study and understanding is a promising target for novel treatments.

3.3 GLUTAMATE RECEPTORS GENE FAMILIES

3.3.1 METABOTROPIC GLUTAMATE RECEPTORS (mGluRs)

mGluRs are members of the family of the G-protein coupled receptors (GPCRs). GPCRs are membrane-bound proteins that are activated by extracellular molecules such as neurotransmitters and peptides. Several metabolic steps involving G-protein signal transduction regulate the flow of ions across the membrane. mGluRs are members of the class C GPCRs which also include the calcium-sensing receptors, γ -amino-butyric acid (GABA) type B receptors, taste T1R receptors and vomeronasal type-2 receptors (Bräuner-Osborne et al. 2007; Chun et al. 2012). GPCRs can be classified into six families, A to F depending on the homology sequence of the conserved heptahelical transmembrane domain (7TM). Class A are the rhodopsin-like family, class B the secretin receptor family, class C metabotropic glutamate/pheromone family, class D fungal mating pheromone receptors, class E cyclic AMP receptors and Class F frizzled/smoothed family (Alexander et al. 2015; IUPHAR/BPS Guide to Pharmacology). The class C family is characterised as presenting two unique structural features, the large extracellular domain with the orthosteric site situated away from the 7TM and the ability to form dimers with unique activation modes compared to other GPCRs families (Chun et al. 2012).

The structure of mGluRs (Fig.3.2) is formed by an extracellular bi-lobed N-terminal domain (glutamate binding site), followed by a cysteine-rich domain, seven spanning transmembrane alpha helices domains and an intracellular C-terminal domain (Kew & Kemp 2005; Niswender & Conn 2010).

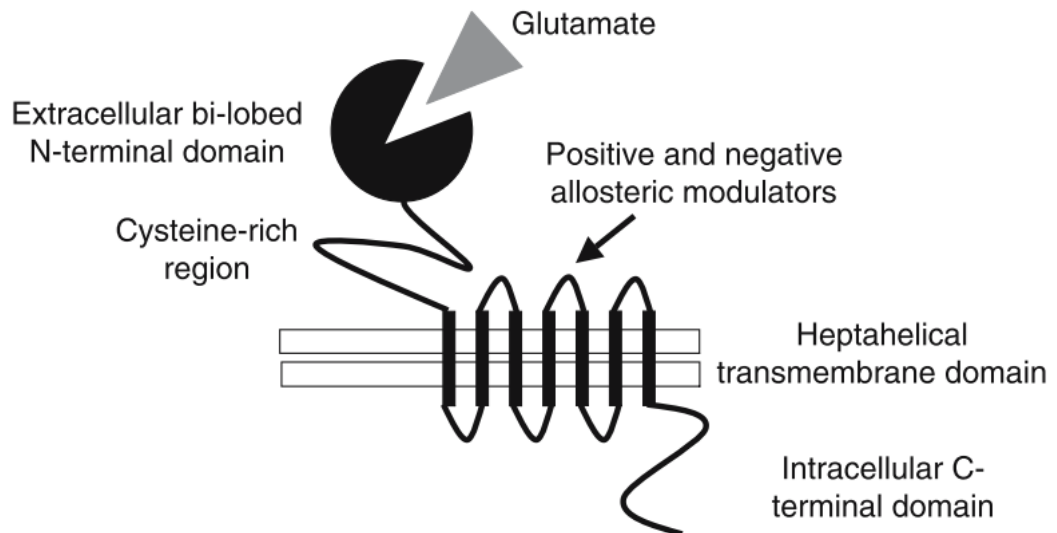


Figure 3.2. Representation of a typical mGluR structure (Kew & Kemp 2005).

The extracellular domain of mGluRs contains a ligand binding site and the intracellular domain binds to G-proteins subunits (α , β and γ). The α subunit binds to guanine nucleotides guanosine triphosphate (GTP) or guanosine diphosphate (GDP). In the inactive state, α subunit binds to GDP to form an inactive heterotrimer with β and γ subunits. The activation of the receptor by an extracellular signal causes the exchange of GDP with GTP. When GTP binds the α subunit the G-protein becomes activated and induces the dissociation of α subunit from the $\beta\gamma$ complex, the dissociated subunits (α -GTP and $\beta\gamma$) can bind to effector proteins such as ion channels or enzymes to mediate a variety of responses in the target cell. This type of activation can induce the opening and closing of an ion channel (Fig. 3.3; Purves et al. 2004).

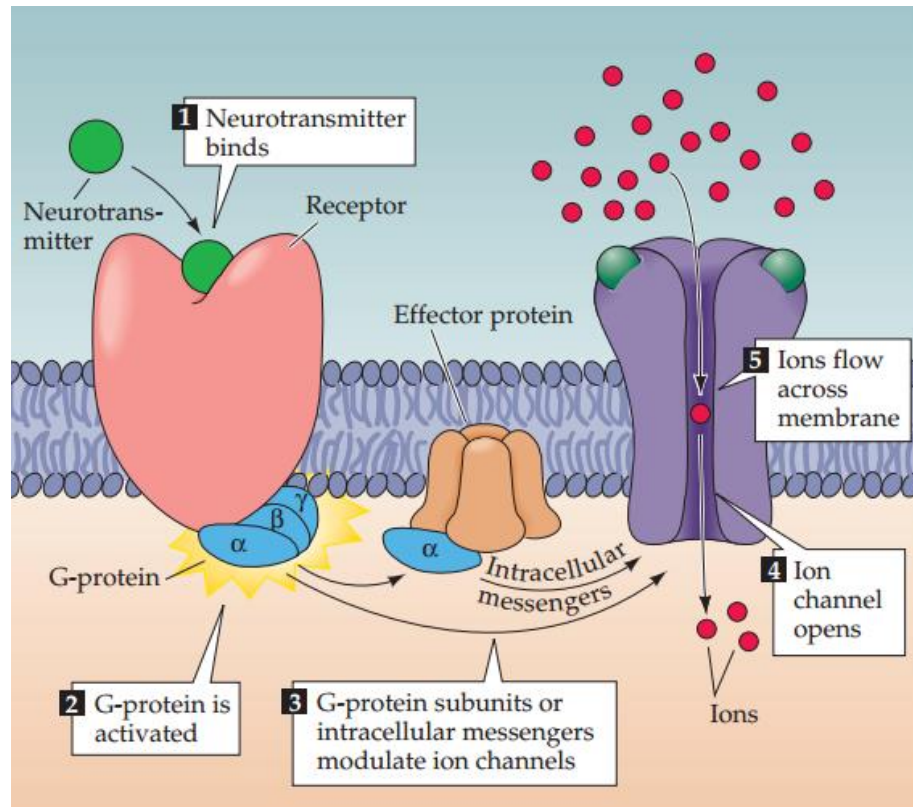


Figure 3.3. Metabotropic Glutamate Receptor. mGluRs activate G-protein subunits (α , β and γ) which trigger several steps to induce the modulation of ion channels (Purves et al. 2004).

mGluRs are classified into three main classes based on their sequence homologies, pharmacology and preferred agonist (Fig. 3.4). Group I (mGluR1 and mGluR5), Group II (mGluR2 and mGluR3) and Group III (mGluR4, mGluR6, mGluR7 and mGluR8). Group I typically couple via G_q/G_{11} to induce the activity of phospholipase C (PLC), resulting in the hydrolysis of phosphatidylinositides and the formation of inositol triphosphate (IP_3) and diacylglycerol. This pathway results in the binding of IP_3 to calcium channels to induce intracellular calcium mobilization and further activation of protein kinase C (PKC; Niswender & Conn 2010). Group II and III couple via G_i/G_o and both inhibit the activity of adenylyl cyclase (AC), avoiding the conversion of adenosine triphosphate (ATP) to cyclic adenosine monophosphate (cAMP) followed by reducing the activity of cAMP-dependent protein kinase and turning off the cAMP pathway (Kew & Kemp 2005; Niswender & Conn 2010).

mGluRs main functions are regulation of neuronal excitability, synaptic transmission and plasticity. Due to the extensive expression of mGluRs in the brain, it has potential therapeutic targets for drug discovery, however the purposes of this project are focused on ionotropic glutamate receptors exclusively.

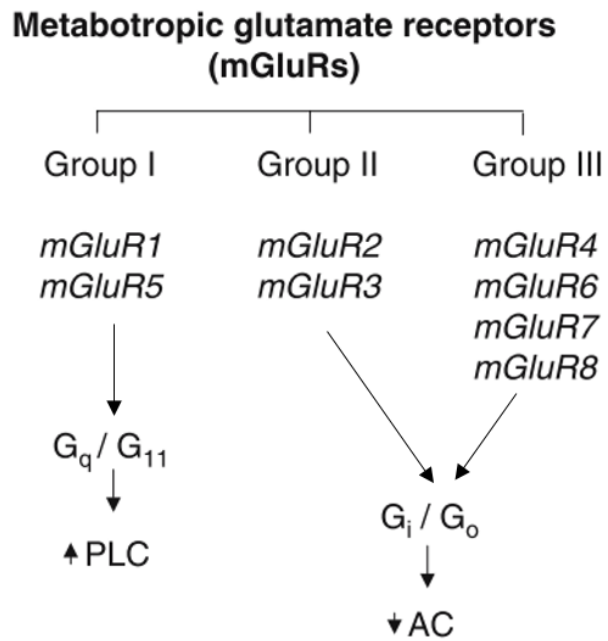


Figure 3.4. Classification of mGluRs families. Group I, activates Phospholipase C (PLC), which results in the formation of inositol triphosphate (IP₃) and the further activation of protein kinase C (PKC). Group II and III inhibit Adenylate cyclase (AC) activity thereby reducing the levels of cyclic adenoside monophosphate (cAMP) turning off the cAMP pathway and reducing cAMP-dependent protein kinase levels (Adapted from Kew & Kemp 2005).

3.3.2 IONOTROPIC GLUTAMATE RECEPTORS (iGluRs)

Ionotropic glutamate receptors (iGluRs) are ligand gated ion channels, meaning that binding of a ligand (usually a neurotransmitter) triggers the opening of the channel allowing the transport of ions such as Na^+ , K^+ and Ca^{2+} through the membrane (Purves et al. 2004). In humans iGluRs are encoded by 18 genes (Fig. 3.5) and they are classified by their selective agonists: α -amino-3-hydroxy-5-methyl-4-isoxazolepropionic acid (AMPA), Kainate, N-methyl-D-aspartic acid (NMDA) and delta (δ) receptors, the latter is not well characterised yet and no endogenous ligands have been identified. More recently it has been found that D-serine and glycine can bind and activate the delta receptor GluD2 (Khan 2016). AMPA receptors family is formed by four receptors GluA1 to GluA4, Kainate formed by five receptors GluK1 to GluK5, NMDA comprises seven sub-types GluN1, GluN2A to D and GluN3A to D (Mayer 2016).

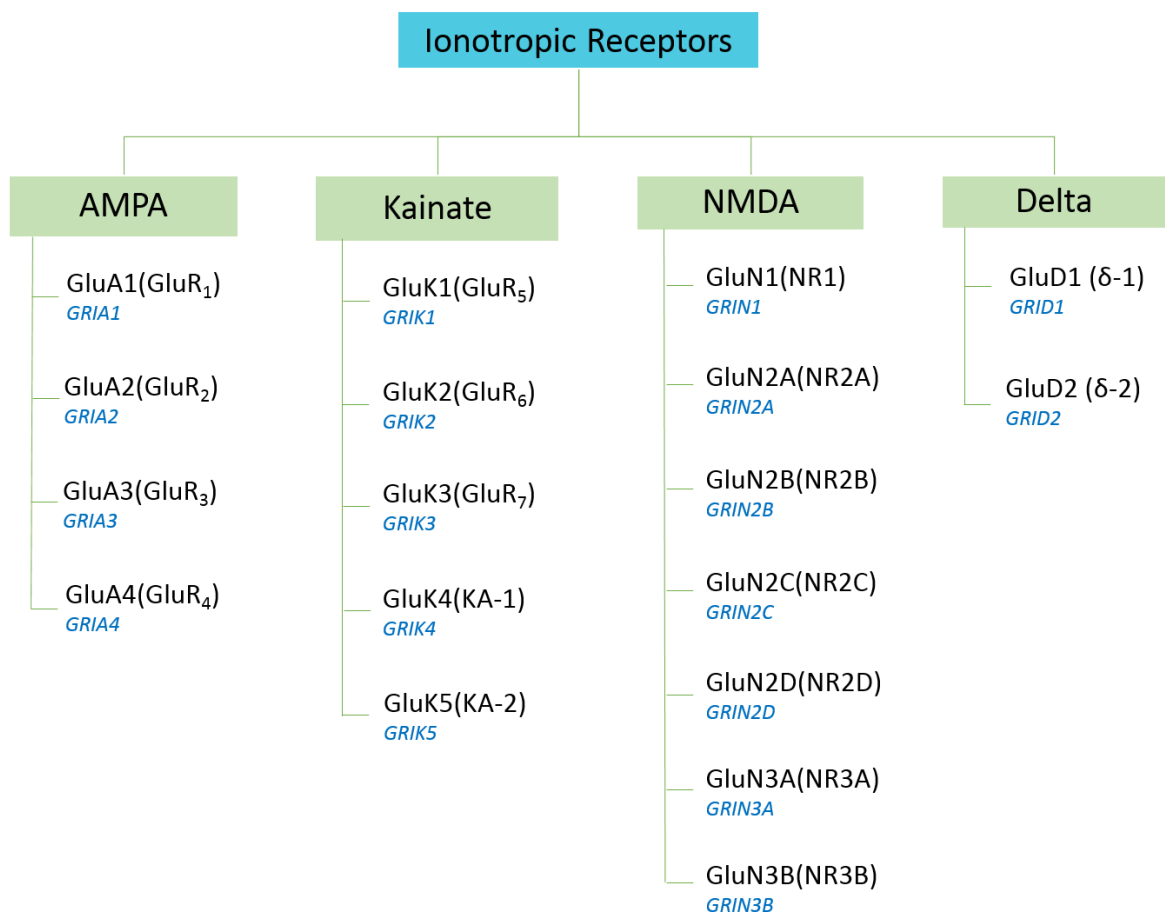


Figure 3.5. The ionotropic receptor gene family. Protein names are shown according to the current nomenclature (with previous nomenclature in parenthesis) and gene names being shown in blue. Genes nomenclature were obtained from UniProt.

3.4 iGluRs STRUCTURE

3.4.1 GENERAL FEATURES

Structural information on iGluRs from high-resolution X-ray crystallography has enabled researchers to explore and gather information of the structure-function relationship. In 1998, the X-ray crystal structure of the soluble LBD of rat GluA2 in complex with kainate provided at 1.9 Å was the first atomic information of the binding site structure of iGluRs (Armstrong et al. 1998). There are currently over one-hundred crystal structures of the LBD of GluA2 in complex with different ligands including kainate, glutamate, L-aspartate, fluoro-willardiine and more (Armstrong et al. 1998; Armstrong & Gouaux 2000; Ahmed et al. 2011; Krintel et al. 2014; Meyerson et al. 2014; Salazar et al. 2017).

In 2009, Sobolevsky obtained the first crystal structure of the full-length rat GluA2 at 3.6 Å providing important information about the global structure and domain organisation of an iGluR (Sobolevsky et al. 2009). Also obtained in the same year was the soluble ATD GluA2 crystal structure at 2.33 Å (Jin et al. 2009). For kainate receptors, in 2005 the first LBD structure of GluK1 and GluK2 was published (Nanao et al. 2005; Naur et al. 2005), currently there are 84 high-resolution crystals of kainate receptors LBD and ATD with agonist, antagonist and ions (Møllerud et al. 2017). In 2014, the full-length of GluK2 was determined at low resolution 7.6 Å using cryo electron microscopy (Meyerson et al. 2014). For NMDA receptors the first ATD of GluN2B subunit at 3.21 Å was reported in 2009 (Karakas et al. 2009) and in 2011 the same research group published the ATD of GluN1 subunit at 2.0 Å (Karakas et al. 2011). Finally, in 2014 two full-length structures of NMDA GluN1/GluN2B were published (Lee et al. 2014; Karakas & Furukawa 2014). All these high- and low-resolution structures have given important information in the structure and topology of iGluRs, several crystal structures will be described in more detail in the following sections.

iGluRs form tetramers assembled as dimer-dimer conformation. Each subunit is formed of four main domains (Fig. 3.6), an extracellular amino terminal domain (ATD), an extracellular ligand-binding domain (LBD), a transmembrane domain (TMD), and an intracellular carboxyl-terminal domain (CTD; Traynelis et al. 2010).

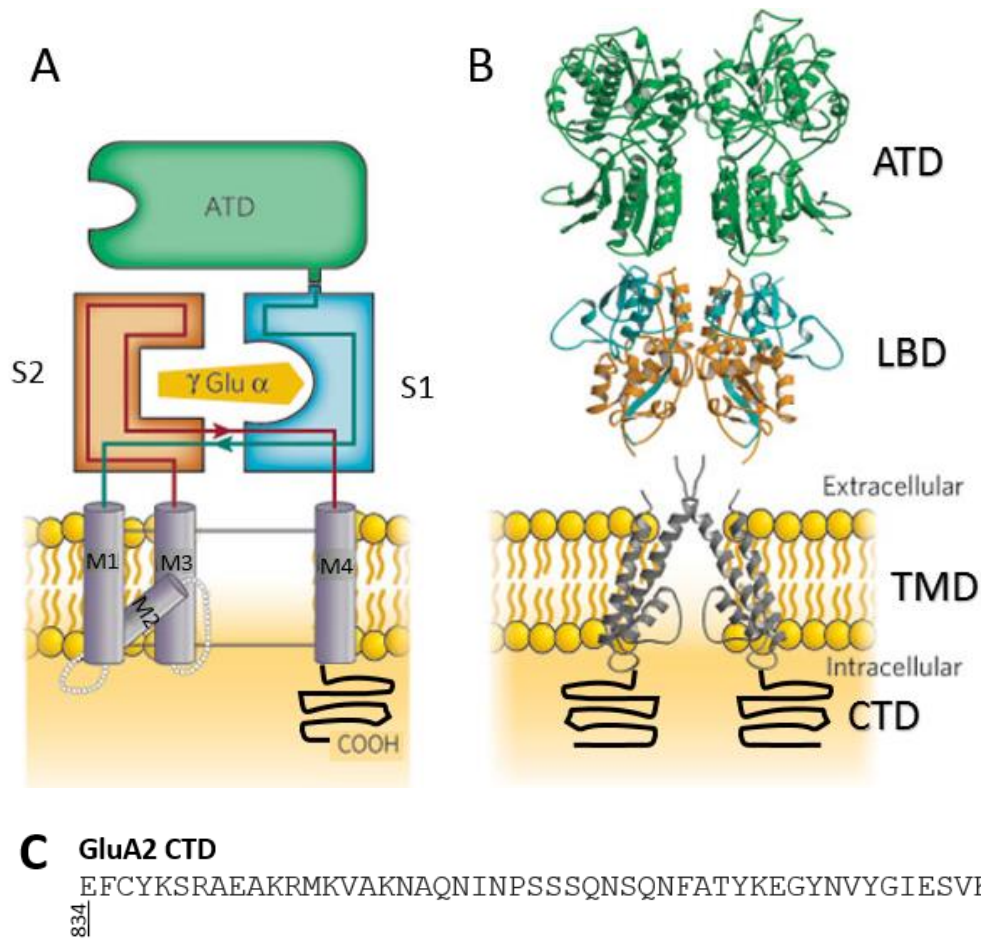


Figure 3.6. Ionotropic glutamate receptor domains. A. Subunit of a monomer structure, amino terminal domain (ATD) in green, ligand binding domain (LBD) formed of segment S1 and S2 ligand binding core (also called D1 and D2) in orange and blue, the transmembrane domain (TMD) formed of three membrane spanning segments (M1, M3 and M4) and a re-entry pore loop (M2) in grey and the C-terminal domain (CTD) in black. B. Representation of the dimer conformation of the ATD, LBD, TM and CTD. ATD and LBD show the clamshell-like structure (Adapted from Mayer 2006b). C. For the CTD of iGluRs there are no structural details in the PDB, the sequence of the CTD of GluA2 is shown, P42262-1 UniProt (Traynelis et al. 2010; Henley & Wilkinson 2016).

The Amino terminal domain (ATD) of iGluRs are allocated in the extracellular region away from the membrane and have a bi-lobed clamshell like structure composed of two lobes (lower and upper). The structural form of the ATD allows a binding site for allosteric modulators. ATD has the most divergent sequence identity of 20-25% comparing other subunits (Furukawa 2012). ATD have an important role in subtype-specific receptor, receptor assembly and trafficking (Garcia 2004; Traynelis et al. 2010; Yelshanskaya et al. 2014; Díaz-alonso et al. 2017).

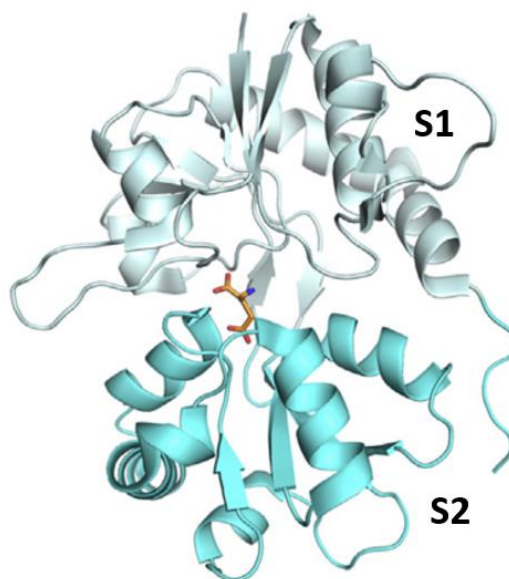


Figure 3.7. GluK1 LBD S1S2 clamshell-like structure. GluK1 LBD (2F36, PDB accession code; Mayer 2006a) in complex with glutamate in orange, LBD forms clamshell-like structure formed of S1 and S2, in light cyan and dark cyan, respectively (Møllerud et al. 2017).

The extracellular ligand binding domain (LBD) is formed of two extended amino acid segments usually named as S1 and S2 (Fig.3.7), both segments form a ligand-binding cavity core where the ligand/neurotransmitter binds (Yelshanskaya et al. 2014; Mayer 2006b). The LBD structure forms a clamshell-like conformation, in which segments S1 (N-terminal of M1 transmembrane spanning domain) and S2 (between M3 and M4 regions) form the two-domain clamshell-like structures for ligand binding, the opening and closing of the clamshell will depend on gating binding and unbinding activities (Traynelis et al. 2010; Hammond 2015). As Fig. 3.6 shows, the ATD also has a clamshell-like structure formed by two lobes (upper and lower lobe). The LBD of glutamate receptors is attached to the TMD with three small linkers, these linkers connect S1-M1, S2-M3 and S2-M4. The TMD forms an ion channel pore by three transmembrane helices M1, M3 and M4 and a re-entrant loop M2 and contributes to receptor tetrameric stability (Balannik et al. 2005; Yelshanskaya et al. 2014; Traynelis et al. 2010). Sequence homology is found in the ATD, LBD and TM, with higher homology in the ligand binding core (up to 80-90% within similar groups), in contrast the CTD has not shown any sequence homology between glutamate receptors (Traynelis et al. 2010; Furukawa 2012). However, the CTD contains several different phosphorylation sites and binding sites for intracellular binding proteins giving it an important role in receptor regulation, synaptic localisation, trafficking, targeting for degradation and post-translational modifications (Traynelis et al. 2010).

Tetramer conformation

iGluRs assemble as four subunits to form tetramers either by different subunits (heterotetramers) or identical subunits (homotetramers). There are two proposed pathways for tetramer assembly “preferential” and “obligatory” (Herguedas et al. 2013). The formation of heterotetramers is obligatory for function of some receptors but preferential for other receptor families. The subunits ATD, LBD and TMD form dimers between them to initiate the assembly of further tetramers. In the preferential route, the subunits (ATD, LBD and TMD) will form homodimers to then form tetramers, a reequilibration step will induce the formation of heterodimers between subunits to obtain a functional heterotetramer (Fig.3.8). For example, AMPA and kainate (GluK1-GluK3) usually forms functional homotetramers, but also has the ability to form native functional heterotetramers. In obligatory assembly the subunits do not form homodimers and directly form functional heterotetramers, NMDA and kainate (GluK4 and GluK5) are examples of this pathway (Sobolevsky et al. 2009; Herguedas et al. 2013).

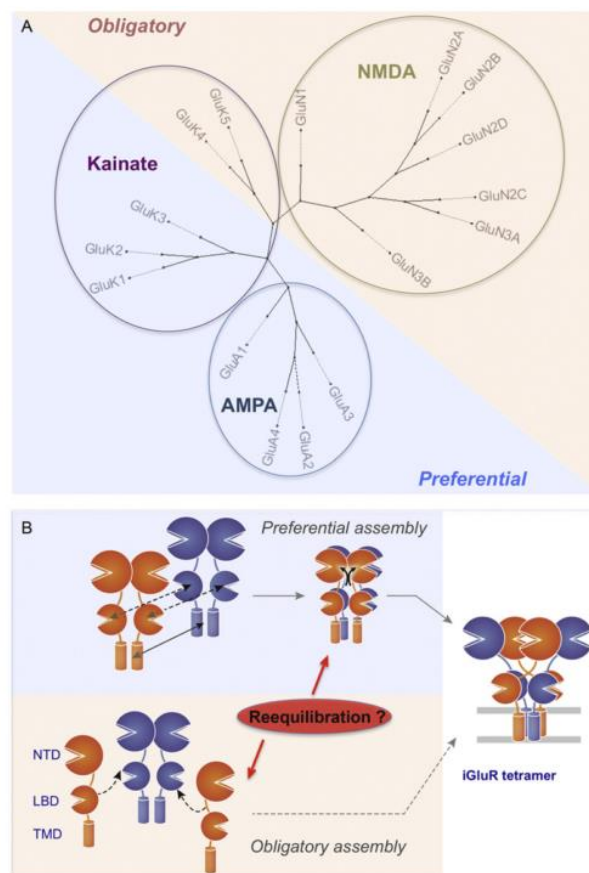


Figure 3.8. iGluR tetramer assembly representation. A. Phylogenetic tree of the main iGluRs (δ has not been fully characterised) divided into preferential and obligatory assembly pathways. B. Schematic representation of the assembly pathway for obligatory or preferential tetramers formation, tetramer structure represents GluA2 (3KG2 PDB code; Herguedas et al. 2013).

3.4.2 AMPA RECEPTORS

α -Amino-3-hydroxy-5-methyl-4-isoxazolepropionic acid (AMPA) is the specific agonist that activates AMPA receptors (Fig. 3.10). As previously described the AMPA receptors are composed of four subunits GluA1 to GluA4. AMPA receptors mediate the fast excitatory synaptic transmission in the central nervous system (CNS). Earlier published high-resolution data of the LBD of rat GluA2 (Armstrong et al. 1998) described a bilobed structure formed by two domains S1 and S2, the domain closure was induced by kainate binding and interdomain contacts were found between the two domains including the formation of a disulphide bond to stabilize the formation of dimers.

X-ray crystallography experiments have confirmed the agonist binding site in the clamshell-like structure in the LBD. As previously discussed the LBD is formed of two segments S1 and S2 that are connected to the TMD; Armstrong and Gouaux were able to design a soluble construct of the LBD (S1 and S2) that was easily expressed in *E. coli* bacteria for protein purification and crystallography experiments. This construct contains the ligand binding domain from N392 to S775 and a GT linker between S1 and S2 (Fig.3.9), sequence numbered according to M36419 flop GluA2 (GenBank-EMBL; Keinänen et al. 1990; Armstrong & Gouaux 2000). This new construct was able to offer better understanding of the binding interactions of various ligands in the LBD pocket. They successfully crystallised and obtained X-ray data for the rat GluA2 LBD in complex with glutamate, DNQX, AMPA and kainate; PDB accession codes 1FTJ, 1FTL, 1FTM and 1FW0 respectively (Armstrong & Gouaux 2000).

In 2009 homotetrameric rat GluA2 subunit was the first full-length crystal structure characterised at 3.6 Å resolution in complex with competitive antagonist ZK200775 (Sobolevsky et al. 2009). The full-length structure of homotetrameric rat GluA2 (Sobolevsky et al. 2009) agrees with the previously described data, however, it provided more detailed information about the full membrane symmetry and tetrameric conformation in glutamate receptors.

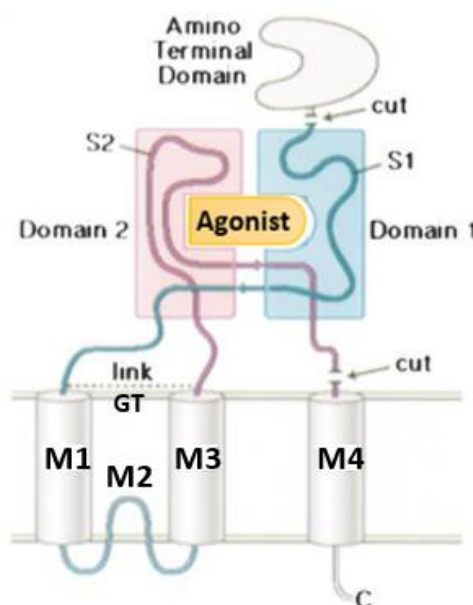


Figure 3.9. Construct of the LBD (S1S2) design. Domain configuration of GluA2 LBD, S1 in blue and S2 in pink, the construct was isolated by cutting above the ATD and before the TMD M4, a Glycine-Threonine was used for linking S1 and S2 between M1 and M2 (Adapted from Armstrong & Gouaux 2000).

The full-length GluA2 rat receptor (PDB accession code, 3KG2) appears as a “Y” shape type structure, with the ATD at the top, the LBD at the middle and the TMD at the bottom to form the ion channel (Fig. 3.11; Sobolevsky 2015). In the paper they used the full-length rat GluA2i (flip variant, from two alternative splicing variants in the LBD) sequence (NP_058957), 36 residues were removed from C-terminus, 6 residues were eliminated from the ATD and the LBD segment, as well as four residues substituted by alanine to stabilize the tetrameric conformation and facilitate crystallography experiments (Sobolevsky et al. 2009). The full-length rGluA2 receptor displayed a 2-fold axis symmetry for the full tetrameric structure, and 4-fold symmetry in the ion channel pore (Sobolevsky et al. 2009).

In addition, they found that the GluA2 tetrameric receptor can form two different subunit conformations, amino acid sequences of each subunit are identical however they fold into A/C (proximal) and B/D (distal) type subunits (Fig. 3.12A). The type A subunit formed a dimer with the B subunit in the ATD, however the A type subunit formed a dimer with D subunit in the LBD, this interaction is called subunit “crossover” or domain “swapping” (Fig.3.12B; Sobolevsky et al. 2009; Hansen et al. 2010; Traynelis et al. 2010).

Structural conformational changes due to the domain swapping might have an important role for tetramer assembly. Domain swapping allows conversion of 2-fold symmetry from LBD to 4-fold symmetry formation in the pore channel. The property of domain swapping results in strong interactions between dimers (disulphide cross-linking) which maintains the stability and flexibility of the tetramer formed by the four subunits (Herguedas et al. 2013; Gan et al. 2015; Sobolevsky 2015).

Crystal structure of rGluA2 (PDB accession code, 3KG2; Sobolevsky et al. 2009) in complex with the competitive antagonist ZK200775 (Fanapanel or MPQX), the antagonist was previously defined by Turski and co-workers (Turski et al. 1998). Fanapanel is a quinoxalinedione drug (Fig. 3.10) which was in phase II clinical trials (Bayer) for the treatment of acute ischemic stroke, however the study was terminated due to intolerable side effects (high levels of sedation, drop of consciousness and transient neurological deterioration) and glial cell toxicity (Elting et al. 2002). Consequently, this first crystal structure of a full-length AMPA GluA2 provided important information about the structure, symmetry, architecture of the ion channel and tetrameric assembly in other families of the ionotropic glutamate receptors.

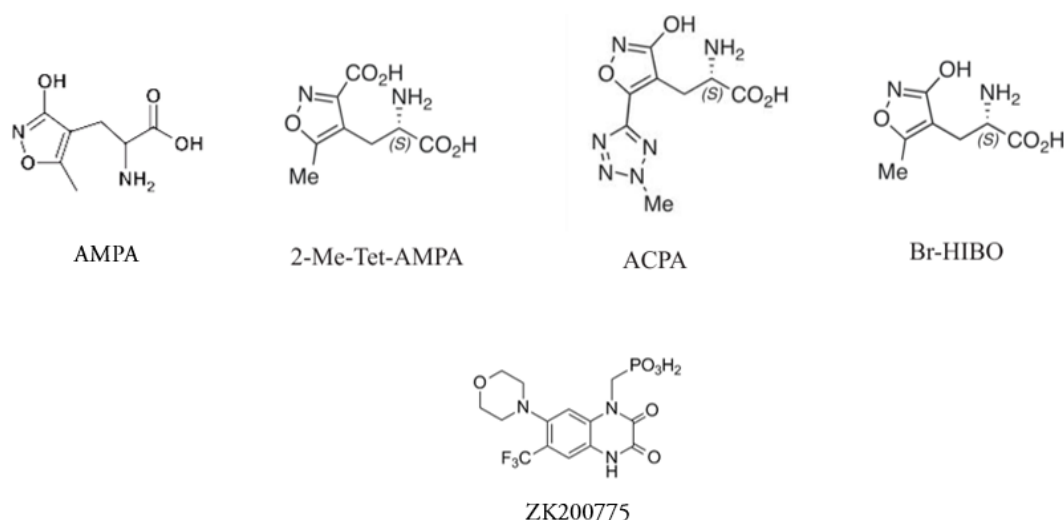


Figure 3.10. AMPA agonists and antagonist. Top, (RS)-AMPA agonist chemical structure, a synthetic analogue of glutamate (Kew & Kemp 2005) and other established agonist of GluA2, 2-methyl-tetrazolyl-[2-amino-3-(3-hydroxy-5-methyl-4-isoxazolyl)propanoic acid (2-Me-Tet-AMPA), (S)-2-amino-3-(3-Carboxy-5-methylisoxazol-4-yl)propionic acid (ACPA) and (S)-2-amino-3-(4-bromo-3-hydroxy-isoxazol-5-yl)propionic acid (Br-HIBO) (Serafimoska & Johansen 2011). Bottom, AMPA competitive antagonist ZK200775, also known as Fanapanel and MPQX, a highly selective AMPA/kainate antagonist. Figure obtained from MedChemExpress (Source <https://www.medchemexpress.com/ZK200775.html>).

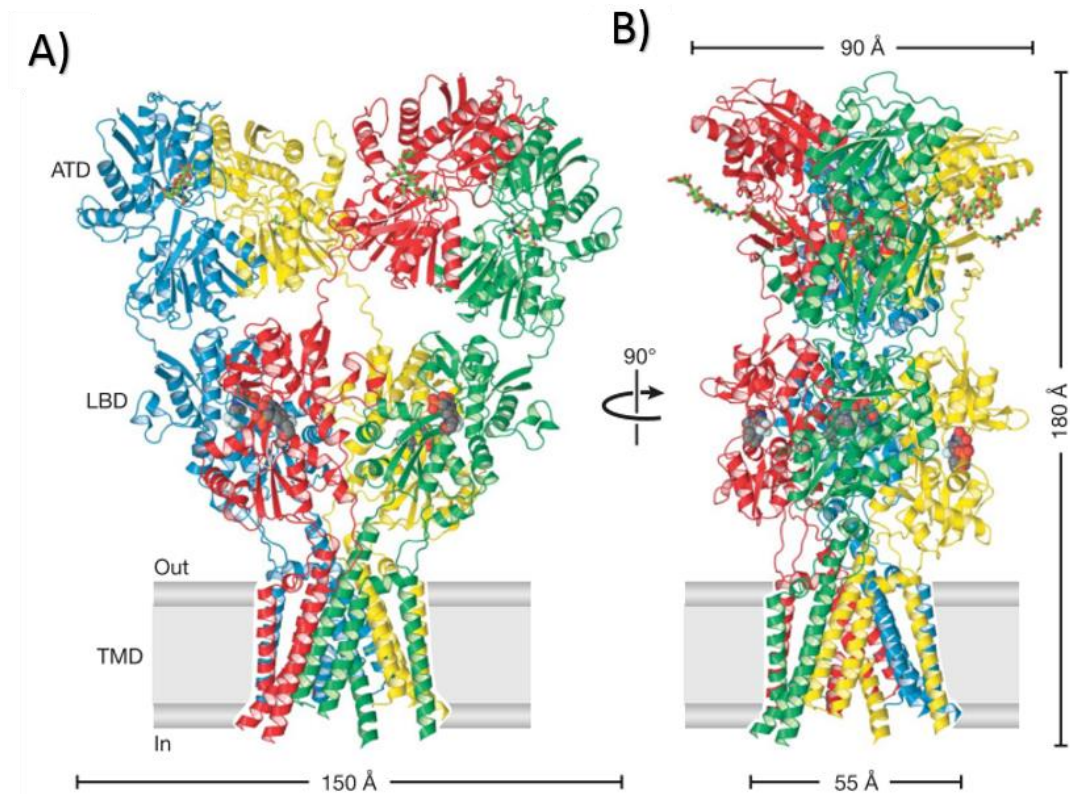


Figure 3.11. Structural architecture and symmetry of rGluA2. Homotetrameric receptor, each subunit is defined in different colours, rGluA2 in complex with antagonist ZK200775. Antagonist inside the LBD clamshell pocket in grey space-filling representation. Open and narrow view of the receptor A and B, respectively. N-acetyl-D-glucosamine (NAG) and beta-D-mannose (BMA) binding the ATD, shown in green (Sobolevsky et al. 2009).

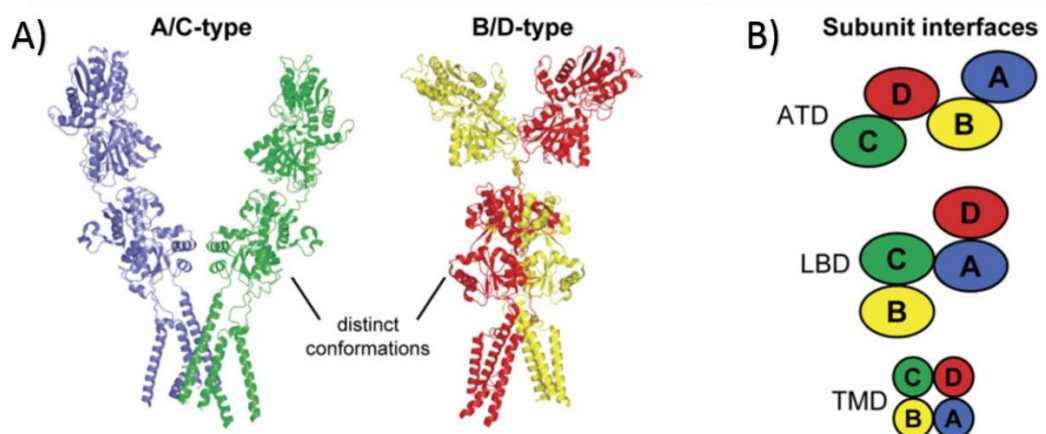


Figure 3.12. Tetrameric distinct conformations. A. Two different structural conformations form A/C type and B/D type subunits. B. Dimer-dimer conformation of the ATD and LBD form 2-fold symmetry and TMD 4-fold symmetry (Hansen et al. 2010).

3.4.2.1 Alternative splicing (Flip/Flop) and RNA editing site (Q/R)

The four AMPA subunits (GluA1-4) can exist in two different alternative splicing versions, commonly named as a “flip/flop”. Exon 14 (flip) and 15 (flop) are RNA segments of ~38 amino acids before the transmembrane domain M4, only nine amino acids are different between them (Fig. 3.13). These two different variants result in different pharmacological and kinetic properties such as channel gating, desensitization and activation (Dingledine et al. 1999; Sommer et al. 1990; Penn & Greger 2009). For example, the flip/flop variants alter the channel opening kinetics of AMPA receptors. They found that the flop variant of GluA2 desensitize faster than the flip variant, this finding suggests an important structural role of the flip/flop sequence in stabilizing the open channel conformation and could be due to the location of the sequence near the transmembrane domain M4 (Pei et al. 2009). The flip/flop segment is located inside the ligand binding domain (S2) and before M4 (TMD), this location might give a structural role to the flip/flop variants for opening/closing the ion channel (Fig. 3.13). In GluA2, GluA3 and GluA4 a selective nuclear RNA editing-site determines the codon change from Arginine to Glycine (conserved site R/G) to regulate receptor assembly and control the speed of recovery from desensitization (Dingledine et al. 1999; Gan et al. 2015).

The regulation of calcium (Ca^{2+}) permeability of the GluA2 subunit is determined by a RNA editing site Q/R located in the transmembrane M2 region of the protein (Fig. 3.13). This post-transcriptional modification changes the amino acid 607 glutamine (Q) to arginine (R) only in the GluA2 mRNA subtype. The GluA2 subtype that contains the R edited residue will be impermeable to Ca^{2+} . In contrast, the other AMPA subtype receptors GluA1, GluA3 and GluA4 maintain the glutamine (Q) residue and therefore they will be permeable to Ca^{2+} (Carlson et al. 2000; Greger et al. 2002; Wright & Vissel 2012). In addition, there are a number of polyamine derivatives and toxins, such as; spermine, spermidine, argiotoxin, Joro spider toxin and philanthotoxin that act as channel blockers in AMPA receptors lacking GluA2 subtype. These spider toxins and polyamines are attracted by the negative charges on the glutamine (Q) residue in GluA1, GluA3 and GluA4 and modify the calcium permeability and voltage-dependent of the receptor. The GluA2 subtype modified by RNA editing has a positive charged residue arginine (R) instead of glutamine (Q) resulting in the repulsion of positive charged polyamides and toxins (Pellegrini-Giampietro 2003 & Isaac et al. 2007).

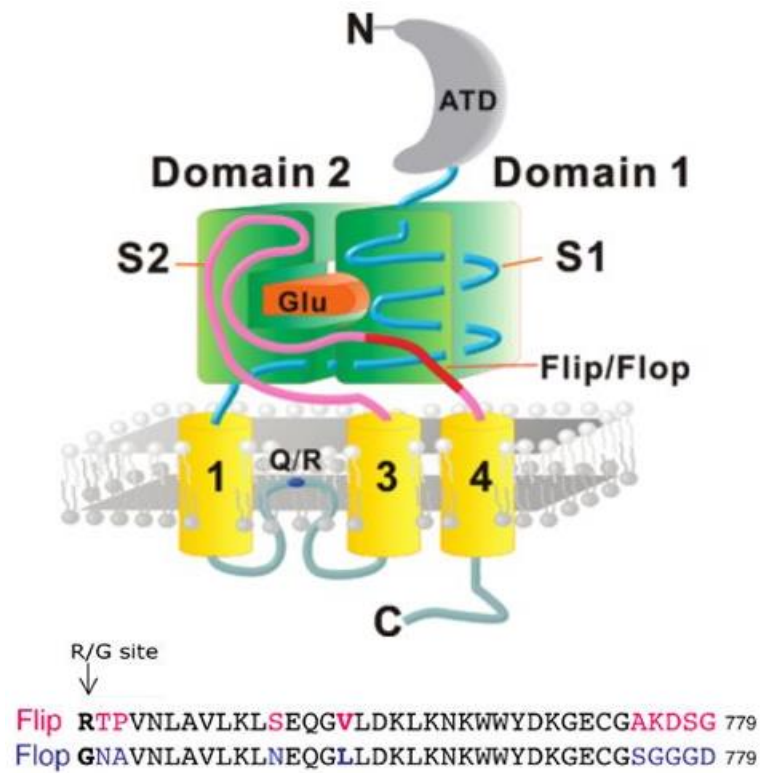


Figure 3.13. Schematic representation of the location and sequence comparison of the Flip/Flop AMPA subunit variations. Top, AMPA receptor structure, ATD in grey, LBD in green (S1 and S2 in blue and pink), TMD in yellow, NTD in light blue. Glutamate in orange, Q/R RNA editing site in TM2 re-entrant loop in dark blue circle and Flip/Flop region in red. Bottom, Flip/Flop sequence alignment in pink and purple, respectively. R/G editing site is indicated in bold for GluA2 receptor (Adapted from Zhang et al. 2008; Pei et al. 2009).

3.4.2.2 Activation and Inactivation of Ion Channel (Gating)

The term *gating* refers to the opening and closing of ion channels caused by conformational changes upon ligand binding/unbinding. This activation and inactivation can be measured electrophysiologically. The three steps involved in gating changes are; 1) activation (agonist binding and channel opening), 2) desensitization (clamshell closure to avoid agonist dissociation) and 3) inactivation (conformational change to induce ion channel closure) (Sobolevsky 2015). Gating might be disturbed at different sites along the receptor by small molecule inhibitors.

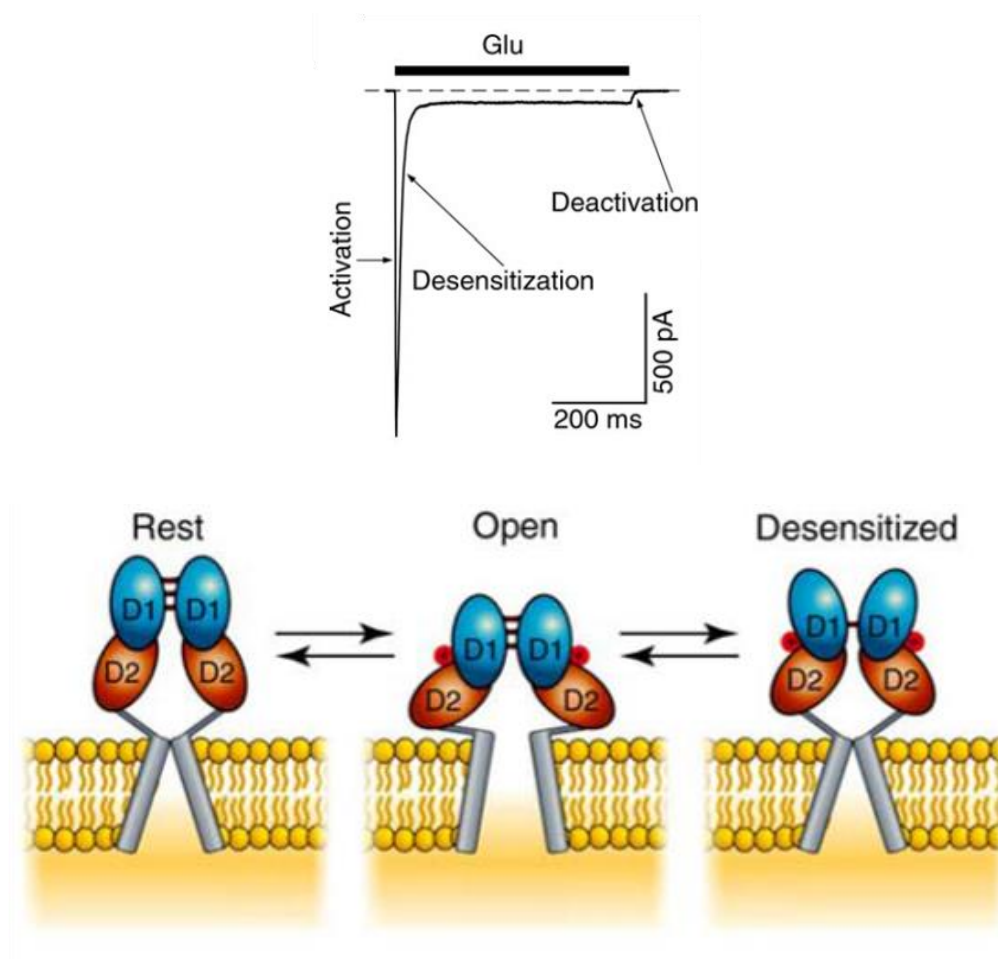


Figure 3.14. Gating steps in glutamate receptors. Top, electrophysiological measurement of the whole-cell current in HEK-293 rGluA2 at holding potential of -60 mV, displaying activation, desensitization and deactivation; 500 ms application of glutamate 3 mM, milliseconds (ms) and picopascal (pA). Bottom, representation of conformational changes involved in gating process; rest, open and desensitized in the LBD formed by domains 1 and 2 (D1 and D2) (Adapted from Perrais et al. 2010; Sobolevsky 2015).

3.4.2.3 AMPAR Auxiliary Proteins

AMPA receptors are able to form complexes with auxiliary proteins that are able to regulate receptor trafficking, channel activity, gating, synaptic transmission and pharmacology (Coombs & Cull-Candy 2009; Henley & Wilkinson 2016). Some of these auxiliary proteins are the AMPA receptor regulatory proteins (TARPs), cornichon homologues (CNIHs), germ cell-specific gene 1-like protein (GSG1L) and cysteine-knot AMPAR modulating proteins (CKAMPs) (Schwenk et al. 2009; Schwenk et al. 2012; Shanks et al. 2012 & Klaassen et al. 2016). These proteins are able to regulate the function of the receptor with both positive and negative gating modulation, in addition to controlling permeation and blockade of the channel (Riva et al. 2017). The most studied and characterized of these AMPAR auxiliary proteins are the TARPs family. There are seven types of TARPs; $\gamma 2$ (stargazin) and $\gamma 3-8$ (Henley & Wilkinson 2016). TARPs control the expression of receptors (postsynaptic membrane) and modulate the gating and pharmacology of AMPA receptors (Carbone & Plested 2016). For example, the TARP stargazin ($\gamma 2$) functions as a chaperone for AMPA receptors and has an essential role in receptor expression in cell surface. A study using in-vitro experiments showed that the absence of stargazin results in retention of the AMPA receptors in the endoplasmic reticulum and the lack of expression in cell surface of cerebellar granule cells (Chen et al. 2000). Recently, a forebrain-selective AMPA receptor antagonist was found to target GluA2- $\gamma 8$ complexes exclusively and might have potential for antiepileptic properties (Kato et al. 2016). This antagonist (LY3130481) prevented seizure types in rodents without presenting motor side effects, hence AMPA receptors auxiliary proteins could be used as potential drug targets (Kato et al. 2016).

3.4.2.4 Agonist Binding

Glutamate, kainate and AMPA shared similar interactions in the binding pocket of the LBD of GluA2. The three agonists showed conserved interaction with LBD residues in Arg-485 and Thr-480, however weak interactions between residues Glu-705, Ser-654 and Pro-478 are similar between agonists (Fig. 3.16; Armstrong & Gouaux 2000).

GluA2 LBD in complex with glutamate displayed specific interactions with Pro-478, Thr-480 and Arg-485 from the S1 domain and Ser-654, Thr-655 and Glu-705 from the S2 domain of the protein (Fig.3.16A). The α -carboxylate and α -amino group of glutamate have a key role in ligand recognition, the carboxylates and amino groups bind to the protein because they become desolvated. In addition, a mutation of the residue Arg-485 led to complete loss of the channel function suggesting the key role of this residue in ligand binding (Speranskiy & Kurnikova 2005; Serafimoska & Johansen 2011).

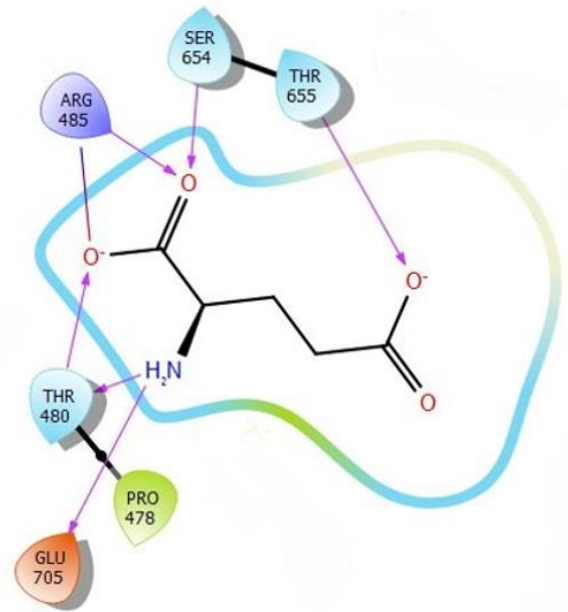
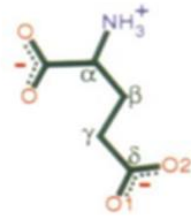
Kainate in complex with GluA2 displays hydrogen bond interactions with Pro-478, Thr-480, Arg-485, Ser-654 and Thr-655. Glu-705 was not observed to interact with kainate however it might form inter protein interactions with other residues inside the binding pocket (Fig. 3.16B). AMPA displayed similar interactions in the binding pocket with Thr-480, Arg-485 and Glu-705 (Fig. 3.16C). For all three agonist residues Arg-485 and Thr-480 bind to the structure forming strong hydrogen bonds with the α -carboxyl group of agonists (Armstrong & Gouaux 2000; Serafimoska & Johansen 2011).



Figure 3.15. GluA2-LBD in complex with glutamate. Glutamate in green ball and stick representation, S1 and S2 in blue and brown respectively. A disulphide bond was observed between S1 domain and S2 domain, 1FTJ PDB accession code (Armstrong & Gouaux 2000; Naur et al. 2005).

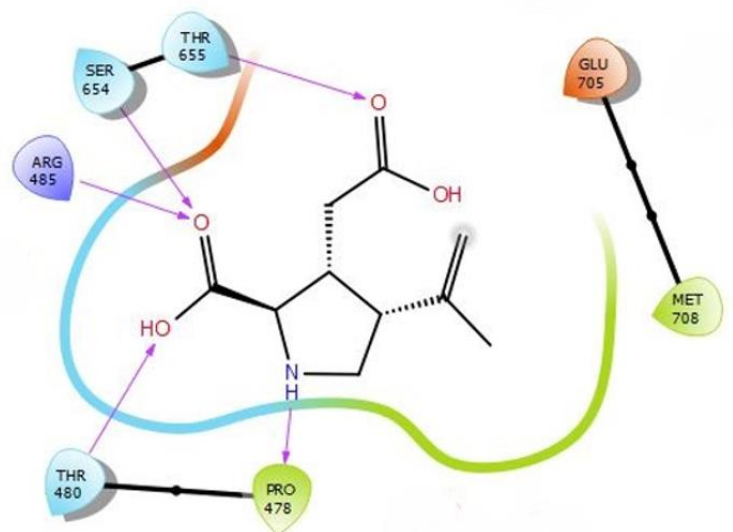
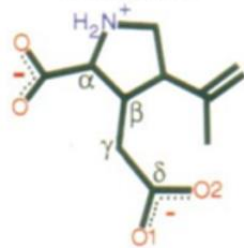
A)

L -Glutamate



B)

Kainate



C)

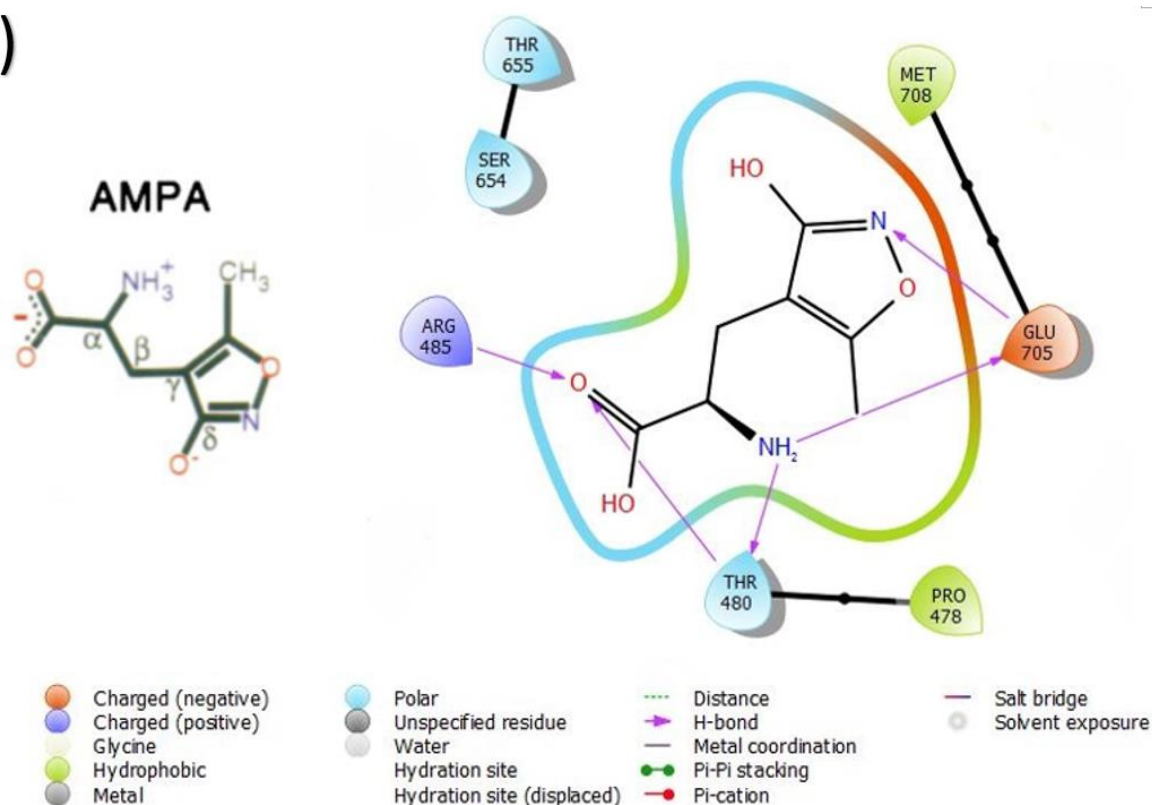


Figure 3.16. Glutamate, kainate and AMPA binding interactions. A) Left, chemical structure of glutamate with carboxyl group designated by α , β , γ and δ . Right, interaction binding pocket of GluA2 with glutamate, 1FTJ accession code. B) Left, chemical structure of kainate with carboxyl group designated by α , β , γ and δ . Right, interaction binding pocket of GluA2 with kainate, 1FW0 accession code. C) Left, chemical structure of AMPA with carboxyl group designated by α , β , γ and δ . Right, interaction binding pocket of GluA2 with AMPA, 1FTM accession code (Armstrong & Gouaux 2000). Diagrams were generated using Maestro Schrödinger.

3.4.2.5 AMPA Antagonist

There are two main classes of antagonists, competitive and non-competitive (Fig. 3.17). Both block and reduce the activation of the channel upon binding. Competitive antagonists compete with the agonist (orthosteric) binding site and the non-competitive antagonists bind to an allosteric site which is different from the agonist, both reduce or interfere with the activation of the channel (Gill & Pulido 2005).

AMPA antagonists will be described in detail in section 3.5.1.2 Antagonist and pharmacology.

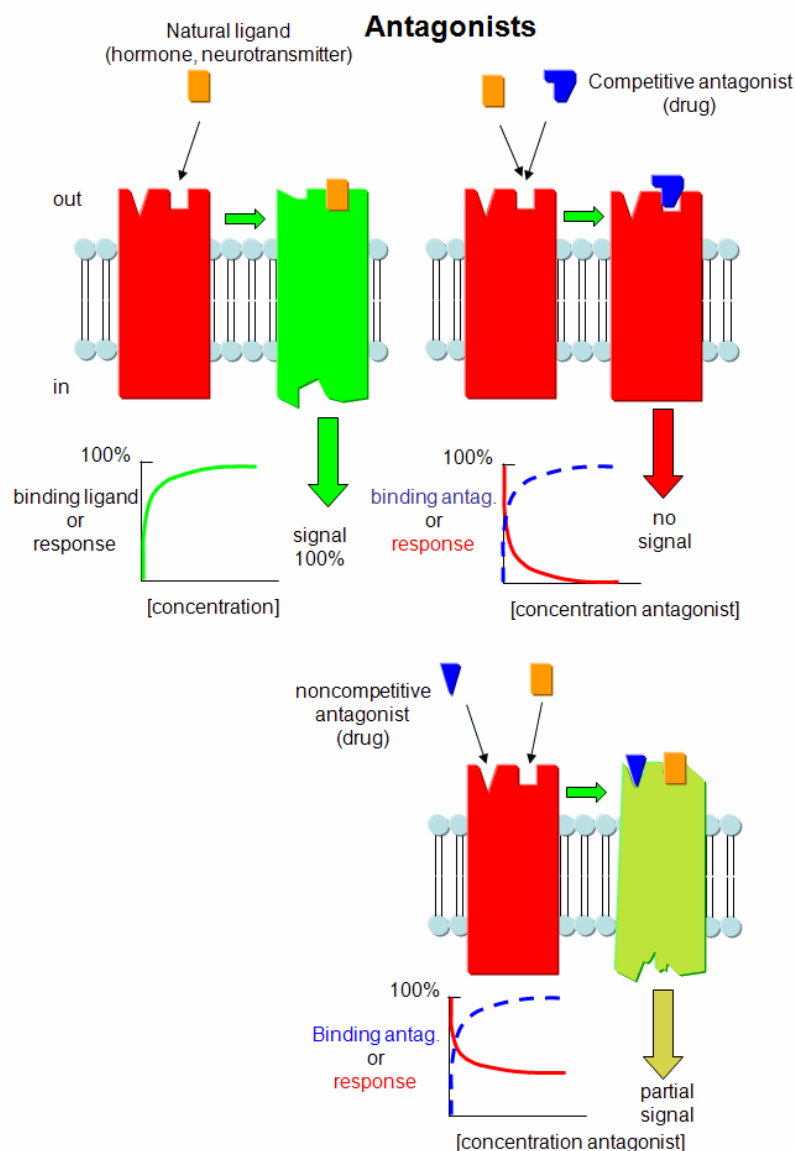


Figure 3.17. Competitive and non-competitive antagonist. Schematic representation of the mechanism of action of antagonist effect in membrane receptors. Image obtained from Biochemistry Online (http://employees.csbsju.edu/hjakubowski/classes/ch331/transkinetics/TK_6C6_Agonist_Anta_Lig_Bind_Recept.html).

3.4.3 KAINATE RECEPTORS

Kainic acid (Kainate) is a natural amino acid derived from the Japanese seaweed *Digenea simplex* (Coyle 1987) and is the preferred agonist for kainate receptors, it has also been shown to activate AMPA receptors. Kainate receptors assemble in five different subunits: GluK1, GluK2, GluK3, GluK4 and GluK5, they assemble as tetramers to form ion channels. GluK1-GluK3 can form functional homomeric and heteromeric receptors, however GluK4 and GluK5 can only form heteromeric receptors with other GluK1-GluK3 subunits to form the ion channel (Fig. 3.8; Lerma & Marques 2013). Compared to AMPA and NMDA receptors kainate receptor physiology is less understood. Kainate receptors are classified into low-affinity (GluK1-3) and high affinity (GluK4-5) receptors based on their affinity for kainate (Kristensen et al. 2016).

3.4.3.1 Kainate Receptor Structure

There are no crystal structures available for a kainate full-length receptor, however in 2014 a cryo-electron microscopy (EM) full-length GluK2 in complex with 2S,4R-4-methylglutamate at 7.6 Å resolution was published, PDB accession code 4UQQ (Meyerson et al. 2014). This full-length structure of a desensitized kainate receptor displays the formation of a tetramer formed by ATD, LBD, TMD and CTD subunits (Fig. 3.18). This full-length GluK2 EM structure displayed drastic conformational changes in the LBD and ion channel assemblies in the TMD (Fig. 3.19); these LBD symmetry changes complement the 4-fold symmetry of the ion channel in the TMD, inducing the closure of the channel (Meyerson et al. 2014; Møllerud et al. 2017). The general conformation of the characterised EM full-length GluK2 displays similarities with AMPA and NMDA general structure subunits, however the low-resolution of the structure makes it difficult to study the specific similarities or differences between both receptor families.

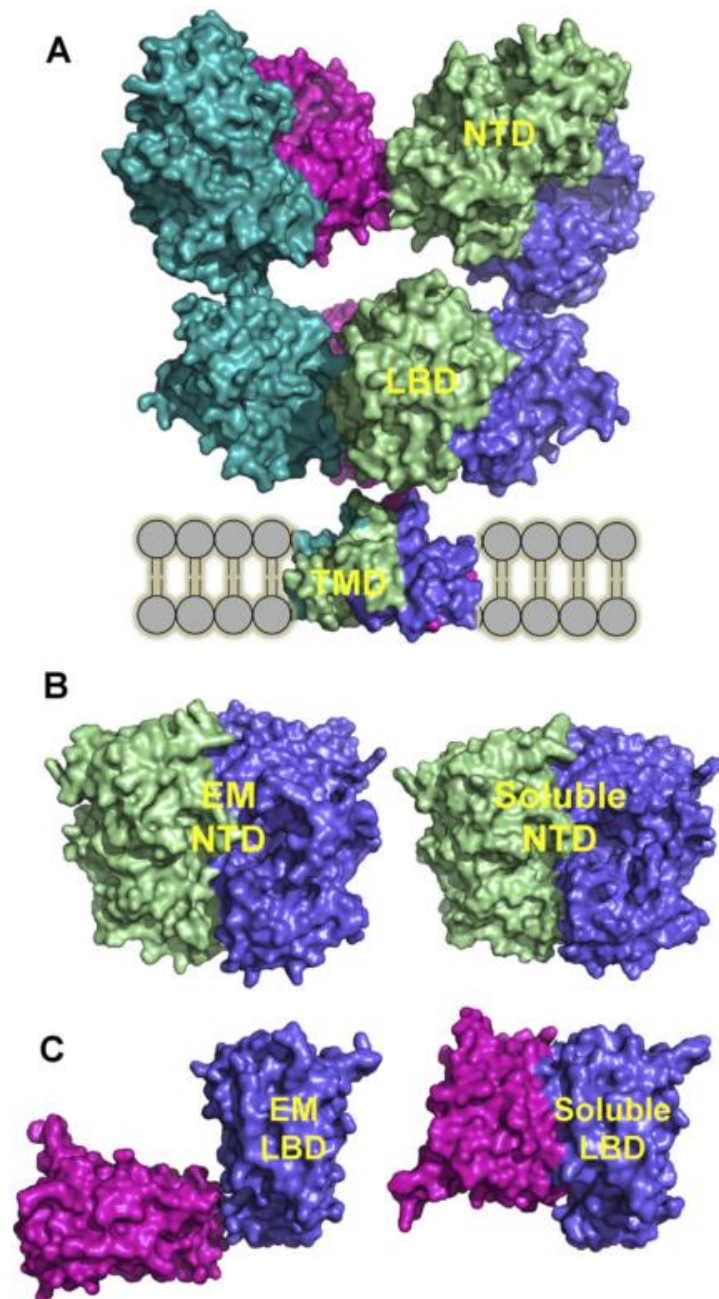


Figure 3.18. Electron microscopy structure of full-length GluK2. A. Full GluK2 structure in surface representation, different subunits are shown in blue, fuchsia, green and turquoise, PDB accession code 4UQQ with 7.6 Å resolution. B. Comparison of the amino terminal domain (NTD) dimer from EM with the soluble dimer construct, PDB accession code 3QLT. C. Comparison of the EM LBD dimer and a soluble construct, PDB accession code 2XXR (Møllerud et al. 2017).

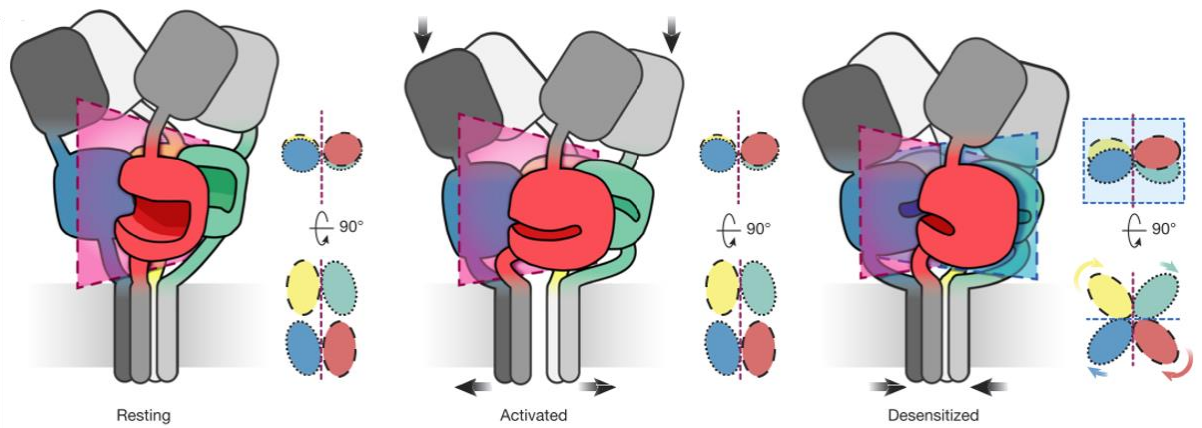


Figure 3.19. Conformational changes in the GluK2 gating process. Structural changes of the receptor in the transition from resting to activated to desensitized state. Circles representing the two-fold and four-fold symmetry of the ATD and the LBD (Adapted from Meyerson et al. 2016).

3.4.3.2 Ligand Binding Domain

There is a vast amount known about the specific structural differences of the ligand binding properties of AMPA, kainate and NMDA receptors, however X-ray crystallography has played an important role in defining the mechanism of binding between different ligands and receptors.

Table 3.1. Crystal structures of the LBD in complex with different ligands

PDB code	Ligand	Resolution Å	Origin	Reference
GluK1				
1TXF	Glutamate	2.1	Rat	(Mayer 2005)
1YCJ	Glutamate	1.95	Rat	(Naur et al. 2005)
2F36	Glutamate	2.11	Rat	(Mayer 2006a)
2PBW	Domoate	2.5	Rat	(Hald et al. 2007)
3C31	Kainate	1.49	Rat	(Plested et al. 2008)
2ZNS	Glutamate	2.0	Human	(Unno et al. 2011)
3FUZ	Glutamate	1.65	Human	(Unno et al. 2011)
GluK2				
1S50	Glutamate	1.65	Rat	(Mayer 2005)
1S7Y	Glutamate	1.75	Rat	(Mayer 2005)
1SD3	*	1.80	Rat	(Mayer 2005)
1TT1	Kainate	1.93	Rat	(Mayer 2005)
1S9T	Quisqualate	1.80	Rat	(Mayer 2005)
1YAE	Domoate	3.11	Rat	(Nanao et al. 2005)
3G3F	Glutamate	1.38	Rat	(Chaudhry et al. 2009)
2XXR	Glutamate	1.6	Rat	(Nayeem et al. 2011)
GluK3				
3S9E	Glutamate	1.6	Rat	(Venskutonytė et al. 2011)
3U93	Glutamate	1.88	Rat	(Veran et al. 2012)
3U94	Glutamate	1.96	Rat	(Veran et al. 2012)
4MH5	Glutamate	1.65	Rat	(Venskutonytė et al. 2011)
3U92	Kainate	1.90	Rat	(Veran et al. 2012)
GluK4	No crystal structures available			
GluK5	No crystal structures available			

*2S,4R-4-methylglutamate

In 2005 the LBD of the GluK1 in complex with glutamate was crystallised for the first time (Naur et al. 2005) see Table 3.1 for list of PDB accession codes. Shortly after, the crystal structures of the LBD of GluK2 in complex with glutamate, 2S,4R-4-methylglutamate, kainate and quisqualate were solved (Mayer 2005). In the same paper they also reproduced the crystal structure of the GluK1 LBD in complex with glutamate (Mayer 2005). These X-ray structures revealed similarities in the binding core between kainate and AMPA receptors, with glutamate binding in the cavity interface between domain one and two (S1 and S2) having the same clamshell-like structure in the LBD (Fig.3.7 & 3.20A).

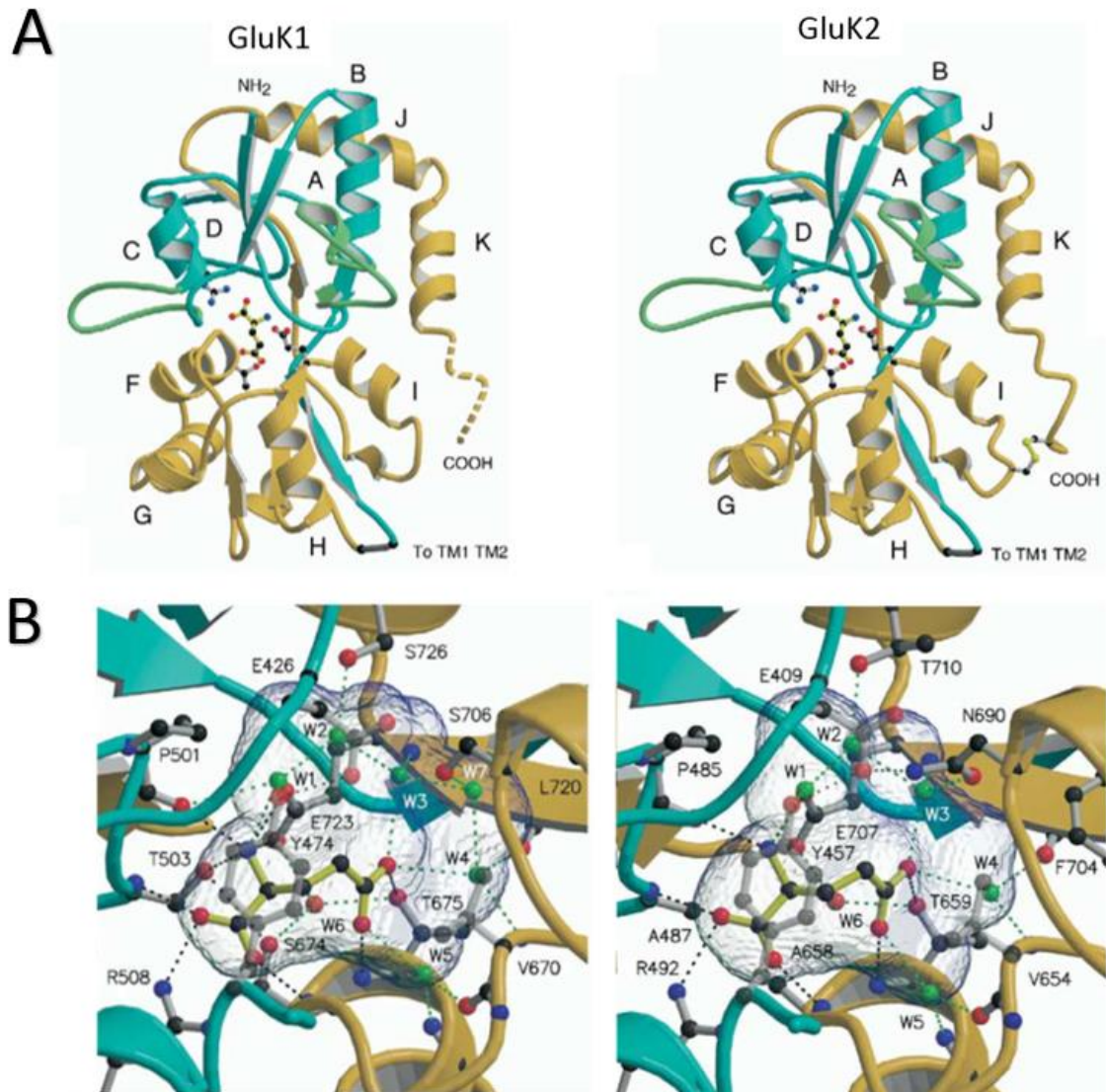


Figure 3.20. LBD binding pocket GluK1 and GluK2 in complex with glutamate. A) LBD formed by S1 and S2 in blue and mustard, loop 1 and 2 in green, helices are numbered alphabetically. Glutamate and conserved amino acids arginine (R), threonine (T) and glutamic acid (E) are displayed in ball and stick representation. B) 3-dimensional view of the binding core with glutamate, conserved amino acids GluK2 (GluK1); R492 (R508), T659 (T675), and E707 (E723). Solvent accessible surface area of the binding cavity with glutamate is displayed as a transparent surface. Black dashes represent hydrogen bonds and ion interactions and green dashes are trapped water molecule interactions (Adapted from Mayer 2005).

Glutamate binding in both GluK1 and GluK2 was conserved between amino acids arginine, glutamate and threonine similar to GluA2 AMPA (Fig. 3.20; Armstrong & Gouaux 2000; Mayer 2005). In one crystal structure of GluK2 Mayer found a conserved disulphide bond between Cys-773 in the extending end of helix K and Cys-719 in the loop linking C terminal of helix I (Fig. 3.20) similar to observed in GluA2 AMPA LBD (Armstrong et al. 1998; Mayer 2005). However the presence or absence of disulphide bond did not modify the structure in both crystal forms (orthorhombic and hexagonal) (Mayer 2005). The importance or function of this conserved disulphide bond formed in the hexagonal crystal form of GluK2 is still not understood. Altogether it was demonstrated that the mechanism of binding between glutamate α -carboxyl and α -amino groups is almost the same between GluK1, GluK2 and GluA2 forming interactions with conserved residues arginine and glutamic acid (Mayer 2005).

The binding mechanism of GluK2 LBD in complex with kainate displays the same binding mode to glutamate with the exception of kainate pyrrolidine ring replacing the water W1 atom and separating the solvent hydrogen bond network, linking the side chain of Thr-710 to the α -amino group of kainate (Fig. 3.21; Mayer 2005).

GluK1 to GluK3 receptors shared several structural similarities in the LBD ligand pocket. A LBD alignment of the three receptors in complex with glutamate reveals the same clamshell-like structure and same binding core for glutamate in the interface between domain 1 and domain 2 (Fig. 3.22; Møllerud et al. 2017). Currently there are five crystal structures of the LBD of GluK1, four structures of GluK2 and four of GluK3 all in complex with glutamate (Table 3.1). All these structures shared similar binding mechanism with glutamate agonist, more specifically the α -carboxylate group of glutamate forms a salt bridge interaction with residue Arg-523 from domain 1 and then will form hydrogen bonds with residues Thr-518 from domain 1 and Ser-689 from domain 2. The α -ammonium group interacts with Glu-738 forming a salt bridge, as well as hydrogen bonds with Pro-516, Thr-518 and a water molecule W1. The γ -carboxylate of glutamate will form hydrogen bonds with Ser-689, Thr-690 and three water molecules W2, W3 and W4 (Fig. 3.21A; Møllerud et al. 2017).

Interestingly glutamate binding pocket shared the same residues in GluK1 rat and human within 4 Å of glutamate. From the ten residues found within 4 Å of glutamate in GluK1, only Thr-518 and Ser-689 are different between GluK1-GluK3 structures (Fig. 3.22). Thr-518 of GluK1 is conserved in GluK3 but changed to alanine for GluK2. Additionally Ser-689 of GluK1 changes to alanine in GluK2 and GluK3. These few differences create a larger binding pocket for glutamate in GluK2 compared to GluK1 (Møllerud et al. 2017).

In summary, the agonist ligand binding pocket of kainate GluK1-GluK3 receptors displayed similarities, suggesting a similar binding mode of action. Ligand binding can induce some small changes in the secondary structure, these differences might be key for understanding selectivity between glutamate receptors and aid in drug design research for therapeutic purposes.

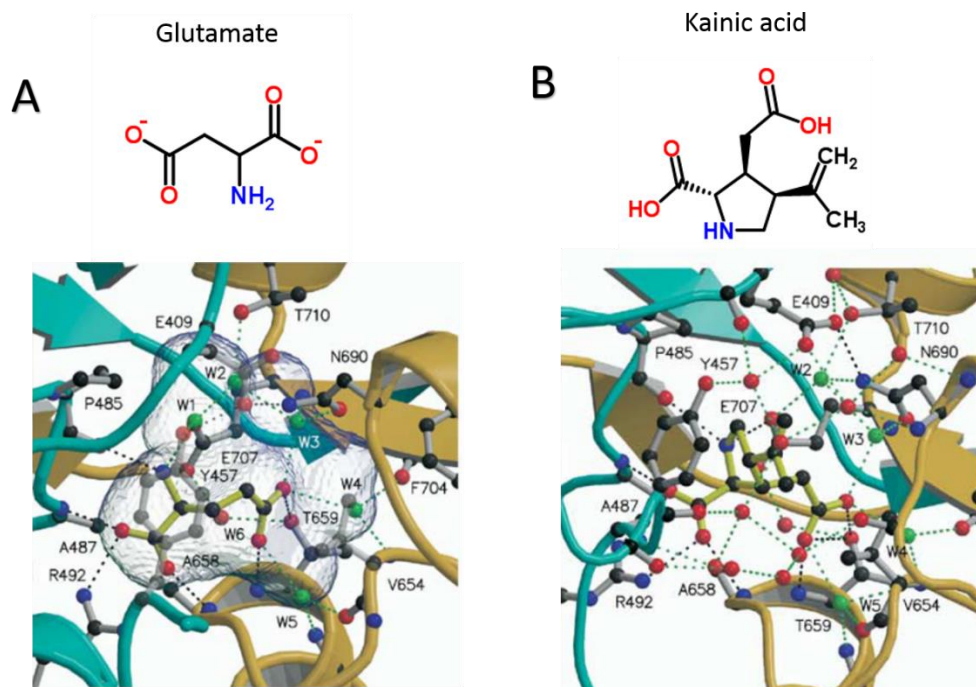


Figure 3.21. GluK2 structure in complex with glutamate and kainate. A) Glutamate binding interactions, previously described in Fig. 3.20. B) 3-dimensional view of the GluK2 in complex with kainate, domain one and two are in blue and mustard. Kainate molecule in yellow ball stick representation, kainate interactions in black dashes, water molecules in green, water atoms forming hydrogen bond are in red (Adapted from Mayer 2005).

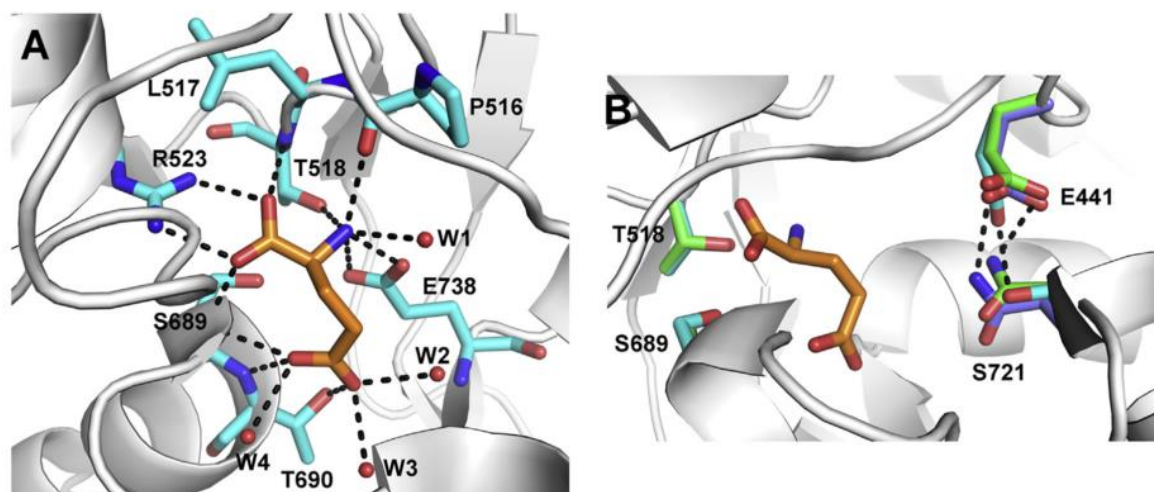


Figure 3.22. Glutamate binding site pocket for kainate receptors GluK1, GluK2 and GluK3. A) Glutamate in orange, GluK1 residues that interact with agonist in cyan, hydrogen bonds in black dashes and water molecules in red spheres. B) Binding sites differences for glutamate binding in GluK1, GluK2 and GluK3 in cyan, purple and green respectively, accession codes 2F36, 2XXR and 4MH5. Amino acids numbering correspond to GluK1 sequence (Møllerud et al. 2017).

3.4.3.3 Kainate Agonists

As previously discussed kainic acid is the natural agonist for kainate receptors, however other molecules such as domoic acid and 5-iodowillardiine can also activate kainate receptors. Domoic acid (domoate) was identified for the first time in a sample of Japanese red algae *Chondria armata* (Daigo 1959) in a study focused on identifying novel anthelmintic compounds. In 1982, domoic acid was synthesised for the first time (Ohfune & Tomita 1982) but it was not discovered until 1987 that domoic acid was toxic for humans when in Canada hundreds of people experienced poisoning symptoms after eating contaminated mussels (Hynie et al. 1990). Domoate is an analogue of glutamate and shares structural similarity with kainic acid, this toxin is responsible for causing amnesic shellfish poisoning (ASP; Pulido 2008). Domoate activates AMPA and kainate receptors by binding in the orthosteric site and causes an uncontrolled influx of calcium in neurons inducing apoptotic and necrotic neuronal cell death; domoate prevents the channel from rapid desensitization in both AMPA and kainate receptors, in addition to synergistic effect with NMDA receptors that results in excitotoxicity (Pulido 2008; Hogberg & Bal-Price 2011). Crystal structure of GluK2 LBD in complex with domoate was solved in 2005 and two years later the GluK1 LBD in complex with domoate was characterised (PDB accession codes 2PBW and 1YAE).

Both crystal structures show similar residue interactions to kainate (Nanao et al. 2005; Hald et al. 2007). Similar to domoate, kainate in high concentrations can cause neuronal cell death and neurotoxic effects (Zhang & Zhu 2011).

A derivative of AMPA agonist results in (S)-2-amino-3-(3-hydroxy-5-ter-butylisoxazol-4-yl) propionic acid (ATPA) a potent and highly selective agonist for GluK1 kainate receptors, with low affinity in AMPA receptors (Goot 2002; Nielsen et al. 2003). Crystal structure of the LBD of GluK1 in complex with ATPA has not been crystallised yet.

(S)-5-Iodowillardiine a willardiine analogue with agonist properties for glutamate receptors, has shown strong selectivity for kainate receptors over AMPA receptors and no interaction with NMDA receptors (Jane et al. 1997; Swanson et al. 1998).

Another selective agonist at kainate receptors is the (2S,4R) 4-methyl glutamic acid (SYM2081), this glutamate analogue displayed preferential selectivity for kainate receptors over AMPA receptors, and displayed similar potencies for GluK1 and GluK2 subtypes, this agonist also induced pronounced desensitization (Zhou et al. 1997; Jane et al. 2009; Traynelis et al. 2010).

Table 3.2. Agonist affinities to AMPA, kainate and NMDA receptors

Agonist	iGluRs		
	AMPA	Kainate	NMDA
Glutamate	++	++	++
Kainate	+	++	+
Domoate	++	++	++
(S)-5-Iodowillardiine	+	++	-
ATPA	+	++	-
SYM2081	+	++	+

++ Strong affinity and + low affinity, – no affinity

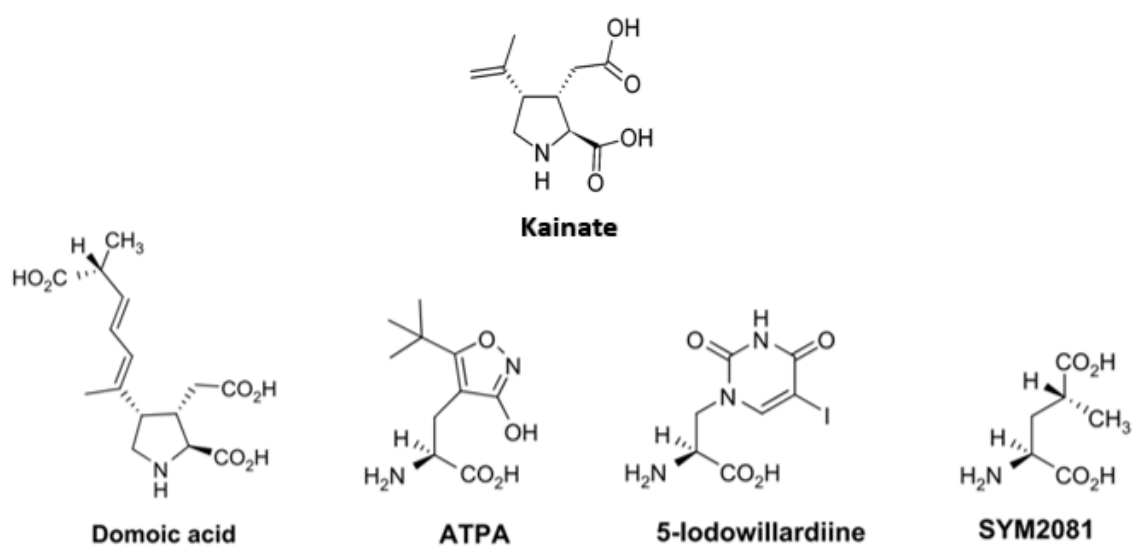


Figure 3.23. Structures of kainate receptor agonists (Adapted from Jane et al. 2009).

Kainate antagonists will be described in detail in iGluRs section 3.5.2.2, antagonist and pharmacology.

3.4.4 NMDA RECEPTORS

NMDA receptors have three different subunits GluN1-GluN3. Post-transcriptional RNA processing of GluN1 results in eight different variants (alternative splicing) of the gene GRIN1 located in two sites of the structure (Fig. 3.24), the N-terminus of the ATD and the C-terminus of the CTD (Vance et al. 2012; Vyklicky et al. 2014; University of Bristol 2017). GluN2 subunits are encoded by four subtypes GluN2A-D and GluN3 by two subtypes GluN3A and GluN3B (Vyklicky et al. 2014).

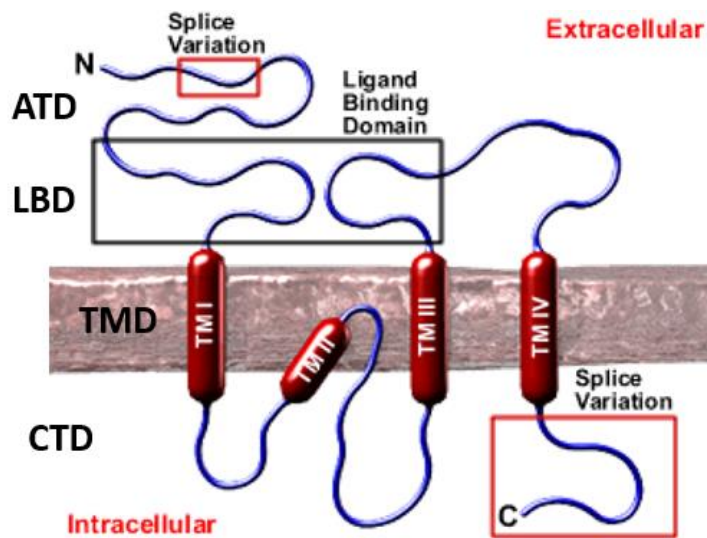


Figure 3.24. RNA alternative splicing in NMDA receptor subunit. Structure of the NMDA receptors, in red boxes show the regions of splice variation (University of Bristol, NMDA receptors; Adapted from <http://www.bristol.ac.uk/synaptic/receptors/nmdar/>).

NMDA receptors form functional heterotetramers containing two obligatory GluN1 subunits in association with two GluN2 and/or GluN3 subunits. This combination of different subunits results in a large number of different NMDA receptors with different pharmacological and biological processes.

The structure of NMDA receptors is similar to AMPA and kainate receptors, an extracellular amino-terminal domain (ATD) linked to a ligand binding domain (LBD) connected to a transmembrane domain (TMD) and an intracellular carboxyl-terminal domain (CTD) (Fig. 3.24 & 3.25). The full heterotetrameric GluN1-GluN2B solved at 3.96 Å (accession code PDB 4PE5) displayed a similarity in the dimer-dimer conformation for tetramer arrangement compared to other iGluRs. One significant structural difference is the more compact structure in the ATD and LBD, compared to the “Y” shape observed with AMPA and kainate receptors (Fig. 3.25; Karakas & Furukawa 2014).

This full-length structure of GluN1-GluN2B was crystallised in complex with glutamate, glycine and an allosteric inhibitor ifenprodil, a highly selective inhibitor for NMDA GluN2B subunit binding in the ATD. The structure represents the allosterically inhibited state of the receptor (Karakas & Furukawa 2014). Interestingly, a recent study using single particle cryo-electron microscopy (cryo-EM) combined with double electron-electron resonance investigated the structures of heterotetramer GluN1-GluN2B in complex with agonists (glutamate and glycine), agonists and allosteric inhibitor (Ro25-6991) and antagonists 5,7-dichlorokynurenic acid (DCKA) and D-(-)-2-amino-5-phosphonopentanoic acid (D-APV) (PDB accession codes in Table 3.3; Zhu et al. 2016). This study proposed a mechanism of NMDA receptor inhibition and activation; firstly the binding of agonist glutamate in combination with glycine helps stabilize the LBD heterodimers and retain the gating ring formed by a dimer-dimer configuration from the LBD. Binding of the allosteric inhibitor Ro25-6981 in the ATD then induces the strength of LBD dimer interactions and stabilizes the LBD layer with ATD. Finally, the binding of competitive antagonist induces the separation and turns over of the LBD disrupting the LBD interactions with ATD and disrupting LBD gating ring (Fig. 3.26). A brief summary of the structural information of NMDA receptors is provided, however the purpose of this research is to focus on AMPA and Kainate receptors in more detail.

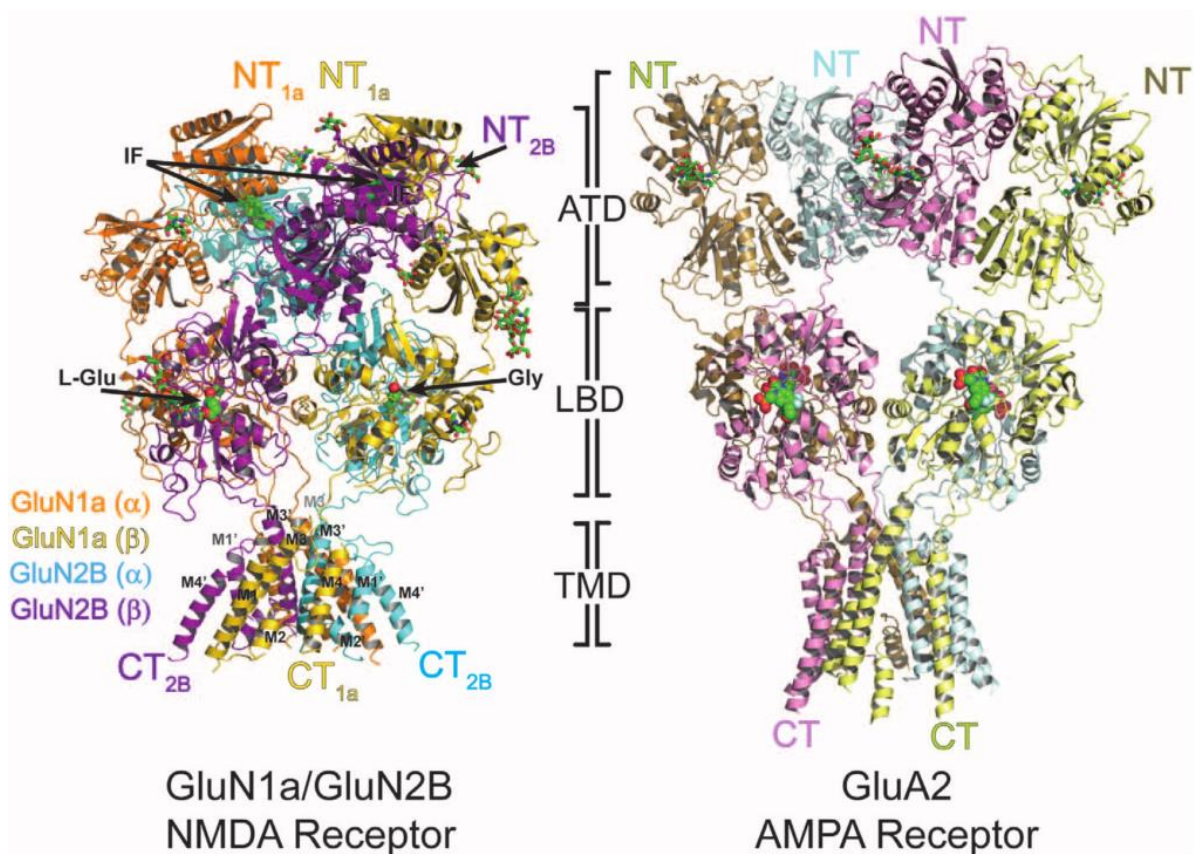


Figure 3.25. Comparison of the heterotetrameric GluN1-GluN2B receptor and the homotetrameric GluA2 receptor. NMDA GluN1a and GluN2B subunits labelled as GluN1a (α), GluN1a (β), GluN2B (α) and GluN2B (β) in orange, yellow, blue and purple respectively. Ifenprodil (IF) situated at the ATD interfaces, glutamate (L-Glu) and glycine (Gly) in the LBD are in green. NT, N-terminal and CT, C-terminal (Karakas & Furukawa 2014).

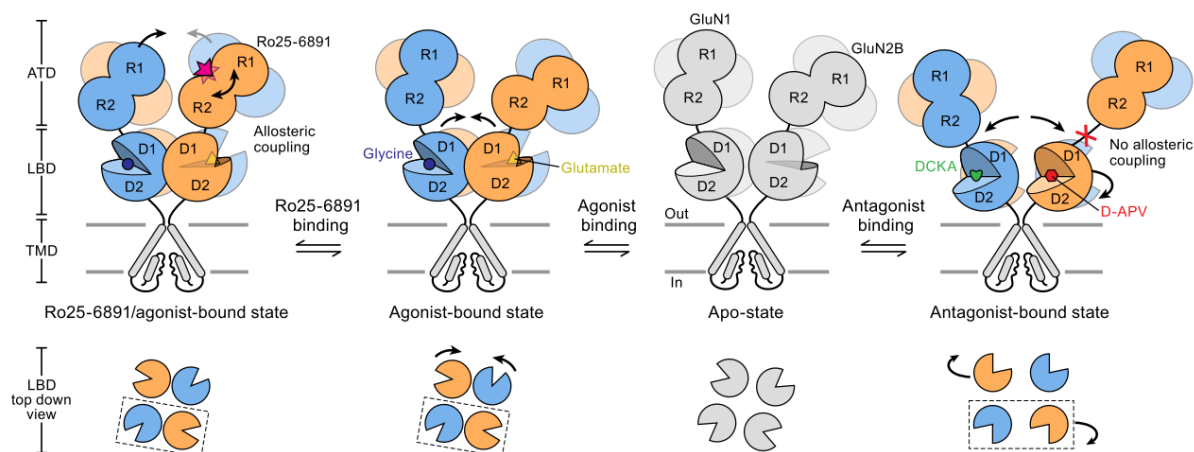


Figure 3.26. Schematic representation of the proposed mechanism of NMDA receptor inhibition and activation. Top, conformational changes of the extracellular domains ATD and LBD with agonist glutamate + glycine, allosteric inhibitor Ro25-6891 and competitive antagonist 5, 7-dichlorokynurenic acid (DCKA) and D-(-)-2-amino-5-phosphonopentanoic acid (D-APV). Bottom, top-down representation of LBD conformations. The Apo-state is shown in grey due to no currently publish structure being available (Zhu et al. 2016).

Table 3.3. Cryo-EM structures of GluN1/GluN2B NMDA receptor

Accession code	In complex with	Resolution Å
5IOU	Glutamate + glycine	7.0
5IOV	Glutamate + glycine + Ro25-6981	7.5
5IPQ	DCKA/D-APV (Class 1)	13.5
5IPR	DCKA/D-APV (Class 2)	14.1
5IPS	DCKA/D-APV (Class 3)	13.5
5IPT	DCKA/D-APV (Class 4)	14.1
5IPU	DCKA/D-APV (Class 5)	15.4
5IPV	DCKA/D-APV (Class 6)	9.25

5,7-dichlorokynurenic acid (DCKA); D-(-)-2-amino-5-phosphonopentanoic acid (D-APV). Six different classes (conformations) of the DCKA/D-APV antagonist using double electron-electron resonance (DEER; Zhu et al. 2016).

3.5 iGluRs FUNCTION AND PHARMACOLOGY

3.5.1 AMPA RECEPTORS

3.5.1.1 FUNCTION AND DISTRIBUTION

AMPA receptor subtypes GluA1-GluA4 have been found in the CNS, specifically with high levels of expression in the brain cerebral cortex, basal ganglia, thalamus, hypothalamus, hippocampus, cerebellum and spinal cord measured using [³H] AMPA binding studies and in-situ hybridization histochemistry (Olsen et al. 1987; Insel et al. 1990; Keinänen et al. 1990; Sommer et al. 1990; Stone 1995; Ozawa et al. 1998; Catarzi et al. 2007). Furthermore, AMPA autoradiography studies have found high density of AMPA anatomical distribution in the hippocampus (CA1 stratum radiatum and dentate gyrus), neurocortex (outer layers) and molecular layers of the cerebellum (Davis 2002). The hippocampus is responsible for short and long-term memory while the neurocortex plays a role in memory, language, cognition, attention and perception. The cerebellum plays an important role in balance and motor control but is also involved in cognitive functions (such as language and attention) and processing of procedural memory (unconscious memory) (Kryukov 2008; Kumaran 2008; Mochizuki-Kawai 2008; Rakic 2009).

AMPA receptors mediate the majority of fast excitatory synaptic transmissions in the CNS and have an important role in long-term potentiation (Joshi et al. 2012). Long-term potentiation (LTP) is the outcome of the increased activity between two neurons and is important for learning and memory processes.

Frequently AMPA and NMDA receptors are located closer to each other in the presynaptic neurons, the traveling of an action potential in neurons results in the release of neurotransmitter glutamate. Glutamate then binds to both AMPA and NMDA receptors, if a small amount of glutamate is released, only AMPA receptors will allow the influx of Na⁺ ions into the postsynaptic neuron to cause a depolarization event; NMDA receptors usually have Mg²⁺ or Zn²⁺ ion that block the transport of ions through the channel. For LTP to occur a high-frequency action potential is necessary to release a larger amount of neurotransmitter from presynaptic neurons. When glutamate binds to AMPA receptors a greater depolarization event causes the AMPA receptors to remain open for longer and increases the influx of Na⁺ into the neuron. The large amount of Na⁺ influx will cause a larger depolarization in the neuron and will cause the release of Mg²⁺ or Zn²⁺ from the NMDA channel pore by a process called electrostatic repulsion, allowing the entering of ions such as Ca²⁺ through the pore (Offermanns & Rosenthal 2008).

The Ca^{2+} influx in the postsynaptic neuron causes the phosphorylation and activation of Ca^{2+} /calmodulin-dependent kinase II (CAMKII), this protein kinase promotes the trafficking and membrane exocytosis processes of AMPA receptors (Fig. 3.27; Lisman et al. 2002; Herring & Nicoll 2016). Protein kinase A (PKA) is also activated by the Ca^{2+} influx and both kinases phosphorylate AMPA receptors to enhance the conductance of the receptor (Kim et al. 2010). The upregulation of AMPA receptors is necessary for the induction of LTP (Cull-Candy et al. 2006; Chater & Goda 2014).

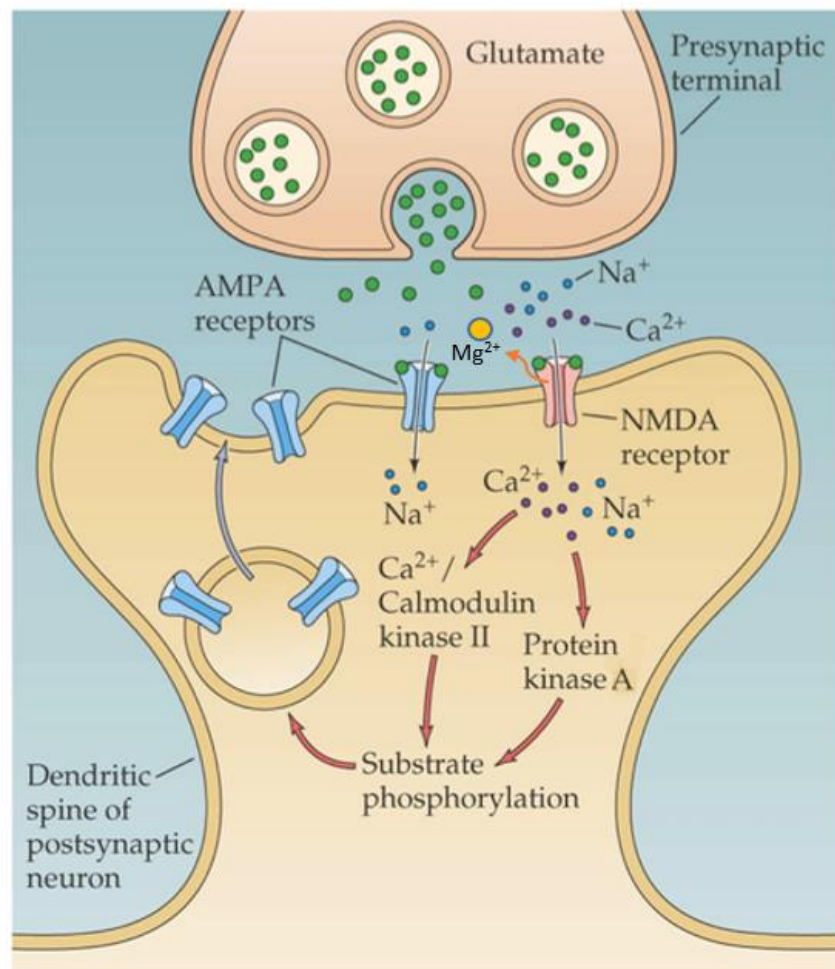


Figure 3.27. Mechanism of long-term potentiation (LTP). (Adapted from The Human Brain: From neuron to nervous system, <http://neurones.co.uk/Neurosciences/Tutorials/M1/M.1.B.4%20Ionotropic.html>).

3.5.1.2 Antagonists and Pharmacology

AMPA receptors have been found to play an important role in epilepsy; prolonged activation of AMPA receptors results in high levels of excitability, also upregulated activation of AMPA can generate proliferation of seizures. Antagonists of AMPA receptors have been shown to protect against seizures *in vitro* and *in vivo* in animal models (Rogawski 2013; Hanada et al. 2014; Twele et al. 2015). AMPA antagonists have shown remarkable reductions in epileptiform, as well as reducing epileptic discharges in human seizures and epilepsy models (Kasteleijn-Nolst Trenité et al. 2015; Twele et al. 2015; Chen et al. 2016). AMPA antagonists such as 2,3-dihydroxy-6-nitro-7-sulfamoyl-benzo[f]quinoxaline-2,3-dione (NBQX), Selurampanel (BGG492) and Perampanel are a promising new target for epilepsy therapy.

Table 3.4. Summary of AMPA antagonist drugs.

Drug	Clinical stage	Use/Treatment	Comments	Reference
Competitive Antagonist				
Fanapanel	Phase II	Acute ischemic stroke	Halted for intolerable side effects: high levels of sedation, drop of consciousness and transient neurological deterioration	(Elting et al. 2002)
Becampanel	Phase II	Epilepsy, anticonvulsant	Discontinued, no more information published	(Suter et al. 2002)
NS1209	Phase II	Refractory status epilepticus	Inconclusive and incomplete results	(Sabers et al. 2013) (Keppel 2017)
Tezampanel	Phase II	Acute migraine	FDA approved phase III but study has not started due to financial constraints	(www.clinicaltrials.gov)
Negative allosteric modulators (NAMs)				
Talampanel	Phase I & II	Anticonvulsant	Halted due to finding various drug interactions	(Bialer et al. 2007; Rogawski 2013)
Perampanel	Marketed	Epilepsy	Commercial name Fycompa by Eisai Co. Adverse side effects: somnolence, dizziness, fatigue, irritability and nausea.	(Besag & Patsalos 2016)
Positive allosteric modulators (PAMs)				
Aniracetam	Marketed	Dementia, supplement for cognitive function	Nootropic drug not approved by the FDA, however it is a prescription drug in Europe	(Nakamura 2006; Koliaki et al. 2012)
Piracetam	Marketed	Myoclonus and supplement for cognitive function	Nootropic drug not approved by FDA but sold in Europe, Asia and South America	(Einstein & McDaniel 2004)
Cyclothiazide	Marketed	Diuretic and antihypertensive	Currently discontinued for marketing by the FDA registry	(Antlitz & Valle 1967; Fucile et al. 2006)

AMPA Competitive Antagonists

The group of quinoxaline compounds were the first selective and potent AMPA receptor antagonist that have been found to display neuroprotection and reduce seizures in epilepsy models (Joshi et al. 2012). The discovery of 2,3-dihydroxy-6-nitro-7-sulfamoyl-benzo[f]quinoxaline-2,3-dione (NBQX) and 6-cyano-7-nitroquinoxaline-2,3-dione (CNQX) as potent and selective antagonists of the AMPA receptor in 1988 (Honoré et al. 1988; Sheardown et al. 1990) has initiated the synthesis and study of several quinoxaline type compounds. NBQX and CNQX were found to have anticonvulsant activity in mouse seizure models (Chapman et al. 1991; Namba et al. 1994; Maj et al. 1995; Szczurowska & Mareš 2013). Other quinoxaline derivatives found with anticonvulsant activity are; DNQX, YM-872, YM-90K, ZK-200775 (Fanapanel) and AMP397 (Becampanel) (Shimizu-Sasamata et al. 1996; Turski et al. 1998; Takahashi et al. 2002; Catarzi et al. 2007; Joshi et al. 2012; Rogawski 2013). Fanapanel was in phase II clinical trials in patients with acute ischemic stroke, however it was terminated due to intolerable side effects such as glial cell toxicity and neurological deterioration (Elting et al. 2002).

Another selective AMPA antagonist pyrazine derivative 9-carboxymethyl-imidazo-[1-2a]indeno[1-2e]pyrazin-4-one-2-carboxylic acid (RPR117824) has been discovered to be a potent compound with anticonvulsant activity in mouse models (Mignani et al. 2002).

Isatin oxime compounds such as NS1209 (SPD502), have also been shown to inhibit GluK1 kainate receptors (Nielsen et al. 1999; Pitkänen et al. 2007). NS1209 was tested in humans in a phase II clinical trial for Refractory Status Epilepticus (RSE). The compound displayed good tolerability in humans, however the results were inconclusive (Sabers et al. 2013). Tezampanel (LY293-558 or NGX-242) a drug developed by Eli Lilly is a competitive antagonist of AMPA receptors and also presents great antagonist potency against GluK1 kainate receptors (Rogawski 2013). This drug has been approved by FDA to initiate phase III clinical trials for acute migraine (NCT00567086, www.clinicaltrial.gov).

AMPA Non-Competitive Antagonists

The non-competitive (negative allosteric) antagonists of AMPA receptors are the most potent and have less toxic side effects compared to other antagonists (Tarnawa & Vize 1998; Donevan & Rogawski 1993). The first non-competitive AMPA receptor antagonist identified was 1-(4-aminophenyl)-4-methyl-7,8-methylenedioxy-5H-2,3-benzodiazepine (GYKI 52466) and was used as a model for the development of novel, more potent, less toxic and more selective 2,3 benzodiazepines. Derivatives of GYKI 52466 include GYKI 53405, GYKI 53655 and GYKI 53773 and have displayed a wide range of anticonvulsant activity in several animal models (Chapman et al. 1991; Szabados et al. 2001; Rogawski 2013; Dhir & Chavda 2016). GYKI 53773, also known as talampanel, displayed great efficacy in reducing seizure frequency in a clinical trial, however various drug interactions were found, specifically with carbamazepine (Bialer et al. 2007; Rogawski 2013).

Other unrelated non-competitive AMPA antagonists include the phthalazine YM928, the imidazole GYKI 47264, the quinazolin-4-one CP-465,022 and the bipyridine benzonitrile Perampanel (Abrahám et al. 2000; Menniti et al. 2000; Ohno et al. 2003). The latter, 2-(2-oxo-1-phenyl-5-pyridin-2-yl-1,2-dihydropyridin-3-yl) benzonitrile (perampanel) is a selective non-competitive AMPA receptor antagonist drug with the commercial name Fycompa (Eisa Co.). It was approved by the FDA in 2012 for the treatment of primary generalized tonic-clonic seizures (PGTCS) in patients with epilepsy; adverse effects include dizziness, somnolence, fatigue, irritability and nausea (Besag & Patsalos 2016).

Balannik and co-workers found using mutagenesis experiments that non-competitive antagonists (GYKI-53655 and CP-465,022) bind in an interface between S1 and S2 of the LBD and the transmembrane spanning regions, more specifically between S1-M1 and S2-M4 linkers (Fig. 3.28; Balannik et al. 2005). In 2016 the full-length GluA2 in complex with the antagonist GYKI 53655, CP 465,022 and Perampanel was successfully crystallised, PDB accession codes 5L1H, 5L1E and 5L1F respectively (Yelshanskaya et al. 2016). These findings confirmed the binding sites of the non-competitive antagonist between the S1-M1 and S2-M4 linkers (Yelshanskaya et al. 2016). A possible model of action of the non-competitive antagonist is that it acts like a wedge between the transmembrane segments, immobilizing the movement towards each other and stabilizing the closure of the channel (Fig. 3.29; Yelshanskaya et al. 2016). These new findings of the antagonist binding pocket can give a new target for the designing of new drugs with improved efficacy and safety.

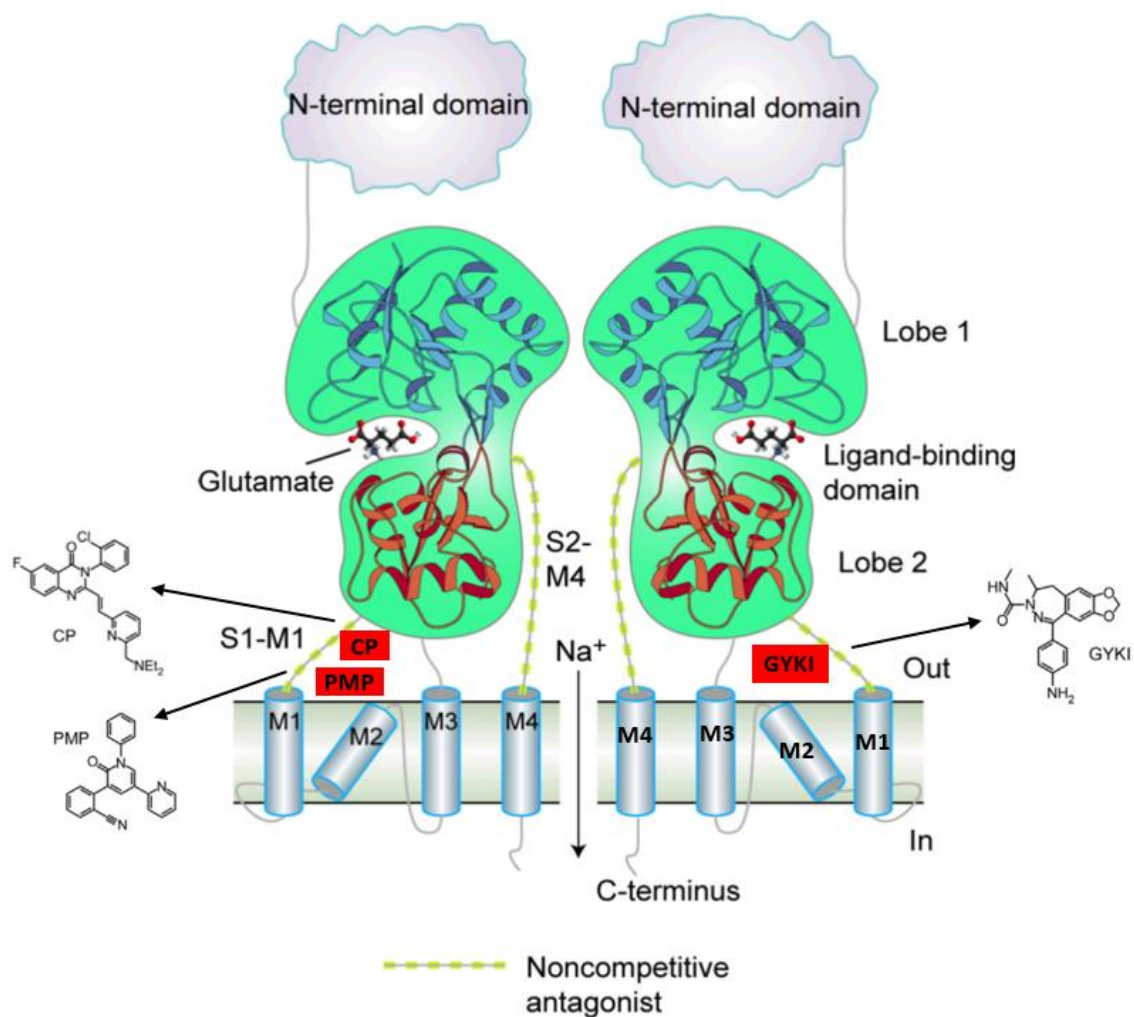


Figure 3.28. AMPA non-competitive antagonist binding site. Schematic representation of the AMPA receptor dimer and binding site of the non-competitive GluA2 inhibitors Perampanel (PMP), GYKI53655 (GYKI) and CP 465,022 (CP) in red squares with structures (Yelshanskaya et al. 2016). Linker segments between S1-M1 and S2-M4 are binding sites for non-competitive AMPA antagonist (Adapted from Rogawski 2013).

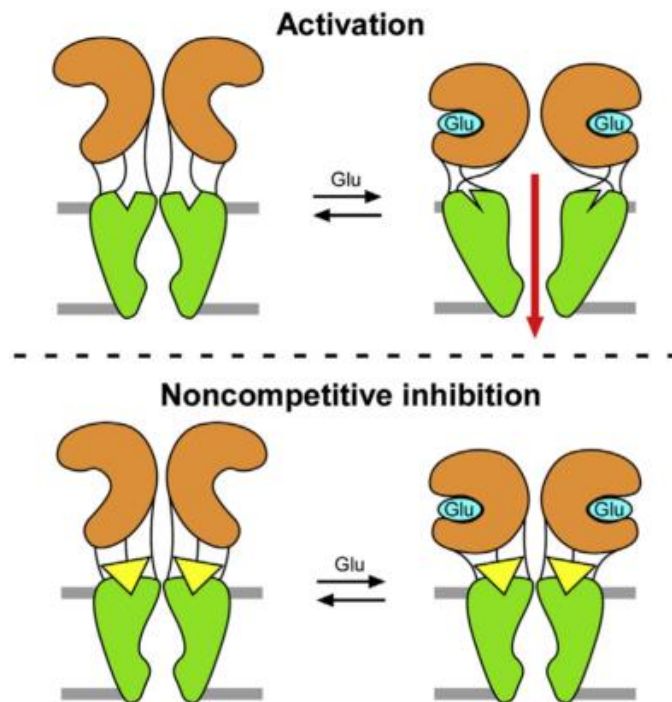


Figure 3.29. Putative model of the mechanism of the non-competitive inhibitor in AMPA receptors. In absence of an inhibitor the glutamate binding domain closes the clamshell-like structure and induces the opening of the pore (red arrow). Inhibitor acts like a wedge (yellow) avoiding the opening of the channel (Yelshanskaya et al. 2016).

3.5.2 KAINATE RECEPTORS

3.5.2.1 FUNCTION AND DISTRIBUTION

Kainate receptors are expressed in postsynaptic and presynaptic neurons, with postsynaptic receptors being involved in excitatory neurotransmission and presynaptic receptors in inhibitory neurotransmission (Kristensen et al. 2016). In situ hybridization studies in the brain have found the expression of mRNA GluK1 subunit in dorsal root ganglion neurons and in the Purkinje cells of the cerebellum. GluK2 mRNA was highly expressed in the cerebellar granule cells, in the dentate gyrus, the striatum and the CA3 region of the hippocampus (Lerma et al. 2001). GluK3 mRNA was detected at low levels of expression in the cerebral cortex, the striatum and in the inhibitory neurons of the molecular layer of the cerebellum (Lerma et al. 2001). In contrast, GluK4 was found almost exclusively in the CA3 region of the hippocampus, with relatively low levels of expression in amygdala and entorhinal cortex (Lerma et al. 2001; Darstein et al. 2003). The GluK5 mRNA was found in the striatum, the inner/outer layers of the cortex and amygdala (Gallyas et al. 2003; Braga et al. 2004).

Kainate receptors have been demonstrated to play an important role in synaptic transmission, presynaptic release of glutamate and γ -aminobutyric acid (GABA) and in the development of epileptogenesis. The function of kainate receptors depends on their cellular distribution. In 1999, kainate receptors (GluK1 subunit) were found to be involved in long-term potentiation in synaptic transmission in mossy fibre of CA1 region of the hippocampus by ligand binding studies and electrophysiology (Bortolotto et al. 1999). Similar to AMPA, kainate receptors function in synaptic plasticity in the postsynaptic cell, however their role is minor compared to AMPA receptors but aid in the influx of Na^+ to induce LTP (Fig. 3.30a). Recently, kainate receptors have been implicated in regulating presynaptic LTP in hippocampus and amygdala. More specifically GluK1 receptors have been associated with pre-LTP mechanisms in anterior cingulate cortex (ACC), pre-LTP in ACC have shown an important role in chronic pain, fear and anxiety (Koga et al. 2015; Yamanaka et al. 2016). In presynaptic neurons active GluK1 receptors allow the influx of Ca^{2+} that leads to the activation of type I adenylyl cyclase (AC1)/protein kinase A (PKA) pathway and hyperpolarization-activated cyclic nucleotide-gated (HCN) channels that result in the regulation of vesicular glutamate transport and in the long lasting increase of glutamate release (Fig. 3.30b; Huang & Trussell 2014; Yamanaka et al. 2016; Zhuo 2017a).

In addition, kainate GluK1 receptors play an important role in modulating the release of GABA neurotransmitter in the pre-synaptic neuron by action potential-dependent GABA release and the activation of voltage-dependent Ca^{2+} channel influx. However, the exact mechanism of kainate in GABA signalling it is not yet fully understood (Fig. 3.30c; Wu et al. 2007; Zhuo 2017a).

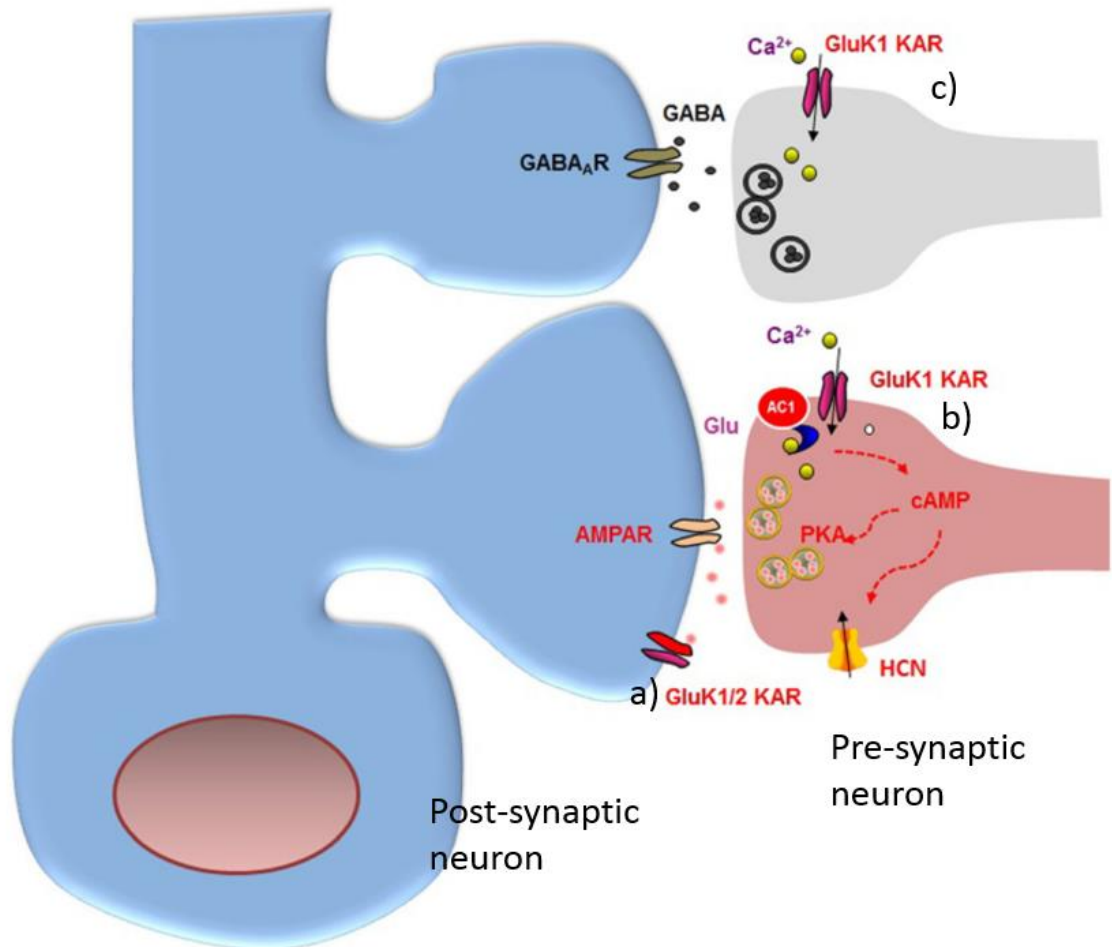


Figure 3.30. Synaptic transmission and pre-synaptic LTP regulation by kainate receptors in the cingulate cortex. a) Postsynaptic GluK1 and GluK2 is involved in mediating synaptic response in addition to AMPA receptors. b) Activation of GluK1 receptor in presynaptic neuron allows the influx of Ca^{2+} ions into the neuron and activates the type I adenylyl cyclase (AC1)/protein kinase A (PKA) pathway and the hyperpolarization-activated cyclic nucleotide-gated (HCN) channels to induce the increase of glutamate release. c) In presynaptic neurons activation of GluK1 receptors triggers action potential-dependent GABA release (Zhuo 2017a).

Seizure generation and epileptogenesis

The first evidence of a link between kainate receptors and epilepsy was in 1998 when it was found that GluK2 receptors in the CNS of mice are important in synaptic transmission and in epileptogenesis induced by kainate (Mulle et al. 1998). In the study, GluK2-deficient mutant mice showed less susceptibility to develop seizures by kainate administration, suggesting the importance of the GluK2 kainate subtype in seizure onset induced by kainate administration (Mulle et al. 1998).

Previous research has demonstrated that selective antagonists for AMPA and kainate can reduce seizure symptoms in animal models. For example, in a GluK1 study antagonists LY-377770 and LY-382884 prevented and interfered with limbic seizures induced by pilocarpine in a rat model (Smolders et al. 2002). Also, the GluK1 and AMPA antagonist NS1209 (discussed in AMPA antagonist section 3.5.1.2) alleviated refractory status epilepticus (RSE) in a small phase II study however no further research followed due to inconclusive results (Pitkänen et al. 2007; Sabers et al. 2013).

Topiramate (Topamax), a current anticonvulsant drug approved by the FDA in 2012 for the treatment of epilepsy, has been shown to interact (antagonize) with AMPA and kainate receptors (Andreou & Goadsby 2011). For example, one study showed that Topiramate inhibits kainate-induced activation in cultured cerebellar granule neurons expressing AMPA and kainate receptors (Skradski & White 2000; Gryder & Rogawski 2003; Braga et al. 2009). In another study, Topiramate selectively inhibited GluK1 kainate receptor-mediated excitatory postsynaptic responses and protected against seizures induced by ATPA in rat neurons (Braga et al. 2009).

In a chemoconvulsive status epilepticus (SE) model in rats, the administration of kainate increased the expression of GluK1, GluK2/GluK3, GluK4 and GluK5 in the CA1 region of the hippocampus measured by immunohistochemistry and colocalization (fluorescence microscopy) studies (Vargas et al. 2013). Higher expression of GluK1 was observed in astrocytes followed by GluK4, GluK2/3 and GluK5; these results demonstrate that after seizure onset astrocytes initiate the overexpression of kainate receptors, indicating a role in epilepsy (Vargas et al. 2013).

There is strong evidence linking kainate receptors in seizure generation and epileptogenesis, for that reason novel antagonists of kainate receptors might be an alternative for the treatment of epilepsy. This thesis research was focused on structure-based studies of kainate receptors GluK1 and GluK2 for the target of epilepsy treatment.

3.5.2.2 Antagonists and Pharmacology

- Competitive Antagonists

Quinoxalinedione derivative compounds such as CNQX and NBQX are relatively non selective competitive antagonists for kainate and AMPA receptors (Kew & Kemp 2005; Jane et al. 2009). A number of tetrazole-substituted decahydroisoquinolines, including LY-293558 (Tezampanel), LY-294486, LY-37770 and LY-382884 have been shown to possess antagonist activity for AMPA and kainate receptors, more specifically with GluK1 receptors compared to AMPA subtypes (Bleakman et al. 1997; Dingledine et al. 1999; Jane et al. 2009; Rogawski 2013). A willardiine analogue UBP302 selectively inhibits GluK1 receptors with low activity versus other kainate subtypes or AMPA receptors (More et al. 2004). Crystal structures of the LBD of GluK1 in complex with UBP302 and UBP310 (PDB accession codes, 2F35 and 2F34) were characterised, both compounds were shown to bind in the orthosteric site using a new mechanism of binding and did not form direct contacts with Glu-723 residue resulting in 22 Å extension of the ligand binding core compared with other crystal structures (Mayer 2006a). These crystal structures in complex with UBP compounds were important for the design of a new antagonist UBP316 (ACET). ACET was found to be a highly potent antagonist for GluK1, and not for GluK2 and GluK3 receptors by adding substituents to the thiophene ring and increasing the hydrophobic interactions with GluK1 receptor in Val-670 and Asn-705 (Dolman et al. 2007). ACET also displays antagonist activity with NMDA receptors, ACET reversibly blocked induction of NMDA receptor-independent long term potentiation (LTP) in vitro experiments (Dolman et al. 2007; Dargan et al. 2009). There is a need for more detailed information on how exactly new antagonists interact with glutamate receptors and their possible effects in therapeutics. Competitive antagonists that bind to the orthosteric site exhibit more side effects because they can also bind to homologous receptors with similar binding sites such as AMPA and NMDA. For that reason, non-competitive antagonists are advantageous; however, a few of non-competitive antagonists have been reported.

- Non-Competitive Antagonists

Although several AMPAR non-competitive antagonists have been described, relatively few non-competitive antagonists have been discovered for kainate receptors. In recent years, efforts have been focused on studying kainate antagonists that bind to the orthosteric site (glutamate site). However, recent evidence shows new allosteric binding sites for AMPA and kainate receptors antagonists, these novel binding sites can have important clinical relevance (Yelshanskaya et al. 2016; Probst Larsen et al. 2017).

5-carboxyl-2,4-di-benzamido-benzoic acid (NS3763), the first non-competitive antagonist for kainate receptors was characterised in 2004 (J. K. Christensen et al. 2004). NS3763 was shown to inhibit domoate-induced responses in homomeric GluK1 receptors expressed in HEK-293 cells but no inhibition was observed in heteromeric GluK1/GluK2 or GluK1/GluK5, AMPA or NMDA receptors (J. K. Christensen et al. 2004; Matute 2011).

Two 2-aryluroidobenzoic acids (AUBAs) identified as 1 and 2a (Fig. 3.31; named accordingly to original paper Valgeirsson et al. 2004) demonstrate to have non-competitive activity against kainate receptors, more specifically, compound 1 displayed higher affinity to GluK1 than GluK2, whereas compound 2a had the same potency for GluK1 and GluK2. Both compounds had no antagonist activity against AMPA subunits expressed in HEK-293 cells (Valgeirsson et al. 2003; Valgeirsson et al. 2004), thereby demonstrating high selectivity for kainate versus AMPA receptors, no studies have been done in NMDA receptors. A more recent study using homology modelling and molecular docking suggests a new non-competitive binding site for kainate receptors GluK1 and GluK2 for indol-derived antagonists. This allosteric site is suggested to occur between S1-M2 and S2-M4 in the transduction domain. However these results not have any X-ray data to prove the exact binding site, they based this experiment on previously discussed AMPA allosteric site (Rogawski 2013; Kaczor et al. 2014).

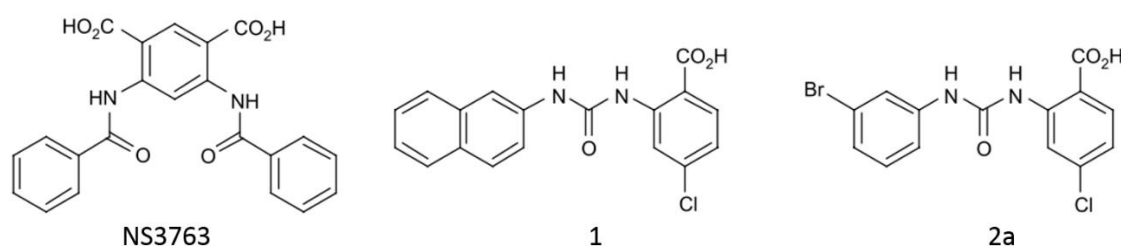


Figure 3.31. Chemical structure of kainate receptors allosteric antagonists (Adapted from Valgeirsson et al. 2004; Jane et al. 2009)

Kainate Allosteric Modulators

Concanavalin A (Con-A) is a member of the sugar lectin family that has shown to block desensitization in kainate receptors by binding to a series of N-glycosylated residues on glutamate receptors extracellular domain. Con-A is a non-selective positive allosteric modulator (PAM) which can increase receptor agonist affinity in kainate, AMPA and NMDA receptors (Partin et al. 1993; Lerma et al. 2001; Bleakman et al. 2002; Mott et al. 2010).

More recently, a new study was able to crystallize GluK1 LBD in complex with three positive allosteric modulators (PAMs) BPAM344, BPAM121 and BPAM521 (PDB accession codes 5MFQ, 5MFW and 5MFV respectively). These kainate modulators (Fig. 3.32) are benzothiadiazine compounds that bind to a novel allosteric binding site in the lower area of the GluK1 LBD dimer interface, near the D1-D2 hinge area (Fig. 3.33; Probst Larsen et al. 2017). BPAM344 and BPAM521 display a potent positive modulatory effect on currents evoked by glutamate in homomeric GluK1b, GluK2a and GluK3a isoform receptors expressed in HEK-293. More specifically, BPAM344 showed a stronger potentiation effect of glutamate-evoked currents in GluK2a and GluK3a compared to AMPA GluA2 receptors. In addition, the allosteric effect showed no differences between GluK1b and GluA2. The three compounds displayed allosteric activity for GluA2 AMPA receptors, in which only BPAM121 significantly potentiates the peak current amplitude of AMPA receptors (Probst Larsen et al. 2017). In previous studies BPAM344 was identified as a strong positive allosteric modulator for AMPA receptors and more interestingly it displayed a specific binding site between the dimer interface of the LBD for all types of benzothiadiazine modulators. It is believed that allosteric modulators of AMPA receptors stabilize the dimer and agonist-bound opening channel conformation, thereby reducing rapid desensitization and deactivation (Nørholm et al. 2013; Krintel et al. 2016). Positive allosteric modulators of iGluRs are promising targets for helping improve cognitive disorders like Alzheimer's disease and schizophrenia in which glutamate transmission is deficient. These new allosteric sites could give an opportunity to find new drugs with improved pharmacological properties and higher target specificity (Menniti et al. 2013; Krintel et al. 2016).

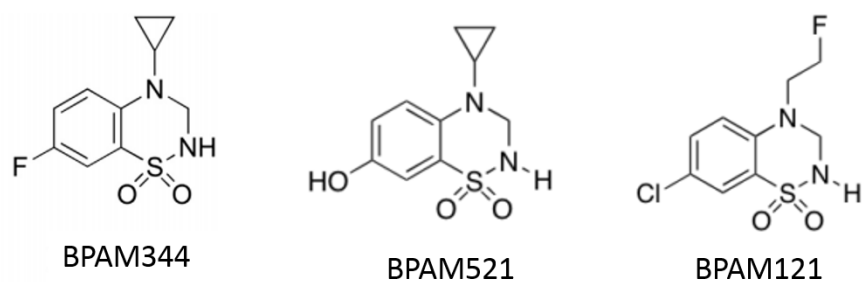


Figure 3.32. Chemical structures of BPAM344, BPAM521 and BPAM121 (Adapted from Probst Larsen et al. 2017).

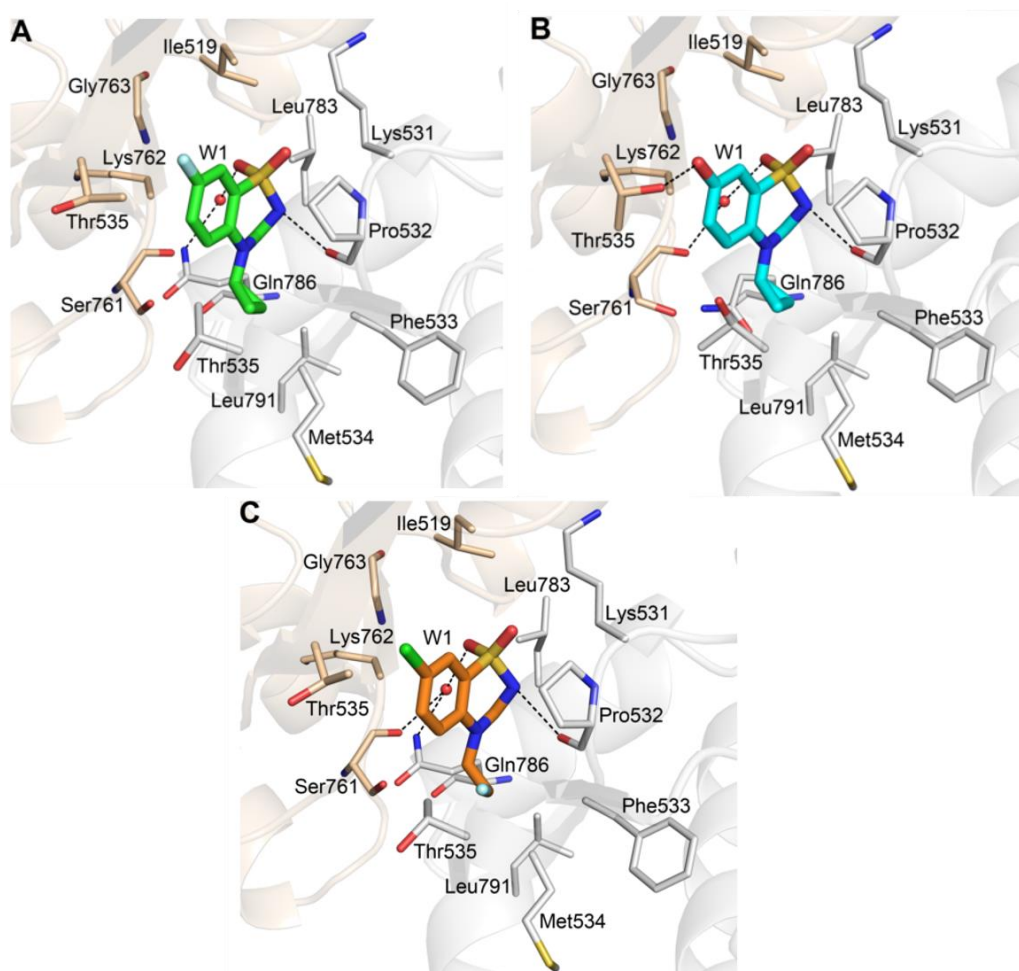


Figure 3.33. Binding interactions of BPAM344, BPAM521 and BPAM121 with LBD-GluK1. Antagonists BPAM344, BPAM521 and BPAM121 in green, cyan and orange respectively. Residues involved in antagonist interaction within 3.5 Å in domains one and two in beige and grey. Water molecules in red spheres and hydrogen bonds in black dashed lines (Probst Larsen et al. 2017).

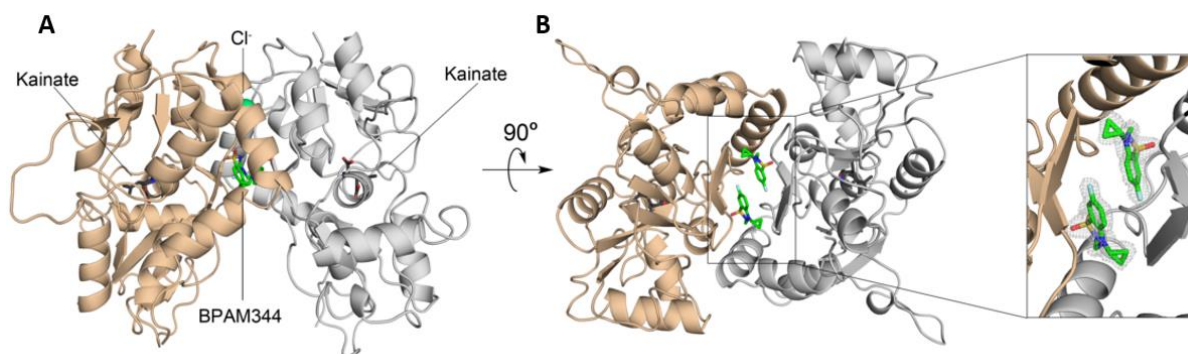


Figure 3.34. GluK1-LBD in complex with BPAM344 and kainate. A) LBD of GluK1 dimer, domains one and two in beige and grey respectively. Kainate and BPAM344 are shown as black and green stick representations, chloride ion used for crystallography in green. B) Rotated view of the LBD in which the antagonist BPAM binds inside the lower part of the dimer interface (Probst Larsen et al. 2017).

The PAM BPAM344 binds between the dimer interface of the GluK1 dimer, more specifically two BPAM344 molecules bind in a lower region of the interface. In addition, kainate agonist binds in the orthosteric site of the LBD between domains one and two (Fig. 3.34). The three PAMs bind with similar interactions, the main differences are residues Thr-535, Ser-761 and Gln-786 that adopt different binding conformations for each PAM (Fig. 3.33) and more specifically Thr-535 side chain turned aside from modulator site in the presence of BPAM121 (Probst Larsen et al. 2017). This binding interface shares a similar binding mode to that previously observed with AMPA GluA2 in complex with other PAMs, such as cyclothiazide, piracetam, aniracetam, LY451646 and 3,4-dihydro-2H-1,2,4-benzothiadiazine dioxide (Menniti et al. 2013; Nørholm et al. 2013). To conclude, the kainate and AMPA receptors display a similar allosteric binding site at the LBD interface; these similarities allow the design of novel PAMs that can be selective for kainate receptors.

3.5.3 NMDA RECEPTORS

3.5.3.1 FUNCTION AND DISTRIBUTION

The N-methyl-D-aspartate (NMDA) receptor is a iGluR important for synaptic plasticity and memory function (Li & Tsien 2009). NMDA receptors are located in the cerebral cortex, the largest region of the brain responsible for information processing, memory, attention, perception, cognition, language, sensation and association (Vidyasagar 1996; Boundless Cerebral Cortex 2016). Immunocytochemistry studies found cortical NMDA receptors in dendritic spines, astrocytes and axon terminals (excitatory and inhibitory) suggesting a large distribution of NMDA receptors in neurons of the cerebral cortex (Conti 1997).

NMDA agonist selectively and exclusively activates NMDA receptors and no other glutamate receptors. The property that differentiates NMDA receptors from other receptors is the requirement of the binding of an agonist (glutamate) and a co-agonist (Glycine or D-serine) for activation of the channel (Fig. 3.35). Extracellular ions such as Mg^{2+} and Zn^{2+} are able to bind inside the pore and block the channel, membrane depolarization results in the release of Mg^{2+} and Zn^{2+} from the pore channel allowing the voltage-dependent flow of ions Na^{+} and Ca^{2+} inside the cell and K^{+} outside the cell (Hashimoto 2017). The opening of the channel results in an influx of Ca^{2+} ions that triggers signal transduction cascades such as protein kinases, calcium-dependent enzymes, second messengers and phosphatases that are important for neuroplasticity (Blanke & VanDongen 2009; Karakas & Furukawa 2014).

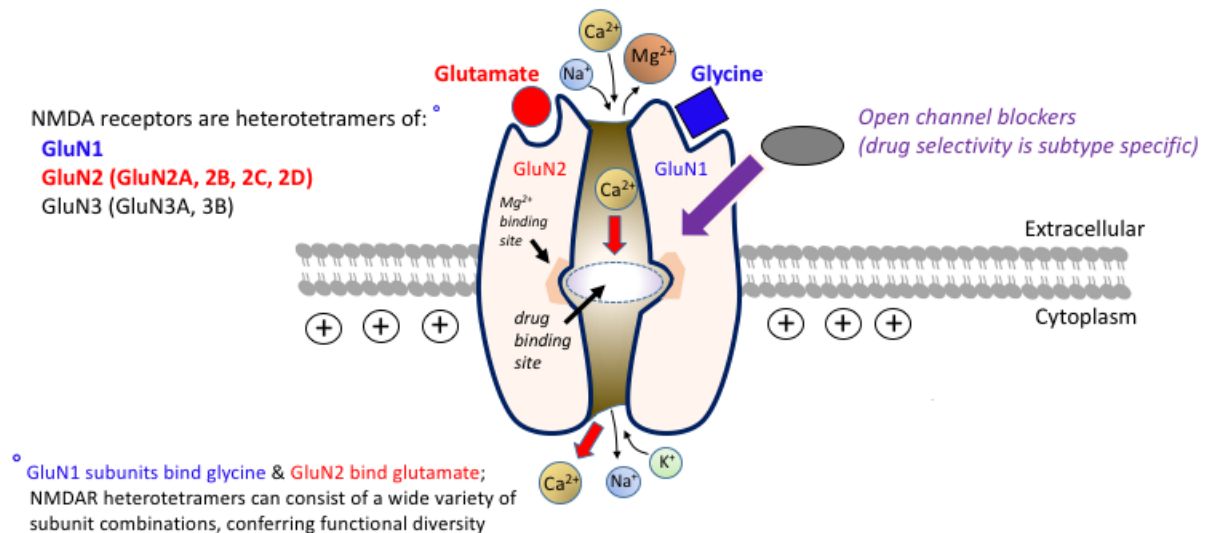


Figure 3.35. Diagram of the topology of activated NMDA receptors. The activation of the NMDA channel requires the binding of neurotransmitter glutamate and co-agonist Glycine or D-serine to allow the influx of Ca^{2+} and Na^{+} and the efflux of K^{+} , membrane depolarization is necessary for the release of Mg^{2+} from the pore (Adapted from Tulane University, Medical Pharmacology TMedWeb).

http://tmedweb.tulane.edu/pharmwiki/doku.php/overview_of_cns_neurotransmitters).

NMDA receptors are important for a large amount of post-synaptic functions; more specifically, long-term potentiation (LTP), a mechanism of synaptic plasticity important for learning and memory, is controlled by NMDA receptors. As previously described in AMPA function section 3.5.1.1; the activation of NMDA receptors in the postsynaptic neuron allows the influx of Ca^{2+} and results in the activation of Ca^{2+} /calmodulin-dependent kinase II (CAMKII) and protein kinases (A and C). Both induce the synaptic insertion of AMPA receptors (Fig. 3.27 & 3.36) to ensure synaptic potentiation by LTP (Newcomer et al. 2000; Lisman et al. 2002; Kim et al. 2010; Herring & Nicoll 2016). In addition, NMDA receptors are also implicated with long-term depression (LTD), a mechanism that is characterised by the longer reduction of synaptic transmission. Once more, the influx of Ca^{2+} by NMDA receptors by low-frequency stimulation activates hippocalcin, a Ca^{2+} binding protein important for synaptic plasticity and learning (Dovgan et al. 2010). Hippocalcin forms a complex with adaptor protein 2 (AP2) to activate the receptor-mediated endocytosis (RME) to initiate the AMPA receptor internalization and as a result the neuron is less responsive to glutamate neurotransmitter (Palmer et al. 2005; Derkach et al. 2007; Dovgan et al. 2010).

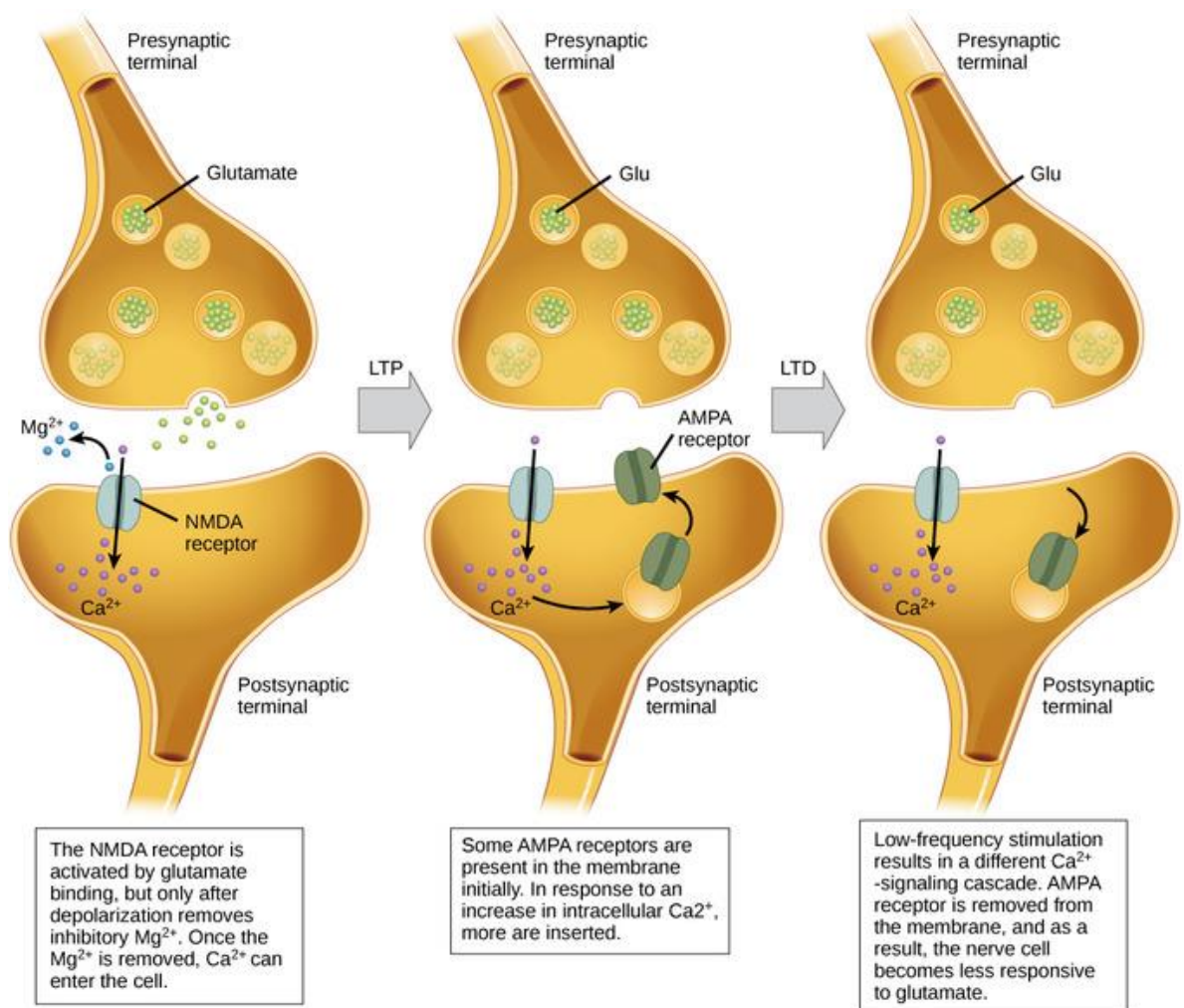


Figure 3.36. NMDA dependent long-term potentiation (LTP) and long-term depression (LTD). In long-term synaptic plasticity the activation of NMDA allows the influx of Ca^{2+} either by increasing the expression of AMPA receptors (high-frequency stimulation) or reducing the expression of AMPA receptors (low-frequency stimulation). (Boundless, Synaptic plasticity; <https://www.boundless.com/biology/textbooks/boundless-biology-textbook/the-nervous-system-35/how-neurons-communicate-200/synaptic-plasticity-765-11998/>).

3.5.3.2 ANTAGONIST AND PHARMACOLOGY

- **Competitive antagonists**

These compounds will compete for the glutamate binding site in the LBD of the receptor. The 2R-amino-5-phosphonopentanoate (AP5) is a selective competitive NMDA receptor antagonist first described in 1981 by Watkins and Evans (Watkins & Evans 1981). AP5 is able to block the induction of LTP and impairs spatial learning (Davis et al. 1992; Morris et al. 2013). One disadvantage of AP5 antagonist is the low selectivity (<10-fold) for other AMPA subunits (Vyklícký et al. 2014). Two phenanthrene compounds (2R*,3S*)-1-(phenanthrene-3-carbonyl)piperazine-2,3-dicarboxylic acid (UBP141) and its 9-brominated homolog (2R*,3S*)-1-(9-bromophenanthrene-3-carbonyl)piperazine-2,3-dicarboxylic acid (UBP145) have shown high selectivity for GluN2D subunits over GluN2B and GluN2A (Morley et al. 2005; Costa et al. 2009).

- **Channel blockers (Non-competitive antagonists)**

Some compounds have the ability to block the channel by binding at the Mg^{2+} site inside the channel pore acting as a non-competitive antagonist (Fig. 3.37). However, the blocking of the channel will require previous receptor activation, otherwise the drug will not be able to enter the open channel (Vyklícký et al. 2014). The most potent NMDA blocker is a dizocilpine maleate, frequently named dizocilpine or MK-801; dizocilpine was discovered and patented by Merck and functions as an anticonvulsant and anaesthetic drug. Unfortunately drug administration in rats demonstrated the development of brain lesions (Olney's lesions), it has also been associated with neurotoxicity and learning impairment (Olney et al. 1986; Kovacic & Somanathan 2010). Two other channel blockers with lower affinity antagonist effect are phencyclidine (PCP) and ketamine (previously discussed in section 3.2, glutamate neurotransmission in disease) both drugs are mainly used as anaesthetics however, both drugs display dissociative effects (hallucinogens) such as memory loss, sedation and delusions (Kapur & Seeman 2002; Sleight et al. 2014; Vyklícký et al. 2014). Medical use of PCP in humans was discontinued for the dissociative side effects; ketamine is used to treat chronic pain and as anaesthetic but only as a prescription and controlled drug. Memantine is another channel blocker, a drug approved by FDA and European medicines agency (EMA) for the treatment of Alzheimer's disease (AD), it is a low-affinity voltage-dependent channel blocker of NMDA receptors and it has been shown to have better clinical tolerability.

The reduction of side effects of memantine is due to their low affinity for NMDA receptors, this drug rapidly binds to the Mg^{2+} binding site and quickly dissociates from the receptor (Kalia et al. 2008; Vyklicky et al. 2014). The major challenge of these channel blockers is that they have low or no subtype selectivity causing large side effects (Dravid et al. 2007).

- **Polyamine site antagonists**

In the amino terminal domain (ATD) of NMDA receptors there is a region that shares homology to the leucine-isoleucine-valine binding protein (LIVBP), this region is an allosteric modulator domain that binds to zinc in GluN2A and polyamines in GluN2B (O'Hara et al. 1993; Masuko et al. 1999; Fayyazuddin et al. 2000; Monaghan & Jane 2009). Ifenprodil, a phenylethanolamine drug, is a selective antagonist of NMDA receptors containing NR2B subunit (Williams 2001). It is currently in clinical trial phase II for the treatment of post-traumatic stress disorder (PTSD) in adolescents, results to be completed in 2020 (NCT01896388, www.clinicaltrials.gov). The highest affinity antagonist for this site is Ro25-6981 which has binding affinity for NMDA receptors containing GluN2B subunit (Fischer et al. 1997). Ro25-6981 has been reported to have antidepressant properties and studies are currently being conducted to determine the clinical actions of this drug in depression (Duman 2014). Traxoprodil (CP-101,606) a drug characterised by Pfizer, displayed a selective antagonist for NMDA receptors containing the GluN2B subunit (Di et al. 1997). Traxoprodil has shown neuroprotective and analgesic properties, and phase II clinical trials were performed in Parkinson disease (PD) and major depressive disorder (MDD) patients (NCT00163085 & NCT00163059, www.clinicaltrials.gov). Unfortunately, the studies were halted due to electrocardiographic abnormalities (QT prolongation) associated with potassium channel blockade (Wolfgang & Rogawski 2002). In addition, traxoprodil was also associated with abnormal thinking and amnesia as undesirable side effects (Nutt et al. 2008).

Subunit selectivity for competitive antagonist is necessary in the new antagonist of NMDA, to avoid adverse side effects; this research was not focused on NMDA receptors.

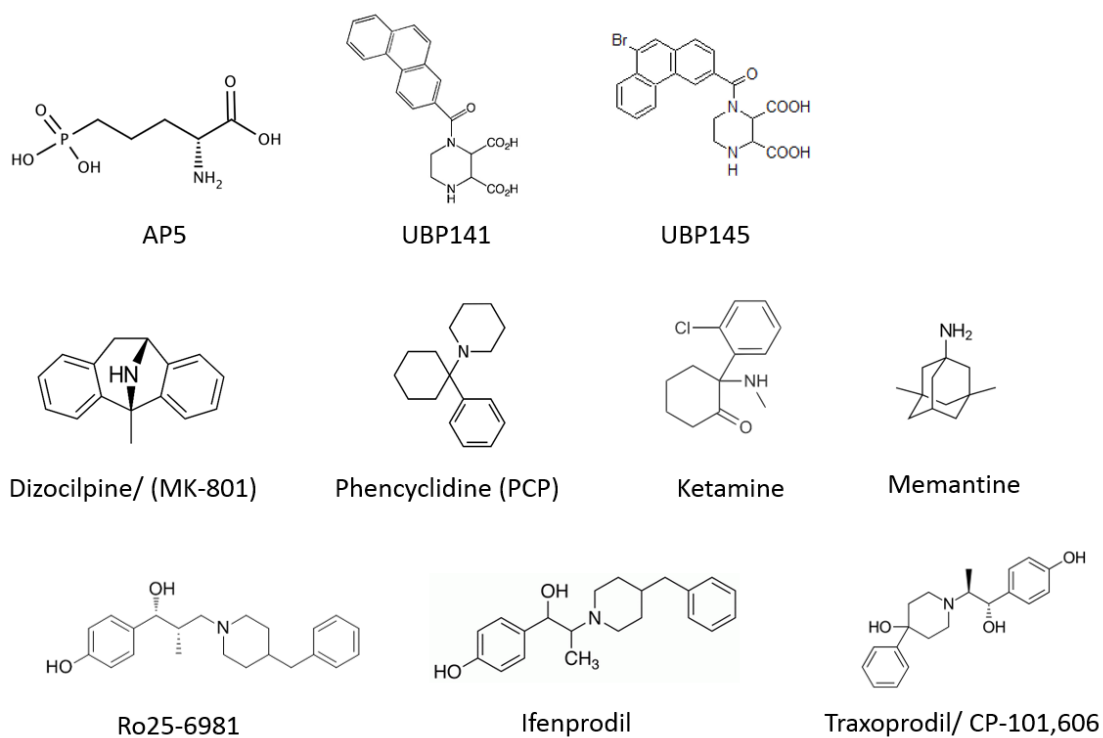


Figure 3.37. Chemical structures of several NMDA antagonists.

CHAPTER 4

AMPA PROJECT

4.1 ABSTRACT

Epilepsy is a chronic neurological disorder and is characterised by recurrent unprovoked seizures. It is one of the most common neurological disorders worldwide; with the overall incidence of epilepsy in Europe and North America being 24 and 53 cases per 100,000 persons per year respectively, affecting 50 million people worldwide according to the World Health Organization (WHO). Epilepsy has a wide variety of phenotypes having more than 15 different seizure types and more than 30 epilepsy syndromes. Several anti-epileptic drugs (AEDs) such as, carbamazepine, perampanel, piracetam and diazepam are available currently, however 25% to 30% of epilepsy patients do not respond to drug treatment (refractory patients; French 2006; Laxer et al. 2014). Additionally, the significant side effects of current AEDs such as fatigue, vertigo, headaches, sedation, drowsiness and nausea may result in treatment discontinuation in approximately 25% of patients (Perucca & Gilliam 2012).

AMPA receptors are a type of ionotropic glutamate receptors (iGluRs), involved in excitatory neurotransmission and are a recent target for AEDs. Currently several anticonvulsant drugs such as Becampanel and Fanapanel can diminish the excitatory neurotransmission of glutamate by antagonising the binding site; however these antagonist drugs can cause significant side effects due to action in other iGluRs in the brain. Perampanel, an antiepileptic drug approved in 2012 for the treatment of partial seizures and generalized tonic-clonic seizures in adults, was found to bind in a new allosteric site in AMPA receptors. This new binding site located in the transduction domain (between the ligand-binding domain and the transmembrane domain) gives great selectivity to negative allosteric modulators (NAMs) including perampanel. Unfortunately, this drug can cause a large number of adverse side effects including behavioural and psychiatric changes, irritability, nausea, somnolence, fatigue and dizziness, for that reason its clinical use is limited (Besag & Patsalos 2016). Hence, we are interested in a different allosteric site than the transduction domain due to a large amount of side effects, as well as the difficulty of obtaining the isolated transmembrane domain with the LBD for purification and crystallography experiments.

AMPA receptors play an important function in the process of synaptic plasticity and are known to be involved with the long-term potentiation mechanism. A group of positive allosteric modulators (PAMs) of AMPA receptors frequently known as AMPAkinases have been shown to

improve cognitive function in a variety of pre-clinical assays (Lynch & Gall 2006; Beneyto et al. 2007; Ward et al. 2011). In addition, a novel binding site for positive allosteric modulators (PAMs) located between the dimer interface of the ligand-binding domain of AMPA receptors has been targeted for drug discovery research focused on cognitive processes (learning and memory). Previous research has shown that AMPA PAMs can improve cognitive performance and be a potential target for Schizophrenia, a chronic mental disorder that affects behaviour, thoughts and perception (Ward et al. 2011).

This project was focused on finding novel negative allosteric modulators (NAMs) and positive allosteric modulators (PAMs) compounds in the LBD of AMPA receptors using fragment-based screening experiments. The experiments resulted in a successful protein production, purification and crystallography for the LBD of AMPA. More than 700 fragment compounds were screened with LBD AMPA crystals using the Diamond fragment screening (XChem) library. Eight fragments were identified, situated in three different sites in the LBD of AMPA, two sites within the dimer interface and one site near the Gly-Thr linker of S1 and S2 of the LBD. These fragment hits found in the dimer interface similar to the literature PAM site are promising for the novel AMPA PAMs characterisation with improved therapeutic properties. Similarly, fragments found near the Gly-Thr linker situated near to the novel NAMs site found in published literature could be a potential target for improved antiepileptic form. These results give important information for the early development of drug discovery in epilepsy and Schizophrenia treatment.

4.2 AIMS

The overall aim of the project was to obtain X-ray structural information about the AMPA receptors GluA2 LBD in complex with small compounds to aid future drug development in the treatment of disorders associated with a dysfunction of AMPA receptors, such as the cognitive deficit associated with schizophrenia as well as epilepsy. The initial aim was to express the LBD construct in *E. coli* bacteria and then purify the protein at a scale large enough to support crystallography method development and then X-ray crystallography to determine the structure of dimeric GluA2 in association with orthosteric ligand (glutamate) as well as small molecule binders. A construct with a sequence encoding a 6xHis-SUMO tag was chosen due to its ability to enhance protein folding (the SUMO sequence) and to purify the protein (the six-residue polyhistidine sequence). The main objective of the fragment screen (XChem, Diamond Light Source) was to identify novel binders of the AMPA protein binding in the dimer of the LBD of the protein.

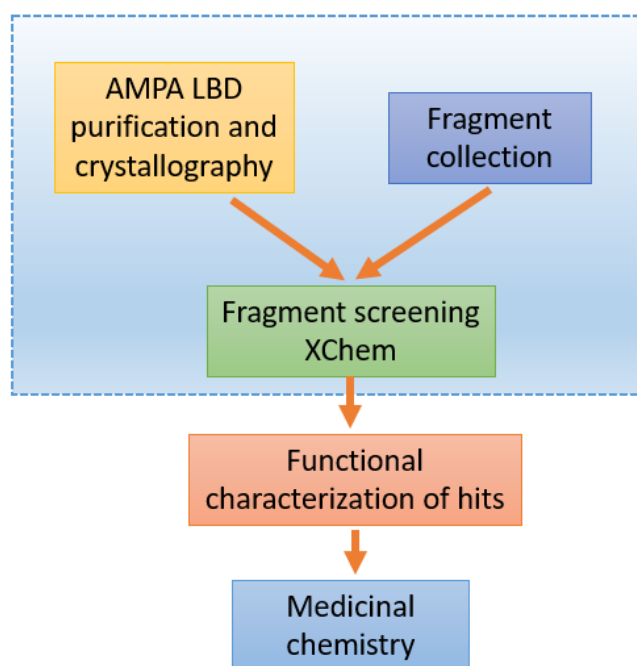


Figure 4.1. AMPA overall project plan. The large blue box with a dashed border represents the experiments covered in this thesis project research. The functional characterisation of hits and potential subsequent iterative medicinal chemistry is planned for future studies.

4.3 MATERIALS AND METHODS

4.3.1 CLONING AND PLASMID VECTOR

The plasmid used for protein expression and purification was the ligand-binding domain (LBD) of rat GluA2, kindly supplied by Dr. Antony W. Oliver from the Genome Damage and Stability Centre (GDSC; University of Sussex). In the GDSC, they used their own pHis-SUMO-3C vector in which they cloned the proteins for purification purposes. Polyhistidine in combination with small ubiquitin-like modifier (SUMO) tags are frequently used due to the ability of increase the expression of recombinant proteins and enhance protein solubility (Costa et al. 2014).

The LBD construct was designed according to previous published experiments (Armstrong & Gouaux 2000) using the segments S1 and S2 from the LBD (Fig. 4.2). The S1S2 construct was produced by deleting the ATD at the beginning of S1 and then link the end of S1 with proximal S2 using a Gly-Thr linker and finally cutting the ending of S2 before the transmembrane segment M4. This dipeptide Gly-Thr was sufficient to covalently join S1 and S2 without modifying the conformation and properties of the LBD of the protein (Reddy et al. 2013).

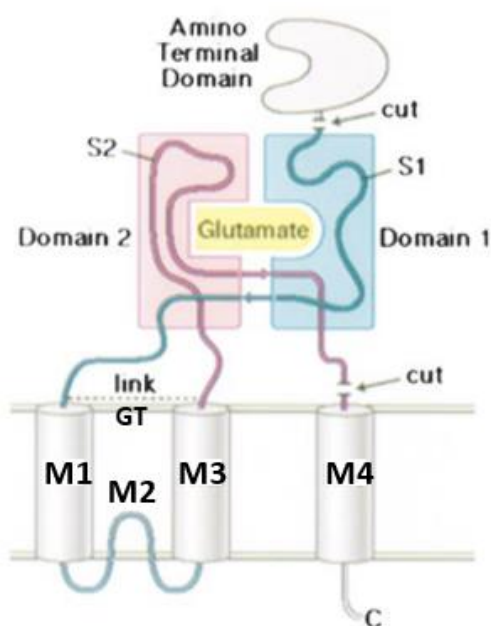


Figure 4.2. Cartoon showing the strategy for the GluA2 ligand-binding domain construct design. The S1S2 construct is based on previous published experiments in which the amino terminal domain (ATD) was deleted at the beginning of S1; a Gly-Thr linker was used to join S2 and S1 and deleting the last segment of S2 closer to M4 (Adapted from Armstrong & Gouaux 2000).

In this case, the LBD of rat GluA2 was cloned into pHis-SUMO-3C vector and consequently sub cloned into pBR322 plasmid using a commercially available pET T7 expression system by Invitrogen (Thermo Fisher Scientific). Similar to previously published studies (Armstrong & Gouaux 2000) the LBD sequence was based on the Flop-splice variant UniProt P19491-1 (Fig. 4.3), with three mutations in the N-terminus of S1 in G410R, L411G and E412A with the purpose of facilitating crystallography experiments. Additionally, one mutation in S2 of N775 to serine corresponding to the flip isoform was designed because compounds such as cyclothiazide have preference to the flip isoform in this specific residue (Partin et al. 1996; Sun et al. 2002; Nørholm et al. 2013). The recombinant protein contains a 6xHis-SUMO tag to improve the solubility and purification experiments. The plasmid was provided by Invitrogen and contained an ampicillin resistance gene to control the production of recombinant protein (Fig. 4.4). Protein expression was induced by β -D-1thiogalactopyranoside (IPTG) under a T7 RNA polymerase/promoter system. In this system the T7 promoter site is located upstream of the recombinant gene and the expression of the gene is controlled by the addition of IPTG. This expression system is highly effective in producing large amounts of target protein.

```
>rGluA2_LBD
MGSHHHHHGS DSEVNQEAKPEVKPEVKPETHINLKVSDGSSEIFFKIKKTTPLRRLMEAFAR
RQ GKEMDSLRF LYDGIRIQADQTPEDLDMEDNDIIEAHREQIGGLEVLFGPHMASNDTSRGA
NKT VVVTTILESPYVMMKKNHEMLEGNERYEGYCVDLAAEIAKHCGFKYKLTIVGDGKYGARD
ADTKIWNGMVGELVYGKADIAIAPLTITLVREEVIDFSKPFMSLGISIMIKKGTPIESAEDLS
KQTEIAYGTLDSGSTKEFFRRSKIAVFDKMWTYMRSAEPSVFVRTTAEGVARVRKSKGKYAYL
LESTMNEYIEQRKPCDTMKVGGNLD SKGYGIATPKGSSLGNAVNLAVLKLSEQGLLDKLNKW
WYDKGECG
```

M - Methionine start codon of recombinant protein expression

6xHis-Ubiquitin-like protein tag

HRV3C Linker

Protein sequence LBD rGluA2

GT linker site connecting S1 and S2 portions of LBD

Mutations for crystallography purposes

Mutation to flip isoform (AMPA PAMs binding preference)

Figure 4.3. rGluA2 LBD sequence construct for protein expression and purification. rGluA2 construct contains an N-terminal 6xHis-SUMO tag, a recognition SUMO cleavage site and the protein sequence consisted of S1 [406-NDTSRGAN....SIMIKK-527] and S2 [653-PIESAEDL....YDKGECG-795], separated by a Gly-Thr linker. Sequence based on rGluA2 P19491-1 Flop Isoform (Uniprot). Positive allosteric modulators (PAMs).

Rat GluA2 protein expression and purification was used because crystals of rat protein are, for whatever reason easier to express and purify and more readily forms crystals (Ward et al. 2011). In addition, there are more published structures of the LBD of GluA2 rat than human.

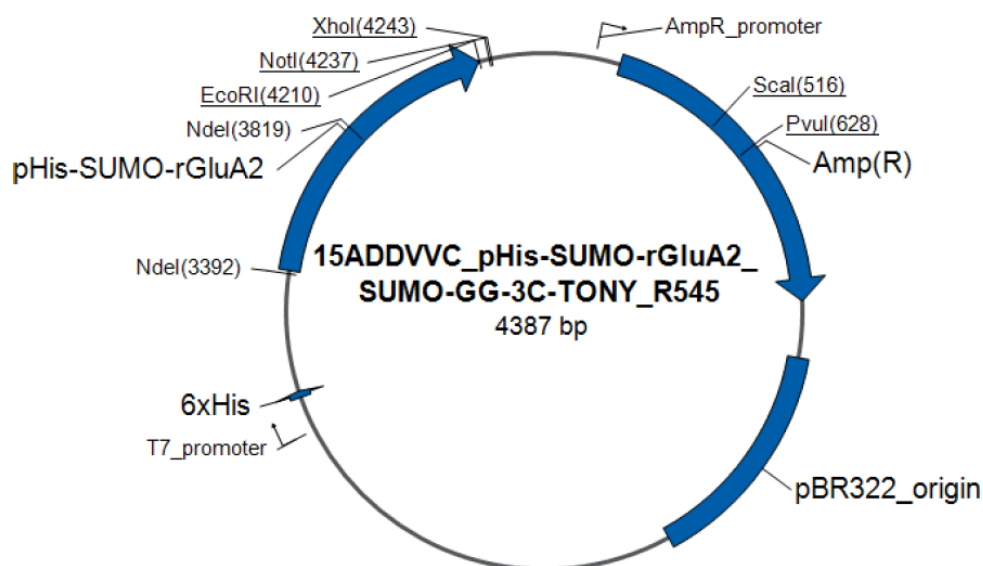


Figure 4.4. Plasmid map of the inserted rat GluA2 LBD gene, of which 5µg of lyophilised plasmid was obtained by Invitrogen. The plasmid PBR322 commonly used as a cloning vector encoding an Ampicillin resistant gene, origin of replication, T7 promote site (control the levels of protein expression by IPTG), 6xHis-SUMO tag, rGluA2 LBD and different restriction enzyme sites. Plasmid used for cloning by Invitrogen (Thermo Fisher Scientific).

4.3.2 COMPETENT CELLS

The competent cells used for transformation experiments were *E. coli* Origami™ B (DE3) by Novagen (Cat. No. 70837-3). Origami B strains have mutations in the thioredoxin reductase (*trxB*) and glutathione reductase (*gor*) genes, these modifications enhance the formation of disulphide bonds in the cytoplasm. Origami bacteria was used for the characteristic of forming disulphide bonds to obtain the correct folding of the protein and subunit assembly. Origami B strains are compatible with ampicillin and carbenicillin resistance plasmids and are adequate for use with pET vectors. Selective antibiotics for Origami strains are kanamycin and tetracycline.

4.3.3 BACTERIA TRANSFORMATION

The vector containing the LBD_rGluA2 (15ADDVVC_pHis-SUMO-rGluA2_SUMO-GG-3C-TONY_R545) was dissolved with 30 µl of purified sterile water. A volume of 1 µl of vector was added into 50 µl of *E. coli* Origami B (DE3) cells and incubated on ice for 30 minutes. Heat shock was performed at 42°C for 40 seconds, and then the vial was transferred on ice for 2 minutes. To finalize with the addition of 200 µl of super optimal broth with catabolite repression medium (SOC) (Invitrogen, Cat. No. 1544-034) and further incubation at 37°C for 1 hour in the shaking incubator. The cell suspension was plated into LB-agar plates (Cat. No. L2897, Sigma-Aldrich) containing 15 µg/ml kanamycin and 50 µg/ml carbenicillin. The use of carbenicillin instead of ampicillin is due to higher stability and selectivity in bacteria containing the selective plasmid. The plates were incubated for 24 hours at 37°C, 5% CO₂.

Antibiotics used: Kanamycin sulphate from *Streptomyces Kanamyceticus* Cat. No. K4000-25G (Sigma-Aldrich) and Carbenicillin disodium salt Cat. No. C1389-5G (Sigma-Aldrich).

4.3.4 PROTEIN EXPRESSION

The colonies which grew in the presence of antibiotic were the ones carrying the plasmid in the competent cells. One single colony was scraped and added into 60 ml of turbo broth (Cat. No. MD12-104-1, Molecular Dimensions) containing 15µg/ml kanamycin and 50µg/ml carbenicillin in a 200 ml flask. Cells were incubated in the shaker incubator at 37°C until the OD₆₀₀ reached ~1.2 and then stored overnight at 4°C. On the next day 10 ml of the 60 ml cell suspension were added into each 1L x 6 flasks of turbo broth containing 15µg/ml kanamycin and 50µg/ml carbenicillin in a 2L glass flask. Cells were grown in a shaker incubator at 30°C at 200 rpm until the OD₆₀₀ was ~1.2, at which point the temperature was reduced to 18°C until the OD₆₀₀ reached ~1.5. Then IPTG (Cat. No. 15529019, Thermo Fisher Scientific) was added to a final concentration of 50µM to each flask and cells were grown over night at 18°C on a shaker incubator. The next day the cells were centrifuged at 6,000 rpm (Rotor JLA 9.1000, Beckman Coulter, Avanti J-26S XP centrifuge) for 20 minutes and pellets were frozen for subsequent purification experiments.

For protein expression tests, a sample of cells were taken before and after IPTG induction and then protein expression was analysed using SDS-PAGE gel electrophoresis at 160 V for one hour (SERVAGel™ TG PRIME 4-20%, Cat. No. 43276.01, SERVA).

4.3.5 PROTEIN PURIFICATION

4.3.5.1 IMMOBILIZED METAL AFFINITY CHROMATOGRAPHY (IMAC)

The purpose of IMAC is to purify a large amount of protein with high selectivity using the method of a chelating agent in a beaded agarose to immobilize the specific desired metal ion followed by binding and purification of the protein of interest. Talon resin has a nitrilotriacetic acid (NTA) group loaded with cobalt divalent metal which produce high selectivity for his-tagged proteins. Protein with a poly-his tag binds in a specific manner to IMAC resins in neutral buffer conditions. Imidazole is also used in the buffer conditions in low concentration (10 mM) as a wash step to remove any nonspecific binding of endogenous proteins that might contain histidine groups. However, a high concentration of imidazole (≥ 300 mM) is used in elution steps for removing the binding of the protein in NTA- Co^{2+} resin owing to the similarity of the side chain to histidine groups (Fig.4.5).

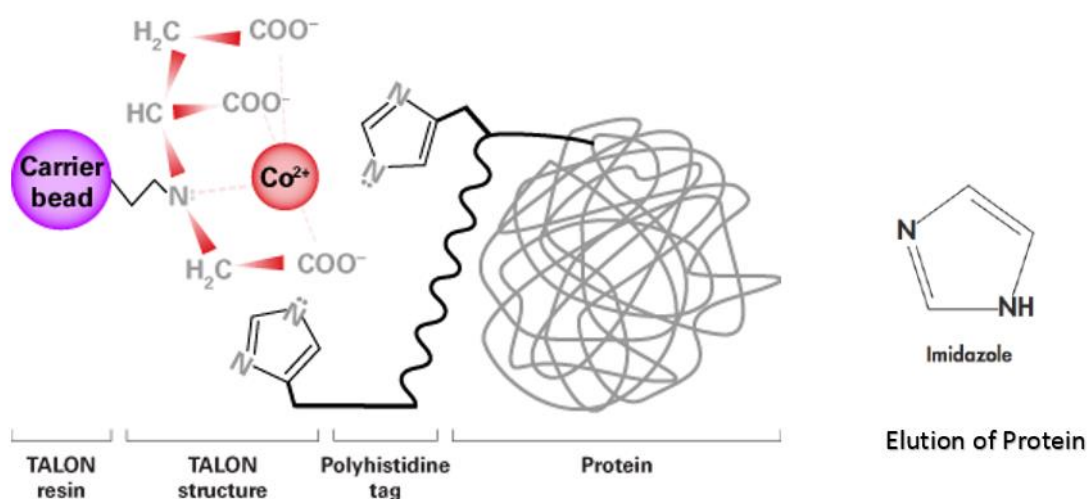


Figure 4.5. Talon resin loaded with NTA- Co^{2+} for protein purification. The bead agarose contains covalently linked NTA which binds to a divalent cobalt. The Co^{2+} then selectively binds to his-tagged protein. Imidazole is used for the elution of the protein of interest because of the similar structure of the histidine side-chain. (Adapted from Takara Clontech supplier website http://www.clontech.com/US/Support/Applications/Tagged_Protein_Purification/Ni-NTA_Resin_vs._Talon)

Experimental procedure

Buffers for protein purification experiment; each buffer was filtered at 0.45 μm (Cellulose nitrate membrane filters, Whatman™ Cat. No. 514-8073, VWR).

Lysis Buffer	Elution Buffer	Cat. No.
20 mM HEPES pH 7.5	20 mM HEPES pH 7.5	BP310-1, Fisher BioReagents
500 mM NaCl	500 mM NaCl	S/3120/63, Fisher Chemical
10 mM Imidazole	300 mM Imidazole	122025000, Acros Organics
0.5 mM TCEP	0.5 mM TCEP	646547-10x1ml, Sigma-Aldrich
Distilled H ₂ O up to 500 ml	Distilled H ₂ O up to 250 ml	N/A

Pellets of cells were defrosted and resuspended in 50 ml of Lysis buffer with one tablet of protease inhibitor cocktail (11055700, Roche) and 250 μM of glutamic acid in 20 mM HEPES-NaOH pH 7.5(L-glutamic acid monosodium salt hydrate Cat. No. G1626, Sigma-Aldrich). Cells were lysed by sonication with a large sonicator probe, 5 sec on, 5 sec off, 40% amplitude for 5 minutes. Cell debris and insoluble fractions were removed by centrifugation at 40,000g for 30 minutes at 4°C. Supernatant (soluble fraction) was filtered through a 0.45 μm syringe filter (Sterile PES syringe filter Cat. No. 15216869, Fisher Scientific). The filtered supernatant was applied to a gravity column containing 7.5 ml of talon metal affinity resin (Clontech Takara Cat. No. 635503) and incubated for 1 hour at 4°C. The column was washed with several applications of lysis buffer (approximately 200 ml). The retained protein was eluted with several applications of elution buffer (~7.5 ml each). Eluted fractions were finally incubated with PreScission protease (27-0843-01, GE Healthcare Life Sciences) at 1 unit per ml at 4°C overnight for the removal of the 6xHis-SUMO tag.

4.3.5.2 SIZE EXCLUSION CHROMATOGRAPHY (SEC)

SEC is a method used for purifying proteins of interest by separating molecules based on the differences in size (Fig. 4.6) and uses a column packed with a resin medium and connected to a FPLC system. In these experiments the HiLoad Superdex 75pg column was used, which is prepacked with a prep grade media Superdex. Superdex is a high resolution resin composed of cross-linked agarose and dextran beads with a molecular weight range of 3,000 to 70,000 Da.

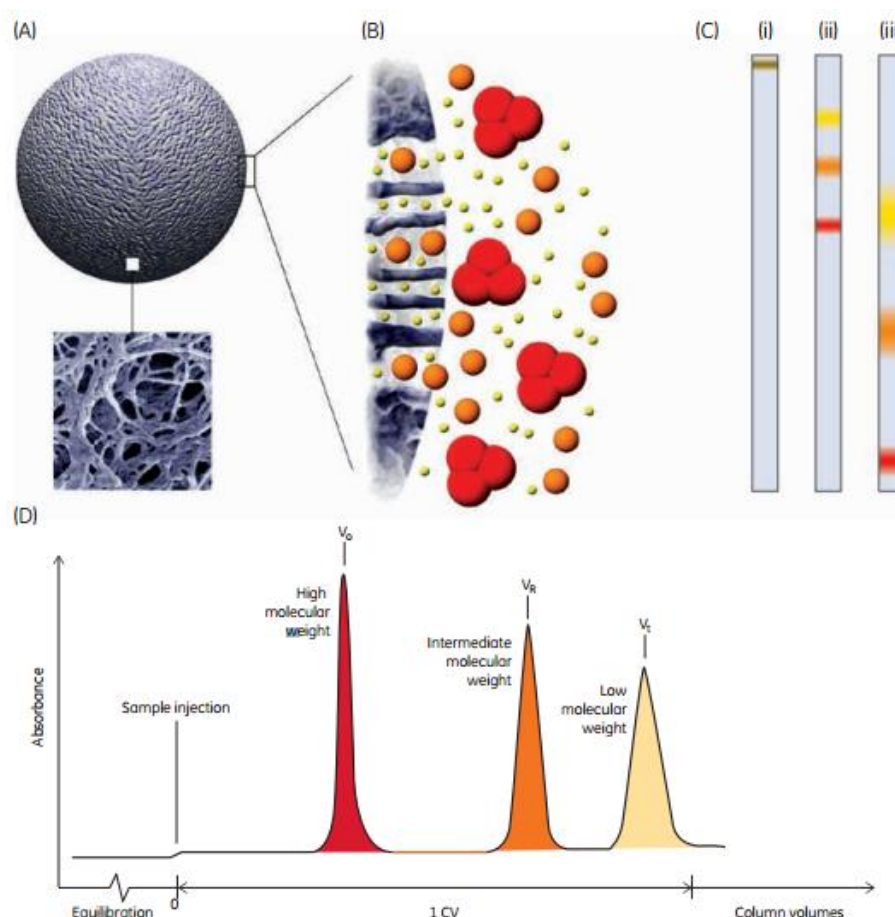


Figure 4.6. SEC principle. A) Electron microscopy image of a Superdex bead illustrating the different pore sizes. B) Sample representation of the column beads passing through and entering the various pores. C) Schematic representation of the separation, i) the top line represents the sample injected into the column, ii) samples passing through the column in which the smallest molecules in yellow diffuse into the pores delaying the flow through, iii) while large molecules pass through the column first. D) Typical chromatogram representing the elution of molecules by size. (Image taken from Size Exclusion Chromatography handbook from GE Healthcare Life Sciences,

https://www.gelifesciences.com/gehcls_images/GELS/Related%20Content/Files/1466158841539/litdoc18102218_20161012165335.pdf)

Experimental procedure

The protein solution from IMAC fractions totalling ~45 to 60 ml was concentrated to 10 ml using a centrifugal filter unit (Vivaspin 20 Molecular weight cut-off (MWCO) 10,000 Cat. No. 28932360, GE Healthcare Life Sciences) at 4,000g for approximately 30 minutes. The ÄKTA purifier system (GE Healthcare Life Sciences) was used for SEC purification with the HiLoad 26/600 Superdex 75 pg column (Cat. No. 28-9893-34, GE Healthcare Life Sciences).

The FPLC buffer used for purification was 20mM HEPES pH 7.5, 500 mM NaCl and 0.5 mM TCEP pH 7.0, filtered and degassed first and the column was equilibrated with FPLC buffer overnight. The next day, 2ml fractions were collected in a 2.4 ml 96-deep block plate (Greiner Master Block M1061-50EA, Sigma-Aldrich); samples of which were analysed using SDS-PAGE gel electrophoresis at 160 V for one hour (SERVAGel™ TG PRIME 4-20%, Cat. No. 43276.01, SERVA) and Coomassie stain for one hour (Cat. No. GEN-QC-STAIN-1L, Generon). Destain was performed by incubating the gel with water for 2 to 3 hours in the shaker. Fractions with most abundant protein were collected (~20ml) and concentrated with a centrifugal filter unit to a final volume of approximately 1 ml. To remove remains of the 6xHis-SUMO tag that remained after Prescission proteolytic digestion and SEC experiments, protein solution was further incubated with 1ml of talon metal affinity resin using a 10 ml centrifuge column for 30 minutes (Pierce™ Centrifuge column 10ml Cat. No. 89898, Thermo Fisher Scientific). After incubation was completed, the eluted solution was concentrated up to 500 µl, the protein concentration was quantified with a nanoDrop at absorbance A_{280} nm and purity of the protein was verified by SDS-PAGE gel electrophoresis. Several batches of protein were obtained and the final yield of purified protein was calculated using the concentration mg/ml adjusted with the final volume obtained.

4.3.6 CRYSTALLOGRAPHY

Crystallography is used to study protein crystallisation, and thereby properties and structures to help determine the arrangement of atoms and their function in biological and biochemical processes. X-ray crystallography is an important technique for the determination of the structure of a protein and plays an important role in structure-based drug discovery. X-ray crystallography can be found in detail in chapter 1, section 1.2.2.1.

The principle of protein crystallisation experiments is based on the solubility properties of a protein. Factors such as thermodynamics, pH and physical chemistry will control the process of crystallisation of the protein. A solubility curve is a schematic representation of the solubility of a protein in relationship with the concentration of precipitant (Fig. 4.7). Crystals will be formed in the supersaturated zone, when the protein concentration surpasses the solubility; the supersaturated zone comprises the metastable, nucleation and precipitation zones (Asherie 2004). The diagram illustrates the different levels of supersaturation; precipitation zone, nucleation zone and metastable zone. The precipitation zone occurs when the supersaturation is extremely high and the protein will form aggregates or precipitates and these conditions will not be favourable for crystal formation. The nucleation zone is when supersaturation is large enough so the nucleation and formation of crystals can occur and metastable zone is when supersaturation is lower and only supports crystal growth (Russo Krauss et al. 2013).

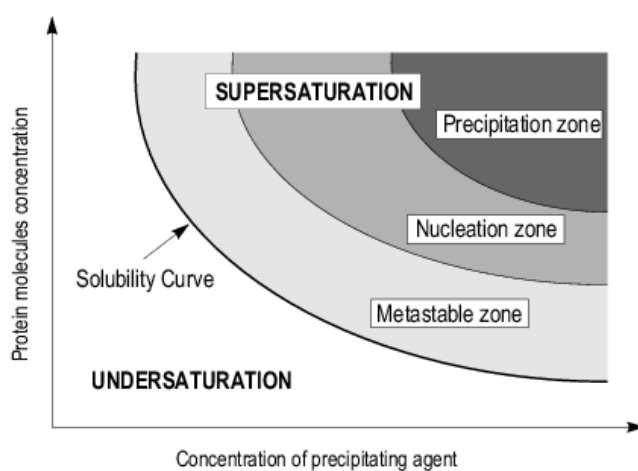


Figure 4.7. Crystallisation phase diagram. The solubility of a protein will depend on the concentration of the precipitant. The more supersaturated the protein becomes in solution the greater the probability of forming nucleation and crystal formation. The supersaturation phase includes the metastable, nucleation and precipitation zones (University of Cambridge, Biochemistry department; http://www.xray.bioc.cam.ac.uk/xray_resources/whitepapers/xtal-in-action/node3.html).

Experimental procedure

Preliminary crystallography screening experiments were performed in 2-drop, 96-MRC polystyrene crystallisation plate (MD11-00-100, Molecular Dimensions). Sitting drop experiments were set up using different commercial matrix screen solutions. A protein solution of 8 mg/ml diluted in FPLC buffer (20mM HEPES pH 7.5, 500 mM NaCl and 0.5 mM TCEP) with the addition of 5 mM zinc acetate and sodium cacodylate final concentration. A drop ratio of 1:1 was prepared using the Art Robbins Crystal Phoenix dispenser (AlphaBiotech). Crystallography plates were incubated at 14°C for 3-5 days. Further optimisation was performed of the crystal hits from screening experiments. Crystals were flash-cooled in liquid nitrogen for short-term storage. The best quality crystals (size and form) were exposed to X-ray beam to obtain diffraction data using the i04-1 beamline at Diamond Light Source synchrotron (Didcot, Oxfordshire).

Crystallography salt additives; zinc acetate (Cat. No. 1724703, Sigma-Aldrich) and Sodium cacodylate (Cat. No. C0250, Sigma-Aldrich).

Table 4.1. Commercial crystallisation screens used for primary crystallography experiments.

Matrix crystallisation screen	Catalogue number and supplier
Morpheus® HT-96	MD1-47, Molecular Dimensions
JCSG-plus™ HT-96	MD1-40, Molecular Dimensions
PACT premier™ HT-96	MD1-36, Molecular Dimensions
MIDASplus™ HT-96	MD1-107, Molecular Dimensions
Crystal Screen HT	HR2-130, Hampton Reserch
SaltRx HT™	HR2-136, Hampton Research

4.3.7 FRAGMENT SCREENING-XCHEM

The purpose of this technique is to identify small fragments binding in the LBD of rat AMPA protein and thereby identify novel or established binding sites for allosteric modulators. The fragment hits will provide the starting points for further chemical optimisation to improve the biological activity and physicochemical properties. The Diamond Fragment Screening (XChem) was performed at Diamond Light Source facilities. At these facilities, they have implemented a highly streamlined process for the screen of compounds in a shorter period of time (less than a week). The full methodology includes crystal targeting, crystal soaking, crystal harvesting, automatic data collection and data analysis. XChem has several fragment libraries, over 2000 compounds available at 100-500 mM in DMSO (Fragment Screening - XChem, Diamond Light Source website). A total of 700 fragments were screened from three different libraries; DSPL-Diamond Poised, Oxxchem and Leeds 3D.

▪ Crystals preparation

The best diffracting crystals grew in the well condition B1 of Morpheus® screen, solutions present in that condition are listed in Table 4.2.

Table 4.2. Conditions of well B1 of commercial Morpheus® screen. (Appendix II)

Well screen condition	Solution mix
0.09 M Halogens	Halogens: Sodium fluoride; sodium bromide and sodium iodide
0.1 M Buffer system 1 pH 6.5	Imidazole; MES monohydrate (acid)
50 % v/v Precipitant Mix 1	PEG 500 MME and PEG 20,000

MES - 2-(N-morpholino) ethanesulfonic acid; PEG – Polyethylene glycol and MME – Mono methyl ether

Solutions were set up in a 96-well SwissCi 3 drop plate (Cat. No. 3W96TPS, SWISSCI Scientific Innovation), using the sitting drop method along with 30 µl of the reservoir solution from the Morpheus screen (Cat. No. MDSR-47-B1, Molecular Dimensions). Experiments were performed using the Oryx8 protein crystallisation robot (Douglas instrument) with 5 mg/ml of protein solution with a final drop ratio of 1:1 of protein and reservoir solution (total volume per drop of 0.30 µl); they were dispensed at least 2 drops in each well of the plate. Plates were stored at 14°C for 1-2 days until crystals appeared and then stored for fragment screening.

▪ Crystal targeting

Crystal plates were transported to the Diamond Light Source facilities where they were given a barcode number. Plates were then imaged to identify the crystals in each drop and with the software TexRank the crystals were targeted for compound injection by selecting an area opposite the crystal.

▪ Crystal Soaking

Compounds were transferred to the crystals using an ECHO® 550 acoustic liquid handler (Labcyte). The dispense coordinates were selected by TexRank software. Plates were inverted and ultrasonic pulses were used for dispensing the compound in nanoliter volume. Compounds were injected at final concentration of 25 mM (5% DMSO) and 50 mM (10% DMSO). After compound injection, the plates were incubated for 1 hour at 14°C.

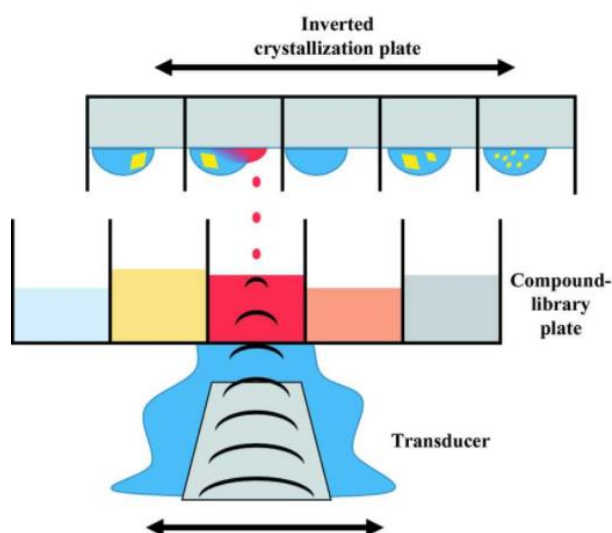


Figure 4.8. ECHO acoustic droplet ejection. Sound waves eject precise drops of compound from a microplate and deposit into inverted crystallisation plate (Adapted Acta Crystallographica Section, <http://journals.iucr.org/d/issues/2017/03/00/ba5268/ba5268fig1.html>). Compounds were injected to have a final concentration of 25 and 50 mM.

- **Crystal Harvesting**

Following a one hour incubation with compound at 14°C, crystals were harvested manually using the OLT Crystal Shifter (Oxford lab technologies). This equipment is automated to speed up the process of crystal harvesting by using a microscope x-y stage, which maintains unsealed plates under a thick plastic cover to avoid quick evaporation of drops and allows the harvesting of one crystal at a time. Usually around 100 crystals can be harvested per hour.

- **X-ray data collection and analysis**

Crystals were exposed to X-rays on beamline i04-1 (Diamond Light Source) with the automated robot BART system, a new sample-changing robot with improved sample exchange times. Data was collected and analysed using XChemExplorer and pan-dataset density analysis (PanDDA software). The process is automated and it gave compound hits as “events” to analyse in the Crystallography object-oriented toolkit (COOT) software package, to then perform model building and space refinement.

4.4 RESULTS

4.4.1 IMMOBILIZED-METAL AFFINITY CHROMATOGRAPHY (IMAC)

Protein IMAC purification experiments resulted in six elution fractions of approximately 7.5 ml each (E1-6; Fig. 4.9) containing rGluA2 LBD protein. The elution fractions, flow through and wash fractions were collected and characterised in a SDS-PAGE gel electrophoresis. In the gel (Fig. 4.9), the flow through fraction showed the proteins that were not retained by the talon beads. More importantly, the band of 45 kDa present in the elution fractions correspond to the purified protein rGluA2 LBD. The rGluA2 was present in high abundance in fraction E2 displaying a strong band of 45 kDa. In addition, the gel displayed a concentrated band in the talon beads sample (B1) before elution, which means the retention of the protein by the talon beads and comparison with the talon beads sample (B2) after elution, indicated that most of the protein bound to the talon beads was eluted with 300 mM Imidazole.

Wash fractions W1 and W2 displayed a number of unspecific proteins of 27 kDa, 70 up to 100 kDa, these observed bands were almost fully removed with the wash buffer with low concentration of imidazole. The remaining bands not corresponding to rGluA2 from elution fractions 1-6 were removed using size exclusion chromatography (SEC).

In order to observe if the protein eluted correspond to rGluA2, samples of elution fractions were collected and incubated with 3C protease enzyme. Samples before and after incubation with 3C protease were run on a SDS-PAGE gel to verify the cleavage of rGluA2-6xHis-SUMO protein by protease 3C. The gel displayed a band of 45 kDa in the sample without 3C protease (Fig. 4.10). Whereas, the sample following 3C protease incubation displayed two bands of 30 kDa and 15 kDa, corresponding to rGluA2 protein and 6xHis-SUMO tag respectively (Fig. 4.10). These results demonstrated the correct purification of rGluA2 protein, to further purify the sample size exclusion chromatography was performed.

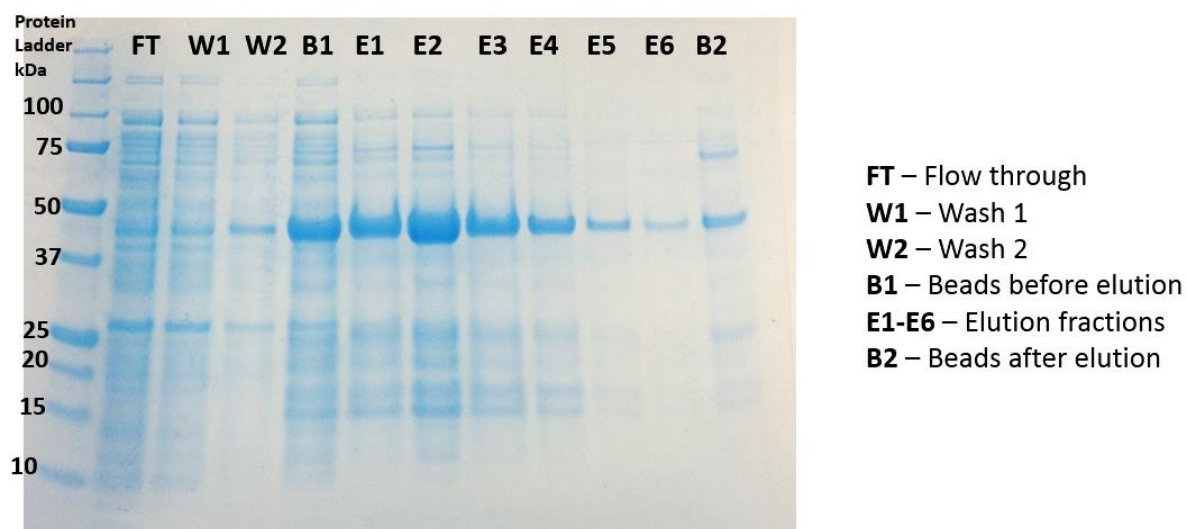


Figure 4.9. SDS-PAGE gel of IMAC purification of the rGluA2 LBD protein. Bands of 45 kDa corresponding to the LBD protein rGluA2. Approximately 50 ml of supernatant was added to 7.5 ml of talon beads, the flow thought was ~50 ml, washes 1 and 2 were ~ 100ml each and samples of 25 μ l were taken for the SDS-PAGE gel. 10 μ g of protein loaded per well, gel stained with Blue Coomassie, protein ladder Precision Plus Protein™ All Blue (Cat. No. 1610373, Bio-Rad).

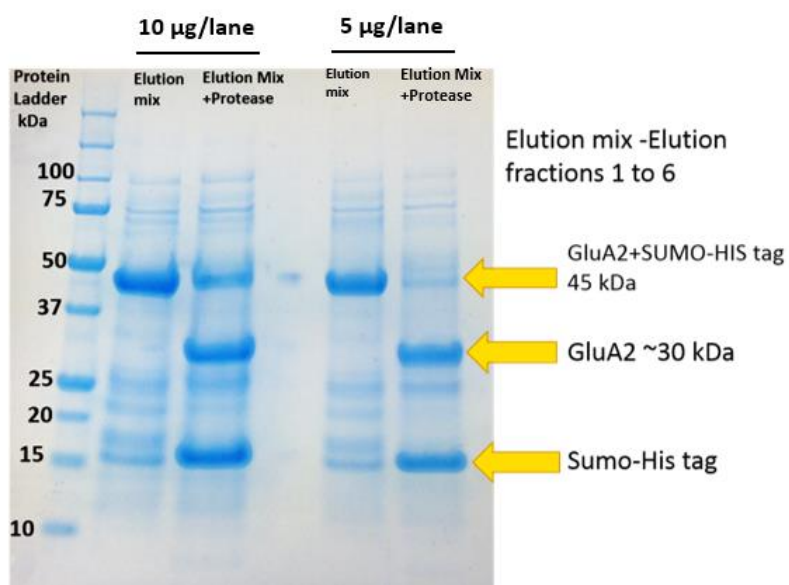


Figure 4.10. SDS-PAGE gel of 3C protease activity. Elution mix samples correspond to the pooled E1-6 fractions (shown in Fig. 4.9) before the addition of 3C protease and displayed a concentrated band of rGluA2 at 45 kDa. Elution mix + Protease correspond to elution fractions after incubation with 3C protease with the production of two bands of 30 kDa and 15 kDa, corresponding to rGluA2 LBD and 6xHis-SUMO tag respectively.

4.4.2 SIZE EXCLUSION CHROMATOGRAPHY (SEC)

Protein SEC purification experiments resulted in a chromatogram displaying the separation of components of the protein sample, measured by ultraviolet (UV) light absorption at A_{280} . The chromatogram displayed two main peaks, first peak around 60 ml and second peak at 80-85 ml (Fig. 4.11A). Fractions from both peaks were collected and run on a SDS-PAGE gel (Fig. 4.11B) which showed that the major peak contained a range of proteins varying from 15 to 120 kDa corresponding to fraction 1E11 and as a result this major peak was not suitable for further purification experiments. More importantly, the second minor peak correspond to the LBD rGluA2 protein with bands of 30 kDa in fractions 1G8 to 1H5. A smear band below the protein band suggest a partial degradation of the protein. A band of 15 kDa was also shown in the gel, this band correspond to 6xHis-SUMO tag remain in the sample. Finally, to remove remain 6xHis-SUMO tag the protein fractions were further purified with IMAC. The final protein solution was highly pure (Fig. 4.12), with a concentration of 9.12 mg/ml in ~1.2 ml, with total yield of 10.9 mg of protein from starting 8 litres of cell culture. Concentration was measured by nanoDrop using the molecular weight of 30.211 kDa and extinction coefficient of $41,370 \text{ M}^{-1} \text{ cm}^{-1}$ at 280 nm. Finally, the band just below the protein observed previously was not present in the final purified protein, suggesting a degraded protein over time (during incubation with further talon beads) or some remain tag present in the sample and further removed with talon beads.

Five batches of purified protein were prepared for crystallography experiments listed in Table 4.3, different starting cell culture were prepared from 2 to 8 litres. It was observed that the larger amount of starting cell culture, the more unspecific proteins were produced.

Table 4.3. Different batches of purified protein obtained after purification experiments

Batch No.	Starting cell culture (L)	Concentration (mg/ml)	Final volume obtained (μ l)	Yield of purified protein (mg)
1	2	8.0	500	4.0
2	4	12.27	1000	12.3
3	8	9.12	1200	10.9
4	6	8.1	800	6.5
5	2	8.0	500	4.0

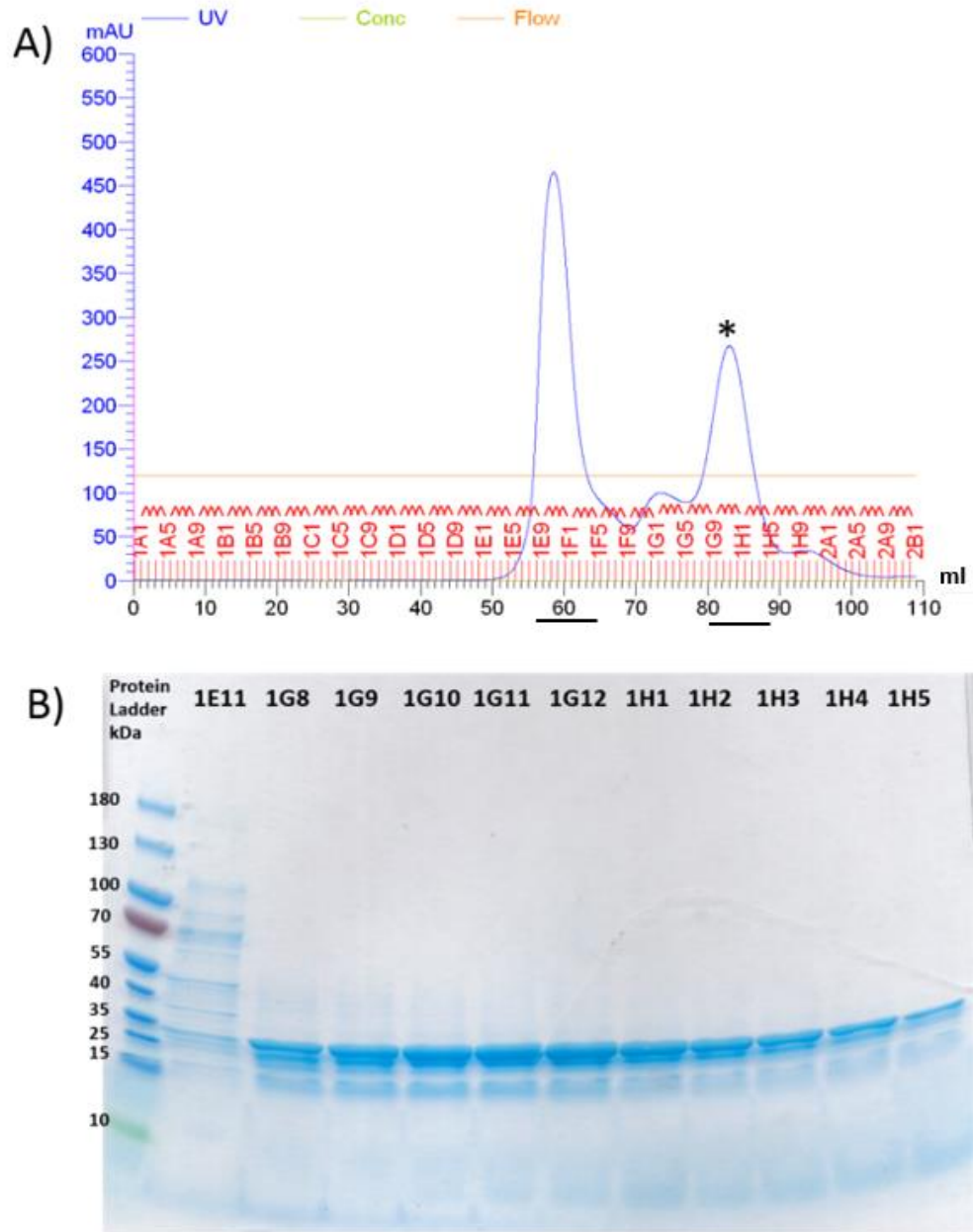


Figure 4.11. Size exclusion chromatography of the rGluA2 LBD after 3C proteolytic removal of the 6xHis-SUMO tag. A) Chromatogram obtained from SEC purification of the LBD rGluA2 protein with the second peak marked with an asterisk corresponding to the protein of interest. B) SDS-PAGE gel of the fractions obtained by SEC, numbering correspond to chromatogram fractions. The protein band at 30 kDa correspond to the LBD of rGluA2. 10 μ g of protein loaded per well, protein ladder use was PageRuler™ prestained ladder (Cat. No. 26616, Thermo Fisher Scientific).

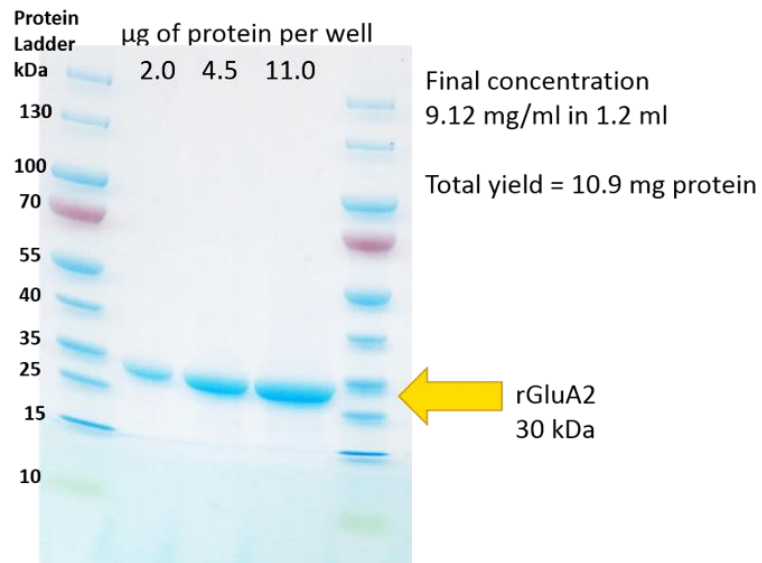


Figure 4.12. Final purity of the protein rGluA2. SDS-PAGE gel verification of the pure protein. One single band of 30 kDa correspond to the LBD of rGluA2 protein. The gel displayed the protein in high purity, with no other bands in the gel. An amount of 2.0, 4.5 and 11.0 µg of protein was loaded in the gel.

4.4.3 CRYSTALLOGRAPHY

In crystallisation screen experiments, the only crystal hits with adequate quality were obtained with the Morpheus® HT-96 plate (Table 4.4). The best crystal in terms of quality, size and diffraction was with the well B1 condition. The rest of the crystals grown were not singular or were too small for the X-ray beam.

Table 4.4. Morpheus® HT-96 crystal hits conditions

Well	Conditions
A1	0.06 divalents, 0.1 M buffer system 1 pH 6.5 and 50 % v/v precipitant Mix 1
B1	0.09 M halogens, 0.1 M buffer system 1 pH 6.5 and 50 % v/v precipitant Mix 1
C4	0.09 M NPS, 0.1 M buffer system 1 pH 6.5 and 50 % v/v precipitant Mix 4
C5	0.09 M NPS, 0.1 M buffer system 2 pH 7.5 and 50 % v/v precipitant Mix 1

Nitrate Phosphate Sulfate (NPS). Full mixes of additives, buffers and precipitants of Morpheus® HT-96 in appendix II.

The condition B1 gave consistently long rectangular single type crystals, in orthorhombic space group (three unequal axes at right angles). Crystals were prepared with 5.0 mg/ml of protein diluted with FPLC buffer, using the hanging drop method with the reservoir solution corresponding to the condition B1 from Morpheus commercial screen.

Crystals grew after 24 -48 hours at 14°C and drops displayed a high amount of precipitation and skin formation. In addition, the crystals presented at least one irregular edge (Fig. 4.13) and size varied from 0.1 to 0.2 mm. The main advantage of the Morpheus® screen is that the solutions already contain cryoprotectant, which makes it suitable for quick storage in liquid nitrogen. The Morpheus solution of B1 contains 40 % v/v of polyethylene glycol (PEG) and monomethyl ether (MME) 500 which both function as a precipitant and cryoprotectant (appendix II) to protect crystals from free radicals from ionising X-rays when collecting diffraction data.

Crystal diffracted at 1.84 Å resolution in the X-ray beamline i04-1 at Diamond Light Source (Didcot). Molecular replacement was carried using a previously described rat GluA2 structure (Armstrong & Gouaux 2000), accession code 1FTJ from the protein data bank (PDB). Final models

were refined using Collaborative Computational Project No.4 (CCP4) and Python-based Hierarchical Environment for Integrated Xtallography (PHENIX) software by Dr. Mark Roe. Crystallographic Object-Oriented Toolkit (COOT) was used for manual model building. The LBD of rGluA2 was in complex with glutamate, from the 250 μ M of glutamate added in the lysis buffer in purification experiments. The final data collection and refinement statistics are presented in Table 4.5.

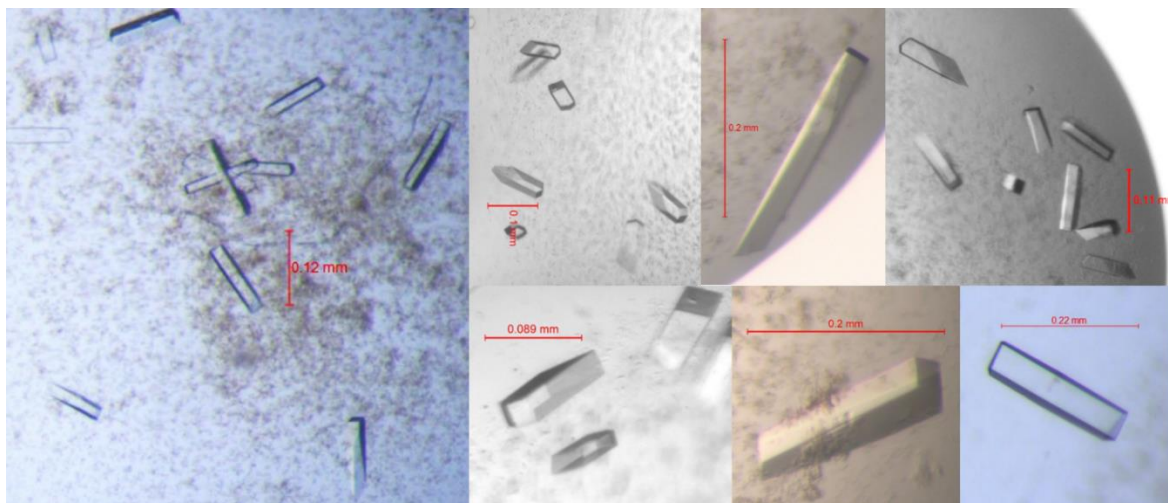


Figure 4.13. Rectangular orthorhombic crystals of the LBD of rGluA2. Crystals were obtained at 5.0 mg/ml using the hanging drop crystallography method. The formation of skin and precipitation was present in all drops. All crystals presented one irregular ending on one side.

Table 4.5. Crystallographic statistics for the rGluA2 LBD in complex with glutamate. Crystal shot at the i04-1 beamline at Diamond Light Source.

Data Set (Highest shell in parentheses)	rGluA2
a (Å)	54.47
b (Å)	113.42
c (Å)	47.41
α (°)	90
β (°)	90
γ (°)	90
Space Group	P 21 21 2
Wavelength (Å)	0.9281
Resolution Limit (Å)	113.42 – 1.84 (1.87-1.84)
Number of Obs.	26305 (1297)
Completeness (%)	100 (100)
Multiplicity	6.5 (6.8)
Rmerge %	0.081 (0.940)
Rpim(I) %	0.046 (0.515)
CC _{1/2}	0.999 (0.783)
I/ σ I	15.2 (2.1)
Refinement	
Resolution Range (Å)	56.71-1.84
Rcryst	0.224
Rfree	0.269
Number of protein atoms	1,924
Number of ligand atoms	10
Number of solvent atoms	81
Mean B	33.718
Rmsd bond lengths (Å)	0.019
Rmsd bond angles (°)	1.980

A monomer of the rGluA2 LBD structure was solved in complex with glutamate. The structure showed that glutamate binds in the cavity space between the interface of S1 and S2 (Fig. 4.14). Zinc ions and acetate are present in the structure, zinc acetate and sodium cacodylate were added in the crystallography experiments as additives to facilitate the nucleation and formation of crystals. It is noteworthy that crystallography experiments without both additives failed to grow crystal suggesting the need of both additives for successful AMPA crystal formation.

More interestingly, the interactions of glutamate with the LBD of rGluA2 are the same as the literature 1FTJ accession code from PDB (Armstrong & Gouaux 2000). The crystal structure showed that glutamate α -carboxyl interacts with Ser-142, Arg-96 and Thr-91 of the protein; the α -amino group of agonist forms interactions with Tyr-61, Glu-193 and Pro-89 and the δ -carboxyl with Thr-143 (Fig. 4.15). The interaction between Arg-96 and the α -carboxyl of glutamate is conserved in all glutamate receptors (Kawamoto et al. 1997; Lampinen et al. 1998; Armstrong & Gouaux 2000). Arg-96 and Glu-193 residues formed strong salt bridge interactions, suggesting their importance for agonist recognition and binding.

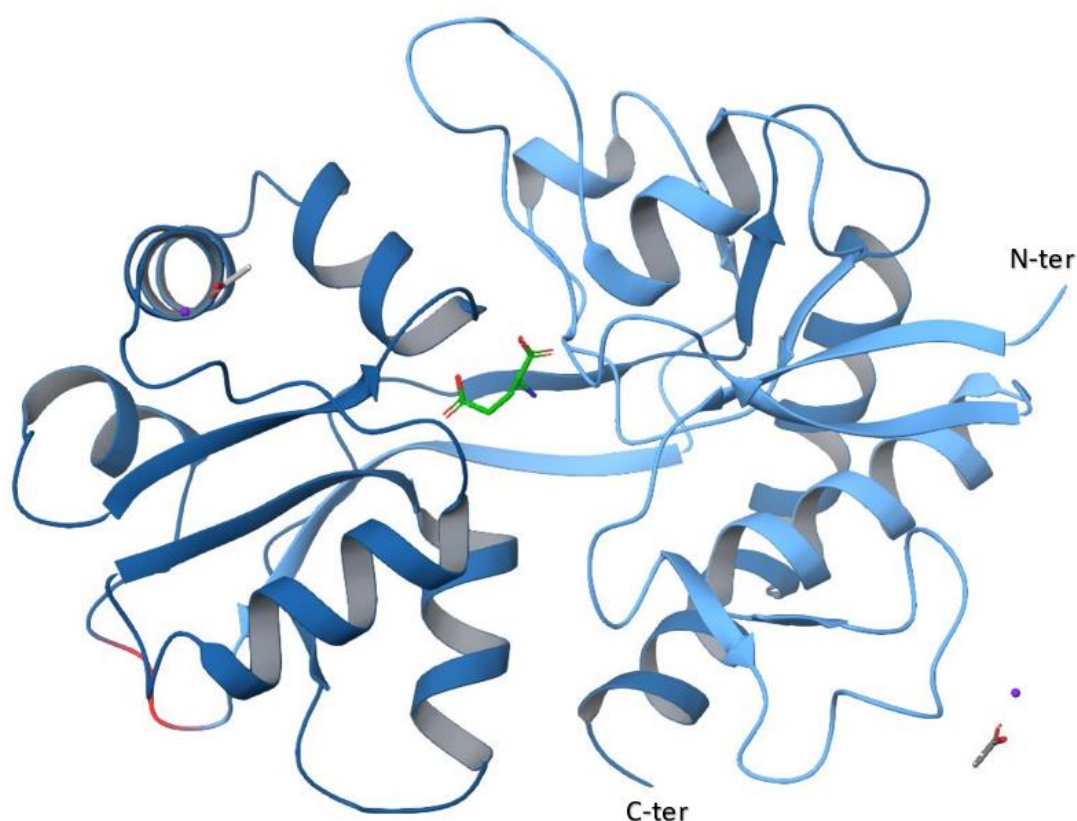


Figure 4.14. Monomer of the LBD of rGluA2 in complex with glutamate. The construct consisted of S1 and S2 domains, dark blue and light blue respectively. Glutamate in green, Gly-Thr linker is displayed in red.

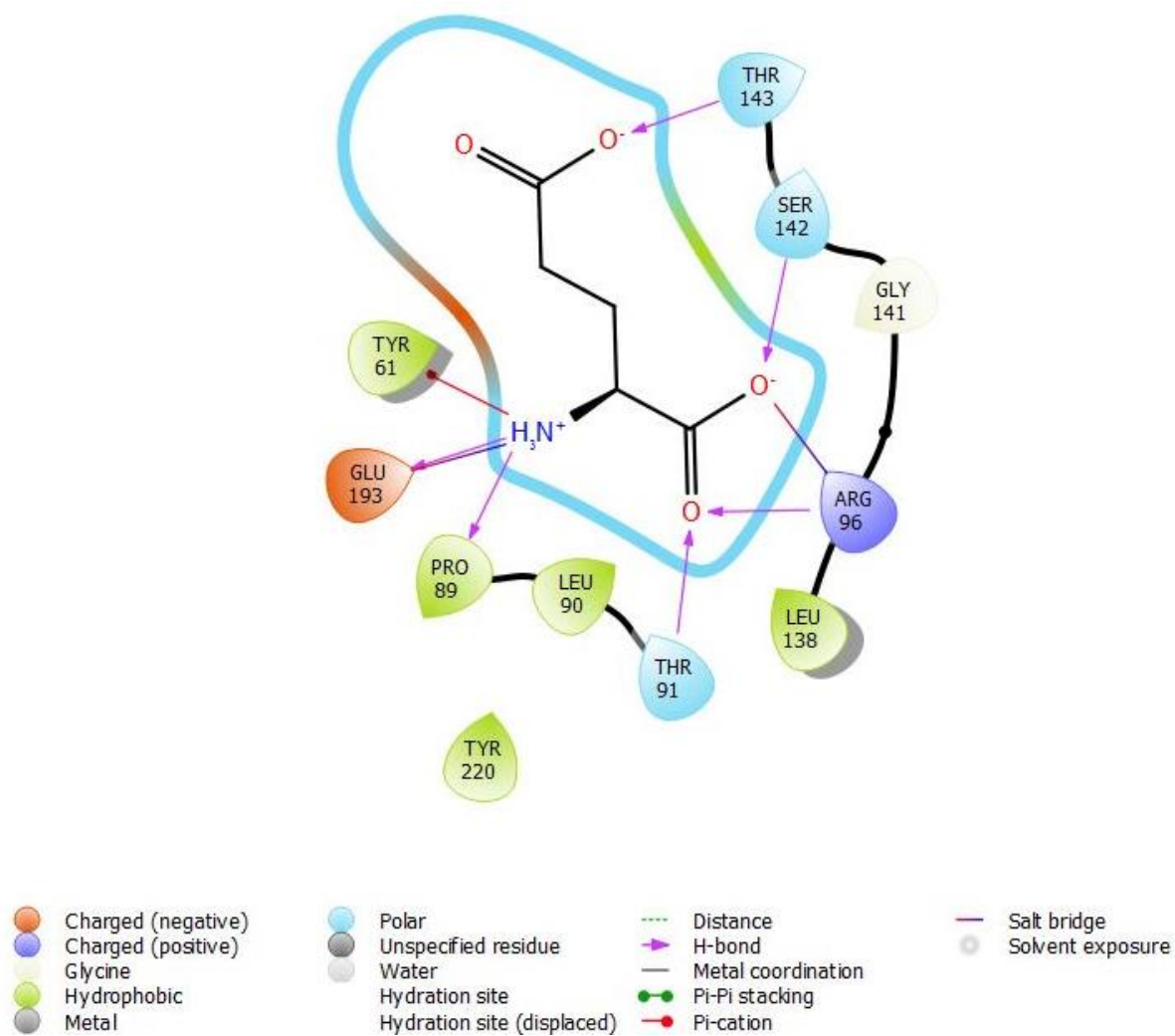


Figure 4.15. Glutamate binding interactions with LBD rGluA2. Arg-96 and Glu-193 are important for agonist binding. Hydrogen bonds are shown in arrows in fuchsia and salt bridges in blue/red line. Interaction diagram generated from Maestro Schrödinger.

4.4.4 FRAGMENT SCREENING-XCHEM

From the 700 compounds soaked into rGluA2 crystals, a number of events were found by PanDDA software, which was further analysed closely to confirm the hits. The hits were analysed using COOT to observe the location of the binding sites. Refinement was carried out using the internal Diamond software XChemExplorer (XCE)-COOT and exported as a PDB file for further refinement performed by Dr. Mark Roe. Crystallography data statistics from crystals with fragments are shown in Table 4.7.

Eight fragments were found to be present in the rGluA2 LBD (Table 4.6). However, these fragments were present at low-occupancy in the structure which means a low-electron density map of the structure making it difficult to distinguish from different structural conformations (amino acid residues). The low-occupancy of the fragment hits could be due to the low concentration of the fragment, suggesting that fragments at higher concentration might improve the percentage of occupancy in the crystal structure.

These results suggest the binding sites of allosteric modulators in the dimer interface and in a site near the Gly-Thr linker. As previously reported (Ward et al. 2011), a binding site in the dimer interface of the LBD was observed. Three different binding sites (at low-occupancy) were observed in the LBD of rat GluA2, two binding sites in the dimer interface (1a and 1b) across the two-fold symmetry axis of the dimer, one binding site (2) near the Gly-Thr linker located in one of the outside loops of the monomer of the structure and one cysteine free site (3) at Cys-58 (Fig. 4.16). The cysteine free site was not explored further due to lack of functionality of these site for drug research.

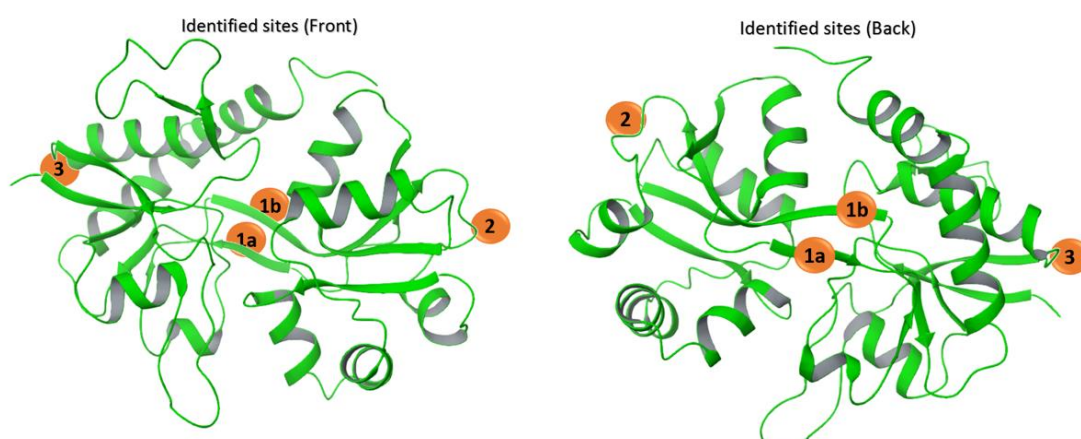


Figure 4.16. Identified sites in the LBD of rGluA2. For clarity of the binding site only one monomer is displayed in this figure. Site 1a and 1b is located inside the dimer interface of the LBD, site 2 near the Gly-Thr linker in one of the external loops of the structure chain, and site 3 corresponding to the free Cys-58, figure generated using Maestro Schrödinger.

Table 4.6. Compound hits found in XChem fragment screening library

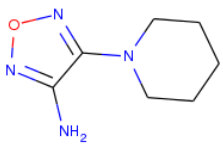
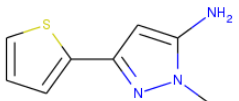
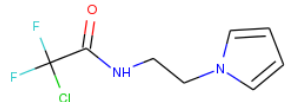
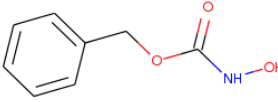
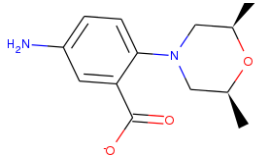
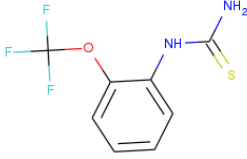
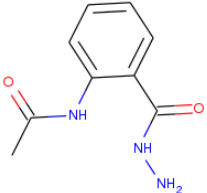
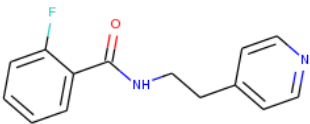
Compound	Structure	Identified sites	Residues in identified sites
Compound 1		Dimer interface Site 1a	Chain A: Lys-104, Pro-105, Phe-106, Met-107 and Ser-108 Chain B: Ile-103, Pro116, Ser-228, Lys-229 and Gly-230
Compound 2		Site 2	Chain B: Lys-217, Gly-129, Thr-130, Pro-131, Lys-196 and Gly-197
Compound 3		Dimer interface Site 1a	Chain A: Lys-104, Pro-105, Phe-106, Met-107 and Ser-108 Chain B: Ile-103, Pro116, Ser-228, Lys-229 and Gly-230
Compound 4		Site 2	Chain B: Lys-217, Gly-129, Thr-130, Pro-131, Lys-196 and Gly-197
Compound 5		Site 2	Chain B: Lys-217, Gly-129, Thr-130, Pro-131, Lys-196 and Gly-197
Compound 6		Dimer interface Site 1b	Chain A: Ile-92, Pro-105, Met-107, Ser-108, Ser-217, Lys-218 and Gly-219 Chain B: Lys-115, Pro-116, Phe-117, Met-118, Ser-119, Leu-250 and Ser-253
Compound 7		Dimer interface Site 1b	Chain A: Ser-92, Pro-105, Ser-108, Ser-217, Lys-218 and Gly-219 Chain B: Lys-115, Pro-116, Phe-117, Met-118, Ser-119
Compound 8		Dimer interface Site 1b	Chain A: Pro-105, Ser-108, Ser-217, Lys-218 and Gly-219 Chain B: Lys-115, Pro-116, Phe-117, Met-118, Ser-119, Lys-229, Gly-230 and Tyr-231

Table 4.7. Crystallographic statistics for the rGluA2 LBD crystals in complex with compound fragments. Crystals shot at the i04-1 beamline at Diamond Light Source.

Data Set (Highest shell in parentheses)	Compound 1	Compound 2	Compound 3	Compound 4
a (Å)	54.07	54.34	54.40	54.69
b (Å)	113.59	133.13	114.73	113.05
c (Å)	47.17	47.44	47.52	47.53
α (°)	90	90	90	90
β (°)	90	90	90	90
γ (°)	90	90	90	90
Space Group	P 21 21 2	P 21 21 2	P 21 21 2	P 21 21 2
Wavelength (Å)	0.9281	0.9281	0.9281	0.9281
Resolution Limit (Å)	56.80 – 2.28 (2.32-2.28)	56.56 – 1.87 (1.90-1.87)	57.36 – 1.88 (1.91-1.88)	56.52 – 1.80 (1.83-1.80)
Number of Obs.	13219 (572)	24891 (1229)	24508 (1196)	27969 (1384)
Completeness (%)	95.2 (82.8)	100 (98.8)	98.8 (98.9)	99.5 (98.3)
Multiplicity	5.9 (5.1)	6.5 (6.8)	6.5 (6.9)	6.3 (6.6)
Rmerge %	0.069 (0.719)	0.054 (0.787)	0.112 (1.385)	0.093 (0.859)
Rpim(I) %	0.041 (0.443)	0.031 (0.445)	0.065 (0.790)	0.055 (0.492)
CC _{1/2}	0.999 (0.709)	0.999 (0.795)	0.997 (0.792)	0.999 (0.757)
I/ σ I	17.0 (2.1)	18.3 (2.1)	12.1 (2.4)	14.6 (2.3)
Refinement				
Resolution Range (Å)	56.90 – 2.19	56.62 – 1.88	57.44 – 1.76	56.60 – 1.74
Rcryst	0.199	0.216	0.241	0.231
Rfree	0.261	0.268	0.279	0.271
Number of protein atoms	1,999	1,999	1,999	1,999
Number of ligand atoms	22	34	24	34
Number of solvent atoms	159	147	160	148
Mean B	47.036	36.944	37.033	29.402
Rmsd bond lengths (Å)	0.015	0.020	0.019	0.020
Rmsd bond angles (°)	1.685	2.071	1.962	2.109

Data Set (Highest shell in parentheses)	Compound 5	Compound 6	Compound 7	Compound 8
a (Å)	53.87	54.56	54.28	54.59
b (Å)	113.32	113.60	113.23	114.19
c (Å)	47.24	47.45	47.30	47.27
α (°)	90	90	90	90
β (°)	90	90	90	90
γ (°)	90	90	90	90
Space Group	P 21 21 2	P 21 21 2	P 21 21 2	P 21 21 2
Wavelength (Å)	0.9281	0.9281	0.9281	0.9281
Resolution Limit (Å)	113.32 – 2.12 (2.15-2.12)	56.80 – 1.81 (1.84-1.81)	56.61 – 1.96 (1.99-1.96)	114.19 – 1.75 (1.78-1.75)
Number of Obs.	17094 (847)	27115 (1328)	21630 (1070)	30250 (1456)
Completeness (%)	100 (99.8)	99.1 (98.8)	100 (99.5)	100 (99.3)
Multiplicity	6.5 (6.7)	6.6 (6.8)	6.5 (6.3)	6.6 (6.8)
Rmerge %	0.089 (0.725)	0.055 (0.744)	0.071 (0.786)	0.062 (0.803)
Rpim(I) %	0.053 (0.405)	0.032 (0.412)	0.041 (0.450)	0.036 (0.440)
CC _{1/2}	0.999 (0.816)	0.999 (0.772)	0.999 (0.770)	0.999 (0.792)
I/ σ I	13.4 (2.3)	19.0 (2.3)	15.0 (2.1)	15.6 (2.1)
Refinement				
Resolution Range (Å)	56.70 – 2.16	56.86 – 1.81	56.69 – 1.96	57.17 – 1.79
Rcryst	0.200	0.219	0.215	0.238
Rfree	0.268	0.263	0.275	0.277
Number of protein atoms	1,999	1,999	1,999	1,999
Number of ligand atoms	28	25	38	28
Number of solvent atoms	164	162	147	167
Mean B	42.750	33.131	39.771	34.748
Rmsd bond lengths (Å)	0.015	0.020	0.017	0.020
Rmsd bond angles (°)	1.699	2.078	1.951	2.121

The crystals obtained resulted in the monomer of the LBD, then the dimers were generated by using the symmetry crystal mate function in COOT and Maestro Schrodinger computational program. Then structure alignment was performed to verify the correct position of the dimer compared to another structure in the PDB (2XX8). Structures and binding sites are listed in Table 4.6.

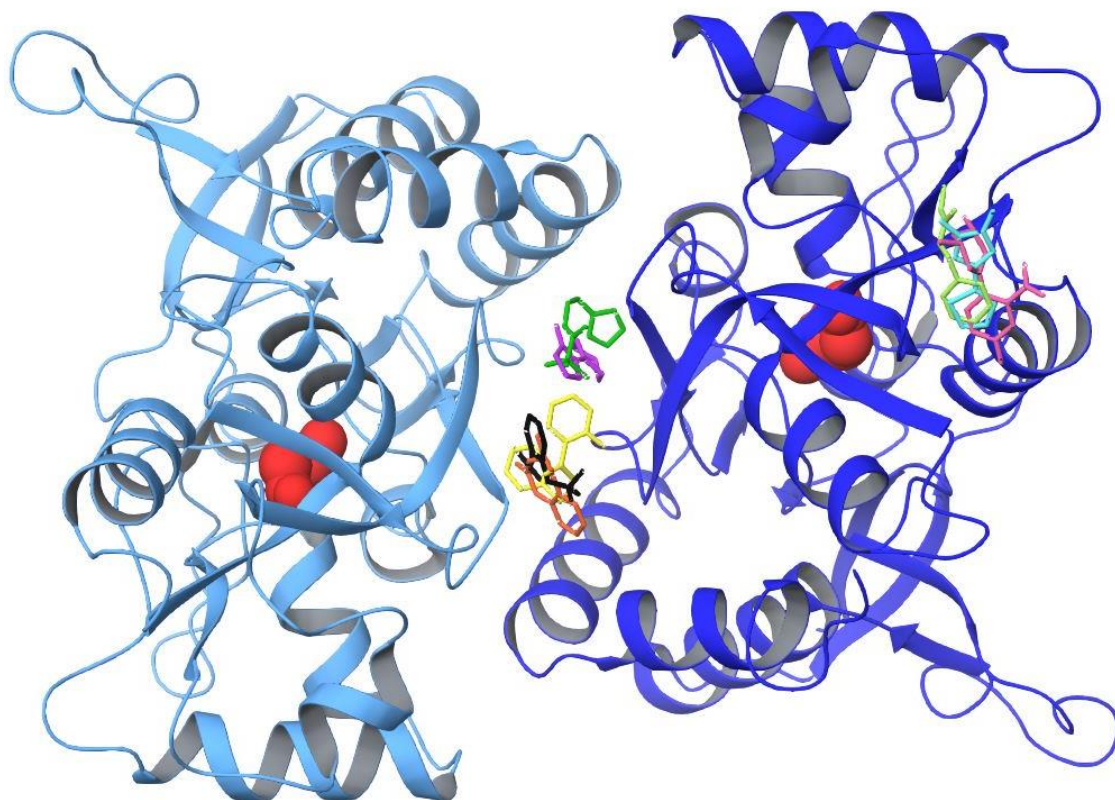


Figure 4.17. Summary of LBD of rGluA2 in complex with fragment hits obtained after XChem fragment screen. Chain A and B forming the LBD of the protein dimer in light and dark blue respectively, glutamate is represented by the red spheres. Positions of the compounds present in the structure; compounds 1 and 3 situated in the dimer interface site 1a in purple and green respectively. Compounds 6, 7 and 8 also in the dimer interface but in site 1b in black, orange and yellow respectively. Compounds 2, 4 and 5 in site 2 of chain B in cyan, mint and pink respectively. All compound structures are shown in a stick representation and generated using Maestro Schrödinger version 11.1.

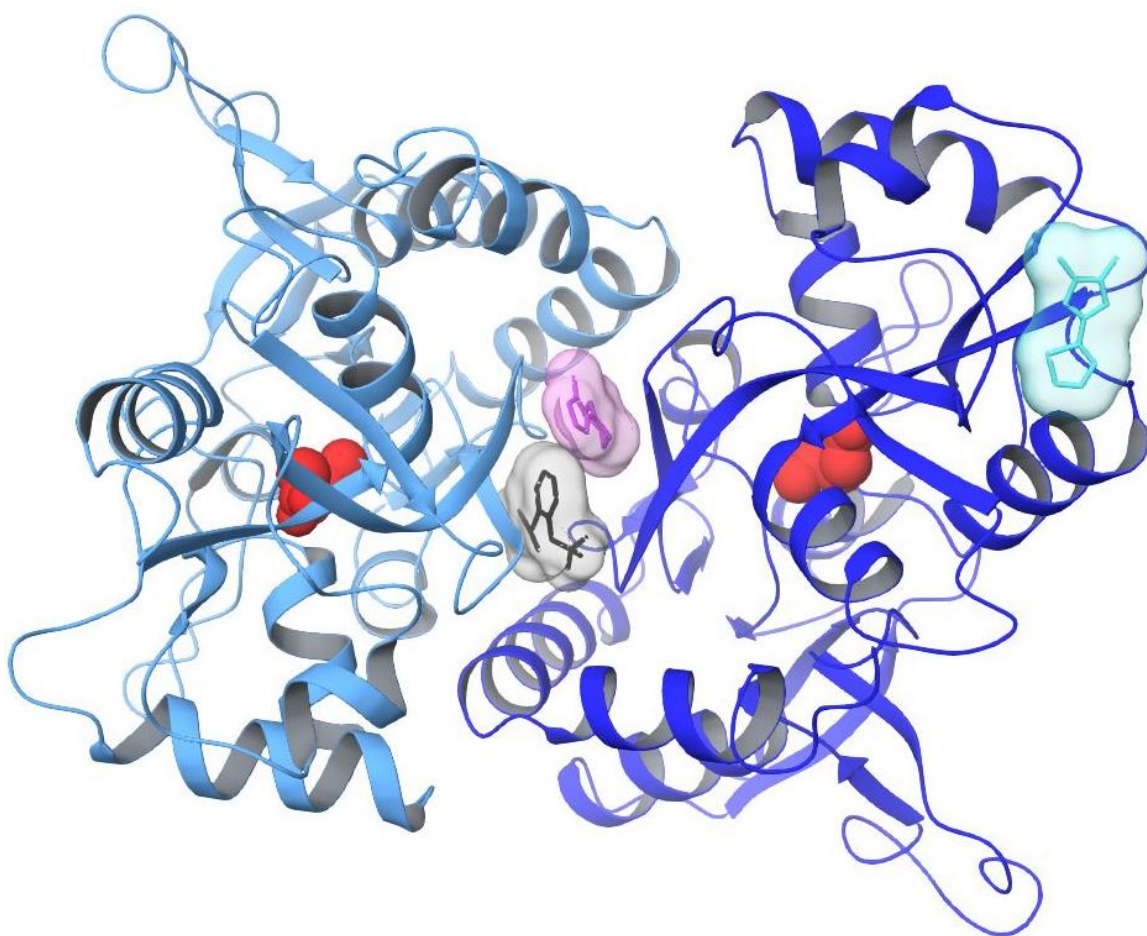


Figure 4.18. Compounds 1, 2 and 6 in the LBD of rGluA2. Glutamate in red spheres representation, chain A and B in light and dark blue respectively. Compound 1 in site 1a in purple and compound 6 in site 1b in black within the dimer interface, both located in the site across the 2-fold symmetry axis. Compound 2 in site 2 in cyan. Structures of dimer and compound with surfaces generated using Maestro Schrödinger version 11.1.

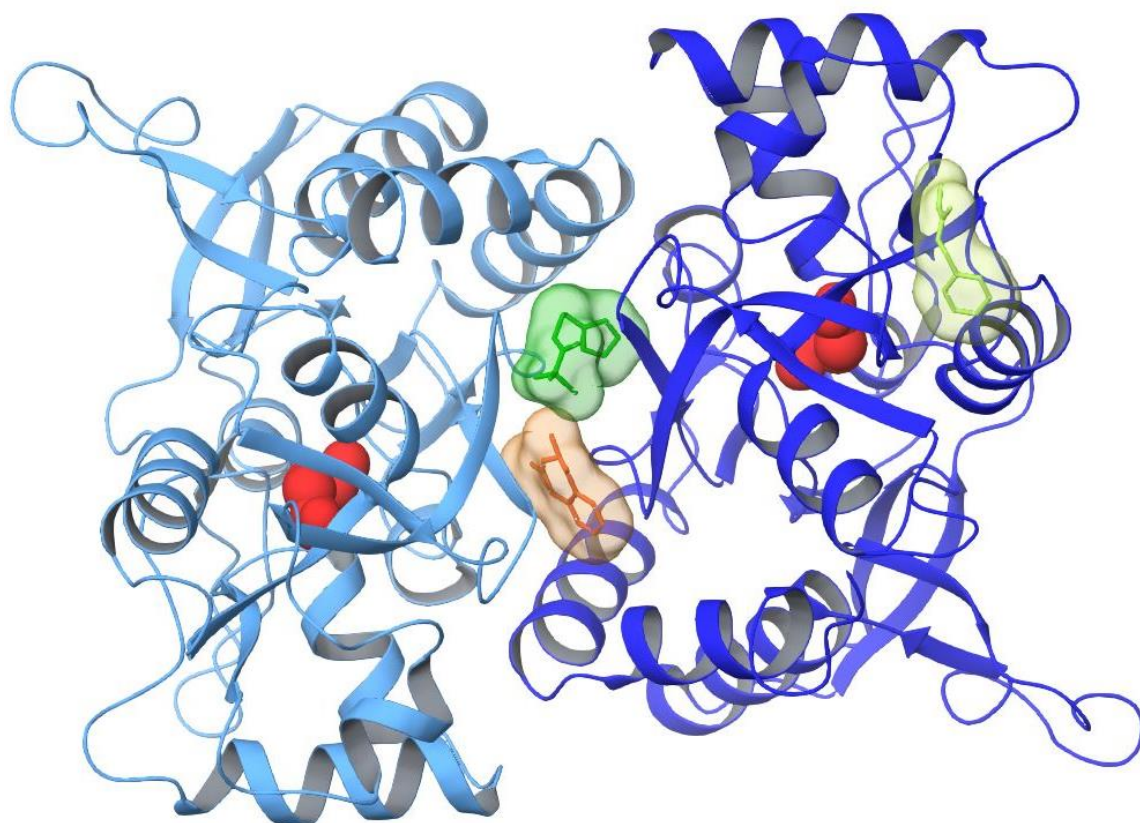


Figure 4.19. Compounds 3, 4 and 7 in the LBD of rGluA2. Glutamate in red spheres representation, chain A and B in light and dark blue respectively. Compound 3 in site 1a in green and compound 7 in site 1b in orange within the dimer interface, both located in the site across the 2-fold symmetry axis. Compound 4 in site 2 in mint. Structures of dimer and compound with surfaces generated using Maestro Schrödinger version 11.1.

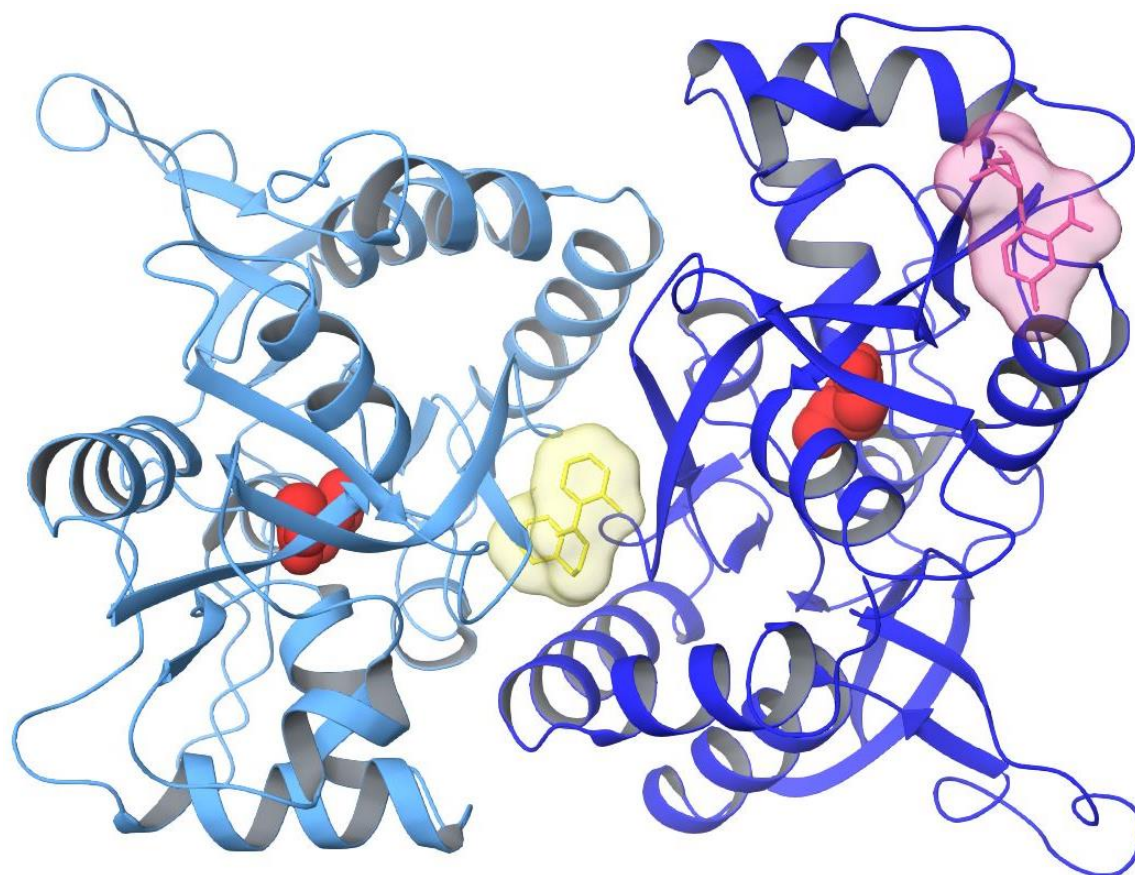


Figure 4.20. Compounds 5 and 8 in the LBD of rGluA2. Glutamate in red spheres representation, chain A and B in light and dark blue respectively. Compound 8 in site 1b in yellow within the dimer interface, located in the site across the 2-fold symmetry axis. Compound 5 in site 2 in pink. Structures of dimer and compound with surfaces generated using Maestro Schrödinger version 11.1.

Compounds found in the binding site 1a are between residues Lys-104, Pro-105, Met-107 and Ser-108 of chain A and Ile-103, Pro-116, Ser-228 and Gly-230 of chain B (Fig. 4.21). This binding site is situated in the dimer interface between the 2-fold symmetry axis similar to other allosteric positive modulators (PAMs) found in the literature to bind close to the “hinge” of clamshell-type structure of the LBD (Sun et al. 2002; Jin et al. 2005; Ward et al. 2011). Similarly, compounds located in site 1b (Fig.4.22) also in the dimer interface of the LBD with residues Pro-105, Ser-108, Ser-217 and Lys-218 from chain A and Pro-116, Met-118 and Ser-119 from chain B. The full list of residues found in these sites are summarised in Table 4.6. Binding site 1a and 1b are close to each other, both sites have residues Pro-105 and Ser-108 (chain A) and Pro-116 from (chain B) near the compounds.

More interestingly, the binding sites of 1a and 1b are similar to previously published LBD GluA2 protein structures in complex with allosteric modulators such as aniracetam and CX614 (Jin et al. 2005). These compounds were shown to bind between two prolines and two serines in a cleft type space formed in the dimer interface of the LBD of rGluA2. Sites 1a and 1b also are located between proline and serine residues. Furthermore, compounds found in site 1a and 1b fit between a cleft formed by prolines and serines (Fig. 4.21 and 4.22); for site 1a these are Pro-105 and Pro-116 and Ser-108 and Ser-228 from chain A and B. For site 1b these are Pro-105 and Pro-116 and Ser-217 and Ser-119. In addition, site 1a is shown to be located in a higher position than 1b, in which the two prolines from chain A and B are situated closer to the base of the cleft, compared to site 1b in which the prolines are situated at the top of the cleft and the serines in the lower part of the cleft in the dimer interface. To summarize, binding sites identified 1a and 1b are located in the dimer interface of the LBD of GluA2, this site is a previously found site for positive allosteric modulators of AMPA receptors and has potential for the improvement of cognitive functions.

The binding site 2 located near the GT linker which connects S1 with S2 near the transmembrane linkers M1 and M3 is located near to a negative allosteric modulator (NAM) site found in 2016 (Yelshanskaya et al. 2016). This published novel NAM site for GluA2 AMPA receptor located in the transduction domain was studied using X-ray crystallography experiments and displayed antagonists Perampanel, GYKI53655 and CP 465,022 binding at the interface between the LBD and the TMD, more specifically between S1-M1 and M3 (Fig. 3.28 & 4.24). Similarly, XChem fragment screening showed compounds 2, 4 and 5 located near the Gly-Thr linker of S1 and S2 segments of the LBD of rGluA2 (Fig. 4.23). In order to observe the position of site 2 it was necessary to superimpose the crystal structure of the LBD of rGluA2 in complex with compound 2 with the literature full length rGluA2 in complex with antagonist CP 465,022 (accession code 5L1E). We found that site 2 is located above the transduction domain site, closer to the position of the Gly-Thr linker joining residues Lys-697 from S1 and Pro-507 from S2 (residues numbering according to full length structure). CP 465,022 a quinazoline-4-one antagonist binds further down in the transduction domain between S1-M1 and M3 (Fig. 4.24). In conclusion, site 2 is located in a higher position than the previous NAM site found in the literature (Yelshanskaya et al. 2016), suggesting a possible novel NAM site for AMPA receptor. Also it could be that the Gly-Thr linker is causing an interaction with the fragments (artefact binding). However, these results need further studies to confirm and verify the exact binding mode of compounds in this site.

Binding site 1a

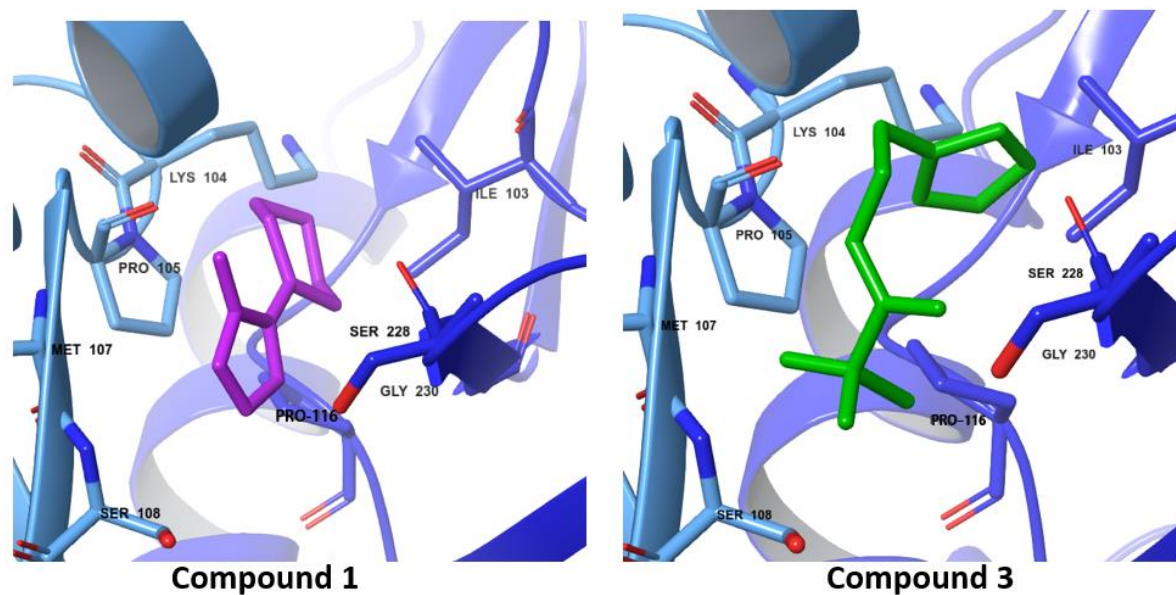


Figure 4.21. Comparison of the possible binding mode of compounds 1 and 3 in the binding site 1a. Compound 1 and 3 in purple and green respectively situated near residues Lys-104, Pro-105, Met-107 and Ser-108 from chain A; and residues of chain B are Ile-103, Pro-116, Ser-228 and Gly-230. No binding interactions were observed due to the low-occupancy of data obtained. Chain A and B in light and dark blue, compounds in stick-model representation, diagram generated using Maestro Schrödinger version 11.1.

Binding site 1b

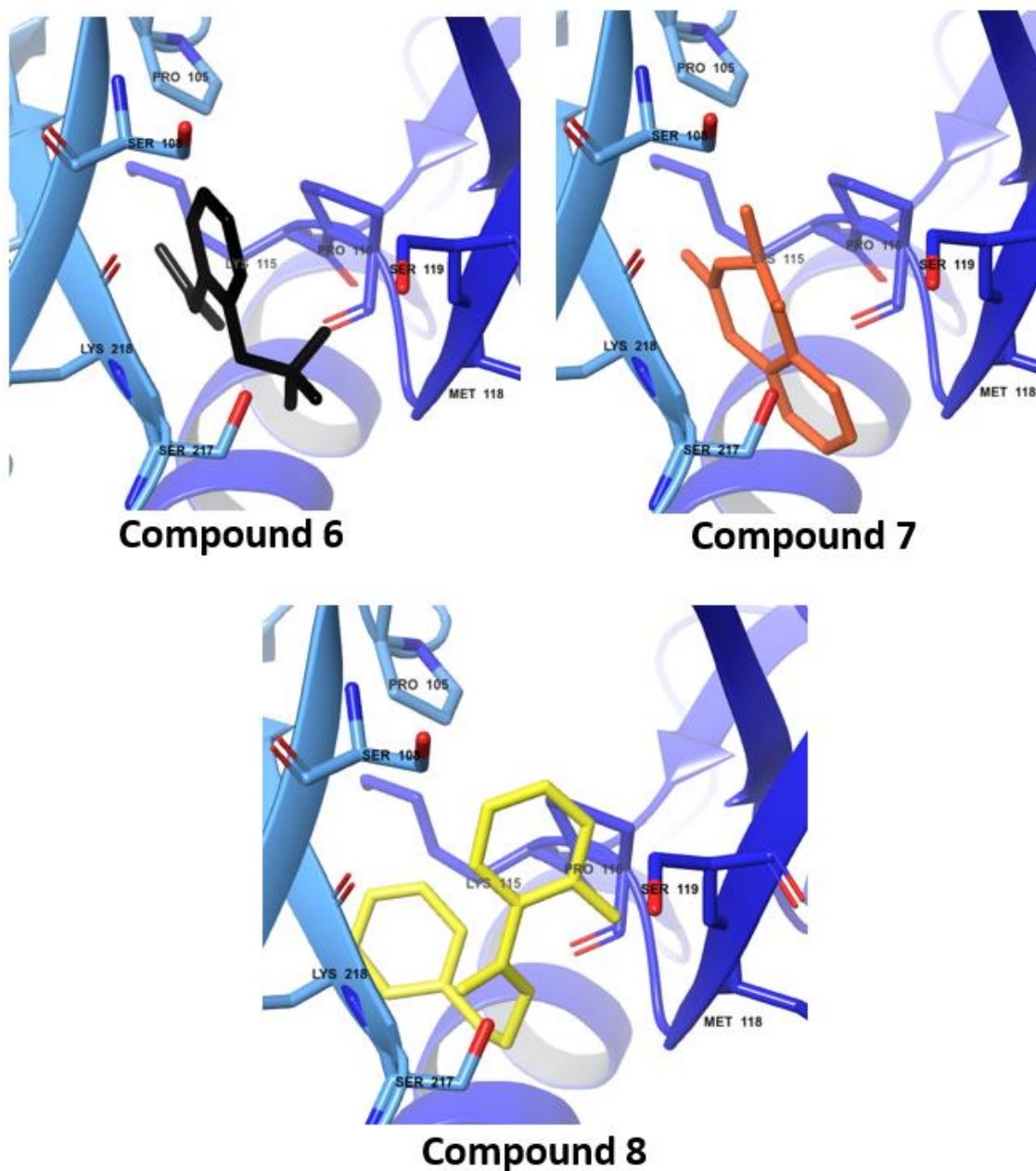


Figure 4.22. Comparison of the possible binding mode of compounds 6, 7 and 8 in the binding site 1b. Compound 6, 7 and 8 in black, orange and yellow respectively, situated near residues Ser-119, Met-118, Pro-116 and Lys-115 from chain B and Ser-108, Lys-218, Pro-105 and Ile-92 from chain A. No binding interactions were observed due to the low-occupancy of data obtained. Chain A in dark blue and chain B in light blue, compounds in stick-model representation, diagram generated using Maestro Schrödinger version 11.1.

Binding site 2

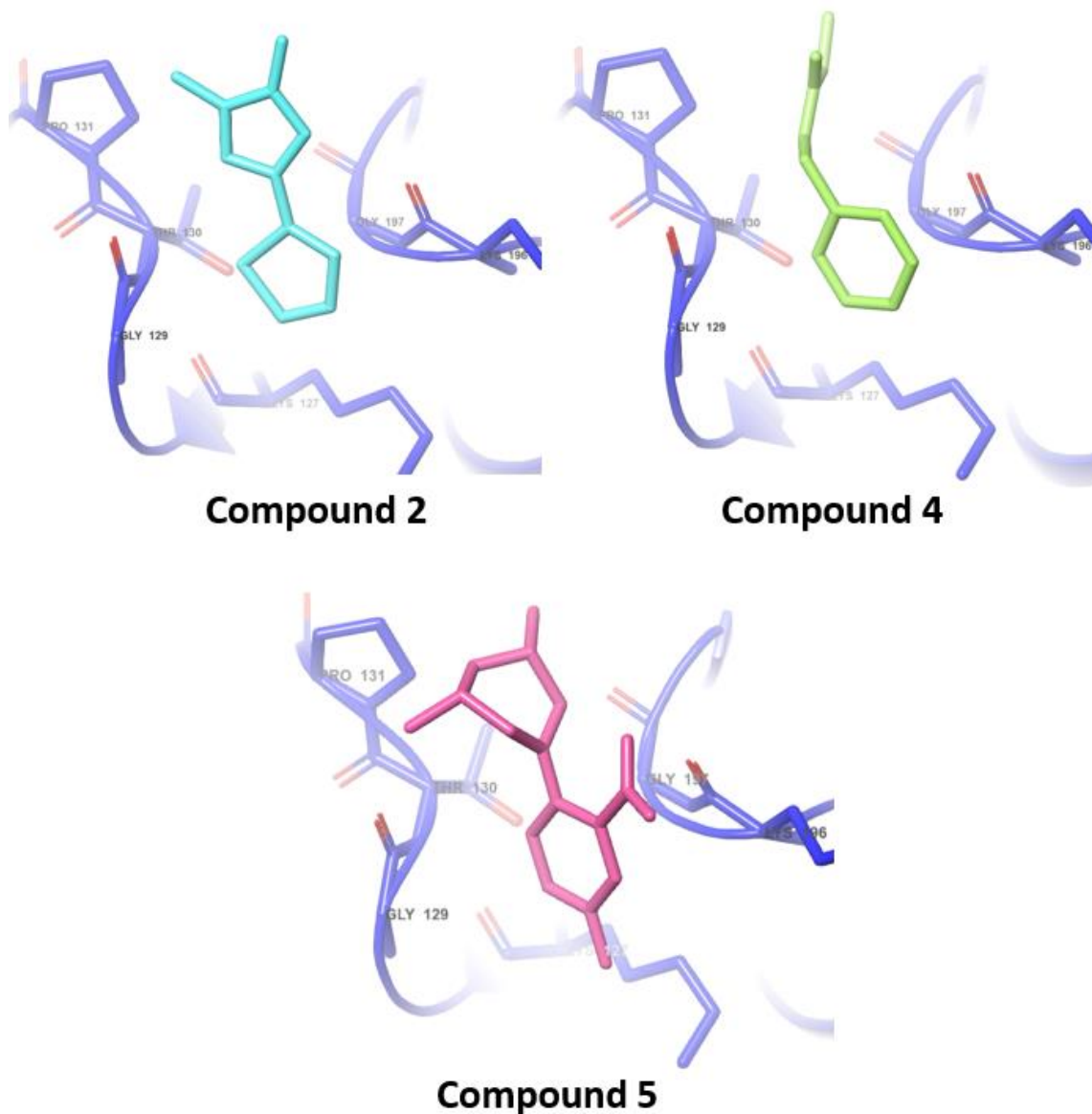


Figure 4.23. Comparison of the possible binding mode of compounds binding site 2. Compounds 2, 4 and 5 in cyan, mint and pink respectively, situated near residues Gly-129, Thr-130, Pro-131 and Gly-197 of chain B in dark blue. No binding interactions were observed due to the low-occupancy of data obtained. Compounds in stick-model representation, diagram generated using Maestro Schrödinger version 11.1.

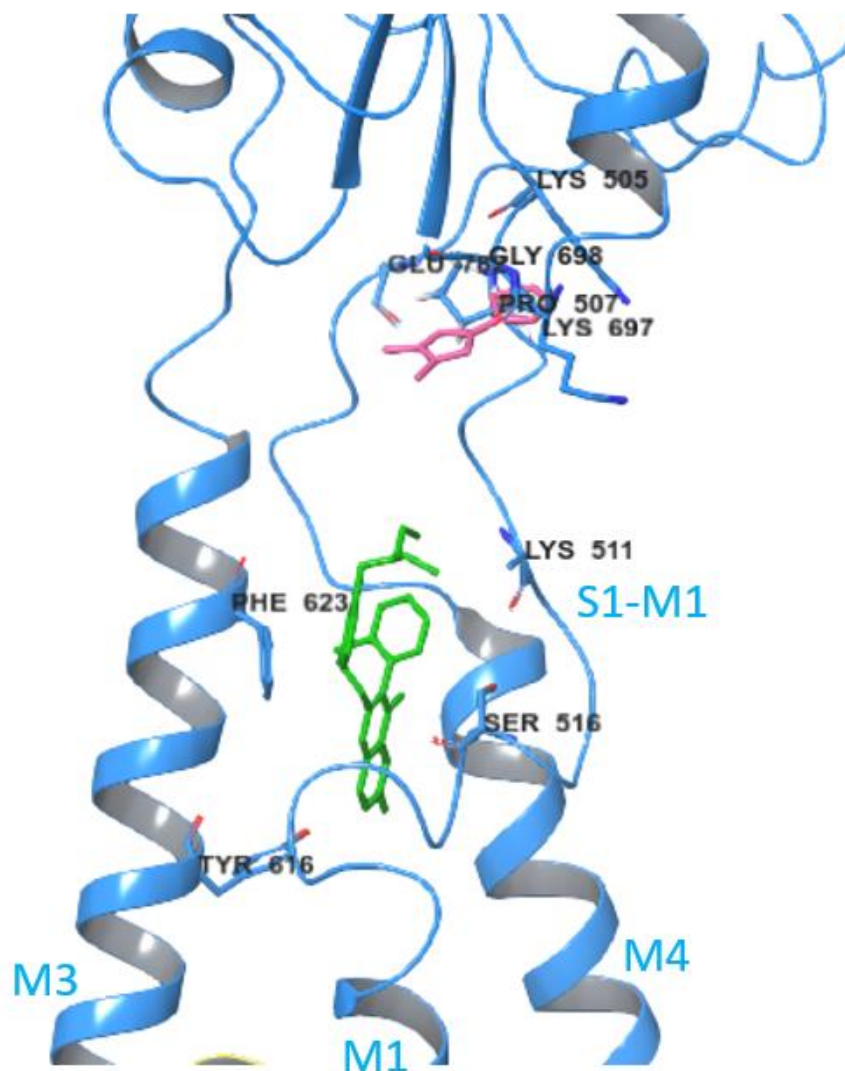


Figure 4.24. Transduction domain of rGluA2 in complex with antagonist CP 465,022 and Compound 2. The full length structure of rGluA2 accession code 5L1E (Yelshanskaya et al. 2016) was superimpose with the structure with compound 2 to observe the different binding sites near the transduciton domain. The NAM antagonist CP 465,022 in green and compound 2 in pink. Compounds in stick-model representation, diagram generated using Maestro Schrödinger version 11.1.

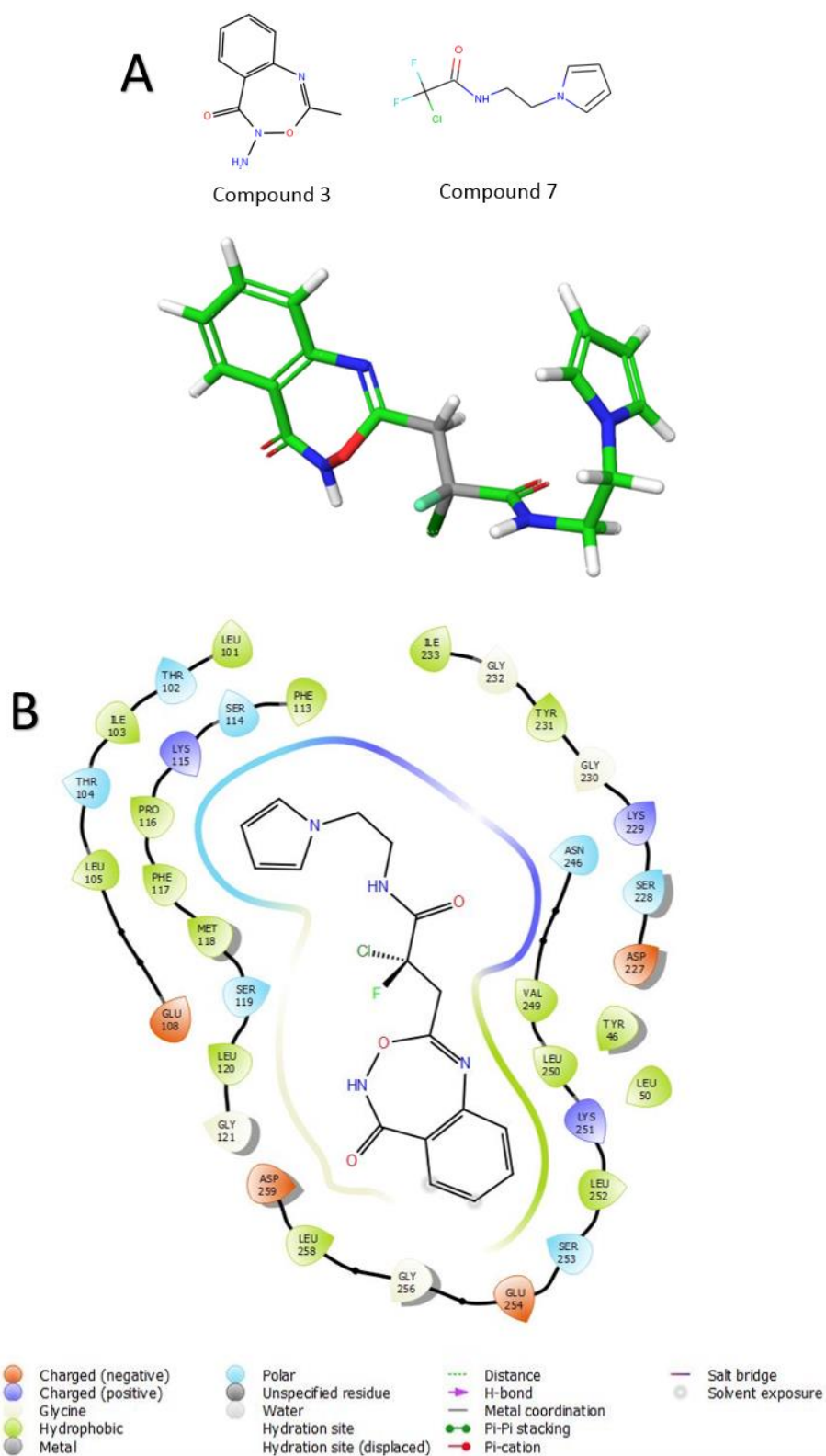


Figure 4.25. Hypothetical ligand “X” formed by two fragment hits. A) Compounds 3 and 7 were joined using a carbon linker shown in gray. B) Ligand X interaction diagram displaying the residues around the ligand in the dimer interface of rGluA2. Diagrams generated using Maestro Schrödinger version 11.1.

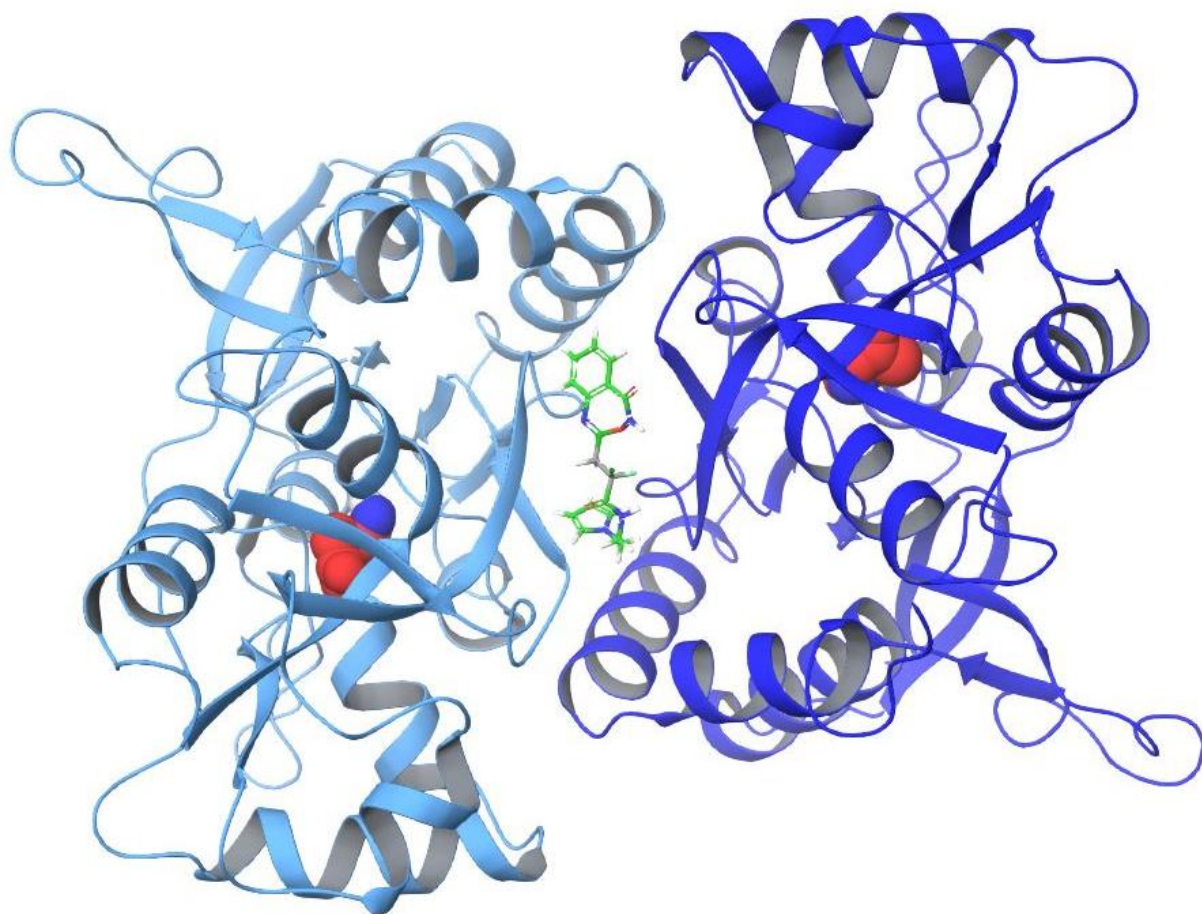


Figure 4.26. Ligand X in the dimer interface of rGluA2. The ligand formed by compounds 3 and 7 are located in the dimer interface of the structure, with a possible higher binding affinity than the fragments alone. Glutamate in red spheres representation, chain A and B in light and dark blue respectively. Structures of dimer and ligand X generated using Maestro Schrödinger version 11.1.

Using computational methods (Maestro Schrödinger) a virtual ligand “X” formed by two fragment hits (compound 3 and 7) was generated to observe the possible binding affinity in the PAM site of rGluA2 (Fig. 4.25 & 4.26).

4.5 DISCUSSION

The purification approach was a multi-step methodology, which successfully gave a homogenous and highly pure protein with an average yield of 7.54 mg of protein. Immobilized metal affinity chromatography (IMAC) and size exclusion chromatography (SEC) were used for purification of the LBD of rGluA2 consistent with previous publications (Chen & Gouaux 1997; Chen et al. 1998). IMAC purification provided an excellent purification step due to the use of a His-SUMO tag on the rGluA2 LBD; the SUMO tag increased the solubility and correct folding of the protein and the six histidines provided metal stable binding sites to permit purification using talon resin which contains cobalt (Block et al. 2009). A resin charged with cobalt instead of nickel was used because cobalt charged resins bind to his-tag recombinant proteins with greater specificity to obtain higher purity of proteins (Clontech, Takara). The rGluA2 LBD recombinant protein was successfully expressed and purified in a large scale format for further structure-based drug discovery research. The cleavage of the protein from the 6xHis-SUMO was performed with high efficiency by the PreScission protease, also helping to identify the correct purification of the recombinant protein.

Preliminary crystallography experiments gave a reproducible hit condition that resulted in crystals with resolution that ranged from 1.87 to 2.5 Å that were further optimised using microseeding experiments for fragment screening. The utilisation of additives in crystallography experiments are essential for crystal formation and the addition of certain salts such as zinc acetate and sodium cacodylate promotes crystallisation as observed in rGluA2 crystals. More specifically, the zinc cause the protein to strongly precipitate and facilitate the nucleation event. Importantly, it was observed that rGluA2 protein without the addition salts did not form crystals or precipitation suggesting an essential role of both salts in controlling the ionic strength interactions for crystal formation. This is similar to the previously published structure of the LBD GluA2 in which zinc acetate and cacodylate were used for crystallisation experiments (Armstrong & Gouaux 2000). Other structures of the GluA2 LBD in complex with the antagonist 2-Me-Tet-AMPA (Hogner et al. 2002) and the amino acid L-Aspartate (Krintel et al. 2014) used zinc acetate and/or sodium cacodylate in crystallisation experiments (1M5B and 4O3A, PDB accession codes). Another reason for the use of zinc acetate in crystallography of AMPA rGluA2 is the evidence of zinc ions located in the crystal packing interfaces (crystal contacts) important for the formation of crystals (Armstrong & Gouaux 2000).

X-ray crystallography data was solved and the final LBD structure in complex with glutamate displayed similar amino acid interactions previously described in the literature. Hence, it was observed that glutamate α -carboxyl, α -amino and δ -carboxyl groups formed interactions with arginine, serine, proline and threonine of the LBD of rGluA2, similar to previously solved structures of rat GluA2 in complex with glutamate (1FTJ, accession code from PDB; Armstrong & Gouaux 2000).

The purpose of the XChem fragment screening was to find small molecules that with further characterisation can act as PAMs or NAMs for AMPA receptors. The results suggest three possible binding sites of AMPA receptors. A total of 8 fragments were found in the LBD crystal structure, in which 5 compounds were found in the dimer interface of the LBD and three compounds found near the Gly-Thr linker. Sites 1a and 1b found in the dimer interface are similar to literature structures binding between two prolines and two serines in the cleft formed in the 2-fold symmetry axis of the LBD of rGluA2 (Sun et al. 2002; Jin et al. 2005; Ward et al. 2011; Nørholm et al. 2013). These possible binding sites found in the dimer interface might allow the further identification and development of new PAMs of AMPA receptors with the potential to improve cognitive performance in Schizophrenia patients. The compounds found need to be confirmed to characterise the binding modes and residues that interact in the binding site, also these compound fragments need to be further optimised using medicinal chemistry properties to identify and confirm any functional effect *in vitro* and *in vivo*.

Other fragments found near the Gly-Thr linker in the S1-S2 of the LBD suggest a possible novel binding site of NAMs of AMPA receptor for epilepsy treatment similar to previously published structures in which an antagonist binding site was found in the interface between S1-S2 and transmembrane M1 and M3 of GluA2 (Yelshanskaya et al. 2016). However, the binding of fragments found in this site has to be confirmed and further characterisation experiments need to be done in order to identify the specific binding mode in this site and the possible therapeutic use in patients with epilepsy. The main disadvantage of this site is the need of the transduction domain in the structure, however the transduction domain has never been identified isolated or with the LBD in X-ray crystallography (only in full-length structure) due to the hydrophilic cell membrane properties. One alternative considered in this project was to identify the full length of rGluA2 AMPA receptors, however the capabilities of our research group are limited, and an external collaboration with other research groups can be a potential for the expression of the full-length protein.

CHAPTER 5

KAINATE PROJECT

5.1 ABSTRACT

The finding of new anti-epileptic drugs (AEDs) is important for avoiding undesirable side effects and for the treatment of refractory (intractable) patients. Kainate is established to induce seizures by binding on iGluRs kainate receptors. Competitive antagonists have been discovered to reduce seizures however the development of these antagonists has been challenging due to the focus on targeting the agonist glutamate binding site (orthosteric site) in kainate and AMPA receptors. High levels of homology in the orthosteric site between iGluRs leads to non-selective drugs that can cause high levels of adverse effects. Novel AEDs targeting new allosteric modulator sites might provide an effective treatment for refractory patients and reduce side effects. This project was focused on obtaining X-ray structural information for GluK1 and GluK2 kainate receptors, more specifically in the LBD for the further finding of negative-allosteric modulators (NAMs) and positive-allosteric modulators (PAMs). NAMs and PAMs can give important structural information for early development of new drugs in the treatment of epilepsy. The experiments resulted in a successful protein production, purification and crystallography for the LBD of GluK1 and GluK2. Both proteins were soaked with fragments synthesised in-house by the SDDC group, however only one compound with 20% occupancy in GluK2 was identified, these results are not suitable for medical chemistry optimisation, nevertheless both crystal structures can potentially be used for further fragment screening experiments. The resulting structural information can help in the identification of new fragments that can be further optimised for the development of new kainate allosteric antagonists. Additionally, the biological functional assay for human GluK1 and GluK2 receptors expressed in HEK-293 cell line was successfully tested with standard agonists and antagonists.

5.2 AIMS

The overall aim of the kainate project was to find novel molecules that bound to the LBD of the GluK1 and the GluK2 proteins with the potential to be negative allosteric modulators that could be suitable for development into a new, more effective and tolerable drug for treating epilepsy. The initial stage of the project was to use kainate antagonist compounds from the literature to perform medicinal chemistry and calcium assay experiments to confirm the activity of compounds (Fig. 5.1, stage 1). The next stage was to characterise these compounds by structure-based X-ray crystallography experiments (Fig. 5.1, stage 2). In parallel, it was planned to conduct a large fragment screen (XChem) to find novel compounds that bind to the LBD of GluK1 and, potentially, GluK2 protein. The work in this chapter of the thesis covers the experiments in stage 2, which serve not only to characterise the compounds originating from stage 1 (work being conducted by Dr. Iain Barret) but also enable a fragment screen to be conducted to identify novel chemotypes (stage 3, planned for 2018). The structural component of the GluK1 project is the critical identification and characterisation of novel compounds that can be further optimised for the development of new kainate allosteric antagonists. In addition, small molecule modulators of GluK2 will be useful in identifying the therapeutic potential of this subtype of glutamate receptor.

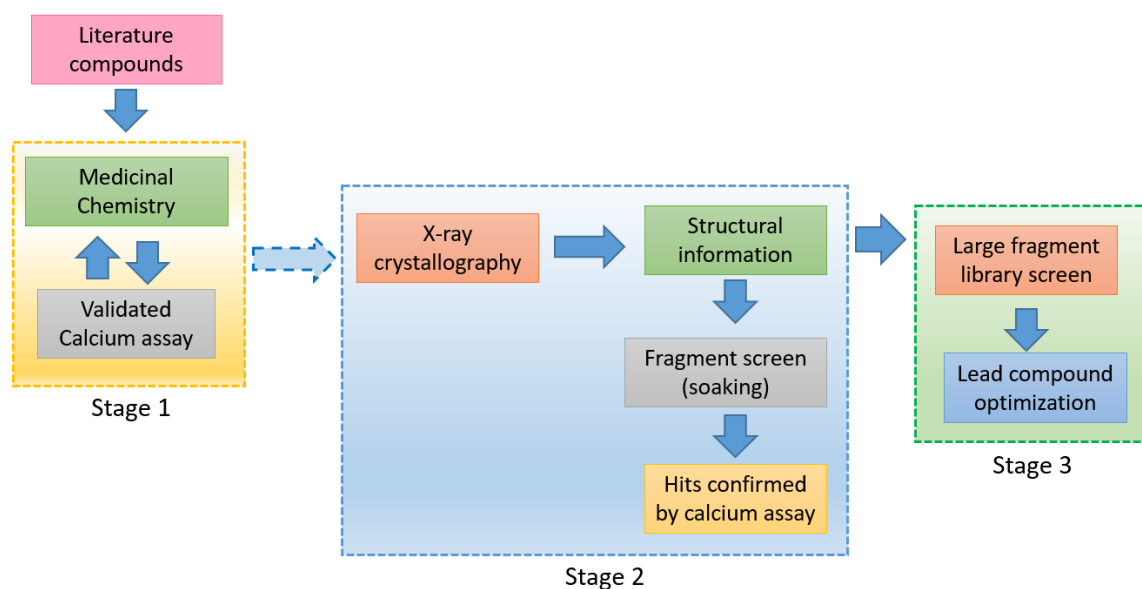


Figure 5.1. Scheme of overall strategy and screening cascade. Stage 1 for the identification and characterisation of compounds for Stage 2, the dash arrow represents this process; however, this order was not followed. Stage 2 started without the completion of stage 1, with a selection of in-house compounds with potential antagonist activity from the literature.

GluK1

5.3 MATERIALS AND METHODS

5.3.1 CLONING AND PLASMID VECTOR

The plasmid used for over-expression and purification of the LBD_rGluk1 (ligand binding domain) was kindly supplied by Dr. Antony W. Oliver from the Genome damage and stability centre (GDSC, University of Sussex). In the GDSC, they used their own pHis-SUMO-3C vector in which they cloned a protein of interest for purification purposes, in this case the S1 and S2 domains forming the ligand-binding core. S1 and S2 are separated by three membrane spanning regions, in order to generate a LBD, S1 and S2 were covalently linked using a Gly-Thr peptide. Similar to AMPA experiments this short linker peptide maintains the structural conformation of the ligand binding domain without causing domains separation or structural changes. Additionally, a 6xHis-SUMO tag was used to enhance expression and solubility of the recombinant protein. Fig. 5.2 shows the protein sequence of fragment S1 and S2 of the LBD, the Gly-Thr linker, the 6xHis-SUMO tag followed by a HRV3C linker protein sequence based on P. Naur and co-workers experiments (Naur et al. 2005). This plasmid was consequently sub cloned into pBR322 plasmid using a pET T7 expression system (Invitrogen) following the manufacturer's commercially available instructions.

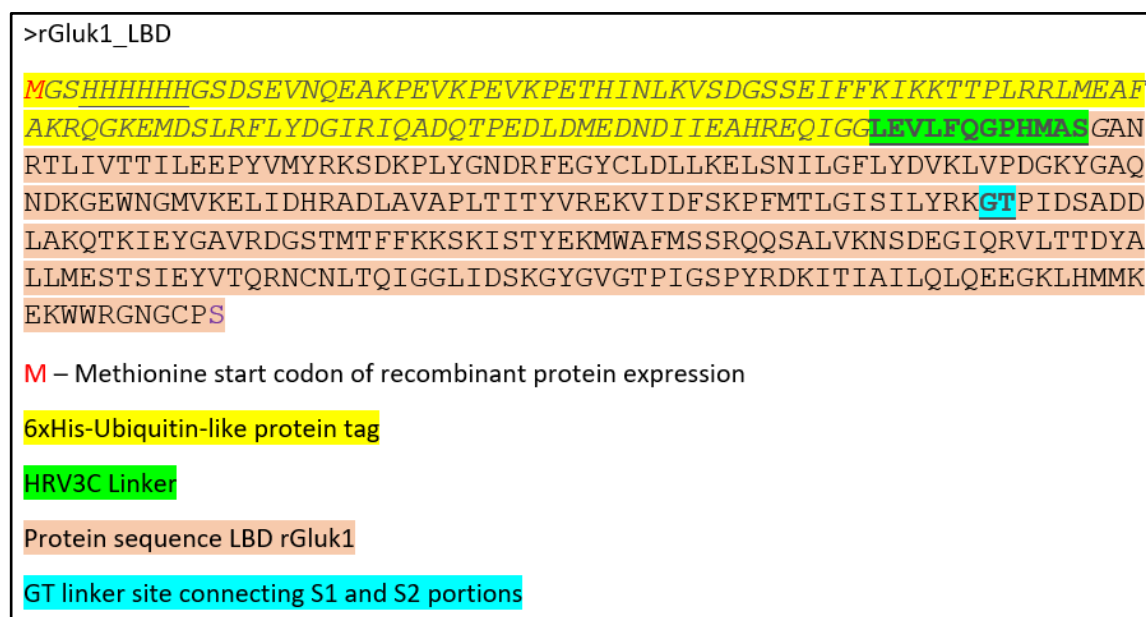


Figure 5.2. LBD rGluk1 sequence design for protein expression and purification. The expressed protein contains an N-terminal 6xHis-SUMO tag, a recognition SUMO cleavage site and the LBD rGluk1 sequence consisting of [430-ANRTL...SILYRK-544], [667-PIDSAD...WRGNGCP-805] separated by a Gly-Thr linker. Sequence based on rGluk1 isoform 2 (Glur5-2, P22756-2 UniProt).

The pBR322 plasmid with a pET T7 expression system (Fig. 5.3) frequently used for the cloning and expression of recombinant proteins in an *E. coli* strain has the advantage of controlling the level of expression by using a T7 RNA polymerase promoter site controlled by isopropyl β -D-1-thiogalactopyranoside (IPTG) induction. The gene cloning and plasmid DNA purification was performed commercially by Invitrogen. The gene of the LBD was from rat GluK1, previously published experiments in GluA2 LBD used rat protein due to the facilitation of crystallisation (Ward et al. 2011). In addition, experiments performed with the plasmid of human GluK1 protein showed that the human protein is difficult to solubilise and express in purification experiments (section 5.4.1).

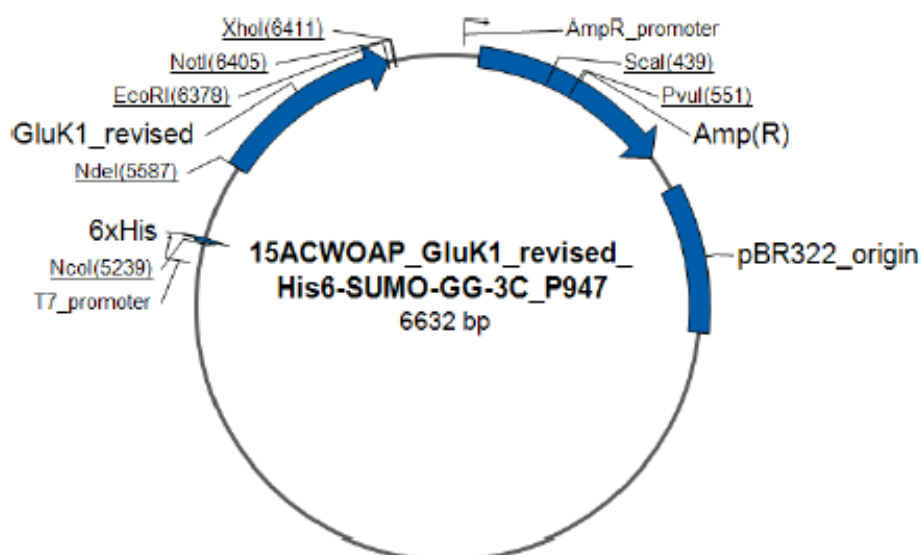


Figure 5.3. Plasmid map of the inserted synthetic rat gene GluK1 LBD, of which 5 μ g of lyophilised plasmid was obtained by Invitrogen. The T7_promoter site controls the levels of protein expression by IPTG induction.

The plasmid was designed to have an N-terminal 6xHis-SUMO tag to improve solubility and purification of the protein, an ampicillin resistance gene to selectively control the recombinant bacteria grown, as well as the inducible expression of T7 promoter by isopropyl β -D-1-thiogalactopyranoside (IPTG).

5.3.2 COMPETENT CELLS

The competent cells used for transformation of the plasmid vector to induce the overexpression of LBD_rGluk1 were *E. coli* Origami™ B (DE3) by Novagen (Cat. No. 70837-3). Origami bacteria was used for the characteristic of forming disulphide bonds to obtain the proper folding of the protein. Since they have mutations in the thioredoxin reductase (*trxB*) and glutathione reductase (*gor*) genes and these modifications enhance the formation of disulphide bonds in the cytoplasm. Bacteria strains with the designation DE3 are lysogenic for a λ prophage that carry an IPTG inducible T7 RNA polymerase. Origami B strains are compatible with ampicillin and carbenicillin resistance plasmids and are suitable for use with pET vectors. Selective antibiotics for Origami strains are kanamycin and tetracycline.

5.3.3 BACTERIA TRANSFORMATION

The vector containing the LBD_rGluk1 (15ACWOAP_Gluk1_revised_His6-SUMO-GC-3C_P947) was prepared by reconstituted lyophilised DNA with 30 μ l of sterile purified water. 1 μ l of the vector was added into 50 μ L of *E. coli* Origami B (DE3) competent cells and incubated on ice for 30 minutes. Heat shock was performed at 42°C for 40s in a heat block, then on ice for 2 minutes and finally at 37°C in the shaking incubator for 1 hour with the addition of 200 μ l of super optimal broth with catabolite repression (SOC) medium (Invitrogen, Cat. No. 1544-034). The cell suspension was plated into LB-agar (Cat. No. L2897, Sigma-Aldrich) containing 15 μ g/ml kanamycin and 50 μ g/ml carbenicillin. The use of carbenicillin instead of ampicillin is due to higher stability and selectivity in bacteria containing the selective plasmid. The plates were incubated for 24 hours at 37°C, 5% CO₂.

Antibiotics: Kanamycin sulphate from *Streptomyces Kanamyceticus* Cat. No. K4000-25G (Sigma-Aldrich), Carbenicillin disodium salt Cat. No. C1389-5G (Sigma-Aldrich).

5.3.4 PROTEIN EXPRESSION

The colonies which grew were ones carrying the plasmid in the competent cells. One single colony was scraped and added into 60 ml of turbo broth (Cat. No. MD12-104-1, Molecular Dimensions) containing 15µg/ml kanamycin and 50µg/ml carbenicillin in a 200 ml flask. Cells were incubated in the shaker incubator at 37°C until the OD₆₀₀ reached approximately 1.2. After it reached the desired optical density it was inoculated with 10 ml of cells suspension into 1L x 6 flasks of turbo broth (15µg/ml kanamycin and 50µg/ml carbenicillin) in a 2L glass flask. Cells were grown in a shaker incubator at 30°C at 200 rpm until the OD₆₀₀ was approximately 1.2, temperature was reduced to 18°C until the OD₆₀₀ reached ~1.5. Then IPTG (Cat. No. 15529019, Thermo Fisher Scientific) was added to a final concentration of 50µM to each flask, cells were grown over night at 18°C. The next day the cells were centrifuged at 6,000 rpm for 20 minutes and pellets were frozen for subsequent purification.

5.3.5 PROTEIN PURIFICATION

5.3.5.1 IMMOBILIZED METAL AFFINITY CHROMATOGRAPHY (IMAC)

Buffers for protein purification experiment, each buffer was filtered at 0.45 μ m (Cellulose nitrate membrane filters, Whatman™ Cat. No. 514-8073, VWR).

Lysis Buffer	Elution Buffer	Cat. No.
50 mM HEPES pH 7.5	50 mM HEPES pH 7.5	BP310-1, Fisher BioReagents
500 mM NaCl	500 mM NaCl	S/3120/63, Fisher Chemical
10 mM Imidazole	300 mM Imidazole	122025000, Acros Organics
1 mM TCEP	1 mM TCEP	646547-10x1ml, Sigma-Aldrich
Distilled H ₂ O up to 500 ml	Distilled H ₂ O up to 250 ml	N/A

Pellets of cells were defrosted and resuspended in 50 ml of Lysis buffer with one tablet of protease inhibitor cocktail (11055700, Roche) and 250 μ M of glutamic acid in 20 mM HEPES-NaOH pH 7.5(L-glutamic acid monosodium salt hydrate Cat. No. G1626, Sigma-Aldrich). Cells were lysate with a large probe sonicator, 5 sec on, 5 sec off, 40% amplitude for 5 minutes. Cell debris and insoluble fractions were removed by centrifugation at 40,000g for 30 minutes at 4°C. Supernatant (soluble fraction) was filtered through a 0.45 μ m syringe filter (Sterile PES syringe filter Cat. No. 15216869, Fisher Scientific). The filtered supernatant was applied to a gravity column containing 7.5 ml of talon metal affinity resin (Clontech Takara Cat. No. 635503) and incubated for 1 hour at 4°C. The column was washed with several applications of lysis buffer (approximately 200 ml). The retained protein was eluted with several applications of elution buffer (~7.5 ml). Eluted fractions were incubated with PreScission protease (27-0843-01, GE Healthcare Life Sciences) at 1 unit per ml at 4°C overnight for the removal of the 6xHis-SUMO tag.

5.3.5.2 SIZE EXCLUSION CHROMATOGRAPHY (SEC)

The protein solution (~45 to 60 ml) was concentrated to 10 ml using a centrifugal filter unit (Vivaspin 20 Molecular weight cut-off (MWCO) 10,000 Cat. No. 28932360, GE Healthcare Life Sciences) at 4,000g for approximately 30 minutes. The ÄKTA purifier system (GE Healthcare Life Sciences) was used for SEC purification with the HiLoad 26/600 Superdex 75 pg column (Cat. No. 28-9893-34, GE Healthcare Life Sciences).

The FPLC buffer used for purification was 20mM HEPES pH 7.5, 500 mM NaCl and 1 mM TCEP pH 7.0, filtered and degassed first. The column was equilibrated with the FPLC buffer overnight. The next day, 2 ml fractions were collected in a 2.4 ml 96-deep block plate (Greiner Master Block M1061-50EA, Sigma-Aldrich). Fractions collected were verified for separation by SDS-PAGE gel electrophoresis 160 V for one hour (SERVAGel™ TG PRIME 4-20%, Cat. No. 43276.01, SERVA) and Coomassie stain (Cat. No. GEN-QC-STAIN-1L, Generon), destain was for 2 hours with distilled water. Fractions with most abundant protein were collected (~20ml) and concentrated with a centrifugal filter unit until a final volume of 1 ml. To ensure the removal of 6xHis-SUMO tag the purified protein solution was further incubated with 1 ml of talon metal affinity resin using a 10 ml centrifuge column for 30 minutes (Pierce™ Centrifuge column 10 ml Cat. No. 89898, Thermo Fisher Scientific). After incubation completed, the eluted solution was concentrated up to 500 µl, the protein concentration was quantified with a nanoDrop at absorbance A_{280} nm and purity of the protein was verified by SDS-PAGE gel electrophoresis. Several batches of protein were obtained and the final yield of purified protein was calculated using the concentration mg/ml adjusted with the final volume obtained.

5.3.6 CRYSTALLOGRAPHY

Preliminary crystal experiments were performed using commercial crystallisation screens, protein solution was tested in different concentrations ranging from 5-10 mg/ml and at two different temperatures 4°C and 14°C. However, none of these conditions were favourable for suitable crystals. A list of commercial screens tested in Table 5.1.

Table 5.1. Commercial crystallisation screens used for preliminary experiments

Crystallisation screen	Supplier	Cat. No
Proplex™	Molecular dimensions	MD1-42
Morpheus®	Molecular dimensions	MD1-47
MIDASplus™	Molecular dimensions	MD1-107
JCSG-plus™	Molecular dimensions	MD1-40
Additive screen™	Molecular dimensions	MD1-11
PACT premier™	Molecular dimensions	MD1-36
Index HT	Hampton Research	HR2-134
PEG/Ion HT	Hampton Research	HR2-139
SaltRx HT	Hampton Research	HR2-136
Natrix HT	Hampton Research	HR2-131
Crystal screen HT	Hampton Research	HR2-130

Crystallography was performed as previously described (Venskutonyte et al. 2012). In brief, concentrated rGluk1 LBD protein was used for crystallography experiments, normally a concentration of ≥ 10 mg/ml was obtained. Protein solution was buffer replaced up to 5.7 mg/ml in crystallography buffer (14.3mM kainate, 20mM NaCl, 1mM EDTA and 10mM HEPES pH 7.0) using a 500 μ L centrifugal concentrator with a membrane of 5,000 MWCO (Cat. No. VS0111, Sartorius). Crystallography experiments were performed using the hanging drop vapour diffusion method at 6°C using a drop ratio of 1:1 (1 μ l of protein solution and 1 μ l of reservoir solution). Reservoir solution containing 21% PEG 4000, 0.45M of lithium sulphate and 0.1 M of cacodylate pH 6.5. Crystals were formed in 4 days incubated at 6°C and crystals were stored with cryoprotectants 30% PEG 400 or 30% ethylene glycol before being flash-cooled in liquid nitrogen. X-ray data was collected to 1.64 Å resolution at the beamline i03 (Diamond Light Source synchrotron, Oxfordshire).

5.3.7 FRAGMENT SCREENING (SOAKING)

Ten fragments synthesised by the SDDC (Chemistry group) were used for soaking experiments (Table 5.2). These fragments were selected for antagonist activity from the literature for kainate receptors or for having binding properties in the dimer interface of AMPA LBD protein (Table 5.3). Some compounds were also tested using the validated calcium assay and by electrophysiology experiments by Dr. Iain Barret. rGluK1 crystals were soaked with fragments at different concentrations 1 mM, 5 mM and 10 mM. A 10 μ l drop was used containing 9 μ l of reservoir solution (from previous crystallography experiments) and 1 μ l of 10 mM, 50 mM or 100 mM stock solution in 100% DMSO, crystals in drops were incubated for 1 hour at 4°C.

Table 5.2. Fragments structures used for soaking experiments, compounds synthesize in-house.

Compound	Structure	Molecular weight (g/mol)	Compound	Structure	Molecular weight (g/mol)
UOS-15592		268.24	UOS-31059		370.32
UOS-14986		190.17	UOS-30693		393.63
UOS-15326		296.29	UOS-30696		369.6
UOS-12344		379.42	UOS-21170		495.88
UOS-12230		282.26	UOS-30695		405.65

Table 5.3. Compound selection criteria for soaking experiments with protein crystals

Compound	Selection criteria
UOS-15592	Compound from previous AMPA research performed by Dr. Simon Ward (Ward et al. 2011)
UOS-14986	Binding in the dimer interface of AMPA, in-house rGluA2 LBD crystal structure
UOS-15326	Binding in the dimer interface of AMPA, in-house rGluA2 LBD crystal structure
UOS-12344	Binding in the dimer interface of AMPA, in-house rGluA2 LBD crystal structure
UOS-12230	Binding in the dimer interface of AMPA, in-house rGluA2 LBD crystal structure
UOS-31059	Preliminary in-house electrophysiology assay experiments reported kainate activity (% of inhibition at 30 μ M, GluK1: 28.3 ± 1.14 ; GluK2: 10.78 ± 1.98)
UOS-30693	Synthesised in-house from literature compound (Valgeirsson et al. 2004)
UOS-30696	Synthesised in-house from literature compound (Valgeirsson et al. 2004)
UOS-21170	Synthesised in-house with structure and chemical similarities from another in-house AMPA compound
UOS-30695	Synthesised in-house from literature compound (Valgeirsson et al. 2004)

5.3.8 KAINATE CALCIUM ASSAY

The calcium assay commercial kit Fluo-4 NW (no-wash) from Thermo Fisher Scientific (Cat. No. F36206) was used. This assay is based on detecting the increase of cytosolic Ca^{2+} with the use of calcium-sensitive dye indicators, such as Fluo-3 and Fluo-4. Fluo-4 is a dye analogue of Fluo-3 (two chloride substituents replaced by fluorines) that increases fluorescence intensity upon binding with intracellular Ca^{2+} , this detection can be measured with a FlexStation microplate reader (Gee et al. 2000). The Fluo-4 NW is a nonfluorescent dye that does not require a wash step or a quencher dye unlike the Fluo-4 and Fluo-3 assay kits. Hence, the opening and closure of the kainate receptors induced by agonists or antagonists can be measured using this calcium-signalling assay.

The validation of the assay was carried out by Dr. Iain Barret from the Sussex Drug Discovery Centre and the validated conditions of the assay were followed to confirm the effect of the reference agonists kainate and domoate, and antagonist CNQX with the Gluk1 and GluK2 cellular assay.

Materials and Reagents

Description	Use for	Supplier and Catalogue
DMEM high glucose	Cell culture media	D0819, Sigma-Aldrich
Fetal bovine serum (FBS)	Media supplement	F7524, Sigma-Aldrich
Penicillin-Streptomycin (PS)	Media supplement (antibiotic)	P4333, Sigma-Aldrich
Trypsin-EDTA, phenol red	Cell detachment	25200056, Thermo Fisher Scientific
PBS	Assay buffer	79382, Sigma-Aldrich
DMSO	Assay buffer	10080110, Fisher chemical
Fluo-4 NW Calcium assay kit Component A: dye mix Component B: assay buffer	Assay kit	F36206, Thermo Fisher Scientific
Corning®96 well flat clear bottom black, sterile microplate	Assay microplate	3904, Corning
96-V well microplate translucent polypropylene	Source dilution plate	MIC9050, Scientific Laboratory Supplies
Concanavalin A	Buffer additive, inhibition of receptor desensitization	J61221, Alfa Aesar
Domoic acid (domoate)	Agonist agent	0269, Tocris Bioscience
Kainic acid (kainate)	Agonist agent	HB0355, Hellobio
CNQX disodium salt hydrate	Antagonist agent	C239, Sigma-Aldrich

Cell Culture

The cell line used for these experiments was HEK-293 stably expressing human GluK1 receptors purchased from Sophion, Biolin Scientific. The GluK1 expression of the cell line was constitutive, meaning that the protein was produced continually at all times. Cells were grown in a T75 flask until they became ≥ 70 % confluent. Cell culture passaging was every 3-4 days.

Calcium Assay procedure

The commercial Fluo-4 NW Calcium assay kit was used for the calcium assay experiments. HEK-293-hGluK1 cells were seeded in a Corning® 96-well black microplate, 40,000 cells per well and incubated at 37°C, 5 % CO₂. Twenty four hours after incubation, media was removed and 50 µl of Fluo-4 NW dye solution was added per well (dye previously prepared by diluting 10 ml of assay buffer into lyophilised dye vial) and incubated for two and a half hours in the dark at room temperature.

On completion of incubation time the dye had entered the cells and the excess was removed and washed with assay buffer 1x. The assay buffer was supplemented with 1 mg/ml of concanavalin A, added to cells and incubated for 30 minutes in the dark at room temperature. Kainate receptor agonists (kainate and domoate) and antagonist 6-cyano-7-nitroquinoxaline-2, 3-dione (CNQX) were prepared in serial dilutions in a source plate in assay buffer. The source plate was prepared with a final maximal concentration of kainate 50 µM prepared from a 25 mM stock solution, domoate 5µM prepared from a 10mM stock solution and CNQX 300µM prepared from a 30 mM stock solution.

Addition of source plate was performed using a FlexStation 3 Multi-mode microplate reader. Fluorescence was read at 495 nm excitation and 516 nm emission using the FlexStation. For the antagonist plate a dual addition protocol was used, in which the first step was the addition of CNQX and the second addition was kainate. Data was analysed using the max-min values with Softmax pro software and graphs were generated using GraphPad Prism 7 (SOP Glutamate/Kainate Ca²⁺ assay by Dr. Iain Barret).

5.4 RESULTS

5.4.1 PROTEIN EXPRESSION AND PURIFICATION OF HUMAN GLUK1 LBD

The construct of the hGluK1 LBD protein was provided by the GDSC. Expression test and small scale purification were performed. The expression test was performed with 500 ml of cultured cells, induction with IPTG (10 μ M) was added when the OD₆₀₀ reached \sim 1.2. The SDS-PAGE gel displayed that after IPTG induction there was no evident protein expression of the human GluK1 LBD (Fig. 5.4A). A small scale purification was then tested using two litres of cells, the obtained protein fractions were incubated with 3C-protease enzyme and samples before and after incubation with protease enzyme were observed in a SDS-PAGE gel. The gel did not display a difference in bands with 3C-protease enzyme (Fig. 5.4B) suggesting that the faint band at 50 kDa does not correspond to the hGluK1 LBD protein. The protein could also be folded in a way so that the 6xHis-SUMO tag is placed inside the structure, making it challenging to purify using IMAC experiments. These results indicate that using the rat Gluk1 construct will increase the solubility and purification of the protein. The purification was then focused on the rGluK1 LBD construct.

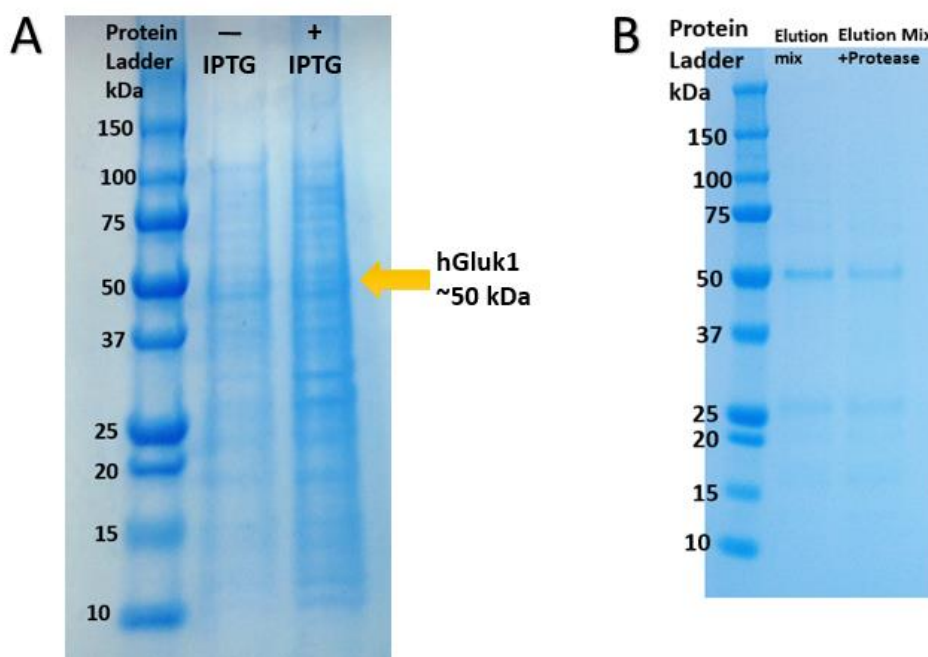


Figure 5.4 Expression test and purification of the hGluK1 LBD. A. Expression test of hGluK1 LBD protein, experiments performed using 250 ml of cultured cells, no evident band of the protein was observed. B. Small scale purification (2L) was performed and the resulted fractions were incubated with 3C-protease enzyme, the gel displayed no difference between bands with or without enzyme incubation. 10 μ g of protein loaded per well, protein ladder used Precision Plus Protein™ All Blue (Cat. No. 1610373, Bio-Rad).

5.4.2 IMMOBILIZED-METAL AFFINITY CHROMATOGRAPHY (IMAC) PURIFICATION

IMAC purification successfully purified the LBD of rGluK1 in 6 elution fractions (Fig. 5.5). The rGluK1 bands are approximately 45 kDa (protein 29.7 kDa + 6xHis-SUMO tag 15 kDa), the gel showed a highly concentrated band in the talon beads before elution which means the retention of the protein. Each elution fraction of 7.5 ml of buffer gives a protein band with higher concentration in elution two and three. The flow through fraction represents all the proteins that do not bind to the talon beads. A sample of beads before and after elution, B1 and B2 respectively (Fig. 5.5), show that most of the protein was eluted providing a large amount of purified protein, although some small fraction of protein was still retained in B2. There were some nonspecific bands around 60-70 kDa and 25 kDa that were further removed by size exclusion chromatography (SEC) experiments as a further purification step.

In order to verify if the concentrated bands are the protein of interest a SDS-PAGE gel of the eluted fractions was run before and after incubation with 3C protease. In Fig. 5.6 it can be observed that elution fractions before 3C protease exhibit a strong band around 45 kDa and after incubation with 3C protease the band of 45 kDa is not present any more. However, two bands are present at 29 kDa and 15 kDa demonstrating the removal of the 6xHis-SUMO tag in rGluK1 protein, this also indicates that the protein eluted and purified was rGluK1 and no other nonspecific protein.

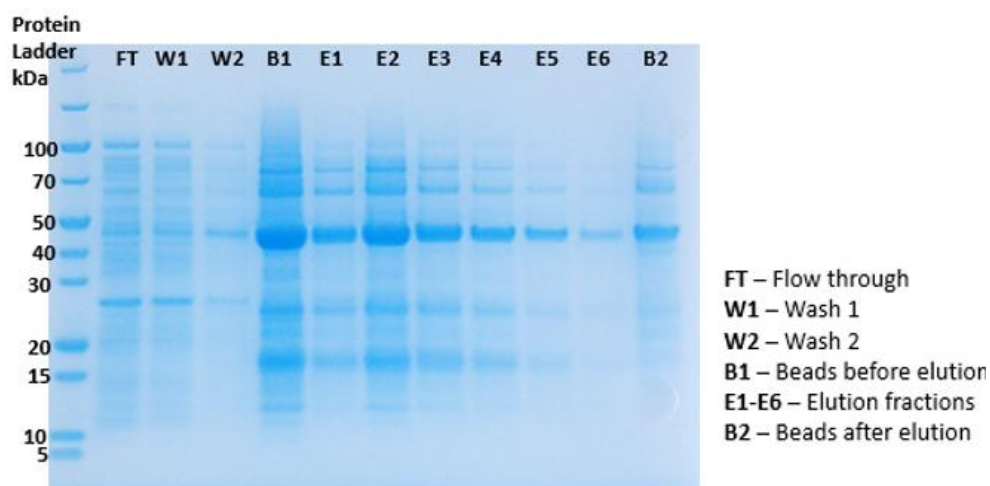


Figure 5.5. SDS-PAGE gel of IMAC purification. Gel stained with Blue Coomassie, strong bands of 45 kDa corresponding to the LBD of rGluK1 protein. Approximately 50 ml of supernatant was added into 7.5 ml of talon beads, the flow through was ~50 ml, wash 1 and 2 was ~ 100ml each and a sample of 25 µl of talon beads was used for running the SDS-PAGE gel. 10 µg of protein loaded per well. Protein ladder PageRuler™ Cat. No. 11892124, Thermo Scientific.

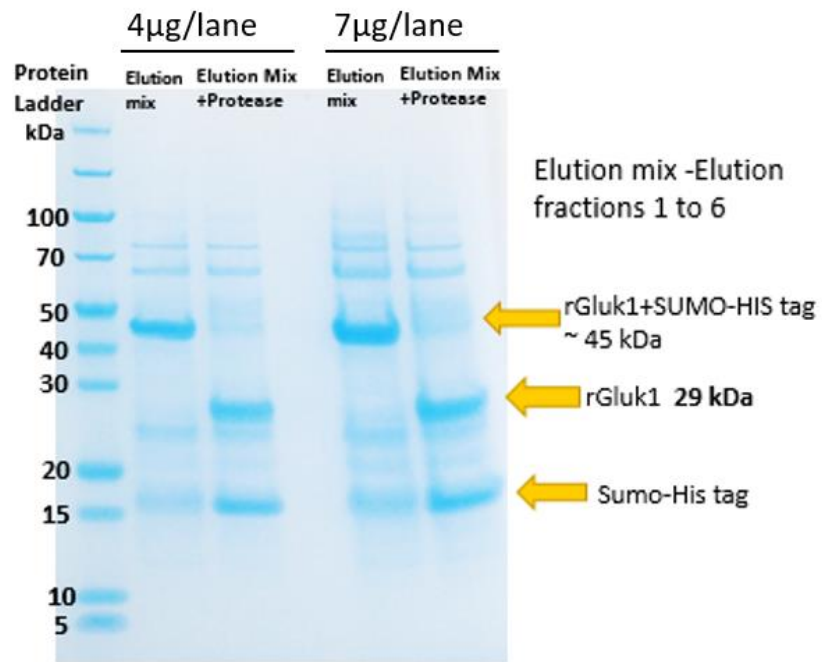


Figure 5.6. SDS-PAGE gel of 3C protease activity. Protein before 3C protease incubation exhibits a band of 45 kDa and after 3C protease incubation exhibits two bands of 29 kDa corresponding to rGluK1 and 15 kDa corresponding to the 6xHis-SUMO tag. Lane one and two loaded with 4 µg of protein and lane three and four with 7 µg of protein.

5.4.3 SIZE EXCLUSION CHROMATOGRAPHY (SEC) PURIFICATION

SEC purification results in a graph (chromatogram) that displays the separation of components of a mixture after a size exclusion chromatography column. Ultraviolet (UV) light absorption at A_{280} was used to measure the fractions separation. A chromatogram was obtained (Fig. 5.7A) with two main peaks, a larger first peak around 120 ml with higher molecular weight molecules that indicates a possible aggregation formation (fractions 1E6-1F2). Additionally, the presence of a 60 kDa band suggests a dimer formation, as this is double the size of the protein of interest. However, these nonspecific bands can be the product of bacteria metabolism products. This larger peak and its respective fractions were not adequate for further purification experiments.

The second peak at 160-180 ml is consistent with the protein rGluk1 with less UV absorption (Fig. 5.7A). Selected fractions collected from FPLC SEC experiments were run in a SDS-PAGE gel electrophoresis (Fig. 5.7B). Fractions between 1G9 and 1H6 display the protein of interest in a higher purity. A degradation band just under 29 kDa was observed and a small amount of 6xHis-SUMO tag around 15 kDa was also observed.

To remove the 6xHis-SUMO tag which remained, the sample was further purified with IMAC, resulting in a flow through with protein rGluk1 with higher purity. This was confirmed by SDS-PAGE gel analysis (Fig. 5.8). The degradation band was not observable in the final purified protein, suggesting a degraded protein over time or the presence of a protein with some tag remain. Final protein concentration was verified by nanoDrop using the molecular weight 29.740 kDa and extinction coefficient of $42,860 \text{ M}^{-1} \text{ cm}^{-1}$ at 280 nm, obtaining a final protein yield of 3.0 mg of protein from 6 litres of culture (8.7 mg/ml in ~350µl). Fifteen batches of purified protein were prepared for crystallography experiments listed in Table 5.4, different starting cell cultures were prepared from 2 to 8 litres.

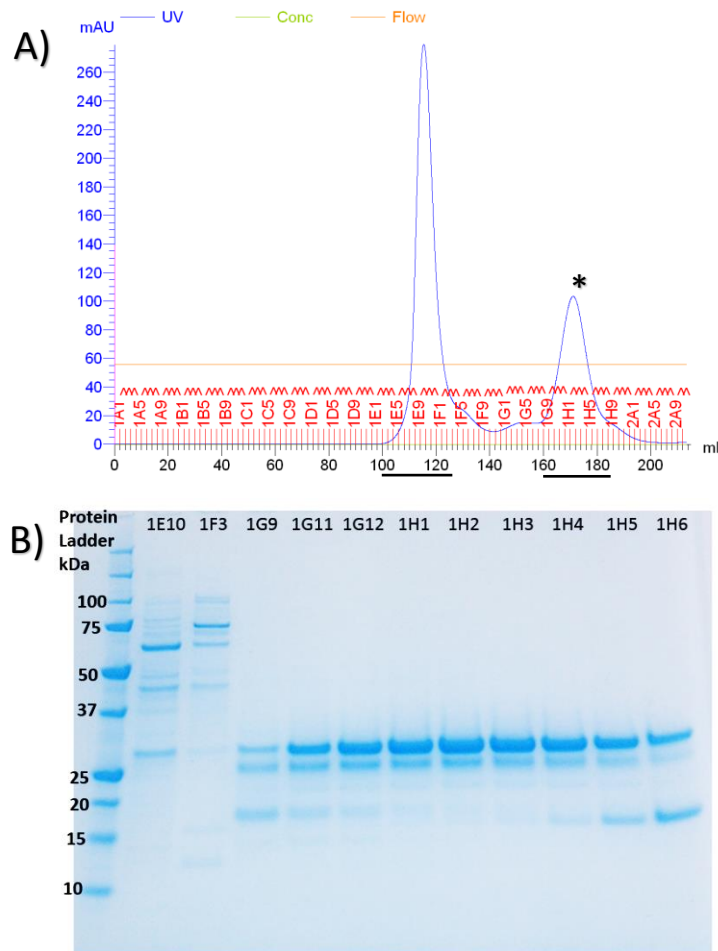


Figure 5.7. Size exclusion chromatography for rGluk1. A) Chromatogram obtained with SEC purification of the rGluk1 protein with 200ml of FPLC buffer through the column. B) SDS-PAGE gel of the fractions obtained by SEC, bands of 29 kDa indicate the rGluk1 protein and a lower band just under 29 kDa suggests proteolytic degradation during the experiment. 10 μ g of protein loaded per well, protein ladder used Precision Plus Protein™ All Blue (Cat. No. 1610373, Bio-Rad).

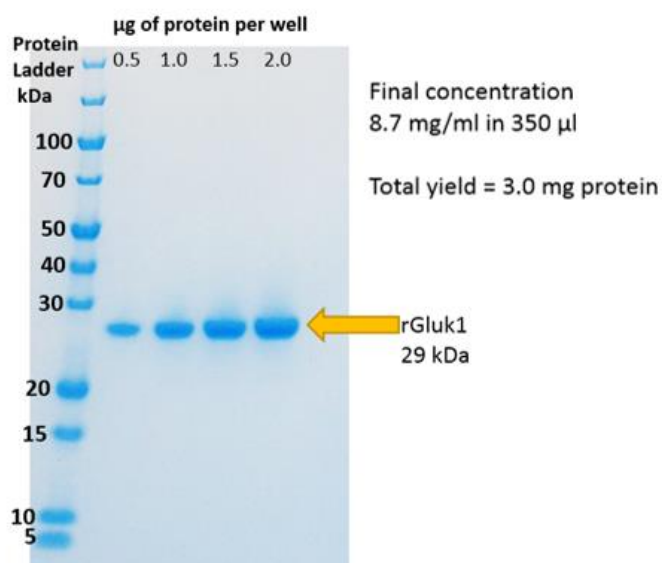


Figure 5.8. SDS-PAGE gel verification of pure rGluK1 protein. 0.5, 1.0, 1.5 and 2.0 µg of protein loaded to verify the purity of the protein, one single band of 29 kDa corresponding to rGluK1, no other proteins were detected in the gel.

Table 5.4. Different batches of purified protein obtained after purification experiments

Batch No.	Starting cell culture (L)	Concentration (mg/m)	Final volume obtained (µl)	Yield of purified protein (mg)
1	2	12.75	60	0.8
2	4	7.21	250	1.8
3	4	7.8	300	2.3
4	4	10	200	2.0
5	6	8.7	350	3.0
6	6	8.0	400	3.2
7	6	9.5	250	2.4
8	6	10.75	300	3.2
9	6	8.81	350	3.1
10	6	12.7	200	2.5
11	6	10.75	300	3.2
12	6	14.5	200	2.9
13	8	8.0	350	2.8
14	8	8.14	200	1.6
15	8	12.6	200	2.5

5.4.4 CRYSTALLOGRAPHY

A wide range of commercial crystallisation screens were tested including: Proplex™, Morpheus®, MIDASplus™, JCSG-plus™, additive screen, PACT premier™, Index, PEG/Ion, SaltRx, Crystal screen and Natrix. None of these gave any suitable crystals for X-ray crystallography.

Crystals were prepared with 5.7 mg/ml protein diluted with crystallography buffer (14.3 mM kainate, 20 mM NaCl, 1 mM EDTA and 10 mM HEPES PH 7.0). Crystals appeared after 4 days of incubation using the hanging drop method at 6°C with a reservoir solution of 21% PEG 4000, 0.45M lithium sulphate and 0.1 M cacodylate pH 6.5.

Crystals had a tetragonal (based on a rectangular inner structure) crystal configuration ranging from 0.2 mm to 0.5 mm length size (Fig. 5.9). It was necessary to separate the cluster of crystals with a needle to obtain single individual crystals. Crystals grew in similar conditions to those described in the literature (PDB 4EOX; Venskutonyte et al. 2012).

The use of cryoprotectant before collecting X-ray diffraction data helps protect the crystal structure from free radicals originating in ionising x-rays that can frequently cause crystal damage. In the literature PEG 400 was used as a cryoprotectant in rGluK1 LBD crystals before collecting X-ray diffraction data (Venskutonyte et al. 2012). PEG 400 and ethylene glycol were compared as a cryoprotectant in rGluK1 crystals before being quick-frozen in liquid nitrogen.

The rGluK1 structures were solved by molecular replacement using a well-known structure PDB 4EOX, models were refined using Collaborative Computational Project No. 4 (CCP4) and Python-based Hierarchical Environment for Integrated Xtallography (PHENIX) software. Crystallographic Object-Oriented Toolkit (COOT) was used for manual model building by Dr. Mark Roe. Diffraction data was collected for both crystals with a final resolution of 1.64 Å for 30% PEG 400 and 1.89 Å for 30% ethylene glycol.

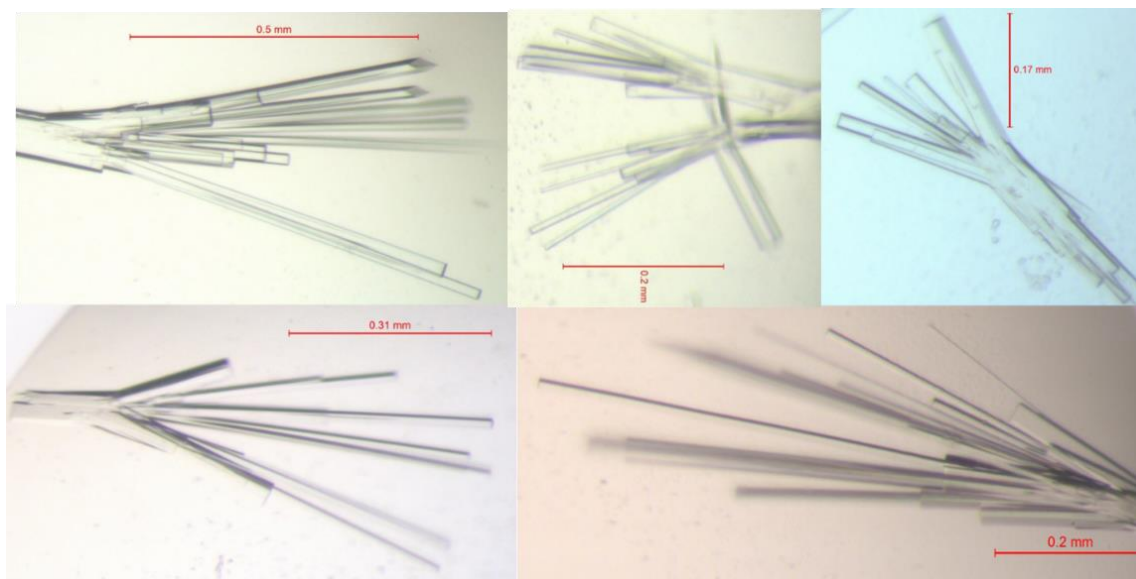
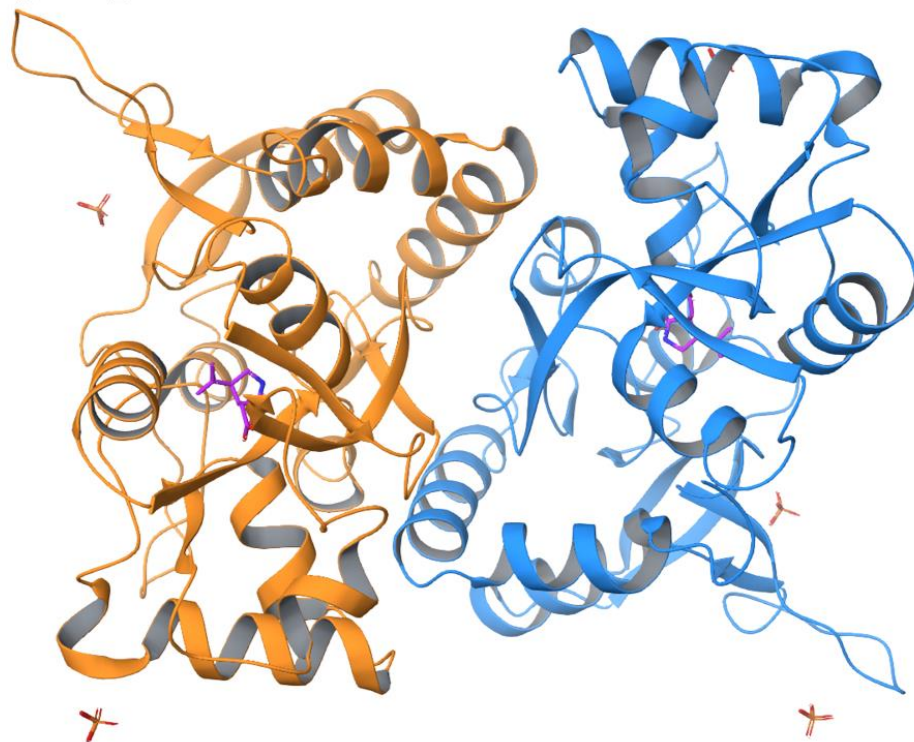


Figure 5.9. rGluk1 tetragonal crystals. Crystals obtained at 5.7 mg/ml protein with a reservoir solution of 21% PEG 4000, 0.45M lithium sulphate and 0.1 M cacodylate pH 6.5. Crystals with a size ranging from 0.2 to 0.5 mm.

Table 5.5. Crystallographic Statistics of rGluK1 LBD. Crystals shot at the i03 beamline at Diamond Light Source.

Data Set (Highest shell in parentheses)	rGluK1 PEG	rGluK1 EG
a (Å)	70.13	70.88
b (Å)	70.13	70.88
c (Å)	232.98	235.9
α (°)	90	90
β (°)	90	90
γ (°)	90	90
Space Group	P 41 21 2	P 41 21 2
Wavelength (Å)	0.9762	0.9762
Resolution Limit (Å)	48.50-1.64 (1.67-1.64)	50.1-1.89 (1.92-1.89)
Number of Unique Obs.	70471 (3435)	49218 (2376)
Completeness (%)	97.2 (95.8)	99.8 (97.9)
Multiplicity	7.3 (7.7)	8.4 (7.2)
Rmerge %	0.111 (1.545)	0.085 (1.532)
Rpim(I) %	0.044 (0.590)	0.032 (0.608)
CC _{1/2}	0.997 (0.505)	0.997 (0.761)
I/ σ I	9.4 (1.3)	12.3 (1.1)
Refinement	0.9762	0.9762
Resolution Range (Å)	232.98 – 1.64	235.97 – 1.89
Rcryst	0.187	0.19555
Rfree	0.225	0.246
Number of protein atoms	3,979	4,013
Number of ligand atoms	31	31
Number of solvent atoms	234	102
Mean B	25.593	44.083
Rmsd bond lengths (Å)	0.020	0.020
Rmsd bond angles (°)	2.037	1.968

LBD_rGluK1_PEG400



LBD_rGluK1_EG

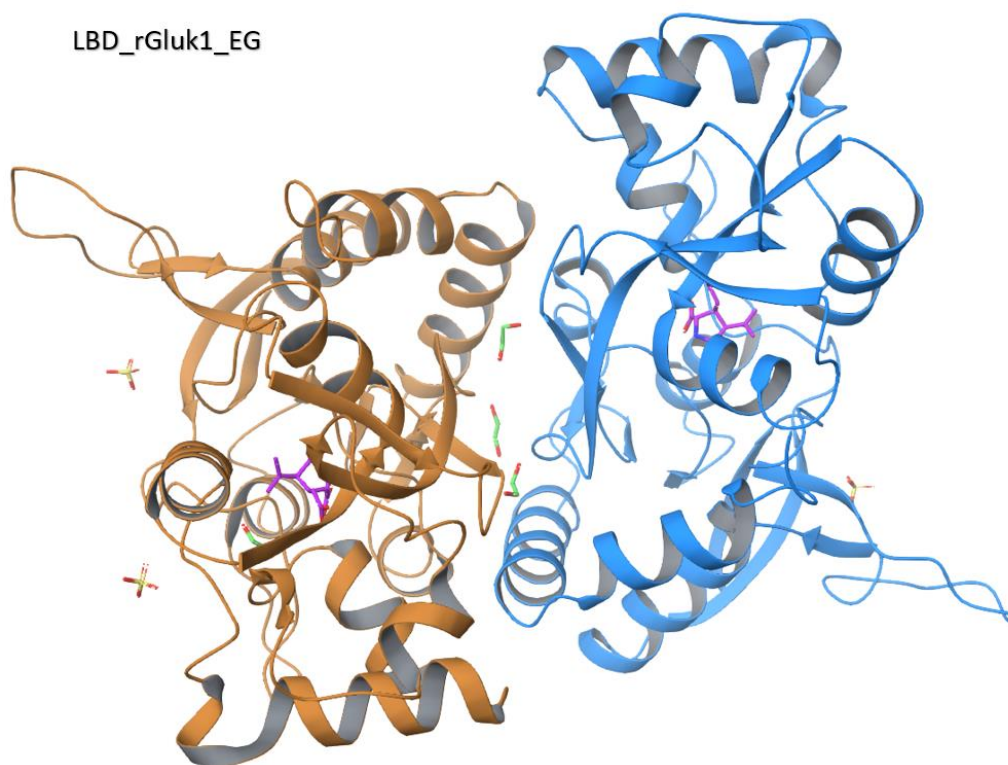


Figure 5.10. LBD rGluK1 structures obtained with X-ray crystallography. Chain A and B, orange and blue respectively. Kainic acid (kainate) shown in fuchsia, SO_4 in yellow and solvent ethylene glycol in green. The dimer interface of ethylene glycol (EG) structure displays solvent molecules but the dimer interface of PEG 400 does not.

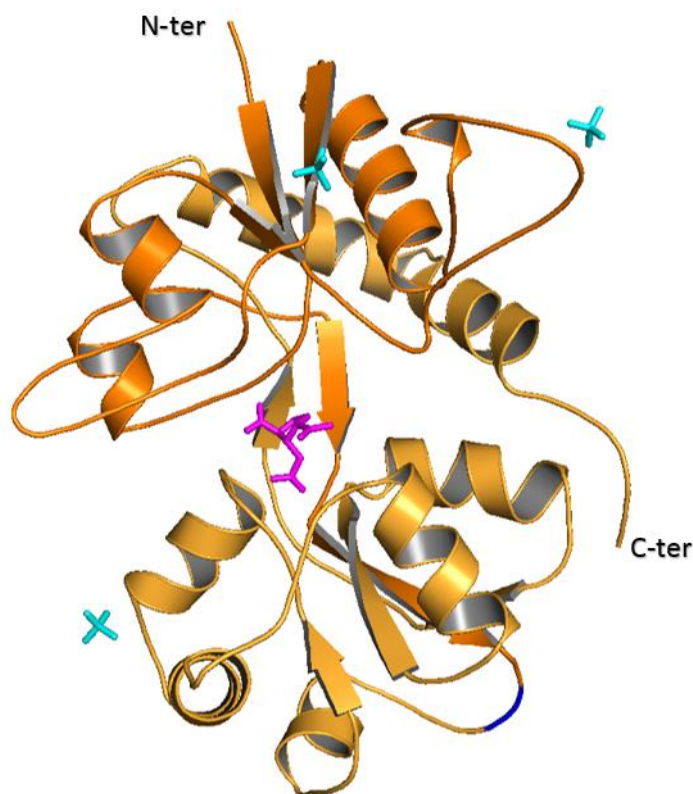


Figure 5.11. Ligand binding domain of rGluK1 in complex with kainic acid. Kainic acid is shown in fuchsia stick representation. The construct consisted of S1 and S2, dark orange and light orange respectively, GT linker in dark blue and SO_4 molecules in cyan. Structure generated using PyMOL 2.0

The solved structures show kainic acid binding in the cavity formed between the interface segment S1 and S2 (Fig. 5.10 & 5.11). Chain A and Chain B of the structure forms a dimer in the LBD of the protein (Fig. 5.10). Crystals with different cryoprotectant (PEG 400 and ethylene glycol) presented similar diffraction data (Table 5.5), however crystals with PEG 400 are better suited for fragment/inhibitor binding studies because there are not solvent molecules present in the dimer interface compared to the structure with ethylene glycol (Fig. 5.10).

Sulphate (SO_4) molecules were present in the structure because of the addition of lithium sulphate in crystals grown; this salt is used as an electrostatic stabilisation agent to stabilize the protein conformation. The monomers of LBD rGluK1 and GluA2 (both produced in-house) were compared and both shared similar conformation and structure. In order to determine ligand/inhibitor binding similarity with GluA2 LBD, the dimer of rGluK1 LBD with kainate obtained was aligned with an in-house LBD structure of GluA2 (Fig. 5.12). Both proteins shared the same dimer conformation suggesting similar ligand binding sites for compounds in the LBD.

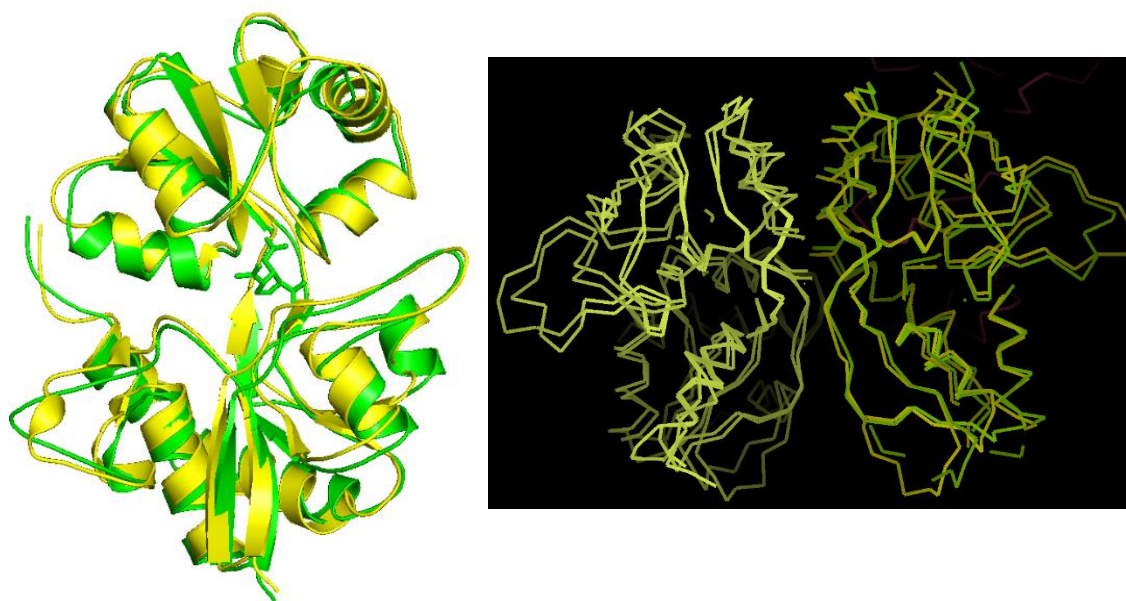


Figure 5.12. Structure alignment between rGluK1 LBD and GluA2 LBD. Left, alignment between rGluK1 LBD monomer with kainate (green) and GluA2 monomer (yellow, in-house structure). Right, LBD dimer alignment between rGluK1 (yellow and green) and GluA2 (yellow). Alignment processed with COOT and PyMOL software.

CLUSTAL multiple sequence alignment by MUSCLE (3.8)

```

GluA2      GPHMASNDTSRGANKTVVVTITLESPYVMKKNHEMLEGNERYEGYCVDLAAEIAKHCGF
GluK1      GPHMAS-----GANRTLIVTTILEEPYVMYRKSDKPLYGNDREFEGYCLDLLKELSNILGF
*****          ***:*:*****:**** *: *: *:*****:*****:*****:

GluA2      KYKLTIVGDGKYGARDADTKIWNMGVGLVYGKADIAIAPLTITLVREEVIDFSKPFMSL
GluK1      LYDVKLVPDGKYGAQN-DKGEWNGMVKELIDHRADLAVAPLTITYVREKVIDFSKPFMTL
*.:*: *****:*. ***** *: *: ***** *****:*****:

GluA2      GISIMIKKGTPIESAEDLSKQTEIAYGTLDSGSTKEFFRRSKIAVFDKMWTYMRSAEPSV
GluK1      GISILYRKGTPIESADDLAKQTKIEYGAVRDGSTMTFFKKSKISTYEKMWAFMSSRQQSA
****. *****:*****:*****: ***** ***** *****:*****:

GluA2      FVRTTAEGVARVRKSKGKYAYLLESTMNEYIEQRKPCDTMKVGGNLDKGYGIATPKGSS
GluK1      LVKNSDEGIQRLVLT--DYALLMESTSIEYVTQRN-CNLTQIGGLIDSKGYGVGTPIGSP
*: *: ***** *: ***** *: ***** *****:*****:*****:

GluA2      LGNAVNLAVLKLSAQGLLDKLNKMWYDKGECG
GluK1      YRDKITIAILQLQEEGKLHMMKEKMWGRNGCPS
: :*:*****:*****:*****:

```

5.13. Sequence alignment of the LBD of rGluA2 and rGluK1. The LBD sequence alignment was performed using Clustal Omega (European Molecular Biology Laboratory-European Bioinformatics Institute, EMBL-EBI). The level of identity between both proteins in the LBD is 53% (259 amino acids analysed) and 73% positives (positives refer to the amino acids which are similar in their physicochemical properties). The amino acid residues involved in the PAMS binding sites in AMPA are highlighted in yellow with their equivalent for rGluK1 (~80% identity between both proteins in the dimer interface pocket).

Kainate binding in the cavity of the LBD was found to form hydrogen bonds with residues of the protein. These interactions observed are: the α -carboxyl group of kainate formed interactions with Thr-90 and Arg-95 and the α -amino group of kainate formed interactions with Glu-190 (Fig. 5.14), similar to a previously published LBD rGluK1 structure 4EOX (PDB, accession code; Venskutonyte et al. 2012). In addition, the residues arginine and glutamic acid showed to be conserved in rGluA2, rGluK1 and rGluK2, forming interactions with the α -carboxyl group and the α -amino group of agonists glutamate and kainate respectively (Fig. 4.15, 5.14 and 5.30).

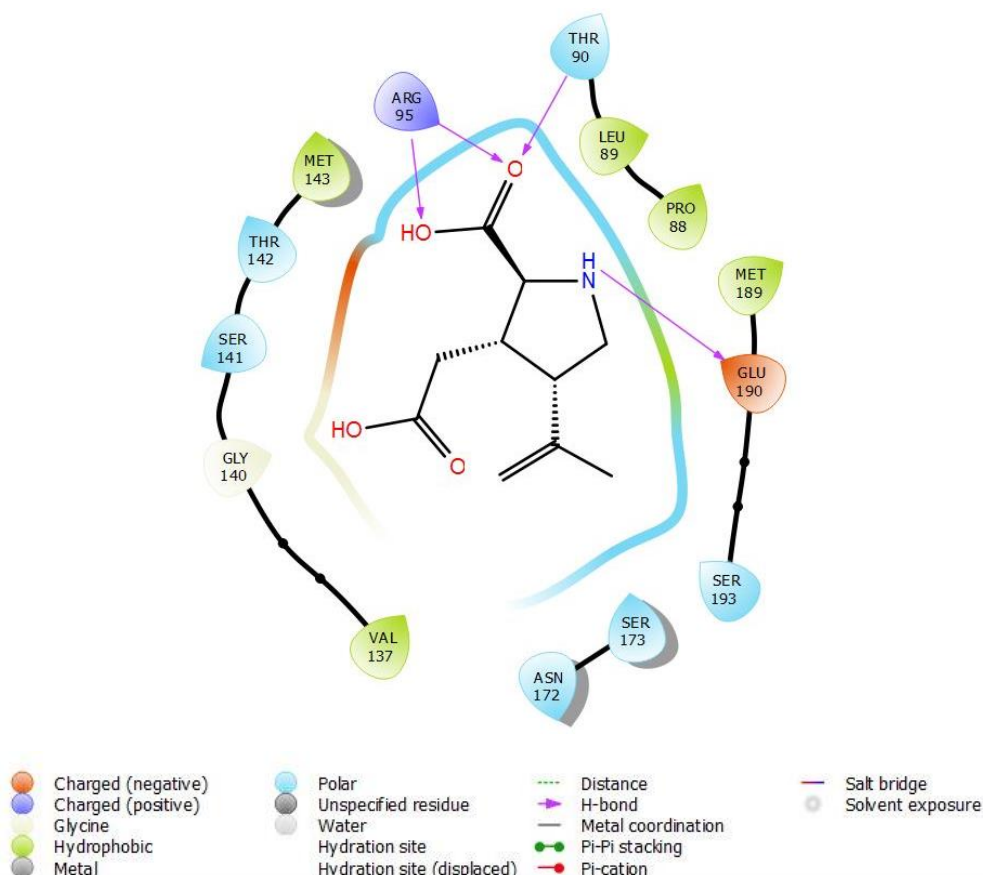


Figure 5.14. Kainate binding interaction diagram for rGluK1 LBD. Kainate agonist forms hydrogen bonds with Residues Thr-90, Arg-95 and Glu-190. Hydrogen bonds are represented in fuchsia arrows. Ligand interaction diagram generated using Maestro Schrödinger version 11.1.

5.4.5 FRAGMENT SCREENING (SOAKING)

A.H Ahmed and co-worker found a new binding site in the LBD of GluA2 for a nootropic drug (Piracetam), binding in multiple positions along the dimer interface (Ahmed & Oswald 2010). This suggests a similar binding pocket for rGluK1 LBD. For that reason, rGluK1 crystals were soaked with ten different fragments synthesised in-house. Fragments were selected according

to the possibility of binding into the LBD (dimer interface or other novel binding site) or their antagonist activity from the literature.

Unfortunately, none of the fragments displayed a binding interaction with rGluK1 protein. At high concentration of compounds, DMSO caused difficulties in handling the crystals and resulted in low-resolution diffractions from 3.5 Å to 6.5 Å resolution.

5.4.6 KAINATE CALCIUM ASSAY

In case compounds were found to bind in the LBD of the protein (after soaking experiments) it was planned to verify the hits using a previously optimised calcium assay, however no compounds were identified as binding in the LBD of rGluK1. In addition, the purpose of these results was to verify the biological calcium assay in determining IC₅₀ values and dose-response curve. The assay development was performed by Dr. Iain Barret and summarised in Table 5.6.

Table 5.6. Parameters tested for 96-well plate for human GluK1/GluK2 Ca²⁺ assay development.

Parameters	Conditions tested	Best parameters
Cell seeding densities	Various densities varying from 10,000 to 30,000 cells per well	Cell density higher than 30,000 cells per well had better resistance to washing off steps and improved assay signal
Poly-D-lysine (PDL) coating	PDL used at 1mg/ml	Increased signal without PDL, final assay without PDL for simplicity.
Dye solution	Dilutions tested from 0.5 to 2x	1x dye improved results
Dye incubation	37°C for 2 hours 37°C for 1 hour then at RT for 1 hour Room temperature for 1-3 hours	Best incubation time was at room temperature for 2.5 hours, followed by at least 30 min in wash buffer (up to 2 hours)
Concanavalin A (ConA)	1.5 to 2.0 mg/ml in assay buffer 0 to 60 minutes incubation time at RT	Improved results with ConA 1mg/ml in assay buffer for 30 minutes at RT

In order to measure the activity of standard agonists and antagonists for GluK1 and GluK2 kainate receptors the commercial Fluo-4 NW calcium assay kit was used. Fluo-4 is a green fluorescent indicator used for the detection of intracellular calcium (Ca²⁺) in which high

fluorescence measurements are directly correlated with Ca^{2+} binding in AMPA and kainate calcium permeable receptors. Fluo-4 NW dye is widely used for identification of agonist/antagonist calcium signalling, having higher sensitivity compared to Fluo-3 and Fluo-4 AM in an assay type format. HEK-293 expressing human protein GluK1 were used to measure the activity of kainate/domoate agonist and CNQX antagonist (Fig. 5.15). The kainate dose-response curve gave an EC_{50} of $3.03\ \mu\text{M}$, 4-fold less than the literature value of $12\ \mu\text{M}$ (Solly et al. 2015) and Domoate dose response curve gave an EC_{50} of $0.077\ \mu\text{M}$ 20-fold less than literature value of $1.6\ \mu\text{M}$ (J. K. Christensen et al. 2004). It was observed that domoate had a lower EC_{50} (higher E_{max}) compared with kainate agonist (Fig. 5.16). Similar EC_{50} values obtained from literature demonstrated that calcium assay using Fluo4 dye is suitable for compound screening characterisation. The signal-to-background ratio (S/B) was calculated for kainate, domoate and CNQX and resulted in 15.01, 37.97 and 30.64 respectively. The calculations were based on the mean of the maximal response divided by the mean of the background. For CNQX the calculation of S/B ratio used the maximal response obtained after addition of kainate. The S/B ratio was higher with domoate suggesting a higher response signal ratio compared to the background.

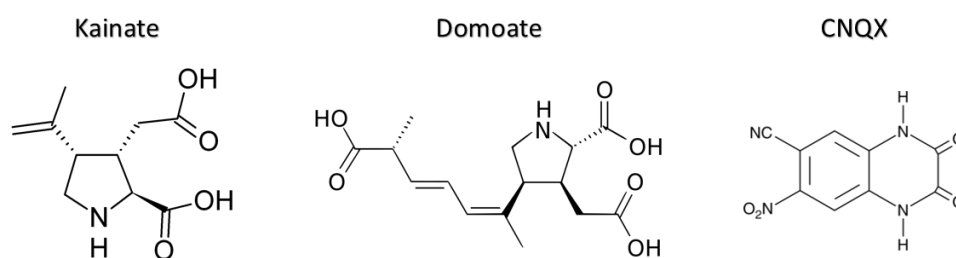
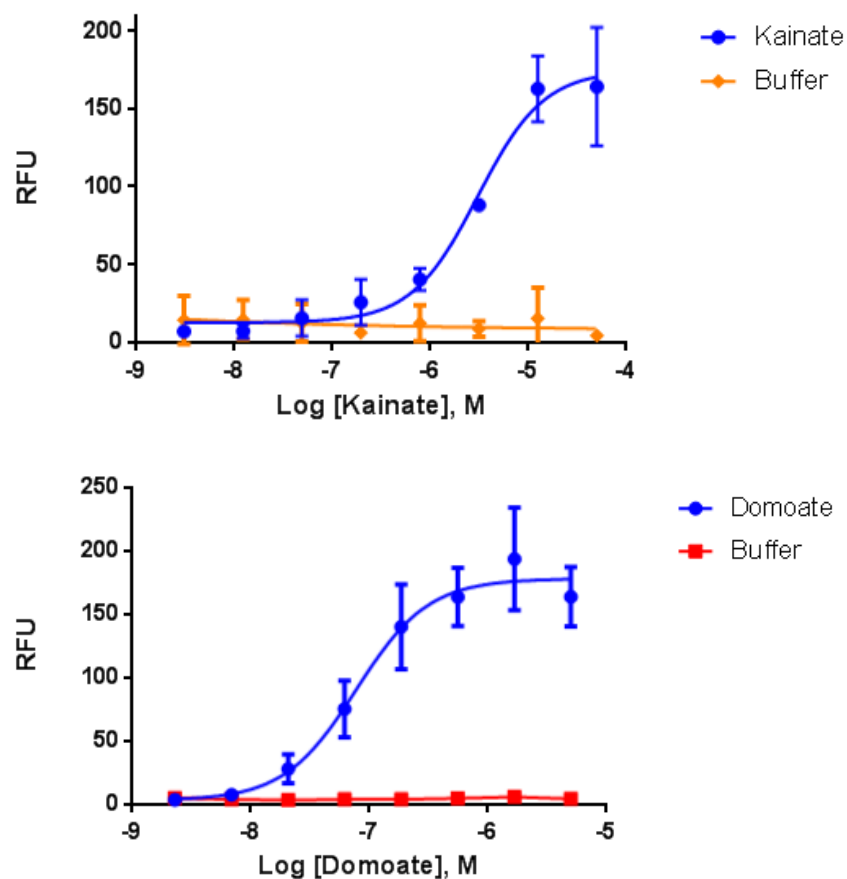


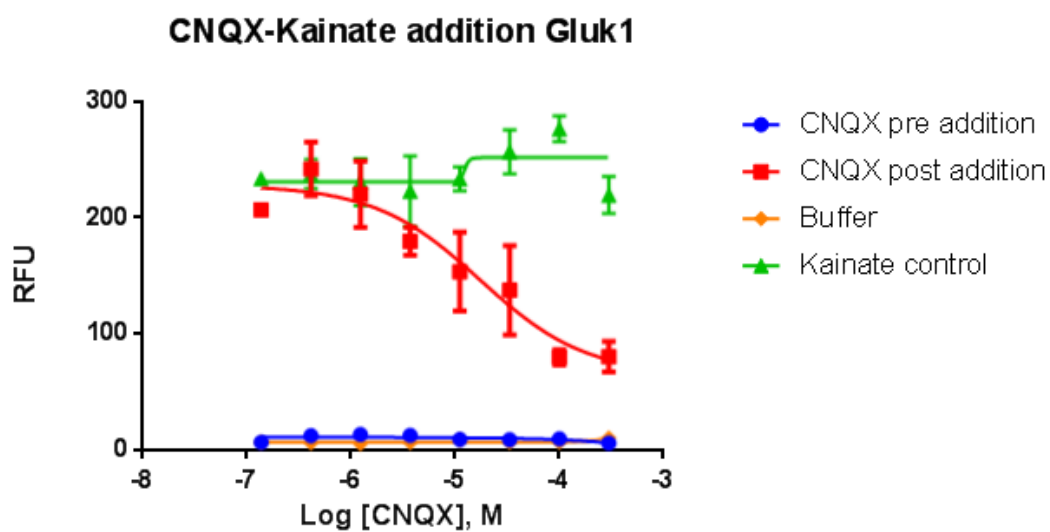
Figure 5.15. Chemical structures of kainate, domoate and CNQX.

CNQX antagonist dose response curve gave IC_{50} of $17.5\ \mu\text{M}$ when kainate was added to final concentration of $50\ \mu\text{M}$, CNQX was added to cells at $300\ \mu\text{M}$ final top concentration in a double addition format experiment, in which the second addition was kainate at single final concentration of $50\ \mu\text{M}$ (Fig. 5.17). The addition of kainate increases fluorescence in the lower concentrations of CNQX. The IC_{50} literature value is $1.5\ \mu\text{M}$ for kainate receptors (value from Cayman chemical supplier).



Agonist	EC ₅₀
Kainate	3.03 μ M
Domoate	0.077 μ M

Figure 5.16. Gluk1 kainate/domoate agonist dose response curves. HEK-293 cells stably expressing Gluk1, cells were incubated with 50 μ M kainate and 5 μ M domoate top concentration. RFU, relative fluorescence units in y-axis. Error bars (SD) are indicated representing n=3 individual experiments.



Antagonist	IC ₅₀
CNQX	17.5 μM

Figure 5.17. Gluk1-CNQX antagonist dose response curve. HEK-293 cells expressing human GluK1 receptors were incubated with CNQX (first addition step) then kainate added at 50μM final concentration (second addition step), labelled as CNQX post addition. Error bars (SD) are indicated representing n=3 individual experiments.

5.5 DISCUSSION

The main objective of these experiments was to express and purify the LBD of the rat GluK1 protein in a large-scale quantity to further continue with crystallography experiments with the aim of obtaining X-ray structure data for further drug discovery design.

Full-length Gluk1 protein has not been purified or crystallised due to being an integral membrane protein. The transmembrane domain is embedded in the phospholipid bilayer and interacts strongly with hydrophobic groups (fatty acyl groups) in the membrane (Uzman et al. 2000; Smith 2011). This property makes the purification and crystallisation extremely difficult, in membrane proteins strong non-polar solvents are usually used to help solubilise the protein. For example, the purification of the full-length rat rGluA2 receptor was achieved using a large amount of detergents such as, n-Dodecyl- β -D-Maltoside and n-undecyl-b-D-thiomaltoside to improve protein solubilisation and purification. For NMDA rat GluN1-GluN2B protein an amphiphilic detergent, lauryl maltose neopentyl glycol (MNG-3), was used to improve the stabilisation and solubilisation of the membrane protein. In addition, in both proteins a baculovirus-insect cell system was used to maximise protein production of membrane proteins (Sobolevsky et al. 2009a; E. Karakas & Furukawa 2014). Furthermore, the recent use of cryo-electron microscopy (EM) gives an advantage for determining structures without the crystal form of the protein, however the structures obtained are at low resolution ranging from 5 Å to 10 Å (Zanotti 2016). For this reason, not all iGluRs subtypes have been identified in a full-length structure because it is a long multi-step procedure with the use of different detergents and expression systems to take into consideration.

For structure based drug design purposes, attention was focused in the ligand binding domain of rat GluK1 as an important drug target structure for the study in epilepsy treatment. Ahmed and Oswald successfully characterised the structure of the LBD of AMPA GluA2 and GluA3 receptors with piracetam and aniracetam (Ahmed & Oswald 2010). Currently these nootropic drugs are marketed as a supplement for improving cognitive function and also used in dementia, however both drugs have not been approved by the FDA (Gouliaev & Senning 1994; Malykh & Sadaie 2010). In Ahmed's review, they found a potential new binding site in the LBD of AMPA receptors, they demonstrated the binding of aniracetam at the centre of the dimer interface and piracetam binding to multiple sites along the dimer interface for GluA2 and GluA3.

Gluk1 protein has over 90% sequence identity in the LBD, it was assumed that Gluk1 may have the same binding site in the dimer interface of the LBD and for that reason it was decided to focus on expressing and purifying the LBD of the rat Gluk1 protein. The rat protein was used due

to the difficulty of expressing human rGluK1 protein and to have uniformity to the AMPA rat GluA2 expression and purification system.

The expression construct was kindly provided by Dr. Antony W. Oliver (GDSC, University of Sussex). The plasmid construct was designed to express the S1 and S2 segments of the LBD following previous purification strategy from M. Mayer for AMPA receptors (Mayer 2005). This construct contains a 6xHis-SUMO tag to improve solubilisation and purification of the protein. The rGluK1 LBD protein was successfully purified on a large scale following a standard purification method used previously for AMPA LBD purification. Several batches of purified protein were produced, from different starting material (cell culture) a sufficient amount of purified protein was observed with six litres of cell culture ranging from 2.4 mg up to 3.2 mg final yield. With eight litres of cell culture it was observed to yield a reduced amount of protein, with a larger amount of unspecific proteins, suggesting a larger amount of aggregate formation from bacteria metabolism. It was also observed that with higher amounts of protein to produce (from higher amounts of cells in the starting culture) it was more difficult to handle the purification experiments, such as sonication, volume of buffers, amount of talon beads, elution fractions and incubation time with beads.

Preliminary crystallisation trials using commercial screening kits resulted in non-single crystals that gave low-resolution diffraction. Previously published crystallography for LBD rGluK1 (PDB 4E0X) was reproducible and single crystals with resolution of 1.64 Å, higher resolution than published crystal structure (2.0 Å) was obtained (Venskutonyte et al. 2012). Crystals obtained of rat GluK1 were high resolution diffracting crystals, however these crystals could be improved in order to facilitate larger fragment screens. rGluK1 protein was crystallised in complex with kainate, because all the crystallography experiments with only glutamate in the purification and without kainate (crystallography buffer) resulted in poor quality crystals. The high affinity of kainate in kainate receptors might give the stability of the structure to crystallize, however this is just a theory due to the difficulty of obtaining crystals with glutamate in the orthosteric site in this recombinant protein.

Finally, Dr. Iain Barret's previously optimised calcium assay was reproduced using standard agonists (kainate and domoate) and antagonist (CNQX). An EC₅₀ dose response curve was obtained with values of 3.03 µM for kainate, 0.077 µM for domoate and 17.5 µM for CNQX. The assay had a signal-to-background ratio (S/B) of 15.01, 37.97 and 30.64 respectively suggesting an adequate assay limit of detection. For future work, other fragments can be screened using this calcium assay optimized methodology.

The overall strategy was to obtain pure rat GluK1 LBD protein for X-ray crystallography experiments. Then using fragment soaking to observe the binding mode of these compounds into the structure to further confirm in a calcium assay format, as well as the possibility to perform in future a larger screen to optimise compounds binding in the structure. However, none of the ten fragments tested at different concentrations (1, 5 and 10 mM) displayed binding properties with the LBD structure of rat GluK1. At higher concentration of compounds more difficulties arose due to the higher % of DMSO affecting the quality and stability of the crystals resulting in poor diffraction values. Structural information obtained from X-ray crystallography and crystals obtained could be used for future work such as larger fragment screening and lead compound optimisation.

GluK2

5.6 MATERIALS AND METHODS

5.6.1 CLONING AND PLASMID VECTOR

The plasmid of the rat ligand binding domain (LBD) of GluK2 was kindly supplied by Dr. Antony W. Oliver from the Genome Damage and Stability Centre (GDSC, University of Sussex). The GDSC frequently used its own pHis-SUMO-3C vector to facilitate protein production and purification. The construct of rat GluK2 containing the LBD is formed by S1 and S2 segments linked by a Gly-Thr dipeptide to maintain the structure of the LBD and to form a stable structure without the amino terminal domain (ATD), transduction domain (TD) and transmembrane domain (TMD). This construct was designed according to previously published experiments (Mayer 2005) based on the design of AMPA receptor rGluA2 S1S2 construct (Armstrong & Gouaux, 2000). Similar to rGluK1, a 6xHis-SUMO tag was used to increase expression and solubility of the recombinant protein. The protein sequence based on rGluK2 P42260-1 from UniProt is shown in Fig. 5.18.

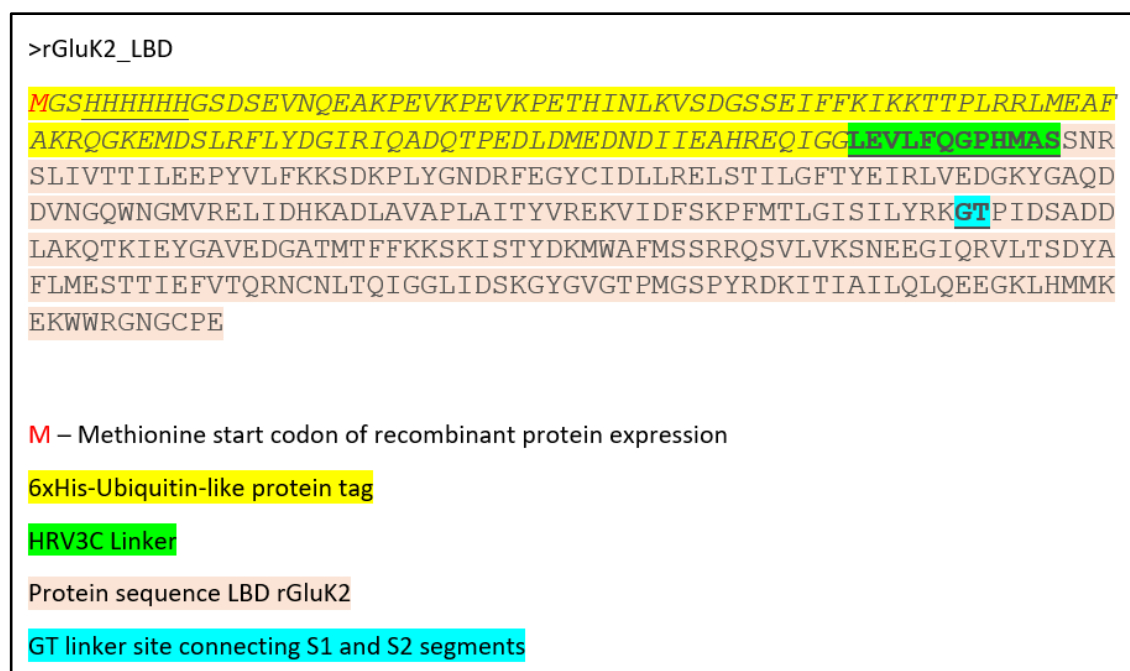


Figure 5.18. LBD rGluK2 sequence design for protein expression and purification. The sequence protein contains a N-terminal 6xHis-SUMO tag, a recognition SUMO cleavage site and the sequence of the LBD of the rGluK2 protein consisting of [429-SNRS...LYRK-544] and [667-PIDS...GCPE-806] linked using a dipeptide Gly-Thr, sequence based on P42260-1 (GRIK6, UniProt).

The pHIS-SUMO-3C plasmid containing the rGluK2 LBD protein was sub cloned externally by Invitrogen. The protein construct was subcloned into a pBR322 plasmid with a pET T7 expression system controlled by isopropyl β -D-1-thiogalactopyranoside (IPTG) using a T7 promoter site. The final plasmid contained an ampicillin resistance gene site to selectively control the bacteria grown carrying the recombinant protein and specific restriction enzymes such as NdeI, EcoRI, NotI, XhoI and Scal (Fig. 5.19). In addition, the plasmid was designed to have an N-terminal 6xHis-SUMO tag to improve the solubility and purification of the protein. The gene cloning and plasmid DNA purification was performed commercially by Invitrogen. Consistent with rGluA2 and rGluK1 experiments, the GluK2 protein was designed on rat protein gene sequence, to facilitate solubility, purification and crystallography experiments.

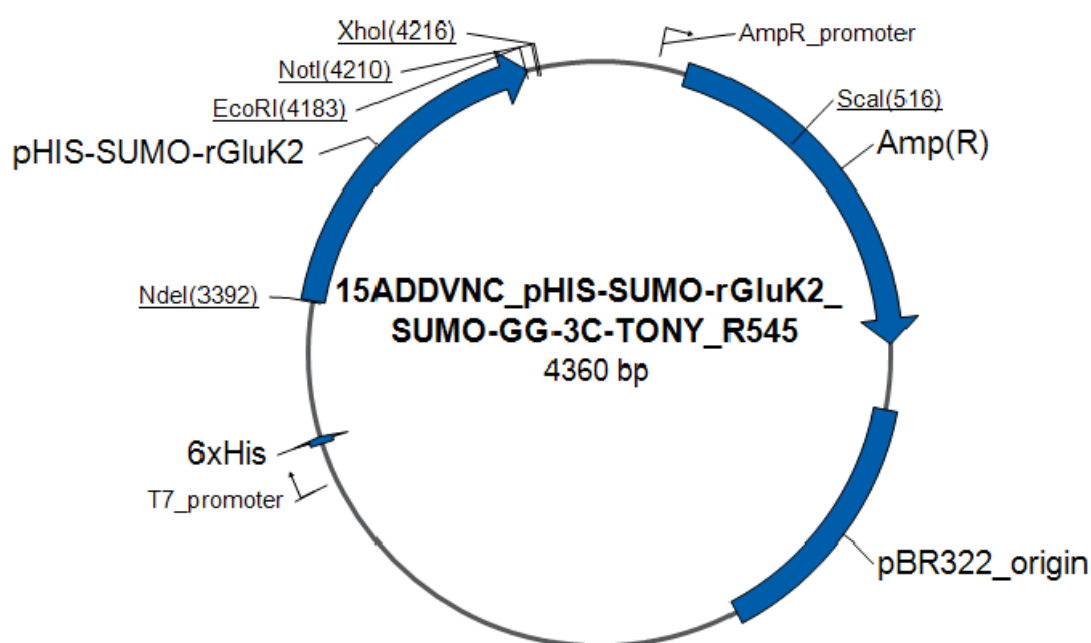


Figure 5.19. Plasmid map of the inserted recombinant rat gene GluK2 LBD. Invitrogen provided 5 μ g of lyophilised plasmid ready to reconstitute with 30 μ l of sterile water and use for transformation experiments.

5.6.2 COMPETENT CELLS

The competent cells used for bacteria transformation were the *E. coli* Origami™ B (DE3) by Novagen (Cat. No. 70837-3). The origami bacteria strain was used due to its ability to form disulphide bonds required for the correct folding of the protein. This bacteria strain is compatible with ampicillin and carbenicillin resistance plasmids. Selective antibiotics for Origami strains are kanamycin and tetracycline.

5.6.3 BACTERIA TRANSFORMATION

The vector containing 5µg of lyophilised DNA was reconstituted with 30µl of sterile purified water. The methodology followed was the same as rGluK1 bacteria transformation section 5.3.3, with the difference of adding 1 µl of the vector 15ADDVNC_pHIS-SUMO-rGluK2_SUMO-GG-3C-TONY_R545 corresponding to the rGluK2 LBD protein. The rest of the plasmid solution was stored at -20°C.

5.6.4 PROTEIN EXPRESSION

Protein expression experiment was the same as rGluK1 experiments, see section 5.3.4. Cells pellets from 6 L of culture broth were frozen at -20°C for further IMAC and SEC purification experiments.

5.6.5 PROTEIN PURIFICATION

5.6.5.1 IMMOBILIZED METAL AFFINITY CHROMATOGRAPHY (IMAC)

Buffers for protein purification experiments below, each buffer was filtered at 0.45 µm (Cellulose nitrate membrane filters, Whatman™ Cat. No. 514-8073, VWR).

Lysis Buffer	Elution Buffer	Cat. No.
20 mM HEPES pH 7.5	20 mM HEPES pH 7.5	BP310-1, Fisher BioReagents
500 mM NaCl	500 mM NaCl	S/3120/63, Fisher Chemical
10 mM Imidazole	300 mM Imidazole	122025000, Acros Organics
0.5 mM TCEP	0.5 mM TCEP	646547-10x1ml, Sigma-Aldrich
Distilled H2O up to 500 ml	Distilled H2O up to 250 ml	N/A

The IMAC purification was the same as followed by rGluK1 experiments, section 5.3.5.1.

5.6.5.2 SIZE EXCLUSION CHROMATOGRAPHY (SEC)

The SEC purification was the same as followed by rGluK1 experiments, section 5.3.5.2

5.6.6 CRYSTALLOGRAPHY

Preliminary crystal experiments were performed using commercial crystallisation screens (Table 5.7). The pure rGluK2 protein was diluted with crystallography buffer (10mM HEPES pH 7.0, 30 mM NaCl, 1 mM EDTA and 20 mM glutamate) to a final concentration of 5 mg/ml. For crystallography screening, the crystal Phoenix liquid handling system (Alpha Biotech) was used. Using the MRC 2-well 1 protein protocol a drop ratio of 1:1 of protein and reservoir solution was dispensed into a 96 MRC crystallography plate. Experiments were performed using the hanging drop vapour diffusion method at 14°C. From crystallography screening, the best crystals grown were under the following conditions: 0.06M Citric acid, 0.04M BIS-TRIS propane pH 4.1 and 16% w/v PEG 3350 corresponding to PEG/Ion HT screen condition H1.

Table 5.7. Commercial crystallisation screens used for preliminary crystallography experiments.

Crystallisation screen	Supplier	Cat. No
JCSG-plus™	Molecular dimensions	MD1-40
Proplex™	Molecular dimensions	MD1-42
Morpheus®	Molecular dimensions	MD1-47
Index HT	Hampton Research	HR2-134
PEG/Ion HT	Hampton Research	HR2-139
SaltRx HT	Hampton Research	HR2-136
Crystal screen HT	Hampton Research	HR2-130

Microseeding

In order to optimise the size and quality of single crystals, a seed stock was prepared from previous crystal hits. Crystals were crushed with a probe and transferred into a seed bead tube (HR2-320, Hampton Research) with 50 μ l of reservoir solution (0.06M Citric acid, 0.04M BIS-TRIS propane pH 4.1 and 16% w/v PEG 3350). The seed bead tube was vortexed for 2 minutes and this solution became the 100% seed stock. 1%, 5% and 10% seed stock dilutions were prepared using the reservoir solution.

The 1%, 5% and 10% seed stocks were seeded (Fig. 5.20) in a 48-well MRC maxi plate (MD11-004-10, Molecular Dimensions). The volumes added per drop were 0.6 μ l protein + 0.4 μ l reservoir solution + 0.2 μ l seed stock using the Oryx8 protein crystallisation robot from Douglas Instruments. Plates were incubated for 5 days at 14°C and crystals which grew after 24 hours were stored with cryoprotectant (30% ethylene glycol) before being flash-cooled in liquid nitrogen. X-ray data was collected to 1.95 Å resolution at the beamline i04 (Diamond Light Source synchrotron, Oxfordshire).

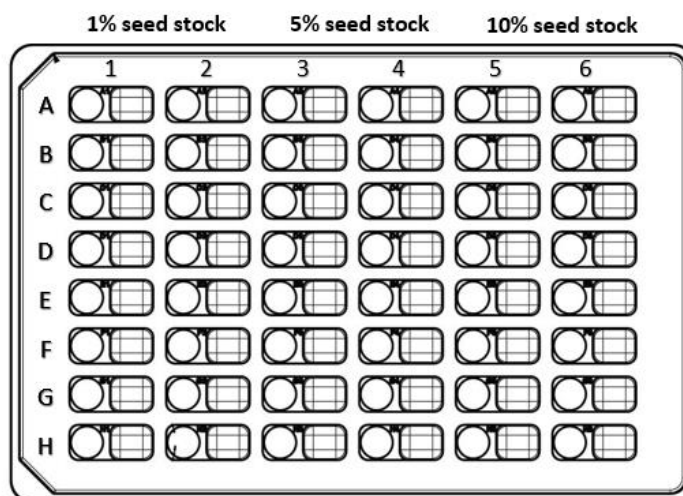


Figure 5.20. Layout plate of the microseeding experiments performed for crystal optimisation. 48-well MRC maxi optimisation plate used for microseeding experiments. This plate type has the characteristic of having wider wells for depositing larger drops to obtain larger crystals by using less reservoir solution.

5.6.7 FRAGMENT SCREENING (SOAKING)

In the same way as rGluK1, ten internally-synthesised fragments (SDDC, Chemistry group) were used for soaked experiments (Table 5.2). Crystals of rGluK2 were soaked with different concentrations of fragments (1, 5 and 10 mM) and incubated for 1 hour at 4°C. Additional detail of the experimental procedure is provided in section 5.3.7.

Table 5.2. Fragments structures used for soaking experiments, compounds synthesized in-house.

Compound	Structure	Molecular weight (g/mol)	Compound	Structure	Molecular weight (g/mol)
UOS-15592		268.24	UOS-31059		370.32
UOS-14986		190.17	UOS-30693		393.63
UOS-15326		296.29	UOS-30696		369.6
UOS-12344		379.42	UOS-21170		495.88
UOS-12230		282.26	UOS-30695		405.65

5.6.8 KAINATE CALCIUM ASSAY

The calcium assay commercial kit Fluo-4 NW (no-wash) from Thermo Fisher Scientific (Cat. No. F36206) was used for detecting the increase of cytosolic Ca^{2+} resulting from activation and pharmacological modulation of the rGluK2 receptor. For more information about the assay principle, see section 5.3.8.

The validation of the assay was carried out by Dr. Iain Barret from the Sussex Drug Discovery Centre and the validated conditions of the assay were followed to confirm the effect of the reference agonist kainate and domoate, and internal antagonist UOS-30693 with the GluK2 cellular assay.

Description	Use for	Supplier and Catalogue
DMEM/F-12 GlutaMAX	Cell culture media	10565018, Thermo Fisher Scientific
Blasticidin S HCl	Media supplement (antibiotic)	R21001, Invitrogen
Hygromycin B	Media supplement (antibiotic)	10687010, Invitrogen
Tetracycline hydrochloride	Induction of receptor expression	233105000, Acros Organics
Fetal bovine serum (FBS)	Media supplement	F7524, Sigma-Aldrich
Penicillin-Streptomycin (PS)	Media supplement (antibiotic)	P4333, Sigma-Aldrich
Trypsin-EDTA, phenol red	Cell detachment	25200056, Thermo Fisher Scientific
PBS	Assay buffer	79382, Sigma-Aldrich
DMSO	Assay buffer	10080110, Fisher chemical
Fluo-4 NW Calcium assay kit Component A: dye mix Component B: assay buffer	Assay kit	F36206, Thermo Fisher Scientific
Corning®96 well flat clear bottom black, sterile microplate	Assay microplate	3904, Corning
96-V well microplate translucent polypropylene	Source dilution plate	MIC9050, Scientific Laboratory Supplies
Concanavalin A	Buffer additive, clamping agent	J61221, Alfa Aesar
Domoic acid (domoate)	Agonist agent	0269, Tocris Bioscience
Kainic acid (kainate)	Agonist agent	HB0355, Hellobio
UOS-30693	Antagonist agent	In-house

Cell culture and assay methodology

Methodology was followed as GluK1 experiments (section 5.3.8) with the following differences:

- I. HEK-293_hGluK2 cells stably expressing human GluK2 receptors purchased from Sophion, Biolin Scientific. The expression of GluK2 receptor was under a tetracycline-inducible promoter.
- II. Cells were grown in DMEM/F12 GlutaMAX supplemented with 10% FBS, 1% PS, 100 µg/ml hygromycin B and 15 µg/ml blasticidin.
- III. 24 hours before calcium assay, cells were incubated with tetracycline at 2.5µg/ml final concentration to induce the expression of the GluK2 receptor.
- IV. The source plate was prepared with a final maximal concentration of kainate of 8.3 µM prepared from a 25 mM stock solution and a final maximal concentration of domoate of 0.83 µM prepared from a 10 mM stock solution. The addition plate was prepared with both agonists at 1:6 serial dilutions format. The antagonist was the compound UOS-30693 with a final maximal concentration of 300µM prepared from a 10 mM stock solution in a 1:3 serial dilutions format, with an extra addition of kainate at 50 µM (two addition format). CNQX antagonist was tested at 300 and 500 µM with GluK2 cells however, no antagonist activity was observed. The internal compound UOS-30693 was used for antagonist experiments due to being previously identified in the literature as a potent antagonist for GluK2 receptors (Valgeirsson et al. 2004).

5.7 RESULTS

5.7.1 IMMOBILIZED-METAL AFFINITY CHROMATOGRAPHY (IMAC)

The rat GluK2 LBD protein was purified using IMAC and talon affinity chromatography as a first step in a purification methodology. The purified protein was obtained in six high-imidazole concentrate elution fractions of approximately 7.5 ml each (Fig. 5.21) with a protein band of 44 kDa (29 kDa of protein + 15 kDa of 6xHis-SUMO tag). The flow-through fraction shown in the gel displays all the proteins that do not bind to the talon beads (nonspecific bands). The wash fractions 1 and 2 represent all unspecific proteins left in the column or proteins that bind weakly to the talon beads. A strong band of protein in the beads sample before elution (B1) demonstrates the protein retained by the talon bead and the sample of beads after elution (B2) shows a small fraction of protein still bound to the beads. This demonstrates the effective retention of the protein of interest for the talon metal affinity resin and the successful first step purification procedure. Elution fractions 1-3 gave a strong band of protein of 44 kDa. Other nonspecific bands of ~15, 25-30 and 60-100 kDa were observed in the SDS-PAGE gel and were further removed by SEC purification experiments.

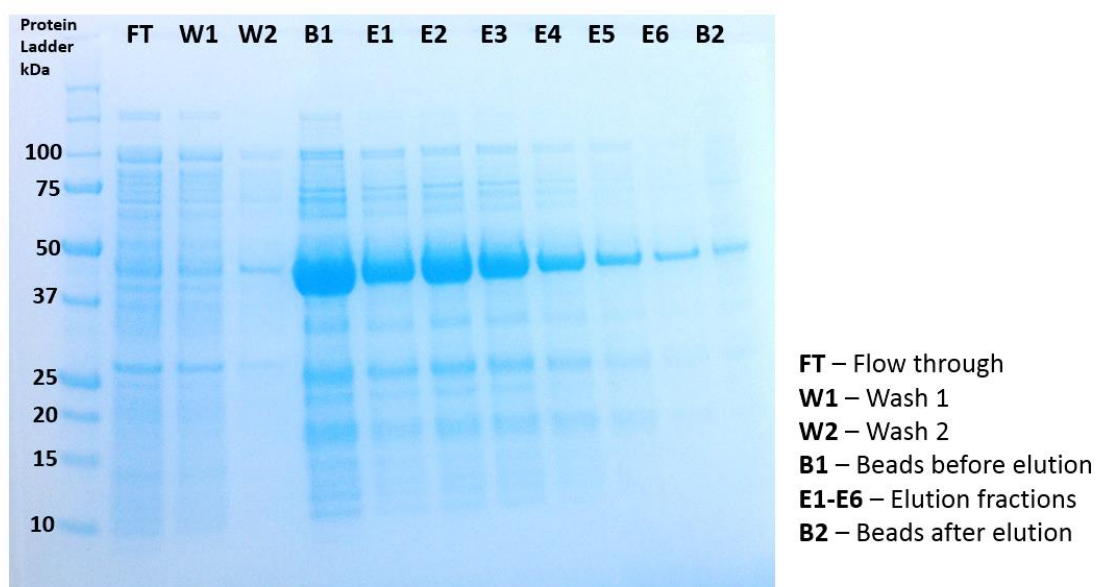


Figure 5.21. SDS-PAGE gel of IMAC purification. Strong bands of 44 kDa corresponding to the LBD of the rat GluK2 protein. Gel stained with Blue Coomassie for 1 hour and destained for 2 hours. Approximately 50 ml of supernatant was added into 7.5 ml of talon beads, the flow through was ~50 ml, washes 1 and 2 ~ 100ml each and a sample of 25 μ l of talon beads was used for running the SDS-PAGE gel. 10 μ g of protein loaded per well, protein ladder used Precision Plus Protein™ All Blue (Cat. No. 1610373, Bio-Rad). Wash buffer contains 10 mM Imidazole and elution buffer 300 mM Imidazole.

To examine if the eluted protein was rGluK2, samples of the elution fractions 1 to 6 (~7.5ml each) were collected and incubated with 3C protease enzyme which specifically cleaves the 6xHis-SUMO recognition site sequence of the protein. One sample of 100µl was taken before adding the enzyme and then another sample of 100 µl was taken after incubation with the protease enzyme. Samples of elution mix with and without 3C protease incubation were run in a SDS-PAGE gel and it was observed that elution fractions without 3C protease incubation exhibit a strong band of 45 kDa (Fig. 5.22). In contrast, samples of elution mix with 3C protease incubation showed two new bands of 29 kDa and 15 kDa corresponding to the protein and the 6xHis-SUMO tag respectively. These results demonstrate that the protein eluted in the previous IMAC experiments correspond to rGluK2 LBD protein containing 6xHis-SUMO tag. The enzyme displayed high protease activity in recognising and cleaving the human rhinovirus (HRV) 3C protease cleavage site of the 6xHis-SUMO tag protein. In the gel a faint band of 45 kDa was still present in the sample with 3C protease however this was a relatively small amount of protein.

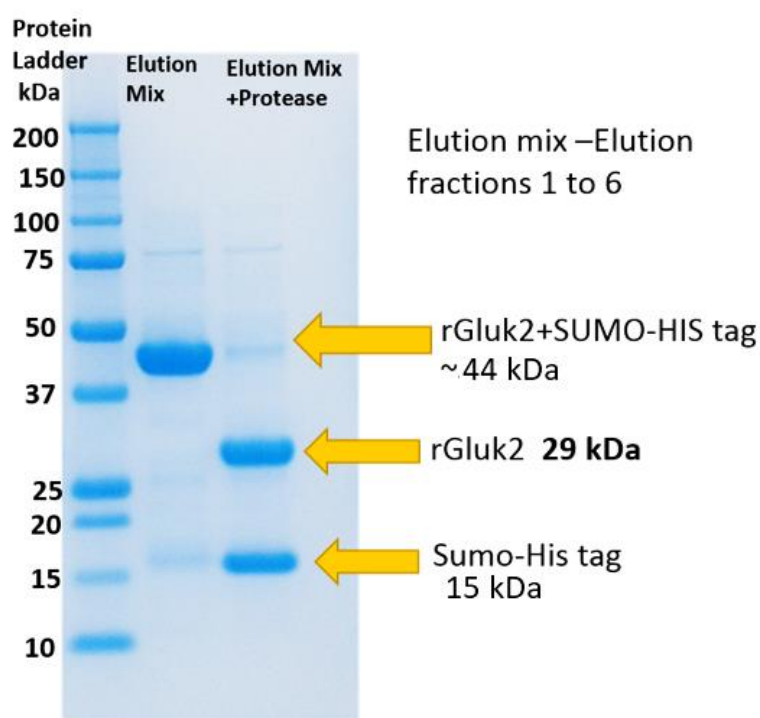


Figure 5.22. SDS-PAGE gel of 3C protease activity. Protein elution fractions before 3C protease incubation exhibit a band of 45 kDa corresponding to rGluK2 with 6xHis-SUMO tag. Protein elution fractions after 3C protease incubation exhibit two bands of 29 kDa and 15 kDa corresponding to the protein rGluK2 and 6xHis-SUMO tag respectively. 15 µg of protein loaded per well, protein ladder used Precision Plus Protein™ All Blue (Cat. No. 1610373, Bio-Rad).

5.7.2 SIZE EXCLUSION CHROMATOGRAPHY (SEC) PURIFICATION

Ultraviolet (UV) light absorption at A_{280} was used to monitor the fractions separated during SEC. The elution profile showed two main peaks (Fig. 5.23A), an initial first peak around 120 ml (~200 mAU) and a second peak at 160-180 ml (~180 mAU). Fractions of both peaks were collected and run in a SDS-PAGE gel electrophoresis to observe the proteins corresponding to each UV absorbance peak. Fractions 1E11 and 1F1 of the first peak displayed two bands, 29 kDa corresponding to the pure rGluK2 protein and 45 kDa corresponding to the protein with remaining 6xHis-SUMO tag (Fig. 5.23B). Fractions 1G9 to 1H4, corresponding to the second peak, exhibit the protein rGluK2 with higher purity, fractions 1H5 and 1H6 displayed a 15 kDa band suggesting a small amount of cleaved 6xHis-SUMO tag remaining in the sample.

Fractions with high purity (1G9-1H4) were collected (~16 ml), concentrated and further purified with IMAC. The concentrated sample was incubated with 1ml of talon beads to remove any amount of cleaved 6xHis-SUMO tag left in the sample because highly pure protein is more effective for crystallography experiments. Final pure protein was confirmed by SDS-PAGE gel analysis (Fig. 5.24), the gel displayed a single band of 29 kDa and no other nonspecific bands. Final protein concentration was verified by nanoDrop using the molecular weight of 29.86 kDa and extinction coefficient of $39,880 \text{ M}^{-1} \text{ cm}^{-1}$ at 280 nm. A final protein yield of 6.1 mg (12.2 mg/ml in ~500 μl) was obtained from 4 litres of starting culture. Six batches of purified protein were prepared for crystallography experiments (listed in Table 5.8).

Table 5.8. Different batches of pure protein obtained after purification experiments

Batch No.	Starting cell culture (L)	Concentration (mg/ml)	Final volume obtained (μl)	Yield of purified protein (mg)
1	2	3.6	100	0.4
2	4	9.5	500	4.8
3	4	7.5	400	3.0
4	4	12.62	400	5.0
5	4	8.1	700	5.7
6	4	12.28	500	6.1

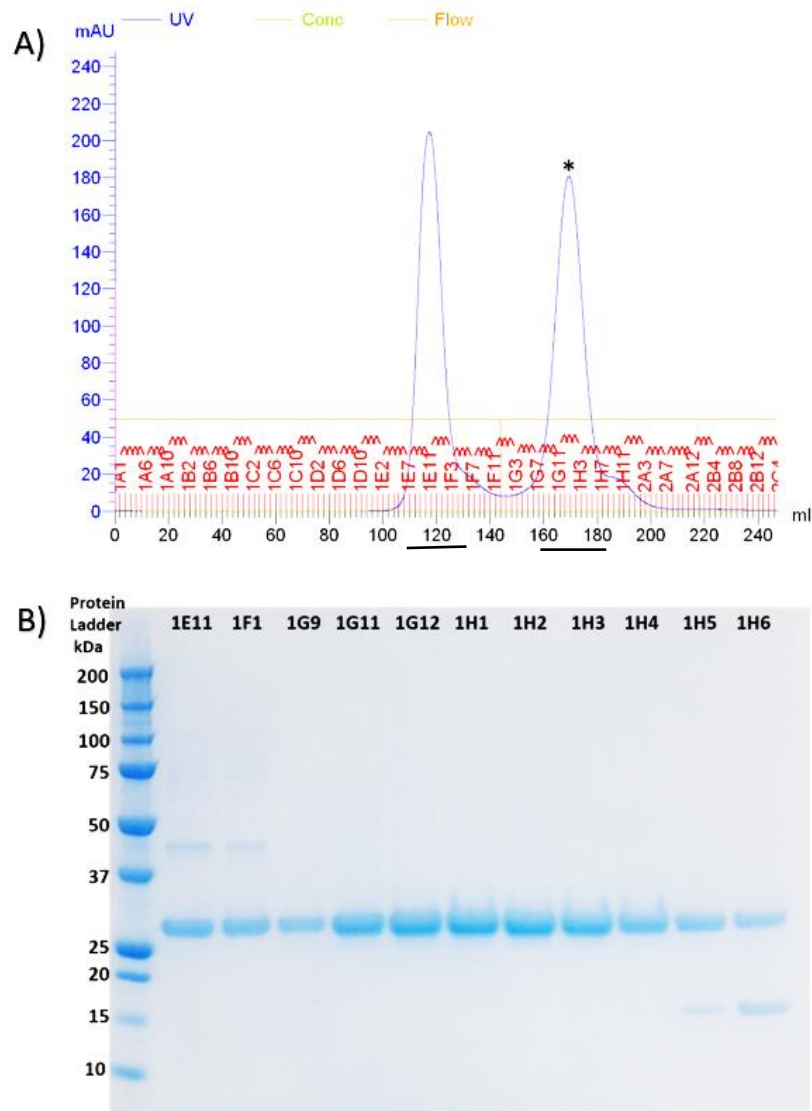


Figure 5.23. Size exclusion chromatography for rGluK2 protein. A) Chromatogram displaying the elution profile of the rGluK2 with SEC purification. B) SDS-PAGE gel of the elution fractions obtained, fractions 1E11 and 1F1 corresponding to first peak; fractions from 1G9 to 1H6 corresponding to second peak marked with an asterisk. Bands of 29 kDa corresponding to rGluK2 LBD. 10 μ g of protein loaded per well and protein ladder used Precision Plus Protein™ All Blue (Cat. No. 1610373, Bio-Rad).

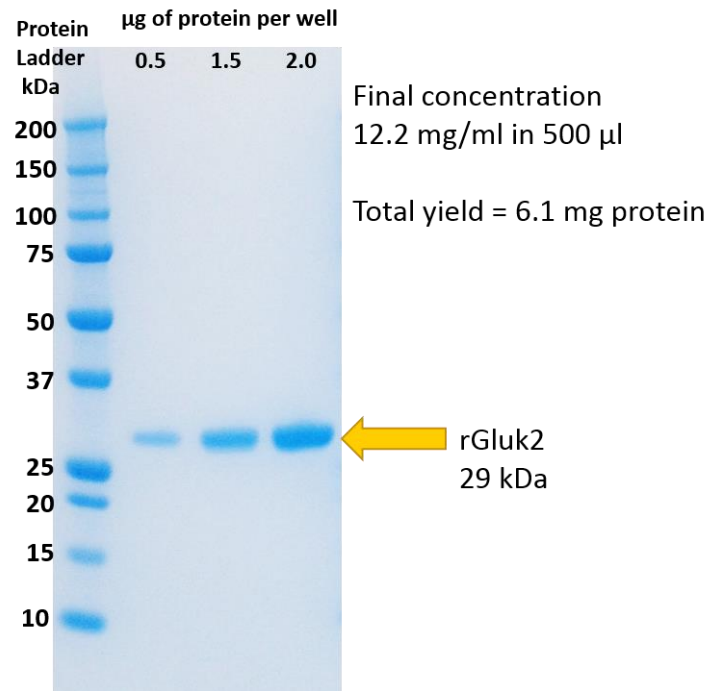


Figure 5.24. SDS-PAGE gel purity verification of rGluK2 protein. 0.5, 1.5 and 2.0 µg of protein loaded, one single band of 29 kDa was observed corresponding to rGluK2 LBD protein.

5.7.3 CRYSTALLOGRAPHY

Preliminary crystallography experiments resulted in the formation of seven crystal hits from three different commercial screen kits (PEG/ION, Salt Rx and JCSG-PLUS) described in Table 5.9. The best single type crystal was condition H1 from PEG/ION HT screen (Fig. 5.25). It was decided not to use any hits containing phosphate salts or buffers to avoid the formation of salt crystals (false positives).

Table 5.9. Conditions of the crystal hits obtained after crystallography screening.

System	Well	Salt	Buffer	Precipitant
PEG/Ion HT	E10	8% v/v Tacsimate pH 4.0	None	20 % w/v PEG 3350
	G7	2% v/v Tacsimate pH 4.0	0.1 M Sodium acetate trihydrate pH 4.6	16% w/v PEG 3350
	H1	None	0.06 M Citric acid, 0.04 M BIS-TRIS propane / pH 4.1	16% w/v PEG 3350
Salt Rx HT	E2	1.8 M Ammonium phosphate monobasic	0.1 M Sodium acetate trihydrate pH 4.6	None
	E8	1.8 M Sodium phosphate monobasic monohydrate, Potassium phosphate dibasic / pH 5.0	None	None
JCSG-PLUS HT-96	C1	0.2 M Sodium chloride	0.1 M Phosphate/citrate pH 4.2	20 % w/v PEG 8000
	D4	0.2 M Lithium sulphate	0.1 M Sodium acetate pH 4.5	30 % w/v PEG 8000

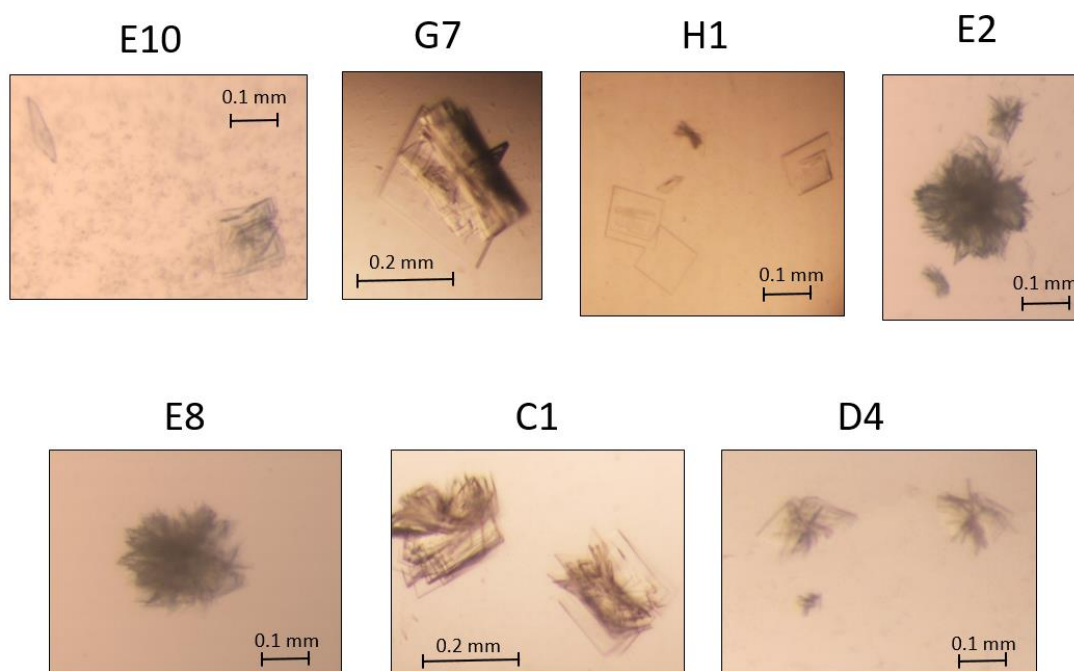


Figure 5.25. Light microscopy images of crystal hits from crystallography commercial screening kits. Different crystal hits were observed after preliminary crystal screening experiments; the conditions of each well are listed in Table 5.9. Crystals obtained were thin plates, most with plate aggregation.

Crystals grew after 24 to 48 hours using the sitting drop method at 14°C with a protein solution of 5 mg/ml diluted in crystallography buffer (10mM HEPES pH 7.0, 30 mM NaCl, 1 mM EDTA and 20 mM glutamate). The drop ratio was 1:1 of protein solution and reservoir solution (0.06 M citric acid, 0.04 M BIS-TRIS propane pH 4.1 and 16% w/v PEG 3350). Single and larger crystals were obtained after microseeding experiments using 1%, 5% and 10% seed stock. The best quality crystals grew with 5% and 10% seed stock, with no significant differences between them.

The final optimised crystals had a monoclinic space group (three unequal axes at right angles) ranging in size from 0.12 to 0.20 mm (Fig. 5.26). Crystals were stored with 30% ethylene glycol as a cryoprotectant to protect crystals from free radicals of ionising X-rays during diffraction collection. rGluK2 crystals diffracted at 1.95 Å resolution. Molecular replacement was performed using an rGluA2 structure obtained in house. Final models were refined using CCP4 and PHENIX software; COOT was used for manual model building and refinement. Molecular replacement and refinement was performed by Dr. Mark Roe. Crystallography statistics of crystal rGluK2 LBD are presented in Table 5.10.

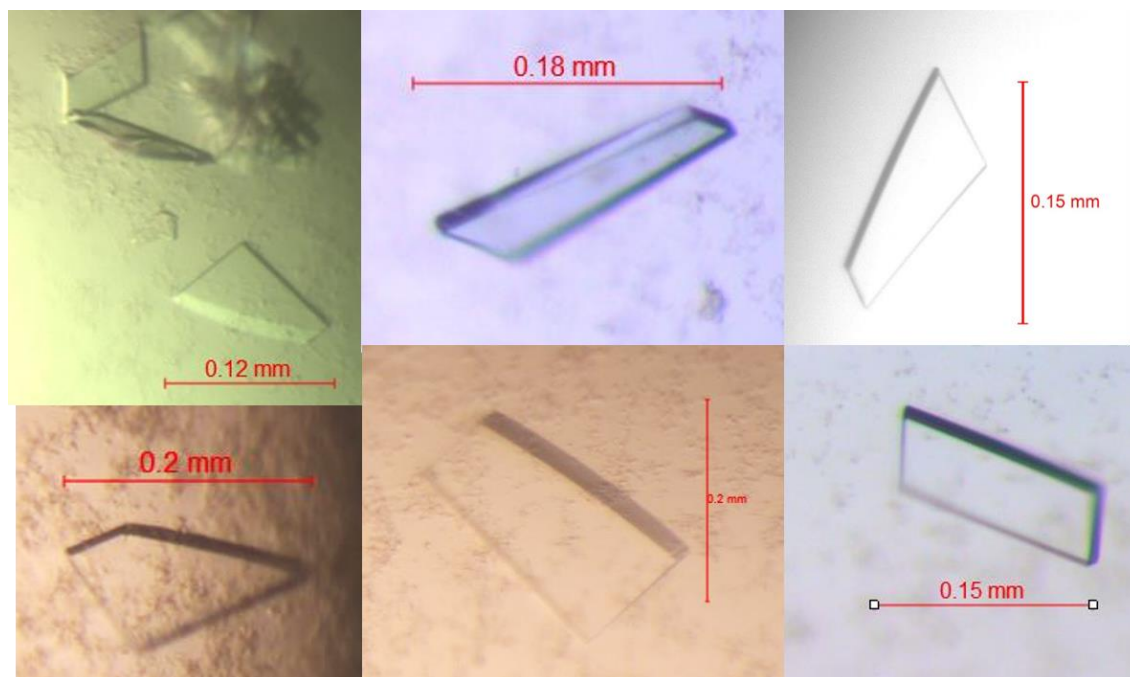


Figure 5.26. Light microscopic images of rGluK2 monoclinic crystals. Crystals obtained at 5.0 mg/ml protein concentration with a reservoir solution of 0.06 M citric acid, 0.04 M BIS-TRIS propane pH 4.1 and 16% w/v PEG 3350.

Table 5.10. Crystallographic statistics of rGluK2 LBD. Crystal shot at the i04 beamline at Diamond Light Source.

Data Set (Highest shell in parentheses)	rGluK2
a (Å)	46.50
b (Å)	105.21
c (Å)	58.06
α (°)	90
β (°)	103.5
γ (°)	90
Space Group	P 1 21 1
Wavelength (Å)	0.9795
Resolution Limit (Å)	49.74-1.95 (1.98-1.95)
Number of Unique Obs.	39197 (1937)
Completeness (%)	99.1 (98.8)
Multiplicity	2.6 (2.5)
Rmerge %	0.106 (0.936)
Rpim(I) %	0.078 (0.692)
CC _{1/2}	0.992 (0.643)
I/ σ I	5.1 (1.2)
Refinement	
Resolution Range (Å)	49.743 – 1.950
Rcryst	0.2390
Rfree	0.2711
Number of protein atoms	3,950
Number of ligand atoms	30
Number of solvent atoms	515
Mean B	27.4
Rmsd bond lengths (Å)	0.003
Rmsd bond angles (°)	0.609

The solved structure of the LBD of rGluK2 displayed glutamic acid (glutamate; the orthosteric agonist) binding in the cavity formed between the interface of S1 and S2 domains (Fig. 5.27). This is the same as other iGluRs LBD receptors such as rGluA2 and rGluK1. Dimers of the LBD of in-house structure rGluK2 in complex with glutamate and the published structure rGluK2 in complex with kainate (PDB accession code 1TT1) were aligned to confirm the same dimer conformation found in the literature (Mayer 2005). The alignment of both dimers confirms the same conformation and same binding core for agonists glutamate and kainate (Fig. 5.28). Interestingly, the dimer structure of rGluK2 has different structural conformation from the rGluK1 dimer. COOT software was used to compare the dimer conformations of rGluK2 and rGluK1 by fixing one monomer of both structures in green (Fig. 5.29), the results show that rGluK1 has a different arrangement of the second monomer in yellow with a wider space at one side of the dimer interface (Fig. 5.29). Previous alignment of the LBD of AMPA rGluA2 and rGluK1 have shown the same dimer conformation suggesting the same binding sites in the dimer interface, however these results now show that rGluK2 might have different residues involved in the binding sites of the dimer interface compared to rGluK1.

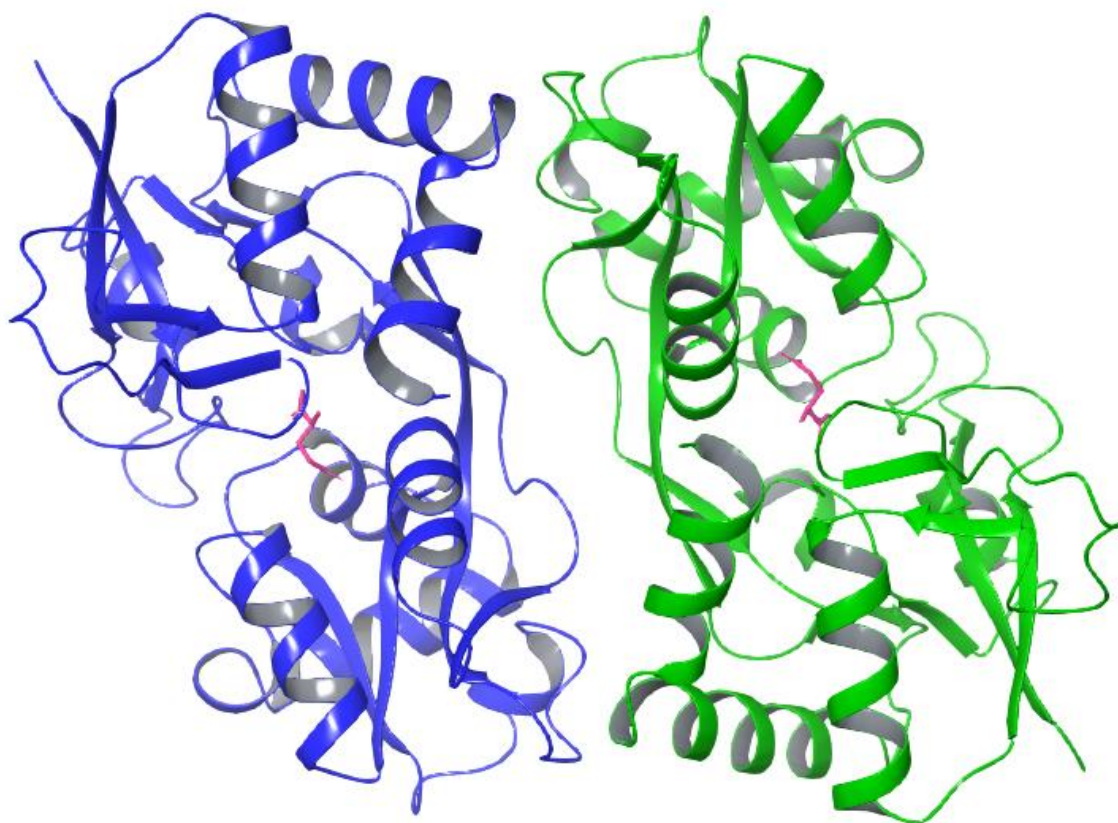


Figure 5.27. LBD rGluK2 dimer structure obtained with X-ray crystallography. Chain A and B are coloured in blue and green respectively. Glutamate shown in pink stick representation. Diagram of structure generated using Maestro Schrödinger version 11.1.

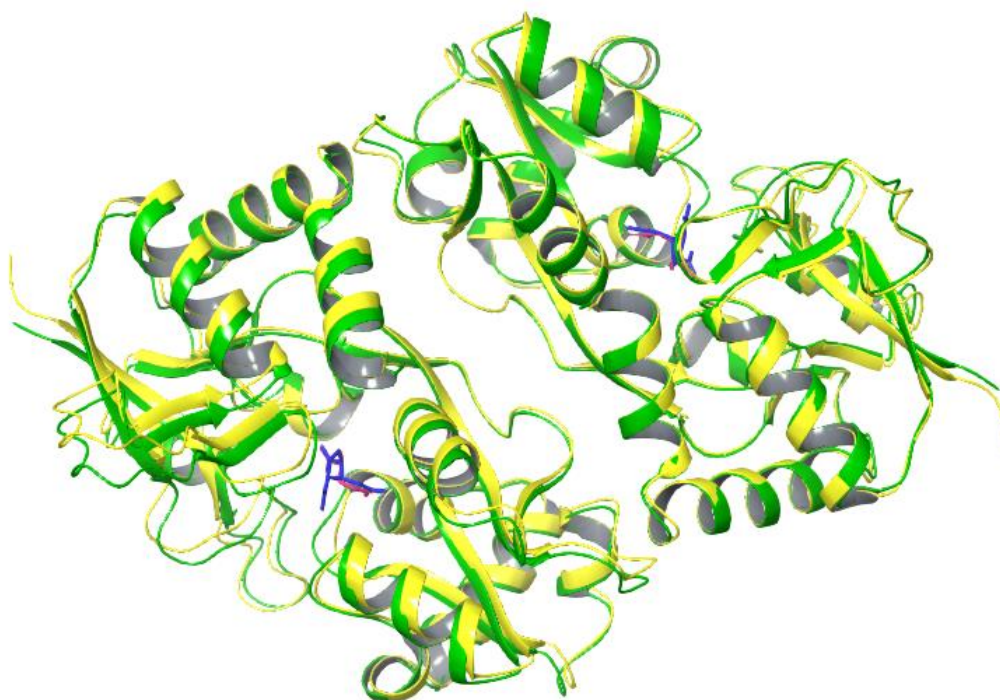


Figure 5.28. Alignment of rGluK2 dimer structures. LBD dimers structures of the in-house rGluK2 protein in complex with glutamate and published rGluK2 in complex with kainate (PDB accession code 1TT1; Mayer 2005) in green and yellow respectively. Glutamate and kainate are displayed in stick representation in pink and blue respectively.

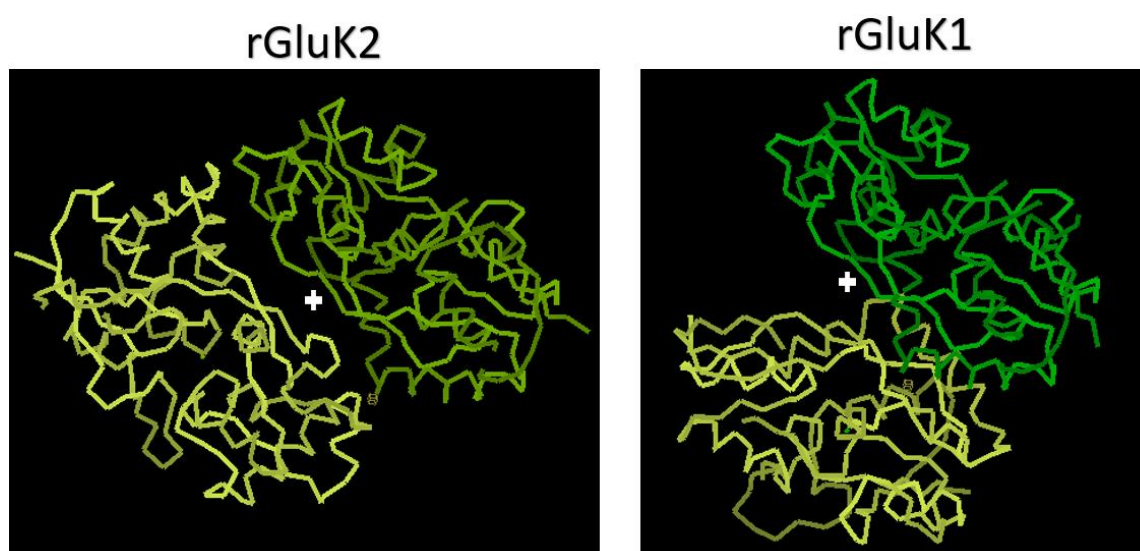


Figure 5.29. Dimer comparison between in-house crystal structures of rGluK1 and rGluK2. Green monomer of both structures were placed in the same position and white cross set in the middle of the dimer 2-symmetry axis to compare dimer conformations. Dimers structures processed with COOT software.

The bond interactions of the agonist-binding pocket showed that glutamate α -carboxyl group formed chemical interactions with residues Ala-102, Arg-107 and Ala-153. The α -amino group of glutamate formed salt bridge and hydrogen bonds with residue Glu-202 and the δ -carboxyl group formed hydrogen interaction with Thr-154 (Fig. 5.30 & 5.31). All these interactions are the same as observed in the published structure of the rat GluK2 LBD in complex with glutamate (PDB accession code 1S50; Mayer 2005). Similarly, the structure of the in-house LBD of rGluA2 has the same three conserved interactions as rGluK2, these residues are: arginine, glutamate and threonine binding to α -carboxyl, α -amino and δ -carboxyl groups of glutamate (Fig. 4.15 & 5.30). In addition, the in-house crystal structure of the rGluK1 LBD in complex with kainate showed that arginine and glutamic acid residues form hydrogen bond interactions with the α -carboxyl group and the α -amino group of kainate respectively (Fig. 5.30). From these results, it can be confirmed that residues arginine and glutamic acid are conserved and important for agonist binding in the cavity of the LBD of rGluA1, rGluK1 and rGluK2.

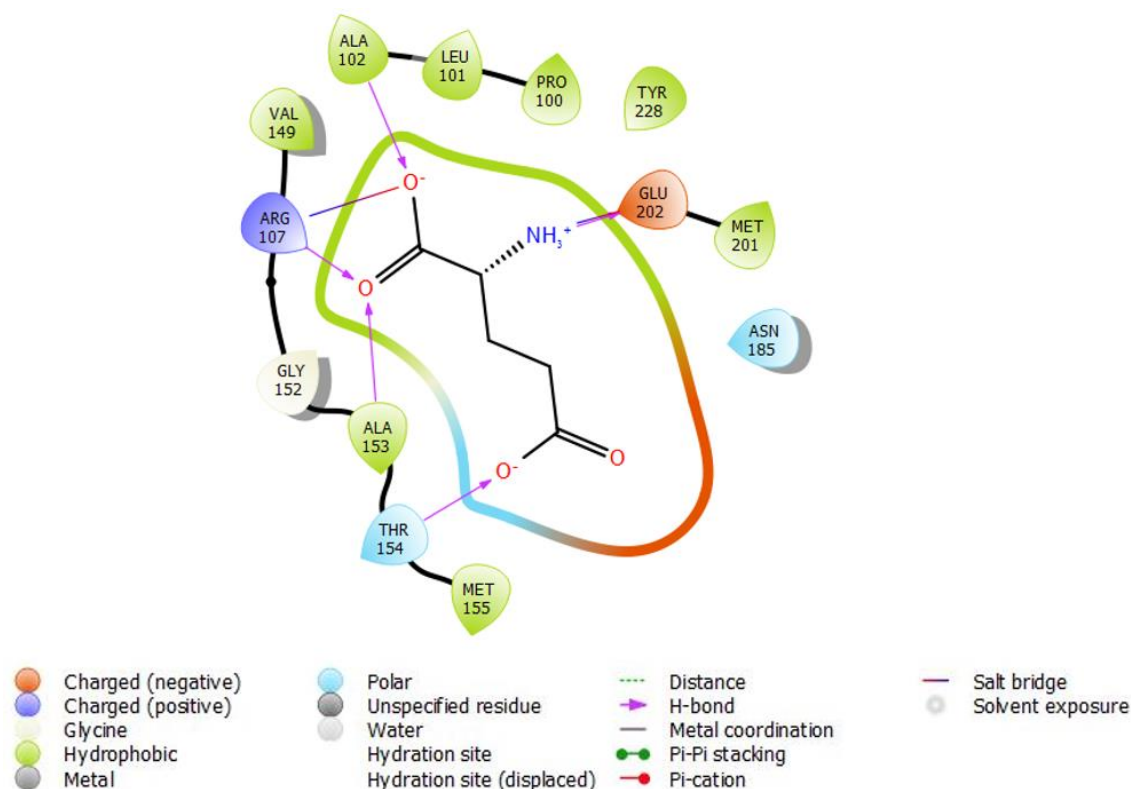


Figure 5.30. Glutamic acid binding interaction diagram for rGluK2 LBD. Bound glutamate interacts with Ala-102, Arg-107, Ala-153, Thr-154, and Glu-202. Hydrogen bonds are represented in fuchsia arrows and salt bridges in blue/red line. Ligand interaction diagram generated using Maestro Schrödinger version 11.1.

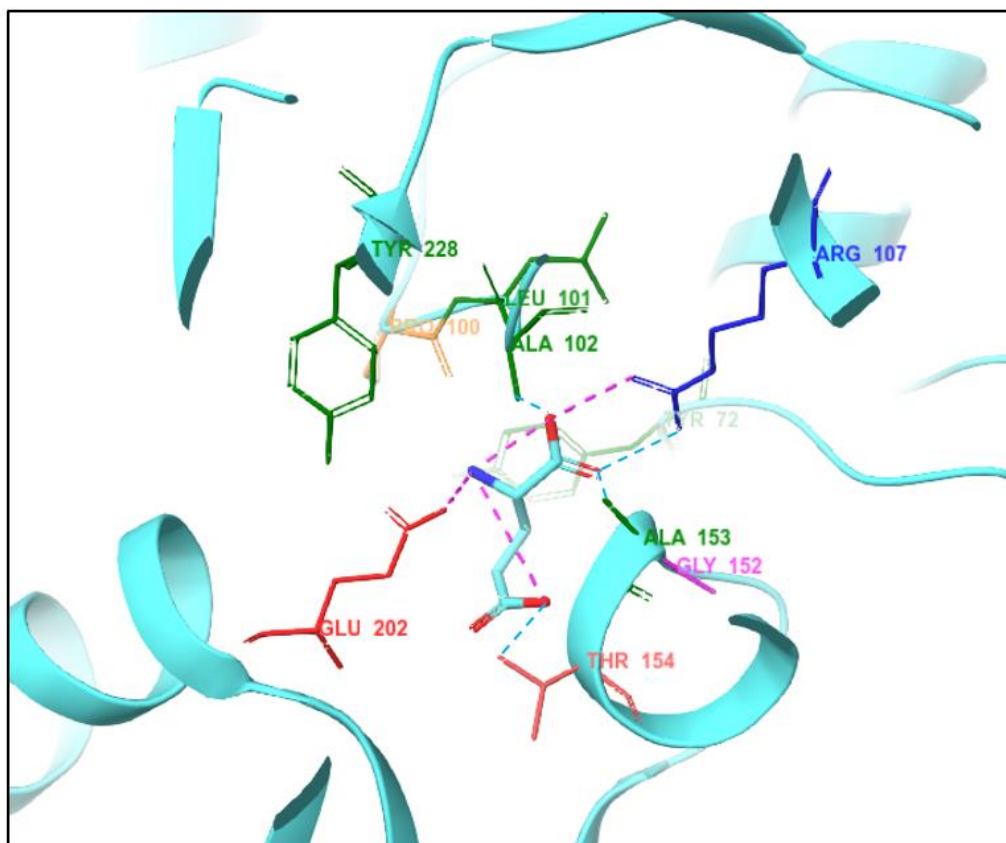


Figure 5.31. Glutamate binding pocket in LBD of rGluK2. Glutamate in stick representation in cyan, salt bridges interactions and Hydrogen bonds are shown in fuchsia and blue dash lines respectively. Diagram generated using Maestro Schrödinger version 11.1.

5.7.4 FRAGMENT SCREEN (SOAKING)

Ten compounds synthesised in-house (SDDC) were incubated with rGluK2 crystals at 1 and 5 mM. In one structure, the electron density observed in the dimer interface does not correspond to water molecules suggesting the presence of the compound UOS-15592 (5 mM) in a low occupancy (~20% map density) and an overlay of AMPA structure displays the same binding site in the dimer interface that corresponds to positive allosteric modulators (PAM) of AMPA (Fig. 5.32). rGluK2 crystals were then soaked with 10 mM compound, however, the compound binding in the structure was not observed. No other compounds displayed binding in the LBD of rGluK2 crystal. At high concentration of compounds, the DMSO caused difficulties in handling and dissolving the crystals which resulted in diffractions from 2.5 Å to 3.0 Å resolution.

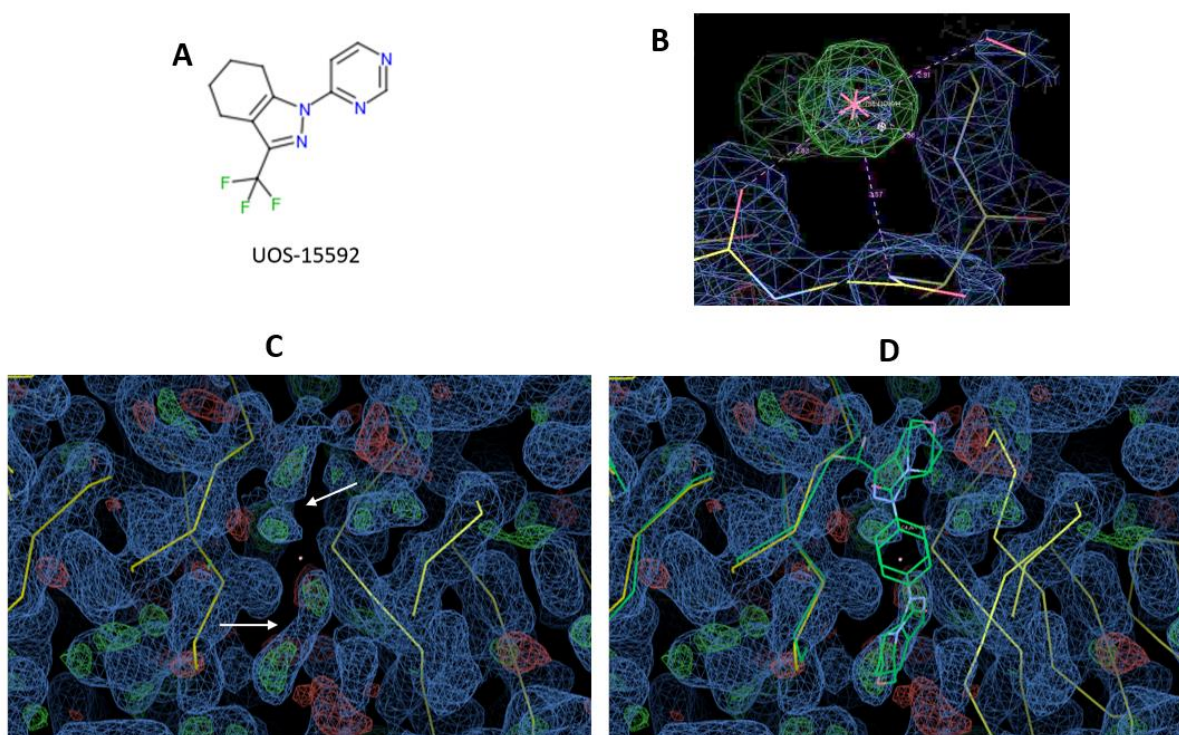


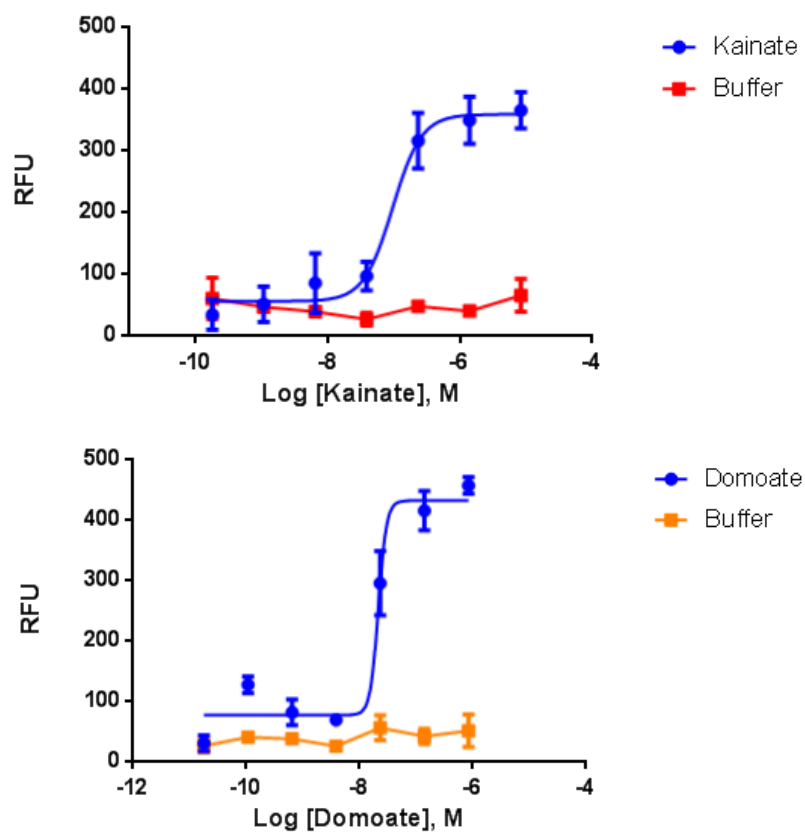
Figure 5.32. Compound UOS-15592 at 5 mM appeared to bind in the dimer interface of rGluK2 structure. **A.** Compound UOS-15592. **B.** Example of the electron density corresponding to a molecule of H₂O. **C.** Gluk2 in yellow displaying the dimer interface with electron density map, white arrows show the low-density corresponding to UOS-15592. **D.** Same dimer interface overlay with AMPA structure (green) with ligand sitting in the PAM site. Figures obtained from Crystallography Object-Oriented Toolkit (COOT) software.

5.7.5 KAINATE CALCIUM ASSAY

The main purpose of performing the calcium assay in human GluK2 cells was to confirm compound hits from soak experiments, however no compounds were found to bind in the LBD of the protein. Dr. Ian Barret previously optimised this calcium assay using the Fluo-4 NW commercial kit for human GluK1 and GluK2 receptors. The parameters of the tested and optimised conditions of the assay are listed in Table 5.6, section 5.4.6. In addition, the purpose of these results was to confirm the activity of the calcium assay in determining IC_{50} values and dose-response curve of agonists and antagonist in cells stably expressing human GluK2 receptors.

The standard agonists kainate and domoate were tested using the calcium assay Fluo-4 NW. The kainate dose response curve gave an EC_{50} of 0.095 μ M, 6-fold less than literature value of 0.6 μ M (obtained from supplier, Hellobio). Domoate dose response curve gave an EC_{50} of 0.021 μ M, 19 fold less than literature value of 0.4 μ M (Christensen et al., 2004; Fig. 5.33). This cell line displayed higher fluorescence signal compared to GluK1 cells in which the maximal signal response was \sim 200 RFU, it is possible that the induction with tetracycline considerably increased the levels of expression of receptors in the membrane. The level of background fluorescence (control buffer) was also increased for agonists kainate and domoate (\sim 40 RFU) but remained low in the antagonist experiments (\sim 9 RFU) compared to kainate of \sim 10 RFU. The signal-to-background ratio (S/B) for kainate and domoate resulted in 8.0 and 10.1 respectively, calculation based on the mean of the maximal response divided by the mean of the background.

CNQX did not display any antagonist activity in this assay, CNQX and CNQX disodium salt hydrate (improved solubility in water) were tested and both failed to display any activity. Compound UOS-30693 is used in literature as a selective antagonist for HEK-293 expressing GluK1 cells (Valgeirsson et al. 2004) and it was synthesised by the SDDC as a selective antagonist for kainate receptors (Fig. 5.34). Compound UOS-30693 displayed an antagonist activity up to 33.33 μ M, at higher concentrations of compound it precipitated out causing high levels of calcium in the cell. This suggests a disruption of the membrane cell, causing cell death and releasing intracellular calcium, as shown in Fig. 5.35. Kainate competitive binding added to UOS-30693 gave an IC_{50} of 11.39 μ M (Fig. 5.35). This compound has an IC_{50} in the literature of 1.5 and 2.0 μ M for cells expressing GluK1 receptors, for cells expressing GluK2 receptors IC_{50} value has not been reported in the literature due to poor solubility to enable the accurate determination of the value (Valgeirsson et al. 2004). The S/B ratio for antagonist UOS-30693 in the assay was 38.31, this value was calculated using the maximal response obtained after the addition of kainate.



Agonist	EC ₅₀
Kainate	0.095 μ M
Domoate	0.021 μ M

Figure 5.33. GluK2 kainate/domoate agonist concentration response curves. HEK-293 cells stably expressing human GluK2 receptor. Cells were incubated with 8.3 μ M kainate and 0.83 μ M domoate. RFU, relative fluorescence units in y-axis. Error bars (SD) are indicated representing n=3 individual experiments.

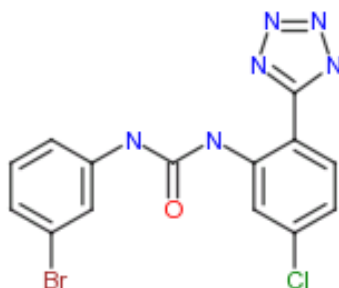


Figure 5.34. In-house compound UOS-30693. Compound used as an antagonist for calcium assays for GluK2 cells.

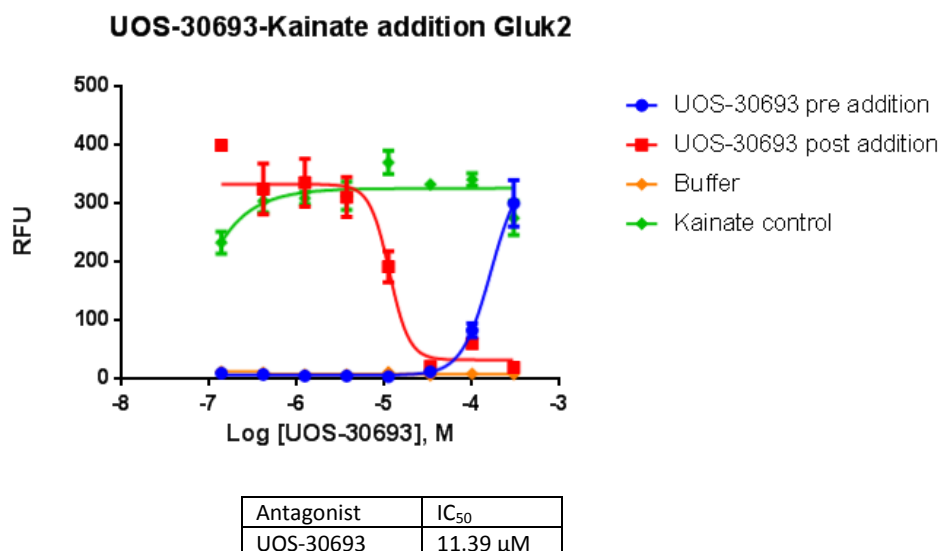


Figure 5.35. GluK2 antagonist concentration response curve. HEK-293 cells expressing GluK2 protein were incubated with 33 μ M UOS-30693 (first addition step) then kainate added at 50 μ M (second addition step), labelled as post addition. Error bars (SD) are indicated representing n=3 individual experiments.

5.8 DISCUSSION

The main objective of these experiments was the large-scale expression and purification of the rat GluK2 LBD protein to then perform crystallography experiments. Sequence alignment of the LBD between rGluK1 and rGluK2 demonstrated high homology identity (86.82%, Identity Matrix created by Clustal2.1) and for that reason, the expression and purification experiments were similar between both proteins. The expression construct was kindly provided by Dr. Antony W. Oliver (GDSC, University of Sussex). The construct contains a 6xHis-SUMO tag to improve solubility and purification of the protein. The small ubiquitin related modifier (SUMO) tag promotes the correct folding and solubility of the protein by having a similar effect as mammalian chaperone proteins; in addition, SUMO tags have been shown to protect target proteins from degradation by promoting the translocation to the nucleus (Peroutka et al. 2011; Costa et al. 2014). Furthermore, the polyhistidine (6xHis) tag was used for improving the purification since it binds to immobilized metal ion matrices in affinity chromatography (Bornhorst & Falke 2000; Costa et al. 2014).

The ligand binding domain of the rat rGluK2 receptors was isolated using a Gly-Thr dipeptide to join S1 and S2 domains, the dipeptide was short but sufficient to covalently bind both domains without changing the rest of the conformation and functionality of the LBD (Reddy et al., 2013). Expression and purification of the LBD of the protein was successful in a large-scale format. Several batches of protein production and purification were performed, an average yield of 4.9 mg of protein was obtained from four litres of starting cell culture. The yield of purified protein from four litres of cells resulted in sufficient protein for the preliminary crystallography and optimisation experiments with some protein left (~10 mg purified protein) stored for long-term at -80°C.

The primary crystallography screen using commercial matrix screen kits resulted in a positive hit that was further optimised and resulted in single crystals that were suitable for X-ray crystallography. The use of 5% and 10% seed stocks in microseeding experiments was necessary for obtaining larger crystals. The quality of rGluK2 protein crystals was reduced after periods of incubation at 14°C longer than one month. Crystals stored at 4°C maintained the quality properties for longer (approximately 3 months). Soaking experiments with ten compounds synthesised in-house resulted in compound UOS-15592 binding with 20% occupancy at 5 mM, higher concentration of compound (10 mM) was tested and no binding to the structure was observed possibly due to the effect of higher DMSO in the crystal. This compound has the potential to be used to generate a medicinal chemistry plan for analogues and test their activity

as potential for positive allosteric modulator drugs. Crystallography experiments were reproducible and optimised for potential future work with a large compound screening format (for example XChem screening) for drug screening studies.

X-ray crystallography data was solved and resulted in a LBD dimer structure. The rGluK2 LBD crystal diffracted at 1.95 Å similar to the literature 1TT1 (1.93 Å). Crystals obtained had a monoclinic space group and space group P 1 21 1, the same as the previously published structure of the LBD of rat GluK2 (Mayer 2005). The X-ray structure showed that the interactions of the glutamate binding pocket of the LBD have similar residues interactions to those previously described in the literature (Mayer 2005). Residues arginine and glutamic acid showed to be conserved in rGluA2, rGluK1 and rGluK2, forming interactions with the α -carboxyl group and the α -amino group of agonists glutamate and kainate respectively. The dimer structural conformation was the same as previously published structure 1TT1 (Mayer 2005) although the dimer conformation of rGluK2 LBD displayed differences with other LBD receptors suggesting a narrowed dimer interface for rGluK2 LBD protein compared with rGluK1 and rGluA2.

The Fluo-4 NW calcium assay was optimised by Dr. Iain Barret and following the optimised conditions of the assay the standard agonists and antagonist were tested to obtain a dose response curve and EC₅₀ value. The calcium assay experiments demonstrated the suitability of the assay for further screening experiments. The agonists kainate and domoate dose response curves displayed activity similar to literature with EC₅₀ values of 0.095 μ M and 0.021 μ M respectively (Christensen et al. 2004 and Hellobio supplier).

The antagonist CNQX failed to display antagonist activity, the reason for this might be due to cell behaviour, dye solution, buffer interaction, compound solubility, etc. In an electrophysiology, experiment published in the literature 100 μ M of CNQX treatment with rGluK2 receptors did not show any change in the effect response of the receptor with the antagonist (Fisher & Housley 2013). Compound UOS-30693 (named as 5d compound in the literature) was synthesised in-house and selected from previous literature experiments as a potential antagonist for kainate receptors (Valgeirsson et al. 2004). This compound has been shown to be a potent non-competitive antagonist for GluK1 cells, suggesting it could have similar antagonist activity for GluK2 cells. The compound UOS-30693 in GluK2 cells gave an antagonist response IC₅₀ of 11.39 μ M tested with a maximal concentration of 33 μ M because higher concentrations caused precipitation and disruption in cells, affecting the intracellular calcium level measurements. The signal-to-background ratio (S/B) for kainate, domoate and UOS-30693 was 8.0, 10.1 and 38.1 respectively. The S/B ratio was higher with antagonist UOS-30693 because of a larger difference

between the maximal response and the background signal values. High levels of response (RFU) were observed with cells expressing GluK2 receptors, this might be the cause of the induction of receptors controlled by tetracycline antibiotic. Novel compounds with predicted antagonist activity for kainate receptors could be tested with this assay format. The LBD structure of the GluK2 receptor resulted in detailed structural information that can be used for the design of novel kainate receptor subtype-selective drugs for the treatment of epilepsy.

CHAPTER 6

CONCLUSIONS AND FUTURE WORK

6.1 NRF2 PROJECT

The aim of this project was to utilise structure-based drug design to identify novel modulators of the Nrf2-Keap1 transcription pathway. The X-ray crystallographic information regarding the Nrf2-Keap1 interface interaction was used as the basis for a virtual screen. A commercial Nrf2 pathway kit (DiscoverX) was then used to evaluate 122 compounds that were purchased from the output of this virtual screen which was useful in identifying potential modulators of the transcription pathway in a cell-based assay format. Two novel compounds were identified as potential modulators of the protein-protein interaction between Nrf2 and its repressor Keap1. The generation of reactive oxygen species (ROS) were monitored and results showed that only two compounds did not increase ROS levels, however Western blot analyses of Nrf2 were unable to demonstrate a translocation of the Nrf2 protein from the cytoplasm into the nucleus since no Nrf2 protein could be detected in the cytoplasm. As a result, it was not possible to confirm whether or not the two compounds of interest were having an effect on Nrf2 translocation and downstream genes expression. Accordingly, given the relatively weak effects of the two compounds and the lack of a reliable assay with which to detect downstream effects, the decision was made to terminate this project.

The DiscoverX assay is a cell-based assay and requires compounds to have a good cell membrane permeability in order to demonstrate effects. An alternative approach would be to take a step backwards to use a biochemical assay to screen for molecules that disrupt the protein-protein interaction and thereafter build in the physicochemical properties required for cell permeability. In this regard, fluorescence polarization biochemical assays have been described using the Keap1 protein and an Nrf2-ETGE peptide as a fluorescein labelled probe (Hancock, Hélène C. Bertrand, et al. 2012; Jiang et al. 2014; Jnoff et al. 2014). Although the Western blot analyses were not successful, fluorescence microscopy could have been used in order to identify nuclear and cytosolic expression of Nrf2 in cells (Theodore et al. 2008; Baird et al. 2013; Malloy et al. 2013; Yu et al. 2014; Zhang et al. 2016). Alternatively, the quantification of the mRNA of Nrf2 downstream genes can be performed using real time PCR (RT-PCR), and these methods were used to identify the effect of compounds in the expression of antioxidant and detoxifying enzymes (Buetler et al. 1995; Kanno et al. 2012b; Mathew et al. 2014; Zhuang et al. 2014).

However, although these alternative methodologies were considered, the low potency of the two compounds of interest did not justify the considerable investment in time and resource required to establish these techniques. Nevertheless, despite the lack of success, the Nrf2 transcription pathway still remains an attractive, albeit challenging, potential therapeutic target for the treatment of neurodegenerative diseases.

6.2 AMPA PROJECT

The aim of this project was to use a structure-based, X-ray crystallography screening approach to identify fragments that bind to, and allosterically modulate, the ligand-binding domain (LBD) of the GluA2 AMPA receptor and which might have the potential to become novel drugs with which to treat neurological disorders. Methods described in the literature have focused on the rat protein due to the increased solubility and crystallography properties in comparison to the human protein. A construct of the rat recombinant protein GluA2 LBD was designed according to previously published methods (Armstrong & Gouaux 2000; Ward et al. 2011) and was expressed and purified to produce a high purity protein suitable for X-ray crystallographic studies. The crystal structure of the rat GluA2 LBD was determined to a resolution of 1.84 Å and the homodimeric structure and agonist (glutamate) binding was consistent with previous data.

In order to find novel compounds that bind to the GluA2 LBD, an XChem fragment screen was performed at the Diamond Light Source (Didcot, UK). The primary methodological challenge was to optimise the methods for crystal production such that they were suitable for large scale fragment screening. The optimised crystallography conditions were in a sitting drop format plate using 5 mg/ml protein with 5 mM zinc acetate and sodium cacodylate and a final drop ratio of 1:1 with reservoir solution (0.09 M halogens, 0.1 M buffer system 1 pH 6.5 and 50% v/v precipitant mix 1, Morpheus® screen Appendix II).

The methods involved in the fragment screen were the crystal targeting, soaking, harvesting, data collection and data analysis of which the crystal harvesting was the most challenging and time consuming due to the need for each crystal to be harvested manually. A total of 700 fragment compounds were soaked with GluA2 LBD crystals (from 1.75 Å to 2.5 Å) in complex with glutamate and resulted in eight fragments located in the ligand binding domain of the protein. Two binding sites were identified, a site near the Gly-Thr dipeptide linker and a site in the dimer interface between domains S1 and S2 of the LBD. The latter had been previously identified as a site for positive allosteric modulators (PAMs) of AMPA receptor, PAMs binding in this interface have been suggested to enhance cognitive performance in animal models. The

binding site near the Gly-Thr linker has not been identified in the literature or any publication. From the eight compounds, five were located in the dimer interface and three near the Gly-Thr site.

In future, functional studies (electrophysiology) will be used to characterise the functional effects of these compounds although it would not be surprising if no effects were observed. Accordingly, more detailed biophysical analyses need to be performed in order to characterise the affinity and other features of the ligand-protein interaction. In addition, close structural analogues of these compounds will need to be ordered or synthesised in the hope of identifying compounds with higher affinity than these presumably weak hits that have been identified in the XChem fragment screen.

6.3 KAINATE PROJECT

The purpose of the kainate receptor project was to provide the structural information that would form the basis of a structure-based drug discovery approach to identifying novel compounds that bound to the LBD of the rat GluK1 and GluK2 subtypes of ionotropic glutamate receptor, in a manner analogous to that used for the GluA2 subtype AMPA receptors. More specifically, the aim was to identify allosteric modulators that might be the starting point in the path to developing novel anti-epileptic drugs that might be more efficacious and/or better tolerated than existing drugs.

The construct of the rat recombinant GluK1 and GluK2 LBD proteins was similar to those used previously (Naur et al. 2005). The crystals of both proteins were solved at 1.64 Å for GluK1 and 1.95 Å for GluK2 and binding interactions with the agonist kainate were comparable to those published previously. In-house compounds based on literature were soaked with both protein crystals and one compound UOS-15592 displayed ~20% occupancy suggesting some evidence of compound binding in the dimer interface of GluK2, more interestingly preliminary electrophysiological data suggests the same activity for GluK1 protein. This result supports the evidence of possible binding sites for positive allosteric modulators (PAMs) of kainate receptors, similar to GluA2 AMPA PAMs.

Further work is required to establish the functional consequences of the binding of this compound in a cellular fluorescence or electrophysiological assay. Nevertheless, these results form the basis of an iterative medicinal chemistry programme based upon increasing the potency of compound UOS-15592. In parallel, the LBDs of GluK1 and GluK2 could be used for

large-scale fragment screening using the XChem screening platform, with a particular focus on GluK1. Fragment hits would then be further analysed in either a biophysical assay or a functional assay, such as the established kainate calcium (Fluo-4 NW) or electrophysiology assays.

Discussions are also underway with the Membrane Protein Laboratory (MPL, Diamond Light Source) in order to establish methodologies for the production and X-ray crystallographic examination of full-length human GluK1. The structural characterisation of the GluK1 and GluK2 LBDs and potentially the full length GluK1 are important components of a structural approach to the development of novel allosteric modulators for the treatment of epilepsy that can reduce undesirable side effects and help in the treatment of refractory (intractable) epilepsy patients.

7.0 BIBLIOGRAPHY

- Abrahám, G., Sólyom, S., Csuzdi, E., Berzsényi, P., Ling, I., Tarnawa, I., Horváth, G. (2000). New non-competitive AMPA antagonists. *Bioorganic & Medicinal Chemistry*, 8(8), 2127–43.
- Abramov, A. Y., Scorziello, A., & Duchen, M. R. (2007). Three distinct mechanisms generate oxygen free radicals in neurons and contribute to cell death during anoxia and reoxygenation. *The Journal of Neuroscience : The Official Journal of the Society for Neuroscience*, 27(5), 1129–38.
- Ahmed, A. H., & Oswald, R. E. (2010). Piracetam Defines a New Binding Site for Allosteric Modulators of α -Amino-3-hydroxy-5-methyl-4-isoxazole-propionic Acid (AMPA) Receptors. *Journal of Medicinal Chemistry*, 53(5), 2197–2203.
- Ahmed, A. H., Wang, S., Chuang, H.H., & Oswald, R. E. (2011). Mechanism of AMPA receptor activation by partial agonists: disulfide trapping of closed lobe conformations. *The Journal of Biological Chemistry*, 286(40), 35257–66.
- Aldred, S., Moore, K. M., Fitzgerald, M., & Waring, R. H. (2003). Plasma amino acid levels in children with autism and their families. *Journal of Autism and Developmental Disorders*, 33(1), 93–7.
- Aleksunes, L. M., & Manautou, J. E. (2007). Emerging role of Nrf2 in protecting against hepatic and gastrointestinal disease. *Toxicologic Pathology*, 35(4), 459–473.
- Alexander, S. P., Kelly, E., Marrion, N., Peters, J. A., Benson, H. E., Faccenda, E., Davies, J. A. (2015). The Concise Guide to PHARMACOLOGY 2015/16: Overview. *British Journal of Pharmacology*, 172(24), 5729–5743.
- Alumkal, J. J., Slotke, R., Schwartzman, J., Cherala, G., Munar, M., Graff, J. N., Mori, M. (2015). A phase II study of sulforaphane-rich broccoli sprout extracts in men with recurrent prostate cancer. *Investigational New Drugs*, 33(2), 480–489.
- Anderson, C. M., & Swanson, R. A. (2000). Astrocyte glutamate transport: review of properties, regulation, and physiological functions. *Glia*, 32(1), 1–14.
- Andreou, A. P., & Goadsby, P. J. (2011). Topiramate in the treatment of migraine: A kainate (glutamate) receptor antagonist within the trigeminothalamic pathway. *Cephalalgia*, 31(13), 1343–1358.
- Anggono, V., Tsai, L. H., Götz, J., tz, J., & rgen. (2016). Glutamate Receptors in Alzheimer's Disease: Mechanisms and Therapies. *Neural Plasticity*, 2016, 1–2.
- Antlitz, A. M., & Valle, N. G. (1967). The antihypertensive effect of cyclothiazide, a double blind study. *Current Therapeutic Research, Clinical and Experimental*, 9(6), 288–92.
- Armstrong, N., Sun, Y., Chen, G. Q., & Gouaux, E. (1998). Structure of a glutamate-receptor ligand-binding core in complex with kainate. *Nature*, 395(6705), 913–917.
- Armstrong, N., & Gouaux, E. (2000). Mechanisms for activation and antagonism of an AMPA-sensitive glutamate receptor: crystal structures of the GluR2 ligand binding core. *Neuron*, 28(1), 165–181.

- Aschner, M. (2000). Neuron-astrocyte interactions: implications for cellular energetics and antioxidant levels. *Neurotoxicology*, 21(6), 1101–7.
- Asherie, N. (2004). Protein crystallisation and phase diagrams. *Methods*, 34, 266–272.
- Atluri, V. S. R., Hidalgo, M., Samikkannu, T., Kurapati, K. R. V., & Nair, M. (2015). Synaptic Plasticity and Neurological Disorders in Neurotropic Viral Infections. *Neural Plasticity*, 2015, 1–14.
- Baird, L., Llères, D., Swift, S., & Dinkova-Kostova, A. T. (2013). Regulatory flexibility in the Nrf2-mediated stress response is conferred by conformational cycling of the Keap1-Nrf2 protein complex. *Proceedings of the National Academy of Sciences of the United States of America*, 110(38), 15259–64.
- Baird, L., Swift, S., Llères, D., & Dinkova-Kostova, A. T. (2014). Monitoring Keap1-Nrf2 interactions in single live cells. *Biotechnology Advances*, 32(6), 1133–44.
- Balannik, V., Menniti, F. S., Paternain, A. V., Lerma, J., & Stern-Bach, Y. (2005). Molecular mechanism of AMPA receptor noncompetitive antagonism. *Neuron*, 48(2), 279–288.
- Barber, S. C., Mead, R. J., & Shaw, P. J. (2006). Oxidative stress in ALS: a mechanism of neurodegeneration and a therapeutic target. *Biochimica et Biophysica Acta*, 1762, 11–12.
- Barbon, A., Fumagalli, F., La Via, L., Caracciolo, L., Racagni, G., Andrea Riva, M., & Barlati, S. (2007). Chronic phencyclidine administration reduces the expression and editing of specific glutamate receptors in rat prefrontal cortex. *Experimental Neurology*, 208(1), 54–62.
- Bataille, A. M., & Manautou, J. E. (2012). Nrf2: a potential target for new therapeutics in liver disease. *Clinical Pharmacology and Therapeutics*, 92(3), 340–8.
- Beamer, L. J., Li, X., Bottoms, C. A., & Hannink, M. (2005). Conserved solvent and side-chain interactions in the 1.35 Å structure of the Kelch domain of Keap1. *Acta Crystallographica. Section D, Biological Crystallography*, 61(Pt 10), 1335–42.
- Begni, S., Popoli, M., Moraschi, S., Bignotti, S., Tura, G. B., & Gennarelli, M. (2002). Association between the ionotropic glutamate receptor kainate 3 (GRIK3) ser310ala polymorphism and schizophrenia. *Molecular Psychiatry*, 7(4), 416–418.
- Beneyto, M., Kristiansen, L. V., Oni-Orisan, A., Mccullumsmith, R. E., & Meador-Woodruff, J. H. (2007). Abnormal Glutamate Receptor Expression in the Medial Temporal Lobe in Schizophrenia and Mood Disorders. *Neuropsychopharmacology*, 32, 1888–1902.
- Berg, J. M. (Jeremy M., Tymoczko, J. L., Stryer, L., & Stryer, L. (2002). Biochemistry. 5th edition. W.H. Freeman.
- Besag, F. M. C., & Patsalos, P. N. (2016). Clinical efficacy of perampanel for partial-onset and primary generalized tonic-clonic seizures. *Neuropsychiatric Disease and Treatment*, 12, 1215–1220.
- Bialer, M., Johannessen, S. I., Kupferberg, H. J., Levy, R. H., Perucca, E., & Tomson, T. (2007). Progress report on new antiepileptic drugs: A summary of the Eighth Eilat Conference (EILAT VIII). *Epilepsy Research*, 73(1), 1–52.
- Blank, V. (2008). Small Maf Proteins in Mammalian Gene Control: Mere Dimerization Partners or Dynamic Transcriptional Regulators? *Journal of Molecular Biology*, 376(4), 913–925.

- Blanke, M. L., & VanDongen, A. M. J. (2009). Activation Mechanisms of the NMDA Receptor. *Biology of the NMDA Receptor*. CRC Press/Taylor & Francis.
- Bleakman, D., Clarke, V. R. J., Ballyk, B. A., Hoo, K. H., Mandelzys, A., Pellizzari, A., Lodge, D. (1997). A hippocampal GluR5 kainate receptor regulating inhibitory synaptic transmission. *Nature*, 389(6651), 599–603.
- Bleakman, D., Gates, M. R., Ogden, A. M., & Mackowiak, M. (2002). Kainate receptor agonists, antagonists and allosteric modulators. *Current Pharmaceutical Design*, 8(10), 873–85.
- Block, H., Maertens, B., Spriestersbach, A., Brinker, N., Kubicek, J., Fabis, R., Schäfer, F. (2009). Chapter 27 Immobilized-Metal Affinity Chromatography (IMAC). A Review. *Methods in Enzymology*, 463(C), 439–473.
- Bonnet-Brilhault, F., Alirol, S., Blanc, R., Bazaud, S., Marouillat, S., Thepault, R.A., Laumonnier, F. (2016). GABA/Glutamate synaptic pathways targeted by integrative genomic and electrophysiological explorations distinguish autism from intellectual disability. *Molecular Psychiatry*, 21(3), 411–418.
- Boots, A. W., Wilms, L. C., Swennen, E. L. R., Kleinjans, J. C. S., Bast, A., & Haenen, G. R. M. M. (2008). In vitro and ex vivo anti-inflammatory activity of quercetin in healthy volunteers. *Nutrition*, 24(7–8), 703–710.
- Borger, D. K., McMahon, B., Roshan Lal, T., Serra-Vinardell, J., Aflaki, E., & Sidransky, E. (2017). Induced pluripotent stem cell models of lysosomal storage disorders. *Disease Models & Mechanisms*, 10(6), 691– 704.
- Bornhorst, J. A., & Falke, J. J. (2000). Purification of proteins using polyhistidine affinity tags. *Methods in Enzymology*, 326, 245–54.
- Bortolotto, Z. A., J Clarke, V. R., Delany, C. M., Parry, M. C., Smolders, I., Vignes, M., Collingridge, G. L. (1999). Kainate receptors are involved in synaptic plasticity. *Nature*, 402(18), 297 – 301.
- Boundless. "Cerebral Cortex." Boundless Psychology Boundless 2016, Accessed on 11/07/2017 [ONLINE]. Available at: <https://www.boundless.com/psychology/textbooks/boundless-psychology-textbook/biological-foundations-of-psychology-3/structure-and-function-of-the-brain-35/cerebral-cortex-152-12687/>
- Boutten, A., Goven, D., Artaud-Macari, E., Boczkowski, J., & Bonay, M. (2011). NRF2 targeting: a promising therapeutic strategy in chronic obstructive pulmonary disease. *Trends in Molecular Medicine*, 17(7), 363–71.
- Bovenschen, H. J., Langewouters, A. M. G., & van de Kerkhof, P. C. M. (2010). Dimethylfumarate for Psoriasis. *American Journal of Clinical Dermatology*, 11(5), 343–350.
- Boyle, J. J., Johns, M., Lo, J., Chiodini, A., Ambrose, N., Evans, P. C., Haskard, D. O. (2011). Heme induces heme oxygenase 1 via Nrf2: role in the homeostatic macrophage response to intraplaque hemorrhage. *Arteriosclerosis, Thrombosis, and Vascular Biology*, 31(11), 2685–91.
- Braga, M. F. M., Aroniadou-Anderjaska, V., & Li, H. (2004). The physiological role of kainate receptors in the amygdala. *Molecular Neurobiology*, 30(2), 127–141.

- Braga, M. F. M., Aroniadou-Anderjaska, V., Li, H., & Rogawski, M. Av. (2009). Topiramate reduces excitability in the basolateral amygdala by selectively inhibiting GluK1 (GluR5) kainate receptors on interneurons and positively modulating GABAA receptors on principal neurons. *The Journal of Pharmacology and Experimental Therapeutics*, 330(2), 558–566.
- Bräuner-Osborne, H., Wellendorph, P., & Jensen, A. A. (2007). Structure, pharmacology and therapeutic prospects of family C G-protein coupled receptors. *Current Drug Targets*, 8(1), 169–84.
- Bridges, R. J., Natale, N. R., & Patel, S. A. (2012). System x c - cystine/glutamate antiporter: An update on molecular pharmacology and roles within the CNS. *British Journal of Pharmacology*, 165(1), 20–34.
- Bryan, H. K., Olayanju, A., Goldring, C. E., & Park, B. K. (2013). The Nrf2 cell defence pathway: Keap1-dependent and -independent mechanisms of regulation. *Biochemical Pharmacology*, 85(6), 705–17.
- Buetler, T. M., Gallagher, E. P., Wang, C., Stahl, D. L., Hayes, J. D., & Eaton, D. L. (1995). Induction of phase I and phase II drug-metabolizing enzyme mRNA, protein, and activity by BHA, ethoxyquin, and oltipraz. *Toxicology and Applied Pharmacology*, 135(1), 45–57.
- Burton, N. C., Kensler, T. W., & Guilarte, T. R. (2006). In vivo modulation of the Parkinsonian phenotype by Nrf2. *Neurotoxicology*, 27(6), 1094–100.
- Büttner, F. M., Renner-Schneck, Michaela, & Stehle, T. (2015). X-ray crystallography and its impact on understanding bacterial cell wall remodeling processes. *International Journal of Medical Microbiology*, 305(2), 209–216.
- Cai, J., Ding, L., Zhang, J.-S., Xue, J., & Wang, L.-Z. (2016). Elevated plasma levels of glutamate in children with autism spectrum disorders. *Cellular Molecular and Developmental Neuroscience*, 27(4), 272–276.
- Calkins, M. J., Johnson, D. A., Townsend, J. A., Vargas, M. R., Dowell, J. A., Williamson, T. P., Johnson, J. A. (2009). The Nrf2 / ARE Pathway as a Potential Therapeutic Target in Neurodegenerative Disease. *Antioxidants & Redox Signaling*, 11(3), 497 – 508.
- Calkins, M. J., Vargas, M. R., Johnson, D. a, & Johnson, J. A. (2010). Astrocyte-specific overexpression of Nrf2 protects striatal neurons from mitochondrial complex II inhibition. *Toxicological Sciences : An Official Journal of the Society of Toxicology*, 115(2), 557–68.
- Carbone, A. L., & Plested, A. J. R. (2016). Superactivation of AMPA receptors by auxiliary proteins. *Nature Communications*, 7, 1–12.
- Carlson, M. D., Penney, J. B., & Young, A. B. (1993). NMDA, AMPA, and benzodiazepine binding site changes in Alzheimer's disease visual cortex. *Neurobiology of Aging*, 14(4), 343–352.
- Carlson, N. G., Howard, J., Gahring, L. C., & Rogers, S. W. (2000). RNA editing (Q/R site) and flop/flip splicing of AMPA receptor transcripts in young and old brains. *Neurobiology of Aging*, 21(4), 599–606.
- Cataldo, A. M., Peterhoff, C. M., Troncoso, J. C., Gomez-Isla, T., Hyman, B. T., & Nixon, R. A. (2000). Endocytic pathway abnormalities precede amyloid beta deposition in sporadic Alzheimer's disease and Down syndrome: differential effects of APOE genotype and presenilin mutations. *The American Journal of Pathology*, 157(1), 277–86.

- Catarzi, D., Colotta, V., & Varano, F. (2007). Competitive AMPA receptor antagonists. *Medicinal Research Reviews*, 27(2), 239–278.
- Chalmers, D. T., Dewar, D., Graham, D. I., Brooks, D. N., & McCulloch, J. (1990). Differential alterations of cortical glutamatergic binding sites in senile dementia of the Alzheimer type. *Proceedings of the National Academy of Sciences of the United States of America*, 87(4), 1352–6.
- Chan, K., & Kan, Y. W. (1999). Nrf2 is essential for protection against acute pulmonary injury in mice. *Proceedings of the National Academy of Sciences of the United States of America*, 96(22), 12731–6.
- Chanas, S. A., Jiang, Q., McMahon, M., McWalter, G. K., McLellan, L. I., Elcombe, C. R., Hayes, J. D. (2002). Loss of the Nrf2 transcription factor causes a marked reduction in constitutive and inducible expression of the glutathione S-transferase Gsta1, Gsta2, Gstm1, Gstm2, Gstm3 and Gstm4 genes in the livers of male and female mice. *The Biochemical Journal*, 365(Pt 2), 405–16.
- Chapman, A. G., Smith, S. E., & Meldrum, B. S. (1991). The anticonvulsant effect of the non-NMDA antagonists, NBQX and GYKI 52466, in mice. *Epilepsy Research*, 9(2), 92–6.
- Chater, T. E., & Goda, Y. (2014). The role of AMPA receptors in postsynaptic mechanisms of synaptic plasticity. *Frontiers in Cellular Neuroscience*, 8, 401.
- Chaudhry, C., Weston, M. C., Schuck, P., Rosenmund, C., & Mayer, M. L. (2009). Stability of ligand-binding domain dimer assembly controls kainate receptor desensitization. *Embo J*, 2009(10), 1518–1530.
- Chen, G. Q., & Gouaux, E. (1997). Overexpression of a glutamate receptor (GluR2) ligand binding domain in Escherichia coli: application of a novel protein folding screen. *Proceedings of the National Academy of Sciences of the United States of America*, 94(25), 13431–6.
- Chen, G. Q., Sun, Y., Jin, R., & Gouaux, E. (1998). Probing the ligand binding domain of the GluR2 receptor by proteolysis and deletion mutagenesis defines domain boundaries and yields a crystallizable construct. *Protein Science : A Publication of the Protein Society*, 7(12), 2623–30.
- Chen, L., Chetkovich, D. M., Petralia, R. S., Sweeney, N. T., Kawasaki, Y., Wenthold, R. J., Nicoll, R. A. (2000). Stargazin regulates synaptic targeting of AMPA receptors by two distinct mechanisms. *Nature*, 408(6815), 936–943.
- Chen, P.-C., Vargas, M. R., Pani, A. K., Smeyne, R. J., Johnson, D. A., Kan, Y. W., & Johnson, J. A. (2009). Nrf2-mediated neuroprotection in the MPTP mouse model of Parkinson's disease: Critical role for the astrocyte. *Proceedings of the National Academy of Sciences of the United States of America*, 106(8), 2933–8.
- Chen, W., Li, Y. S., Gao, J., Lin, X. Y., & Li, X. H. (2016). AMPA receptor antagonist NBQX decreased seizures by normalization of perineuronal nets. *PLoS ONE*, 11(11), 1–16.
- Chin, M. P., Reisman, S. A., Bakris, G. L., O'Grady, M., Linde, P. G., McCullough, P. A., Meyer, C. J. (2014). Mechanisms contributing to adverse cardiovascular events in patients with type 2 diabetes mellitus and stage 4 chronic kidney disease treated with bardoxolone methyl. *American Journal of Nephrology*, 39(6), 499–508.

- Cho, H.-Y. Y., Jedlicka, A. E., Reddy, S. P. M., Kensler, T. W., Yamamoto, M., Zhang, L.-Y., & Klee. (2002). Role of Nrf2 in protection against hyperoxic lung injury in mice. *Am. J. Respir. Cell Mol. Biol.*, 26, 175–182.
- Cho, H.-Y. Y., Reddy, S. P. M., Yamamoto, M., & Kleeberger, S. R. (2004). The transcription factor NRF2 protects against pulmonary fibrosis. *Faseb J*, 18(11), 1258–1260.
- Christensen, J. K., Varming, T., Ahring, P. K., Jorgensen, T. D., & Nielsen, E. O. (2004). In Vitro Characterization of 5-Carboxyl-2,4-di-benzamidobenzoic Acid (NS3763), a Noncompetitive Antagonist of GLUK5 Receptors. *Journal of Pharmacology and Experimental Therapeutics*, 309(3), 1003–1010.
- Chun, L., Zhang, W., & Liu, J. (2012). Structure and ligand recognition of class C GPCRs. *Acta Pharmacologica Sinica*, 33(3), 312–23.
- Conti, F. (1997). Localization of NMDA receptors in the cerebral cortex: A schematic overview. *Brazilian Journal of Medical and Biological Research*, 30(5), 555–560.
- Coombs, I. D., & Cull-Candy, S. G. (2009). Transmembrane AMPA receptor regulatory proteins and AMPA receptor function in the cerebellum. *Neuroscience*, 162(3), 656–65.
- Copple, I. M. (2012). *The Keap1-Nrf2 Cell Defense Pathway - A Promising Therapeutic Target? Advances in Pharmacology* (Vol. 63). Elsevier Inc.
- Costa, B. M., Feng, B., Tsintsadze, T. S., Morley, R. M., Irvine, M. W., Tsintsadze, V., Monaghan, D. T. (2009). N-Methyl-D-aspartate (NMDA) Receptor NR2 Subunit Selectivity of a Series of Novel Piperazine-2,3-dicarboxylate Derivatives: Preferential Blockade of Extrasynaptic NMDA Receptors in the Rat Hippocampal CA3-CA1 Synapse. *Journal of Pharmacology and Experimental Therapeutics*, 331(2), 618–626.
- Costa, S., Almeida, A., Castro, A., & Domingues, L. (2014). Fusion tags for protein solubility, purification and immunogenicity in *Escherichia coli*: the novel Fh8 system. *Frontiers in Microbiology*, 5(63), 1 – 20.
- Coyle, J. T. (1987). Kainic acid: insights into excitatory mechanisms causing selective neuronal degeneration. *Ciba Foundation Symposium*, 126, 186–203.
- Cull-Candy, S., Kelly, L., & Farrant, M. (2006). Regulation of Ca²⁺-permeable AMPA receptors: synaptic plasticity and beyond. *Current Opinion in Neurobiology*, 16(3), 288–297.
- Cullinan, S. B., Zhang, D., Hannink, M., Arvisais, E., Kaufman, R. J., & Diehl, J. A. (2003). Nrf2 Is a Direct PERK Substrate and Effector of PERK-Dependent Cell Survival. *Molecular and Cellular Biology*, 23(20), 7198–7209.
- Daigo, K. (1959). Studies on the Constituents of *Chondria armata*. I Detection of the Anthelmintical constituents. *YAKUGAKU ZASSHI*, 79(3), 350–353.
- Dargan, S. L., Clarke, V. R. J., Alushin, G. M., Sherwood, J. L., Nisticò, R., Bortolotto, Z. A., Collingridge, G. L. (2009). ACET is a highly potent and specific kainate receptor antagonist: Characterisation and effects on hippocampal mossy fibre function. *Neuropharmacology*, 56(1), 121–130.
- Darnell, J. C., & Klann, E. (2013). The translation of translational control by FMRP: therapeutic targets for FXS. *Nature Neuroscience*, 16(11), 1530–1536.

- Darstein, M., Petralia, R. S., Swanson, G. T., Wenthold, R. J., & Heinemann, S. F. (2003). Distribution of kainate receptor subunits at hippocampal mossy fiber synapses. *The Journal of Neuroscience : The Official Journal of the Society for Neuroscience*, 23(22), 8013–9.
- Davis, S., Butcher, S. P., & Morris, R. G. (1992). The NMDA receptor antagonist D-2-amino-5-phosphonopentanoate (D-AP5) impairs spatial learning and LTP in vivo at intracerebral concentrations comparable to those that block LTP in vitro. *The Journal of Neuroscience : The Official Journal of the Society for Neuroscience*, 12(1), 21–34.
- Davis, K. L. (2002). Neuropsychopharmacology : an official publication of the American College of Neuropsychopharmacology. [ONLINE] Available from https://books.google.co.uk/books?id=BKwkonZwZD0C&pg=PA72&dq=ampa+receptor+distribution&hl=en&sa=X&ved=0ahUKEwjWhvvi_fUAhWQh7QKHekZDplQ6AEIPTAF#v=onepage&q=ampa+receptor+distribution&f=false
- Dawson, V. L., & Dawson, T. M. (1996). Free radicals and neuronal cell death. *Cell Death and Differentiation*, 3(1), 71–8.
- de Zeeuw, D., Akizawa, T., Audhya, P., Bakris, G. L., Chin, M., Christ-Schmidt, H., Chertow, G. M. (2013). Bardoxolone methyl in type 2 diabetes and stage 4 chronic kidney disease. *The New England Journal of Medicine*, 369(26), 2492–503.
- Derkach, V. A., Oh, M. C., Guire, E. S., & Soderling, T. R. (2007). Regulatory mechanisms of AMPA receptors in synaptic plasticity. *Nature Reviews Neuroscience*, 8(2), 101–113.
- Dewar, D., Chalmers, D. T., Graham, D. I., & McCulloch, J. (1991). Glutamate metabotropic and AMPA binding sites are reduced in Alzheimer's disease: an autoradiographic study of the hippocampus. *Brain Research*, 553 (1991), 58–64.
- Dhir, A., & Chavda, V. (2016). Pre- and post-exposure talampanel (GYKI 53773) against kainic acid seizures in neonatal rats. *Pharmacological Reports*, 68(1), 190–195.
- Di, X., Bullock, R., Watson, J., Fatouros, P., Chenard, B., White, F., & Corwin, F. (1997). Effect of CP101, 606, a novel NR2B subunit antagonist of the N-methyl-D-aspartate receptor, on the volume of ischemic brain damage off cytotoxic brain edema after middle cerebral artery occlusion in the feline brain. *Stroke*, 28(11), 2244–51.
- Díaz-alonso, J., Sun, Y. J., Granger, A. J., Levy, J. M., Blankenship, S. M., & Nicoll, R. A. (2017). Subunit-specific role for the amino-terminal domain of AMPA receptors in synaptic targeting. *Proceedings of the National Academy of Sciences of the United States of America*, 114(27), 7136–7141.
- Dingledine, R., Borges, K., Bowie, D., & Traynelis, S. F. (1999). The glutamate receptor ion channels. *Pharmacological Reviews*, 51(1), 7-61.
- Dolman, N. P., More, J. C. A., Alt, A., Knauss, J. L., Pentikäinen, O. T., Glasser, C. R., Jane, D. E. (2007). Synthesis and Pharmacological Characterization of N 3 -Substituted Willardiine Derivatives: Role of the Substituent at the 5-Position of the Uracil Ring in the Development of Highly Potent and Selective GLU K5 Kainate Receptor Antagonists. *Journal of Medicinal Chemistry*, 50(7), 1558–1570.
- Donevan, S. D., & Rogawski, M. A. (1993). GYKI 52466, a 2,3-benzodiazepine, is a highly selective, noncompetitive antagonist of AMPA/kainate receptor responses. *Neuron*, 10(1), 51–59.

- Dovgan, A. V., Cherkas, V. P., Stepanyuk, A. R., Fitzgerald, D. J., Haynes, L. P., Tepikin, A. V., Belan, P. V. (2010). Decoding glutamate receptor activation by the Ca²⁺ sensor protein hippocalcin in rat hippocampal neurons. *European Journal of Neuroscience*, 32(3), 347–358.
- Dravid, S. M., Erreger, K., Yuan, H., Nicholson, K., Le, P., Lyuboslavsky, P., Traynelis, S. F. (2007). Subunit-specific mechanisms and proton sensitivity of NMDA receptor channel block. *The Journal of Physiology*, 581(1), 107–128.
- Duman, R. S. (2014). Pathophysiology of depression and innovative treatments: remodeling glutamatergic synaptic connections. *Dialogues in Clinical Neuroscience*, 16(1), 11–27.
- Einstein, G. O., & McDaniel, M. A. (2004). Memory fitness : a guide for successful aging. Yale University Press. Available from https://books.google.co.uk/books?id=Q_Tsvv4VUZ0C&pg=PA217&lpg=PA217&dq=piracetam+sold+europe+asia+and+south+america&source=bl&ots=aLI0mRDB7H&sig=b3wAZr4Cgu5hepDz8U4v1fJnrYc&hl=en&sa=X&ved=0ahUKEwidrenhrffUAhVCaIAKHRQPB-YQ6AEILzAB#v=onepage&q=piracetam sold europe asia and south america&f=false
- Elting, J.-W., Sulter, G. A., Kaste, M., Lees, K. R., Diener, H. C., Hommel, M., De Keyser, J. (2002). AMPA Antagonist ZK200775 in Patients with Acute Ischemic Stroke. *Stroke*, 33(12), 2813–2818.
- Enomoto, A., Itoh, K., Nagayoshi, E., Haruta, J., Kimura, T., O'Connor, T., Yamamoto, M. (2001). High sensitivity of Nrf2 knockout mice to acetaminophen hepatotoxicity associated with decreased expression of ARE-regulated drug metabolizing enzymes and antioxidant genes. *Toxicological Sciences*, 59(1), 169–177.
- Ernst, B., & Magnani, J. L. (2009). From carbohydrate leads to glycomimetic drugs. *Nature Reviews Drug Discovery*, 8(8), 661–677.
- Evers, L. J. M., Van Amelsvoort, T. A. M. J., Bakker, J. A., De Koning, M., Drukker, M., & Curfs, L. M. G. (2015). Glutamatergic markers, age, intellectual functioning and psychosis in 22q11 deletion syndrome. *Psychopharmacology*, 232(18), 3319–3325.
- Fayyazuddin, A., Villarroel, A., Le Goff, A., Lerma, J., & Neyton, J. (2000). Four residues of the extracellular N-terminal domain of the NR2A subunit control high-affinity Zn²⁺ binding to NMDA receptors. *Neuron*, 25(3), 683–94.
- Fischer, G., Mutel, V., Trube, G., Malherbe, P., Kew, J. N., Mohacsi, E., Kemp, J. A. (1997). Ro 25-6981, a highly potent and selective blocker of N-methyl-D-aspartate receptors containing the NR2B subunit. Characterization in vitro. *The Journal of Pharmacology and Experimental Therapeutics*, 283(3), 1285–92.
- Fisher, J. L., & Housley, P. R. (2013). Agonist binding to the GluK5 subunit is sufficient for functional surface expression of heteromeric GluK2/GluK5 kainate receptors. *Cellular and Molecular Neurobiology*, 33(8), 1099–108.
- Fox, R. J., Miller, D. H., Phillips, J. T., Hutchinson, M., Havrdova, E., Kita, M. (2012). Placebo-controlled phase 3 study of oral BG-12 or glatiramer in multiple sclerosis. *The New England Journal of Medicine*, 367(12), 1087–97.
- Fragment Screening – Xchem, Diamond Light Source, Available [Online] at <http://www.diamond.ac.uk/Beamlines/Mx/Fragment-Screening.html>

- French, J. A. (2006). Refractory epilepsy: one size does not fit all. *Epilepsy Currents*, 6(6), 177–80.
- Fritsch, B., Reis, J., Gasior, M., Kaminski, R. M., & Rogawski, M. a. (2014). Role of GluK1 Kainate Receptors in Seizures, Epileptic Discharges, and Epileptogenesis. *The Journal of Neuroscience : The Official Journal of the Society for Neuroscience*, 34(17), 5765–75.
- Fucile, S., Miledi, R., & Eusebi, F. (2006). Effects of cyclothiazide on GluR1/AMPA receptors. *Proceedings of the National Academy of Sciences of the United States of America*, 103(8), 2943–7.
- Fukutomi, T., Takagi, K., Mizushima, T., Ohuchi, N., & Yamamoto, M. (2014). Kinetic, thermodynamic, and structural characterizations of the association between Nrf2-DLGex degenon and Keap1. *Molecular and Cellular Biology*, 34(5), 832–46.
- Furukawa, H. (2012). Structure and function of glutamate receptor amino terminal domains. *The Journal of Physiology*, 590(1), 63–72.
- Gallyas, F., Ball, S. M., & Molnar, E. (2003). Assembly and cell surface expression of KA-2 subunit-containing kainate receptors. *Journal of Neurochemistry*, 86(6), 1414–27.
- Gan, L., Vargas, M. R., Johnson, D. A., & Johnson, J. A. (2012). Astrocyte-specific overexpression of Nrf2 delays motor pathology and synuclein aggregation throughout the CNS in the alpha-synuclein mutant (A53T) mouse model. *The Journal of Neuroscience : The Official Journal of the Society for Neuroscience*, 32(49), 17775–87.
- Gan, Q., Salussolia, C. L., & Wollmuth, L. P. (2015). Assembly of AMPA receptors: mechanisms and regulation. *The Journal of Physiology*, 593(1), 39–48.
- Garcia, K. C. (2004). Cell surface receptors. Academic Press.
- Gee, K. R., Brown, K. A., Chen, W.-N. U., Bishop-Stewart, J., Gray, D., & Johnson, I. (2000). Chemical and physiological characterization of fluo-4 Ca²⁺-indicator dyes. *Cell Calcium*, 27(2), 97–106.
- Gershwin, M. E., & Belay, A. (2008). Spirulina in human nutrition and health. Taylor & Francis.
- Gharavi, N., & El-Kadi, A. O. S. (2005). tert-Butylhydroquinone is a novel aryl hydrocarbon receptor ligand. *Drug Metabolism and Disposition: The Biological Fate of Chemicals*, 33(3), 365–72.
- Gharavi, N., Haggarty, S., & El-Kadi, A. O. S. (2007). Chemoprotective and carcinogenic effects of tert-butylhydroquinone and its metabolites. *Current Drug Metabolism*, 8(1), 1–7.
- Giacinti, C., & Giordano, A. (2006). RB and cell cycle progression. *Oncogene*, 25(38), 5220–5227.
- Gill, S., & Pulido, O. (2005). Glutamate receptors in peripheral tissue : excitatory transmission outside the CNS. Kluwer Academic/Plenum Publishers. Available from <https://books.google.co.uk/books?id=wcjiZ58myplC&pg=PA29&dq=competitive+antagonist+GLUTAMATE+RECEPTOR&hl=en&sa=X&ved=0ahUKewjhjJbRx5LTAhXKOxoKHXn5CmgQ6AEIGjAA#v=onepage&q=competitive+antagonist+GLUTAMATE+RECEPTOR&f=false>
- Gilroy, D. J., Kauffman, K. W., Hall, R. A., Huang, X., & Chu, F. S. (2000). Assessing potential health risks from microcystin toxins in blue-green algae dietary supplements. *Environmental Health Perspectives*, 108(5), 435–9.

- Gold, R., Kappos, L., Arnold, D. L., Bar-Or, A., Giovannoni, G., Selmaj, K. (2012). Placebo-Controlled Phase 3 Study of Oral BG-12 for Relapsing Multiple Sclerosis. *New England Journal of Medicine*, 367(12), 1098–1107.
- González-Reyes, S., Guzmán-Beltrán, S., Medina-Campos, O. N., & Pedraza-Chaverri, J. (2013). Curcumin pretreatment induces Nrf2 and an antioxidant response and prevents hemin-induced toxicity in primary cultures of cerebellar granule neurons of rats. *Oxidative Medicine and Cellular Longevity*, 2013.
- Goodman, B. K., Rutberg, J., Lin, W. W., Pulver, A. E., & Thomas, G. H. (2000). Hyperprolinaemia in patients with deletion (22)(q11.2) syndrome. *Journal of Inherited Metabolic Disease*, 23(8), 847–8.
- Goot, H. van der. (2002). Trends in drug research III : proceedings of the 13th Noordwijkerhout-Caminero [sic] Symposium, the Netherlands, 6-11 May 2001. Elsevier.
- Gopinathan, A., Morton, J. P., Jodrell, D. I., & Sansom, O. J. (2015). GEMMs as preclinical models for testing pancreatic cancer therapies. *Disease Models & Mechanisms*, 8(10), 1185 – 1200.
- Gouliarov, A. H., & Senning, A. (1994). Piracetam and other structurally related nootropics. *Brain Research Reviews*, 19(2), 180-222.
- Greger, I. H., Khatri, L., & Ziff, E. B. (2002). RNA editing at Arg607 controls AMPA receptor exit from the endoplasmic reticulum. *Neuron*, 34(5), 759–772.
- Grootaert, M. O. J., da Costa Martins, P. A., Bitsch, N., Pintelon, I., de Meyer, G. R. Y., Martinet, W., & Schrijvers, D. M. (2015). Defective autophagy in vascular smooth muscle cells accelerates senescence and promotes neointima formation and atherogenesis. *Autophagy*, 11(11), 2014–2032.
- Grosdidier, A., Zoete, V., & Michielin, O. (2011). SwissDock, a protein-small molecule docking web service based on EADock DSS. *Nucleic Acids Research*, 39, 270-7.
- Gryder, D. S., & Rogawski, M. a. (2003). Selective antagonism of GluR5 kainate-receptor-mediated synaptic currents by topiramate in rat basolateral amygdala neurons. *The Journal of Neuroscience : The Official Journal of the Society for Neuroscience*, 23(18), 7069–74.
- Guo, W., Zou, S., Tal, M., & Ren, K. (2002). Activation of spinal kainate receptors after inflammation: Behavioral hyperalgesia and subunit gene expression. *European Journal of Pharmacology*, 452(3), 309–318.
- Hald, H., Naur, P., Pickering, D. S., Sprogø, D., Madsen, U., Timmermann, D. B., Kastrup, J. S. (2007). Partial agonism and antagonism of the ionotropic glutamate receptor iGluR5: Structures of the ligand-binding core in complex with domoic acid and 2-amino-3-[5-tert-butyl-3-(phosphonomethoxy)-4-isoxazolyl]propionic acid. *Journal of Biological Chemistry*, 282(35), 25726–25736.
- Hammond, C. (2015). Chapter 10 – The ionotropic glutamate receptors. In *Cellular and Molecular Neurophysiology* (pp. 221–244).
- Hampson, D. R., & Manalo, J. L. (1998). The activation of glutamate receptors by kainic acid and domoic acid. *Natural Toxins*, 6(June), 153–158.

- Hanada, T., Ido, K., & Kosasa, T. (2014). Effect of perampanel, a novel AMPA antagonist, on benzodiazepine-resistant status epilepticus in a lithium-pilocarpine rat model. *Pharmacology Research & Perspectives*, 2(5), e00063.
- Hancock, R., Bertrand, H. C., Tsujita, T., Naz, S., El-Bakry, A., Laoruchupong, J., Wells, G. (2012). Peptide inhibitors of the Keap1-Nrf2 protein-protein interaction. *Free Radical Biology & Medicine*, 52(2), 444–51.
- Hansen, K. B., Furukawa, H., & Traynelis, S. F. (2010). Control of assembly and function of glutamate receptors by the amino-terminal domain. *Molecular Pharmacology*, 78(4), 535–49.
- Harris, S. L., & Levine, A. J. (2005). The p53 pathway: positive and negative feedback loops. *Oncogene*, 24(17), 2899–2908.
- Harwood, M., Danielewska-Nikiel, B., Borzelleca, J. F., Flamm, G. W., Williams, G. M., & Lines, T. C. (2007). A critical review of the data related to the safety of quercetin and lack of evidence of in vivo toxicity, including lack of genotoxic/carcinogenic properties. *Food and Chemical Toxicology*, 45(11), 2179–2205.
- Hashimoto, K. (2017). The NMDA Receptors. (K. Hashimoto, Ed.) (1st ed.). Cham: Springer International Publishing.
- Hasler, G., van der Veen, J. W., Tumonis, T., Meyers, N., Shen, J., & Drevets, W. C. (2007). Reduced Prefrontal Glutamate/Glutamine and Gamma-Aminobutyric Acid Levels in Major Depression Determined Using Proton Magnetic Resonance Spectroscopy. *Archives of General Psychiatry*, 64, 193–200.
- Hassan, T. H., Abdelrahman, H. M., Abdel Fattah, N. R., El-Masry, N. M., Hashim, H. M., El-Gerby, K. M., & Abdel Fattah, N. R. (2013). Blood and brain glutamate levels in children with autistic disorder. *Research in Autism Spectrum Disorders*, 7(4), 541–548.
- Hendrickson, W. A., & Ogata, C. M. (1997). [28] Phase determination from multiwavelength anomalous diffraction measurements. *Methods in Enzymology*, 276(1997), 494–523.
- Henley, J. M., & Wilkinson, K. A. (2016). Synaptic AMPA receptor composition in development, plasticity and disease. *Nature Reviews Neuroscience*, 17(6), 337–350.
- Herguedas, B., Krieger, J., & Greger, I. H. (2013). Receptor heteromeric assembly - How it works and why it matters: The case of ionotropic glutamate receptors. *Progress in Molecular Biology and Translational Science* (1st ed., Vol. 117). Copyright © 2013, Elsevier Inc. All Rights Reserved.
- Herring, B. E., & Nicoll, R. A. (2016). Long-Term Potentiation: From CaMKII to AMPA Receptor Trafficking. *Annual Review of Physiology*, 78(1), 351–365.
- Hiatt, W. R., & Smith, R. J. (2014). Assessing the Clinical Benefits of Lipid-Disorder Drugs. *New England Journal of Medicine*, 370(5), 396–399.
- Hirota, A., Kawachi, Y., Yamamoto, M., Koga, T., Hamada, K., & Otsuka, F. (2011). Acceleration of UVB-induced photoageing in nrf2 gene-deficient mice. *Experimental Dermatology*, 20(8), 664–668.
- Hogberg, H. T., & Bal-Price, A. K. (2011). Domoic acid-induced neurotoxicity is mainly mediated by the AMPA/KA receptor: Comparison between immature and mature primary cultures of neurons and glial cells from rat cerebellum. *Journal of Toxicology*, 2011, 1–14.

- Hogner, A., Kastrup, J. S., Jin, R., Liljefors, T., Mayer, M. L., Egebjerg, J., Gouaux, E. (2002). Structural basis for AMPA receptor activation and ligand selectivity: Crystal structures of five agonist complexes with the GluR2 ligand-binding core. *Journal of Molecular Biology*, 322(1), 93–109.
- Hong, F., Freeman, M. L., & Liebler, D. C. (2005). Identification of sensor cysteines in human Keap1 modified by the cancer chemopreventive agent sulforaphane. *Chemical Research in Toxicology*, 18(12), 1917–1926.
- Hong, Y., Yan, W., Chen, S., Sun, C., & Zhang, J. (2010). The role of Nrf2 signaling in the regulation of antioxidants and detoxifying enzymes after traumatic brain injury in rats and mice. *Acta Pharmacologica Sinica*, 31(11), 1421–30.
- Honoré, T., Davies, S. N., Drejer, J., Fletcher, E. J., Jacobsen, P., Lodge, D., & Nielsen, F. E. (1988). Quinoxalinediones: potent competitive non-NMDA glutamate receptor antagonists. *Science (New York, N.Y.)*, 241(4866), 701–3.
- Hörer, S., Reinert, D., Ostmann, K., Hoevels, Y., & Nar, H. (2013). Crystal-contact engineering to obtain a crystal form of the Kelch domain of human Keap1 suitable for ligand-soaking experiments. *Acta Crystallographica. Section F, Structural Biology and Crystallisation Communications*, 69(Pt 6), 592–6.
- Houghton, C. A., Fassett, R. G., & Coombes, J. S. (2016). Sulforaphane and Other Nutrigenomic Nrf2 Activators: Can the Clinician's Expectation Be Matched by the Reality? *Oxidative Medicine and Cellular Longevity*, 2016, 1–17.
- Huang, H.C., Nguyen, T., & Pickett, C. B. (2002). Phosphorylation of Nrf2 at Ser-40 by protein kinase C regulates antioxidant response element-mediated transcription. *The Journal of Biological Chemistry*, 277(45), 42769–74.
- Huang, H., & Trussell, L. O. (2014). Presynaptic HCN Channels Regulate Vesicular Glutamate Transport. *Neuron*, 84(2), 340–346.
- Hubbard, R. E. (2011). Structure-based drug discovery and protein targets in the CNS. *Neuropharmacology*, 60(1), 7–23.
- Huber, K. M., Sawtell, N. B., & Bear, M. F. (1998). Effects of the Metabotropic Glutamate Receptor Antagonist MCPG on Phosphoinositide Turnover and Synaptic Plasticity in Visual Cortex. *The Journal of Neuroscience*, 1(18), 1–9.
- Hughes, J. P., Rees, S. S., Kalindjian, S. B., & Philpott, K. L. (2011). Principles of early drug discovery. *British Journal of Pharmacology*, 162(6), 1239–1249.
- Hussain, N. K., Diering, G. H., Sole, J., Anggono, V., & Huganir, R. L. (2014). Sorting Nexin 27 regulates basal and activity-dependent trafficking of AMPARs. *Proceedings of the National Academy of Sciences*, 111(32), 11840–11845.
- Hynie, I., Hockin, J., Wright, J., & Iverson, F. (1990). Panel discussion: evidence that domoic acid was the cause of the 1987 outbreak. Canada Diseases Weekly Report = Rapport Hebdomadaire Des Maladies Au Canada, 37–40.
- Ichimura, Y., Waguri, S., Sou, Y., Kageyama, S., Hasegawa, J., Ishimura, R., Komatsu, M. (2013). Phosphorylation of p62 Activates the Keap1-Nrf2 Pathway during Selective Autophagy. *Molecular Cell*, 51(5), 618–631.

- Iizuka, T., Ishii, Y., Itoh, K., Kiwamoto, T., Kimura, T., Matsuno, Y., Sekizawa, K. (2005). Nrf2-deficient mice are highly susceptible to cigarette smoke-induced emphysema. *Genes to Cells : Devoted to Molecular & Cellular Mechanisms*, 10(12), 1113–25.
- Insel, T. R., Miller, L. P., & Gelhard, R. E. (1990). The ontogeny of excitatory amino acid receptors in rat forebrain—I. N-methyl-D-aspartate and quisqualate receptors. *Neuroscience*, 35(1), 31–43.
- Isaac, J. T. R., Ashby, M., & McBain, C. J. (2007). The Role of the GluR2 Subunit in AMPA Receptor Function and Synaptic Plasticity. *Neuron*, 54(6), 859–871.
- Ishii, T. (2000). Transcription Factor Nrf2 Coordinately Regulates a Group of Oxidative Stress-inducible Genes in Macrophages. *Journal of Biological Chemistry*, 275(21), 16023–16029.
- Ishii, Y., Itoh, K., Morishima, Y., Kimura, T., Kiwamoto, T., Iizuka, T., Sekizawa, K. (2005). Transcription factor Nrf2 plays a pivotal role in protection against elastase-induced pulmonary inflammation and emphysema. *Journal of Immunology*, 175(10), 6968–75.
- Itoh, K., Wakabayashi, N., Katoh, Y., Ishii, T., O'Connor, T., & Yamamoto, M. (2003). Keap1 regulates both cytoplasmic-nuclear shuttling and degradation of Nrf2 in response to electrophiles. *Genes to Cells*, 8(4), 379–391.
- IUPHAR/BPS Guide to Pharmacology. Metabotropic glutamate receptors. Available online at: <http://www.guidetopharmacology.org/GRAC/FamilyDisplayForward?familyId=40>
- Jancova, P., Anzenbacher, P., & Anzenbacherova, E. (2010). Phase II drug metabolizing enzymes. *Biomed Pap Med Fac Univ Palacky Olomouc Czech Repub*, 154(2), 103–116.
- Jane, D. E., Hoo, K., Kamboj, R., Deverill, M., Bleakman, D., & Mandelzys, A. (1997). Synthesis of Willardiine and 6-azawillardiine analogs: Pharmacological characterization on cloned homomeric human AMPA and kainate receptor subtypes. *Journal of Medicinal Chemistry*, 40(22), 3645–3650.
- Jane, D. E., Lodge, D., & Collingridge, G. L. (2009). Kainate receptors: Pharmacology, function and therapeutic potential. *Neuropharmacology*, 56(1), 90–113.
- Jansen, K. L. R., Faull, R. L. M., & Dragunow, M. (1989). Excitatory amino acid receptors in the human cerebral cortex: a quantitative autoradiographic study comparing the distributions of [³H]TCP, [³H]glycine, L-[³H]glutamate, [³H]ampa and [³H]kainic acid binding sites. *Neuroscience*, 32(3), 587–607.
- Jenner, P. (2003). Oxidative stress in Parkinson's disease. *Annals of Neurology*, 53 Suppl 3, S26–36–8.
- Jiang, Z.-Y., Lu, M.-C., Xu, L. L., Yang, T.-T., Xi, M.-Y., Xu, X.-L., Sun, H.-P. (2014). Discovery of potent keap1-nrf2 protein-protein interaction inhibitor based on molecular binding determinants analysis. *Journal of Medicinal Chemistry*, 57(6), 2736–45.
- Jin, R., Clark, S., Weeks, A. M., Dudman, J. T., Gouaux, E., & Partin, K. M. (2005). Mechanism of Positive Allosteric Modulators Acting on AMPA Receptors. *Journal of Neuroscience*, 25(39), 9027–9036.
- Jin, R., Singh, S. K., Gu, S., Furukawa, H., Sobolevsky, A. I., Zhou, J., Gouaux, E. (2009). Crystal structure and association behaviour of the GluR2 amino-terminal domain. *The EMBO Journal*, 28(12), 1812–23.

- Jin, F., Nieman, D. C., Shanely, R. A., Knab, A. M., Austin, M. D., & Sha, W. (2010). The variable plasma quercetin response to 12-week quercetin supplementation in humans. *European Journal of Clinical Nutrition*, 64(7), 692–697.
- Jnoff, E., Albrecht, C., Barker, J. J., Barker, O., Beaumont, E., Bromidge, S., Courade, J.-P. (2014). Binding Mode and Structure-Activity Relationships around Direct Inhibitors of the Nrf2-Keap1 Complex. *ChemMedChem*, 1–7.
- Jolly, C. (2000). Role of the Heat Shock Response and Molecular Chaperones in Oncogenesis and Cell Death. *Journal of the National Cancer Institute*, 92(19), 1564–1572.
- Joshi, P. P., Moradipour, M., Nerkar, A. G., & Sawant, S. D. (2012). AMPA receptor: A review. *International Journal of Pharmacy and Pharmaceutical Sciences*, 4(SUPPL.3), 39–44.
- Joshi, G., Biederman, J., Wozniak, J., Goldin, R. L., Crowley, D., Furtak, S., Gönenç, A. (2013). Magnetic resonance spectroscopy study of the glutamatergic system in adolescent males with high-functioning autistic disorder: A pilot study at 4T. *European Archives of Psychiatry and Clinical Neuroscience*, 263(5), 379–384.
- Juge, N., Mithen, R. F., & Traka, M. (2007). Molecular basis for chemoprevention by sulforaphane: a comprehensive review. *Cellular and Molecular Life Sciences*, 64(9), 1105–1127.
- Kaczor, A. A., Karczmarzyk, Z., Fruzi Ski, A., Pihlaja, K., Sinkkonen, J., Wiinämäki, K., Matosiuk, D. (2014). Structural studies, homology modeling and molecular docking of novel non-competitive antagonists of GluK1/GluK2 receptors. *Bioorganic & Medicinal Chemistry*, 22, 787–795.
- Kalia, L. V, Kalia, S. K., & Salter, M. W. (2008). NMDA receptors in clinical neurology: excitatory times ahead. *The Lancet Neurology*, 7(8), 742–755.
- Kanematsu, S., Uehara, N., Miki, H., Yoshizawa, K., Kawanaka, A., Yuri, T., & Tsubura, A. (2010). Autophagy inhibition enhances sulforaphane-induced apoptosis in human breast cancer cells. *Anticancer Research*, 30(9), 3381–90.
- Kanno, T., Tanaka, K., Yanagisawa, Y., Yasutake, K., Hadano, S., Yoshii, F., Ikeda, J.-E. (2012). A novel small molecule, N-(4-(2-pyridyl)(1,3-thiazol-2-yl))-2-(2,4,6-trimethylphenoxy) acetamide, selectively protects against oxidative stress-induced cell death by activating the Nrf2-ARE pathway: therapeutic implications for ALS. *Free Radical Biology & Medicine*, 53(11), 2028–42.
- Kapur, S., & Seeman, P. (2002). NMDA receptor antagonists ketamine and PCP have direct effects on the dopamine D2 and serotonin 5-HT2 receptors—implications for models of schizophrenia. *Molecular Psychiatry*, 7(8), 837–844.
- Karakas, E., Simorowski, N., & Furukawa, H. (2009). Structure of the zinc-bound amino-terminal domain of the NMDA receptor NR2B subunit. *The EMBO Journal*, 28(24), 3910–20.
- Karakas, E., Simorowski, N., & Furukawa, H. (2011). Subunit arrangement and phenylethanolamine binding in GluN1/GluN2B NMDA receptors. *Nature*, 475(7355), 249–53.
- Karakas, E., & Furukawa, H. (2014). Crystal structure of a heterotetrameric NMDA receptor ion channel. *Science*, 344(6187), 992–997.

- Kasteleijn-Nolst Trenité, D., Brandt, C., Mayer, T., Rosenow, F., Schmidt, B., Steinhoff, B. J., Kucher, K. (2015). Dose-dependent suppression of human photoparoxysmal response with the competitive AMPA/kainate receptor antagonist BGG492: Clear PK/PD relationship. *Epilepsia*, 56(6), 924–932.
- Kato, A. S., Burris, K. D., Gardinier, K. M., Gernert, D. L., Porter, W. J., Reel, J., Witkin, J. M. (2016). Forebrain-selective AMPA-receptor antagonism guided by TARP λ 3-8 as an antiepileptic mechanism. *Nature Medicine*, 22(12), 1496–1501
- Katsuoka, F., Motohashi, H., Ishii, T., Aburatani, H., Engel, J. D., & Yamamoto, M. (2005). Genetic Evidence that Small Maf Proteins Are Essential for the Activation of Antioxidant Response Element-Dependent Genes. *Molecular and Cellular Biology*, 25(18), 8044–8051.
- Kavsan, V. M., Iershov, A. V., & Balynska, O. V. (2011). Immortalized cells and one oncogene in malignant transformation: old insights on new explanation. *BMC Cell Biology*, 12(1), 23.
- Kawai, Y., & Arinze, I. J. (2006). Valproic acid-induced gene expression through production of reactive oxygen species. *Cancer Research*, 66(13), 6563–6569.
- Kawamoto, S., Uchino, S., Xin, K. Q., Hattori, S., Hamajima, K., Fukushima, J., Okuda, K. (1997). Arginine-481 mutation abolishes ligand-binding of the AMPA-selective glutamate receptor channel α 1-subunit. *Brain Research. Molecular Brain Research*, 47(1–2), 339–44.
- Kawasaki, Y., Ishigami, S., Arigami, T., Uenosono, Y., Yanagita, S., Uchikado, Y., Natsugoe, S. (2015). Clinicopathological significance of nuclear factor (erythroid-2)-related factor 2 (Nrf2) expression in gastric cancer. *BMC Cancer*, 15(1), 5.
- Keinänen, K., Wisden, W., Sommer, B., Werner, P., Herb, A., Verdoorn, T. A., Seeburg, P. H. (1990). A family of AMPA-selective glutamate receptors. *Science (New York, N.Y.)*, 249(4968), 556–60.
- Kemmerer, Z. A., Ader, N. R., Mulroy, S. S., & Eggler, A. L. (2015). Comparison of human Nrf2 antibodies: A tale of two proteins. *Toxicology Letters*, 238(2), 83–89.
- Kensler, T. W., Wakabayashi, N., & Biswal, S. (2007). Cell survival responses to environmental stresses via the Keap1-Nrf2-ARE pathway. *Annual Review of Pharmacology and Toxicology*, 47, 89–116.
- Keppel Hesselink, J. M. (2017). NS1209/SPD 502, A Novel Selective AMPA Antagonist for Stroke, Neuropathic Pain or Epilepsy? Drug Development Lessons Learned. *Drug Development Research*, 78(2), 75–80.
- Keum, Y.-S., Yu, S., Chang, P. P.-J., Yuan, X., Kim, J.-H., Xu, C., Kong, A.-N. T. (2006). Mechanism of Action of Sulforaphane: Inhibition of p38 Mitogen-Activated Protein Kinase Isoforms Contributing to the Induction of Antioxidant Response Element-Mediated Heme Oxygenase-1 in Human Hepatoma HepG2 Cells. *Cancer Research*, 66(17).
- Kew, J. N. C., & Kemp, J. A. (2005). Ionotropic and metabotropic glutamate receptor structure and pharmacology. *Psychopharmacology*, 179(1), 4–29.
- Khan, M. Z. (2016). Ionotropic glutamate receptors (iGluRs) of the delta family (GluD1 and GluD2) and synaptogenesis. *Alexandria Journal of Medicine*, 53(3), 201–206.

- Kim, M., Huang, T., Abel, T., Blackwell, K. T., & Yamada, K. (2010). Temporal Sensitivity of Protein Kinase A Activation in Late-Phase Long Term Potentiation. *PLoS Computational Biology*, 6(2), e1000691.
- Kimelberg, H. K., & Nedergaard, M. (2010). Functions of Astrocytes and their Potential As Therapeutic Targets. *Neurotherapeutics*, 7(4), 338–353.
- Kimura, S., Warabi, E., Yanagawa, T., Ma, D., Itoh, K., Ishii, Y., Ishii, T. (2009). Essential role of Nrf2 in keratinocyte protection from UVA by quercetin. *Biochemical and Biophysical Research Communications*, 387(1), 109–114.
- Klaassen, C. D., & Reisman, S. A. (2010). Nrf2 the rescue: effects of the antioxidative/electrophilic response on the liver. *Toxicology and Applied Pharmacology*, 244(1), 57–65.
- Klaassen, R. V., Stroeder, J., Coussen, F., Hafner, A.-S., Petersen, J. D., Renancio, C., Smit, A. B. (2016). Shisa6 traps AMPA receptors at postsynaptic sites and prevents their desensitization during synaptic activity. *Nature Communications*, 7, 10682.
- Ko, S., Zhao, M.-G., Toyoda, H., Qiu, C.-S., & Zhuo, M. (2005). Altered Behavioral Responses to Noxious Stimuli and Fear in Glutamate Receptor 5 (GluR5)- or GluR6-Deficient Mice. *Journal of Neuroscience*, 25(4), 977–984.
- Kobayashi, A., Kang, M.-I., Watai, Y., Tong, K. I., Shibata, T., Uchida, K., & Yamamoto, M. (2006). Oxidative and electrophilic stresses activate Nrf2 through inhibition of ubiquitination activity of Keap1. *Molecular and Cellular Biology*, 26(1), 221–9.
- Kobayashi, M., Li, L., Iwamoto, N., Nakajima-Takagi, Y., Kaneko, H., Nakayama, Y., Yamamoto, M. (2009). The antioxidant defense system Keap1-Nrf2 comprises a multiple sensing mechanism for responding to a wide range of chemical compounds. *Molecular and Cellular Biology*, 29(2), 493–502.
- Koga, K., Descalzi, G., Chen, T., Ko, H.G., Lu, J., Li, S., Zhuo, M. (2015). Coexistence of Two Forms of LTP in ACC Provides a Synaptic Mechanism for the Interactions between Anxiety and Chronic Pain. *Neuron*, 85(2), 377–389.
- Koliaki, C. C., Messini, C., & Tsolaki, M. (2012). Clinical Efficacy of Aniracetam, Either as Monotherapy or Combined with Cholinesterase Inhibitors, in Patients with Cognitive Impairment: A Comparative Open Study*. *CNS Neuroscience & Therapeutics*, 18(4), 302–312.
- Komatsu, M., Kurokawa, H., Waguri, S., Taguchi, K., Kobayashi, A., Ichimura, Y., Yamamoto, M. (2010). The selective autophagy substrate p62 activates the stress responsive transcription factor Nrf2 through inactivation of Keap1. *Nature Cell Biology*, 12(3), 213–23.
- Konradi, C., & Heckers, S. (2003). Molecular aspects of glutamate dysregulation: Implications for schizophrenia and its treatment. *Pharmacology and Therapeutics*, 97(2), 153–179.
- Kopeck, K. K., Bozyczko-Coyne, D., & Williams, M. (2005). Target identification and validation in drug discovery: the role of proteomics. *Biochemical Pharmacology*, 69(8), 1133–1139.
- Kovacic, P., & Somanathan, R. (2010). Clinical Physiology and Mechanism of Dizocilpine (MK-801): Electron Transfer, Radicals, Redox Metabolites and Bioactivity. *Oxidative Medicine and Cellular Longevity*, 3(1), 13–22.

- Kraft, A. D., Johnson, D. a, & Johnson, J. a. (2004). Nuclear factor E2-related factor 2-dependent antioxidant response element activation by tert-butylhydroquinone and sulforaphane occurring preferentially in astrocytes conditions neurons against oxidative insult. *The Journal of Neuroscience: The Official Journal of the Society for Neuroscience*, 24(5), 1101–12.
- Kreuter, A., Knierim, C., Stucker, M., Pawlak, F., Rotterdam, S., Altmeyer, P., & Gambichler, T. (2005). Fumaric acid esters in necrobiosis lipoidica: results of a prospective noncontrolled study. *British Journal of Dermatology*, 153(4), 802–807.
- Krintel, C., Frydenvang, K., Ceravalls de Rabassa, A., Kaern, A. M., Gajhede, M., Pickering, D. S., & Kastrup, J. S. (2014). I-Asp is a useful tool in the purification of the ionotropic glutamate receptor A2 ligand-binding domain. *The FEBS Journal*, 281(10), 2422–30.
- Krintel, C., Francotte, P., Pickering, D. S., Juknaite, L., Pøhlsgaard, J., Olsen, L., Kastrup, J. S. (2016). Enthalpy-Entropy Compensation in the Binding of Modulators at Ionotropic Glutamate Receptor GluA2. *Biophysical Journal*, 110(11), 2397–2406.
- Kristensen, O., Kristensen, L. ., Mollerud, S., Frydenvang, K., Pickering, D. ., & Kastrup, J. S. (2016). The Structure of a High-Affinity Kainate Receptor: GluK4 Ligand-Binding Domain Crystallised with Kainate. *Structure*, 24(9), 1582–1589.
- Kryukov, V. I. (2008). The role of the hippocampus in long-term memory: is it memory store or comparator? *Journal of Integrative Neuroscience*, 7(1), 117–84.
- Kuehne, A., Emmert, H., Soehle, J., Lucius, R., Hildebrand, J., & Zamboni Correspondence JanoschHildebrand, N. (2015). Acute Activation of Oxidative Pentose Phosphate Pathway as First-Line Response to Oxidative Stress in Human Skin Cells. *Molecular Cell*, 59, 359–371.
- Kulkarni, S. K., & Dhir, A. (2010). An overview of curcumin in neurological disorders. *Indian Journal of Pharmaceutical Sciences*, 72(2), 149–54.
- Kumagai, Y., Kanda, H., Shinkai, Y., & Toyama, T. (2013). The role of the Keap1/Nrf2 pathway in the cellular response to methylmercury. *Oxidative Medicine and Cellular Longevity*, 2013, 848279.
- Kumaran, D. (2008). Short-Term Memory and the Human Hippocampus. *Journal of Neuroscience*, 28(15), 3837–3838.
- Kuo, P.-C., Brown, D. A., Scofield, B. A., Yu, I.-C., Chang, F.-L., & Yen, J.-H. (2016). 3H-1,2-Dithiole-3-thione as a novel therapeutic agent for the treatment of experimental autoimmune encephalomyelitis. *Brain, Behaviour and Immunity*, 57, 173–186.
- Kwak, M.-K., Wakabayashi, N., Itoh, K., Motohashi, H., Yamamoto, M., & Kensler, T. W. (2003). Modulation of gene expression by cancer chemopreventive dithiolethiones through the Keap1-Nrf2 pathway. Identification of novel gene clusters for cell survival. *The Journal of Biological Chemistry*, 278(10), 8135–8145.
- Lahti, A., Weiler, M. A., Michaelidis, T. B. A., Parwani, A., & Tamminga, C. A. (2001). Effects of Ketamine in Normal and Schizophrenic Volunteers. *Neuropsychopharmacology*, 25(4), 455–467.
- Lampinen, M., Pentikäinen, O., Johnson, M. S., & Keinänen, K. (1998). AMPA receptors and bacterial periplasmic amino acid-binding proteins share the ionic mechanism of ligand recognition. *EMBO Journal*, 17(16), 4704–4711.

- Lange, P. S., Chavez, J. C., Pinto, J. T., Coppola, G., Sun, C.-W., Townes, T. M., Ratan, R. R. (2008). ATF4 is an oxidative stress-inducible, prodeath transcription factor in neurons in vitro and in vivo. *The Journal of Experimental Medicine*, 205(5), 1227–42.
- Lau, A., & Tymianski, M. (2010). Glutamate receptors, neurotoxicity and neurodegeneration. *Pflügers Archiv - European Journal of Physiology*, 460(2), 525–542.
- Lau, A., Tian, W., Whitman, S. a, & Zhang, D. D. (2013). The predicted molecular weight of Nrf2: it is what it is not. *Antioxidants & Redox Signaling*, 18(1), 91–3.
- Laxer, K. D., Trinka, E., Hirsch, L. J., Cendes, F., Langfitt, J., Delanty, N., Benbadis, S. R. (2014). The consequences of refractory epilepsy and its treatment. *Epilepsy & Behavior*, 37, 59–70.
- Lee, J.-M., Li, J., Johnson, D. a, Stein, T. D., Kraft, A. D., Calkins, M. J., Johnson, J. a. (2005). Nrf2, a multi-organ protector? *FASEB Journal : Official Publication of the Federation of American Societies for Experimental Biology*, 19(9), 1061–6.
- Lee, B., Cao, R., Choi, Y.-S., Cho, H.-Y., Rhee, A. D., Hah, C. K., Obrietan, K. (2009). The CREB/CRE transcriptional pathway: protection against oxidative stress-mediated neuronal cell death. *Journal of Neurochemistry*, 108(5), 1251–65.
- Lee, C.-H., LU, W., Michel, J. C., Goehring, A., Du, J., Song, X., & Gouaux, E. (2014). NMDA receptor structures reveal subunit arrangement and pore architecture. *Nature*, 511(7508), 191–197.
- Lerma, J., Paternain, A., Rodríguez-Moreno, A., & López-García, J. (2001). Molecular physiology of kainate receptors. *Physiological Reviews*, 81(3), 971–998.
- Lerma, J., & Marques, J. M. (2013). Kainate receptors in health and disease. *Neuron*, 80(2), 292–311.
- Li, P., Wilding, T. J., Kim, S. J., Calejesan, A., Huettner, J. E., & Zhuo, M. (1999). Kainate-receptor-mediated sensory synaptic transmission in mammalian spinal cord. *Nature*, 397(6715), 161–164.
- Li, J., & Johnson, J. A. (2002). Time-dependent changes in ARE-driven gene expression by use of a noise-filtering process for microarray data. *Physiological Genomics*, 9(3), 137–44.
- Li, Y., Seacat, A., Kuppusamy, P., Zweier, J. L., Yager, J. D., & Trush, M. A. (2002). Copper redox-dependent activation of 2-tert-butyl(1,4)hydroquinone: formation of reactive oxygen species and induction of oxidative DNA damage in isolated DNA and cultured rat hepatocytes. *Mutation Research*, 518(2), 123–33.
- Li, X., Zhang, D., Hannink, M., & Beamer, L. J. (2004). Crystal structure of the Kelch domain of human Keap1. *The Journal of Biological Chemistry*, 279(52), 54750–8.
- Li, F., & Tsien, J. Z. (2009). Memory and the NMDA receptors. *The New England Journal of Medicine*, 361(3), 302–3.
- Li, Y., Paonessa, J. D., & Zhang, Y. (2012). Mechanism of chemical activation of Nrf2. *PloS One*, 7(4), e35122.
- Li, K., Yang, S., Gong, Y., Yang, H., Li, X., Zhao, Y., Cao, C. (2016). 3H-1,2-dithiole-3-thione protects retinal pigment epithelium cells against Ultra-violet radiation via activation of Akt-mTORC1-dependent Nrf2-HO-1 signaling. *Scientific Reports*, 6(1), 25525.

- Li, S., Wang, W., Niu, T., Wang, H., Li, B., Shao, L., Cui, T. (2014a). Nrf2 deficiency exaggerates doxorubicin-induced cardiotoxicity and cardiac dysfunction. *Oxidative Medicine and Cellular Longevity*, 2014, 748524.
- Li, T., Wang, H., Ding, Y., Zhou, M., Zhou, X., Zhang, X., Wei, W. (2014b). Genetic elimination of Nrf2 aggravates secondary complications except for vasospasm after experimental subarachnoid hemorrhage in mice. *Brain Research*, 1558, 90–9.
- Liao, G., Li, R., Chen, X., Zhang, W., Du, S., & Yuan, Y. (2016). Sodium valproate prevents radiation-induced injury in hippocampal neurons via activation of the Nrf2/HO-1 pathway. *Neuroscience*, 331, 40–51.
- Lionta, E., Spyrou, G., Vassilatis, D. K., & Cournia, Z. (2014). Structure-based virtual screening for drug discovery: principles, applications and recent advances. *Current Topics in Medicinal Chemistry*, 14(16), 1923–1938.
- Lisman, J., Schulman, H., & Cline, H. (2002). The molecular basis of CaMKII function in synaptic and behavioural memory. *Nature Reviews Neuroscience*, 3(3), 175–190.
- Lo, S.-C., Li, X., Henzl, M. T., Beamer, L. J., & Hannink, M. (2006). Structure of the Keap1:Nrf2 interface provides mechanistic insight into Nrf2 signaling. *The EMBO Journal*, 25(15), 3605–17.
- Lynch, G., & Gall, C. M. (2006). Ampakines and the threefold path to cognitive enhancement. *Trends in Neurosciences*, 29(10), 554–562.
- Lyne, P. D. (2002). Structure-based virtual screening: An overview. *Drug Discovery Today*, 7(20), 1047–1055.
- Maj, J., Rogóz, Z., Skuza, G., & Jaros, T. (1995). Some behavioral effects of CNQX AND NBQX, AMPA receptor antagonists. *Polish Journal of Pharmacology*, 47(4), 269–77.
- Malloy, M. T., McIntosh, D. J., Walters, T. S., Flores, A., Goodwin, J. S., & Arinze, I. J. (2013). Trafficking of the transcription factor Nrf2 to promyelocytic leukemia-nuclear bodies: implications for degradation of NRF2 in the nucleus. *The Journal of Biological Chemistry*, 288(20), 14569–83.
- Malykh, A. G., & Sadaie, M. R. (2010). Piracetam and piracetam-like drugs: From basic science to novel clinical applications to CNS disorders. *Drugs*. 12;70(3)287-312.
- Marcel, A.-K., Ekali, L. G., Eugene, S., Arnold, O. E., Sandrine, E. D., Von der Weid, D., Mbanya, J. C. (2011). The Effect of Spirulina platensis versus Soybean on Insulin Resistance in HIV-Infected Patients: A Randomized Pilot Study. *Nutrients*, 3(12), 712–724.
- Marcotte, D., Zeng, W., Hus, J.-C., McKenzie, A., Hession, C., Jin, P., Silvian, L. (2013). Small molecules inhibit the interaction of Nrf2 and the Keap1 Kelch domain through a non-covalent mechanism. *Bioorganic & Medicinal Chemistry*, 21(14), 4011–9.
- Masuko, T., Kashiwagi, K., Kuno, T., Nguyen, N. D., Pahk, A. J., Fukuchi, J., Williams, K. (1999). A regulatory domain (R1-R2) in the amino terminus of the N-methyl-D-aspartate receptor: effects of spermine, protons, and ifenprodil, and structural similarity to bacterial leucine/isoleucine/valine binding protein. *Molecular Pharmacology*, 55(6), 957–69.

- Mathew, S. T., Bergström, P., & Hammarsten, O. (2014). Repeated Nrf2 stimulation using sulforaphane protects fibroblasts from ionizing radiation. *Toxicology and Applied Pharmacology*, 276(3), 188–194.
- Matute, C. (2011). Therapeutic potential of kainate receptors. *CNS Neuroscience & Therapeutics*, 17(6), 661–9.
- Mayer, M. L. (2005). Crystal structures of the GluR5 and GluR6 ligand binding cores: molecular mechanisms underlying kainate receptor selectivity. *Neuron*, 45(4), 539–52.
- Mayer, M. L., Ghosal, A., Dolman, N.P. and Jane, D.E. (2006a). Crystal Structures of the Kainate Receptor GluR5 Ligand Binding Core Dimer with Novel GluR5-Selective Antagonists. *Journal of Neuroscience*, 26(11), 2852–2861.
- Mayer, M. L. (2006b). Glutamate receptors at atomic resolution. *Nature*, 440(7083), 456–462.
- Mayer, M. L. (2016). Structural biology of glutamate receptor ion channel complexes. *Current Opinion in Structural Biology*, 41(1), 119–127.
- McEntee, W. J., & Crook, T. H. (1993). Glutamate: its role in learning, memory, and the aging brain. *Psychopharmacology*, 111(4), 391–401.
- Menniti, F. S., Chenard, B. L., Collins, M. B., Ducat, M. F., Elliott, M. L., Ewing, F. E., White, W. F. (2000). Characterization of the binding site for a novel class of noncompetitive alpha-amino-3-hydroxy-5-methyl-4-isoxazolepropionic acid receptor antagonists. *Molecular Pharmacology*, 58(6), 1310–7.
- Menniti, F. S., Lindsley, C. W., Conn, P. J., Pandit, J., Zagouras, P., & Volkmann, R. A. (2013). Allosteric modulators for the treatment of schizophrenia: targeting glutamatergic networks. *Current Topics in Medicinal Chemistry*, 13(1), 26–54.
- Merz, K. M., Ringe, D., & Reynolds, C. H. (2010). Drug Design: Structure and ligand-based approaches (First edti). New York: Cambridge University Press.
- Meyerson, J. R., Kumar, J., Chittori, S., Rao, P., Pierson, J., Bartesaghi, A., Subramaniam, S. (2014). Structural mechanism of glutamate receptor activation and desensitization. *Nature* (7522), 328–334.
- Meyerson, J. R., Chittori, S., Merk, A., Rao, P., Han, T. H., Serpe, M., Subramaniam, S. (2016). Structural basis of kainate subtype glutamate receptor desensitization. *Nature*, 537(7621), 567–571.
- Mignani, S., Bohme, G. A., Birraux, G., Boireau, A., Jimonet, P., Damour, D., Stutzmann, J. M. (2002). 9-Carboxymethyl-5H,10H-imidazo[1,2-a]indeno[1,2-e]pyrazin-4-one-2-carboxylic acid (RPR117824): Selective anticonvulsive and neuroprotective AMPA antagonist. *Bioorganic and Medicinal Chemistry*, 10(5), 1627–1637.
- Mochizuki-Kawai, H. (2008). [Neural basis of procedural memory]. *Brain and Nerve*, 60(7), 825–32.
- Møllerud, S., Frydenvang, K., Pickering, D. S., & Kastrup, J. S. (2017). Lessons from crystal structures of kainate receptors. *Neuropharmacology*, 112, 16–28.
- Monaghan, D. T., & Jane, D. E. (2009). Pharmacology of NMDA Receptors. Biology of the NMDA Receptor. CRC Press/Taylor & Francis.

- More, J. C. A., Nistico, R., Dolman, N. P., Clarke, V. R. J., Alt, A. J., Ogden, A. M., Jane, D. E. (2004). Characterisation of UBP296: A novel, potent and selective kainate receptor antagonist. *Neuropharmacology*, 47(1), 46–64.
- Moreno, H., Borjas, L., Arrieta, A., Sáez, L., Prasad, A., Estévez, J., & Bonilla, E. (1992). [Clinical heterogeneity of the autistic syndrome: a study of 60 families]. *Investigacion Clinica*, 33(1), 13–31.
- Moreno-Fuenmayor, H., Borjas, L., Arrieta, A., Valera, V., & Socorro-Candanoza, L. (1996). Plasma excitatory amino acids in autism. *Investigacion Clinica*, 37(2), 113–28.
- Morley, R. M., Tse, H., Feng, B., Miller, J. C., Monaghan, D. T., & Jane, D. E. (2005). Synthesis and Pharmacology of N 1 -Substituted Piperazine-2, 3-dicarboxylic Acid Derivatives Acting as NMDA Receptor Antagonists. *Journal of Medicinal Chemistry*, 48(2005), 2627–2637.
- Morris, B. J., Cochran, S. M., & Pratt, J. A. (2005). PCP: from pharmacology to modelling schizophrenia. *Current Opinion in Pharmacology*, 5(1), 101–106.
- Morris, R. G. M., Steele, R. J., Bell, J. E., & Martin, S. J. (2013). N-methyl- d -aspartate receptors, learning and memory: chronic intraventricular infusion of the NMDA receptor antagonist d -AP5 interacts directly with the neural mechanisms of spatial learning. *European Journal of Neuroscience*, 37(5), 700–717.
- Morrisette, D. A., & Stahl, S. M. (2011). Affective symptoms in schizophrenia. *Drug Discovery Today: Therapeutic Strategies*, 8(1–2), 3–9.
- Motohashi, H., & Yamamoto, M. (2004). Nrf2-Keap1 defines a physiologically important stress response mechanism. *Trends in Molecular Medicine*, 10(11), 549–57.
- Mott, D. D., Rojas, A., Fisher, J. L., Dingledine, R. J., & Benveniste, M. (2010). Subunit-specific desensitization of heteromeric kainate receptors. *The Journal of Physiology*, 588(4), 683–700.
- Mullard, A. (2016). mRNA-based drug approaches Phase I milestone. *Nature Reviews Drug Discovery*, 15(9), 595–595.
- Mulle, C., Sailer, A., Pérez-Otaño, I., Dickinson-Anson, H., Castillo, P. E., Bureau, I., Heinemann, S. F. (1998). Altered synaptic physiology and reduced susceptibility to kainate-induced seizures in GluR6-deficient mice. *Nature*, 392(6676), 601–605.
- Mullin, R. (2014). Cost to Develop New Pharmaceutical Drug Now Exceeds \$2.5B - Scientific American. Available from <https://www.scientificamerican.com/article/cost-to-develop-new-pharmaceutical-drug-now-exceeds-2-5b/>
- Murphy, T. H., De Long, M. J., & Coyle, J. T. (1991). Enhanced NAD(P)H:Quinone Reductase Activity Prevents Glutamate Toxicity Produced by Oxidative Stress. *Journal of Neurochemistry*, 56(3), 990–995.
- Nair, S., Doh, S., Chan, J., Kong, A.-N., & Cai, L. (2008). Regulatory potential for concerted modulation of Nrf2-and Nfkb1-mediated gene expression in inflammation and carcinogenesis. *British Journal of Cancer*, 99, 2070–2082.
- Nakamura, K. (2006). Aniracetam: Its Novel Therapeutic Potential in Cerebral Dysfunctional Disorders Based on Recent Pharmacological Discoveries. *CNS Drug Reviews*, 8(1), 70–89.

- Nakaso, K., Yano, H., Fukuhara, Y., Takeshima, T., Wada-Isoe, K., & Nakashima, K. (2003). PI3K is a key molecule in the Nrf2-mediated regulation of antioxidative proteins by hemin in human neuroblastoma cells. *FEBS Letters*, 546(2–3), 181–4.
- Namba, T., Morimoto, K., Sato, K., Yamada, N., & Kuroda, S. (1994). Antiepileptogenic and anticonvulsant effects of NBQX, a selective AMPA receptor antagonist, in the rat kindling model of epilepsy. *Brain Research*, 638(1–2), 36–44.
- Nanao, M. H., Green, T., Stern-Bach, Y., Heinemann, S. F., & Choe, S. (2005). Structure of the kainate receptor subunit GluR6 agonist-binding domain complexed with domoic acid. *Proceedings of the National Academy of Sciences of the United States of America*, 102(5), 1708–1713.
- Naur, P., Vestergaard, B., Skov, L. K., Egebjerg, J., Gajhede, M., & Kastrup, J. S. (2005). Crystal structure of the kainate receptor GluR5 ligand-binding core in complex with (S)-glutamate. *FEBS Letters*, 579(5), 1154–1160.
- Nayeem, N., Mayans, O., & Green, T. (2011). Conformational Flexibility of the Ligand-Binding Domain Dimer in Kainate Receptor Gating and Desensitization. *Journal of Neuroscience*, 31(8), 2916–2924.
- Newcomer, J. W., Farber, N. B., & Olney, J. W. (2000). NMDA receptor function, memory, and brain aging. *Dialogues in Clinical Neuroscience*, 2(3), 219–32.
- Newsholme, P., Lima, M. M. R., Procopio, J., Pithon-Curi, T. C., Doi, S. Q., Bazotte, R. B., & Curi, R. (2003). Glutamine and glutamate as vital metabolites. *Brazilian Journal of Medical and Biological Research*, 36(2), 153–163.
- Nguyen, T., Nioi, P., & Pickett, C. B. (2009). The Nrf2-antioxidant response element signaling pathway and its activation by oxidative stress. *The Journal of Biological Chemistry*, 284(20), 13291–5.
- NHS, Alzheimer's disease, available at: <http://www.nhs.uk/conditions/Alzheimers-disease/Pages/Introduction.aspx>
- Niciu, M. J., Kelmendi, B., & Sanacora, G. (2012). Overview of glutamatergic neurotransmission in the nervous system. *Pharmacology Biochemistry and Behavior*, 100(4), 656–664.
- Nielsen, E. O., Varming, T., Mathiesen, C., Jensen, L. H., Møller, A., Gouliarov, A. H., Drejer, J. (1999). SPD 502: a water-soluble and in vivo long-lasting AMPA antagonist with neuroprotective activity. *The Journal of Pharmacology and Experimental Therapeutics*, 289(3), 1492–501.
- Nielsen, M. M., Liljefors, T., Krosgaard-Larsen, P., & Egebjerg, J. (2003). The Selective Activation of the Glutamate Receptor GluR5 by ATPA is Controlled by Serine 741. *Molecular Pharmacology*, 63(1), 19–25.
- Niswender, C. M., & Conn, P. J. (2010). Metabotropic glutamate receptors: physiology, pharmacology, and disease. *Annual Review of Pharmacology and Toxicology*, 50, 295–322.
- Niture, S. K., & Jaiswal, A. K. (2012). Nrf2 protein up-regulates antiapoptotic protein Bcl-2 and prevents cellular apoptosis. *The Journal of Biological Chemistry*, 287(13), 9873–86.
- Nørholm, A. B., Francotte, P., Olsen, L., Krintel, C., Frydenvang, K., Goffin, E., Kastrup, J. S. (2013). Synthesis, pharmacological and structural characterization, and thermodynamic aspects of

GluA2-positive allosteric modulators with a 3,4-dihydro-2 H -1,2,4-benzothiadiazine 1,1-dioxide scaffold. *Journal of Medicinal Chemistry*, 56(21), 8736–8745.

Nowack, U., Gambichler, T., Hanefeld, C., Kastner, U., & Altmeyer, P. (2002). Successful treatment of recalcitrant cutaneous sarcoidosis with fumaric acid esters. *BMC Dermatology*, 2, 15.

Nutt, J. G., Gunzler, S. A., Kirchhoff, T., Hogarth, P., Weaver, J. L., Krams, M., Landen, J. W. (2008). Effects of a NR2B selective NMDA glutamate antagonist, CP-101,606, on dyskinesia and Parkinsonism. *Movement Disorders : Official Journal of the Movement Disorder Society*, 23(13), 1860–6.

O'Hara, P. J., Sheppard, P. O., Thógersen, H., Venezia, D., Haldeman, B. A., McGrane, V., Mulvihill, E. R. (1993). The ligand-binding domain in metabotropic glutamate receptors is related to bacterial periplasmic binding proteins. *Neuron*, 11(1), 41–52.

Offermanns, S., & Rosenthal, W. (2008). Encyclopedia of molecular pharmacology. Springer. Available from <https://books.google.co.uk/books?id=iwwo5gx8aX8C&pg=PA658&lpg=PA658&dq=electrostatic+repulsion+nmda&source=bl&ots=Uw6XCkfe0g&sig=bWshC5rCfJdLITbGdvienDnMtCo&hl=en&sa=X&ved=0ahUKEwjP28uYgPXUUhUPaVAKHSrKBCwQ6AEIUTAG#v=onepage&q=electrostatic+repulsion+nmda&f=false>

Ohfuné, Y., & Tomita, M. (1982). Total synthesis of (-)-domoic acid. A revision of the original structure. *Journal of the American Chemical Society*, 104(12), 3511–3513.

Ohno, K., Tsutsumi, R., Matsumoto, N., Yamashita, H., Amada, Y., Shishikura, J., Yamaguchi, T. (2003). Functional characterization of YM928, a novel noncompetitive α -amino-3-hydroxy-5-methyl-4-isoxazolepropionic acid (AMPA) receptor antagonist. *The Journal of Pharmacology and Experimental Therapeutics*, 306(1), 66–72.

Ohrmann, P., Siegmund, A., Suslow, T., Spitzberg, K., Kersting, A., Arolt, V., Pfeleiderer, B. (2005). Evidence for glutamatergic neuronal dysfunction in the prefrontal cortex in chronic but not in first-episode patients with schizophrenia: a proton magnetic resonance spectroscopy study. *Schizophrenia Research*, 73(2–3), 153–157.

Oliver, P. L., Finelli, M. J., Edwards, B., Bitoun, E., Butts, D. L., Becker, E. B. E., Davies, K. E. (2011). Oxr1 is essential for protection against oxidative stress-induced neurodegeneration. *PLoS Genetics*, 7(10), e1002338.

Olney, J. W., Collins, R. C., & Sloviter, R. S. (1986). Excitotoxic mechanisms of epileptic brain damage. *Advances in Neurology*, 44, 857–77.

Olsen, R. W., Szamraj, O., & Houser, C. R. (1987). [3H]AMPA binding to glutamate receptor subpopulations in rat brain. *Brain Research*, 402(2), 243–54.

Otwinowski, Z., & Minor, W. (1997). [20] Processing of X-ray diffraction data collected in oscillation mode. *Methods in Enzymology*, 276, 307–326.

Ozawa, S., Kamiya, H., & Tsuzuki, K. (1998). Glutamate receptors in the mammalian central nervous system. *Progress in Neurobiology*, 54(5), 581–618.

- Padmanabhan, B., Tong, K. I., Ohta, T., Nakamura, Y., Scharlock, M., Ohtsuji, M., Yamamoto, M. (2006). Structural basis for defects of Keap1 activity provoked by its point mutations in lung cancer. *Molecular Cell*, 21(5), 689–700.
- Padmanabhan, B., Nakamura, Y., & Yokoyama, S. (2008). Structural analysis of the complex of Keap1 with a prothymosin alpha peptide. *Acta Crystallographica. Section F, Structural Biology and Crystallisation Communications*, 64(Pt 4), 233–8.
- Page, L. A., Daly, E., Schmitz, N., Simmons, A., Toal, F., Deeley, Q., Murphy, D. G. M. (2006). In Vivo ¹H-Magnetic Resonance Spectroscopy Study of Amygdala-Hippocampal and Parietal Regions in Autism. *American Journal of Psychiatry*, 163(12), 2189–2192.
- Palecek, J., Neugebauer, V., Carlton, S. M., Iyengar, S., & Willis, W. D. (2004). The effect of a kainate GluR5 receptor antagonist on responses of spinothalamic tract neurons in a model of peripheral neuropathy in primates. *Pain*, 111(1), 151–161.
- Palmer, C. L., Lim, W., Hastie, P. G. R., Toward, M., Korolchuk, V. I., Burbidge, S. A., Henley, J. M. (2005). Hippocalcin functions as a calcium sensor in hippocampal LTD. *Neuron*, 47(4), 487–94.
- Pan, H., Lin, M., Yang, Y., Callaway, K., Baker, J., Diep, L., Artis, D. R. (2012). Crystal Structures of apo Keap1, Keap1-peptide, and Keap1-compound complexes. *Acta Crystallogr., Sect. D*.
- Partin, K. M., Fleck, M. W., & Mayer, M. L. (1996). AMPA receptor flip/flop mutants affecting deactivation, desensitization, and modulation by cyclothiazide, aniracetam, and thiocyanate. *The Journal of Neuroscience*, 16(21), 6634–6647.
- Partin, K. M., Patneau, D. K., Winters, C. A., Mayer, M. L., & Buonanno, A. (1993). Selective modulation of desensitization at AMPA versus kainate receptors by cyclothiazide and concanavalin A. *Neuron*, 11(6), 1069–82.
- Paul, D. S., & Gautham, N. (2016). MOLS 2.0: software package for peptide modeling and protein–ligand docking. *Journal of Molecular Modeling*, 22(10), 239.
- Pei, W., Huang, Z., Wang, C., Han, Y., Jae, S. P., & Niu, L. (2009). Flip and flop: A molecular determinant for AMPA receptor channel opening. *Biochemistry*, 48(17), 3767–3777.
- Pellegrini-Giampietro, D. E. (2003). An activity-dependent spermine-mediated mechanism that modulates glutamate transmission. *Trends in Neurosciences*, 26(1), 9–11.
- Penn, A. C., & Greger, I. H. (2009). Sculpting AMPA receptor formation and function by alternative RNA processing. *RNA Biology*, 6(5), 517–521.
- Penney, J. B., Maragos, W. F., Greenamyre, J. T., Debowey, D. L., Hollingsworth, Z., & Young, A. B. (1990). Excitatory amino acid binding sites in the hippocampal region of Alzheimer's disease and other dementias. *Journal of Neurology, Neurosurgery, and Psychiatry*, 53(4), 314–20.
- Pergola, P. E., Raskin, P., Toto, R. D., Meyer, C. J., Huff, J. W., Grossman, E. B., Warnock, D. G. (2011). Bardoxolone methyl and kidney function in CKD with type 2 diabetes. *The New England Journal of Medicine*, 365(4), 327–36.
- Perkins, A., Nelson, K. J., Parsonage, D., Poole, L. B., & Karplus, P. A. (2015). Peroxiredoxins: guardians against oxidative stress and modulators of peroxide signaling. *Trends in Biochemical Sciences*, 40(8), 435–45.

- Peroutka III, R. J., Orcutt, S. J., Strickler, J. E., & Butt, T. R. (2011). SUMO Fusion Technology for Enhanced Protein Expression and Purification in Prokaryotes and Eukaryotes. *Methods in Molecular Biology*, 705, 15-30.
- Perrais, D., Veran, J., & Mulle, C. (2010). Gating and permeation of kainate receptors: differences unveiled. *Trends in Pharmacological Sciences*, 31(11), 516–22.
- Perry, G., Cash, A. D., & Smith, M. A. (2002). Alzheimer Disease and Oxidative Stress. *Journal of Biomedicine & Biotechnology*, 2(3), 120–123.
- Perucca, P., & Gilliam, F. G. (2012). Adverse effects of antiepileptic drugs. *The Lancet Neurology*, 11(9), 792–802.
- Phan, K. L., Fitzgerald, D. A., Cortese, B. M., Seraji-Bozorgzad, N., Tancer, M. E., & Moore, G. J. (2005). Anterior cingulate neurochemistry in social anxiety disorder: 1H-MRS at 4 Tesla. *Neuroreport*, 16(2), 183–186.
- Piantadosi, C. A., Withers, C. M., Bartz, R. R., MacGarvey, N. C., Fu, P., Sweeney, T. E., Suliman, H. B. (2011). Heme Oxygenase-1 Couples Activation of Mitochondrial Biogenesis to Anti-inflammatory Cytokine Expression. *Journal of Biological Chemistry*, 286(18), 16374–16385.
- Pickard, B. S., Malloy, M. P., Christoforou, A., Thomson, P. A., Evans, K. L., Morris, S. W., Muir, W. J. (2006). Cytogenetic and genetic evidence supports a role for the kainate-type glutamate receptor gene, GRIK4, in schizophrenia and bipolar disorder. *Molecular Psychiatry*, 11(9), 847–57.
- Pistollato, F., Casado-Poblador, J., & Bal-Price, A. (2016). In vitro methods for Nrf2 pathway induction. JRC technical reports, European Commission. Available at: http://publications.jrc.ec.europa.eu/repository/bitstream/JRC103676/jrc%20technical%20report_nrf2-rotenone_revised_07-11-16.pdf
- Pitkänen, A., Mathiesen, C., Rønn, L. C. B., Møller, A., & Nissinen, J. (2007). Effect of novel AMPA antagonist, NS1209, on status epilepticus. An experimental study in rat. *Epilepsy Research*, 74(1), 45–54.
- Platt, S. R. (2007). The role of glutamate in central nervous system health and disease - A review. *Veterinary Journal*, 173(2), 278–286.
- Plested, A. J. R., Vijayan, R., Biggin, P. C., & Mayer, M. L. (2008). Molecular basis of kainate receptor modulation by sodium. *Neuron*, 58(5), 720–35.
- Pop, A. S., Gomez-Mancilla, B., Neri, G., Willemsen, R., & Gasparini, F. (2014). Fragile X syndrome: a preclinical review on metabotropic glutamate receptor 5 (mGluR5) antagonists and drug development. *Psychopharmacology*, 231(6), 1217–1226.
- Probst Larsen, A., Fièvre, S., Frydenvang, K., Francotte, P., Pirotte, B., Sandholm Kastrup, J., Apl, D. (2017). Identification and structure-function study of positive allosteric modulators of kainate receptors. *Molecular Pharmacology*, 91(6), 576–585.
- ProFrontal, Iris Nutraceuticals 2017. Accessed on 05/07/2017 [ONLINE]. Available at: <http://profrontal.com/nmda/>
- Pulido, O. M. (2008). Domoic acid toxicologic pathology: A review. *Marine Drugs*, 6(2), 180–219.

- Purves, D., Augustine, G. J., & Fitzpatrick, D. (2004). Neuroscience, 3rd Edition. Nature Reviews Neuroscience.
- Rakic, P. (2009). Evolution of the neocortex: a perspective from developmental biology. *Nature Reviews. Neuroscience*, 10(10), 724–35.
- Ramos-Gomez, M., Kwak, M. K., Dolan, P. M., Itoh, K., Yamamoto, M., Talalay, P., & Kensler, T. W. (2001). Sensitivity to carcinogenesis is increased and chemoprotective efficacy of enzyme inducers is lost in nrf2 transcription factor-deficient mice. *Proceedings of the National Academy of Sciences of the United States of America*, 98(6), 3410–3415.
- Ramsey, C. P., Glass, C. A., Montgomery, M. B., Lindl, K. A., Ritson, G. P., Chia, L. A., Jordansciutto, K. L. (2008). Expression of Nrf2 in Neurodegenerative Diseases. *NIH Public Access*, 66(1), 75–85.
- Rangasamy, T., Cho, C. Y., Thimmulappa, R. K., Zhen, L., Srisuma, S. S., Kensler, T. W., Biswal, S. (2004). Genetic ablation of Nrf2 enhances susceptibility to cigarette smoke-induced emphysema in mice. *Journal of Clinical Investigation*, 114(9), 1248–1259.
- Reddy, C., Kumar, V., & Sivaraman, J. (2013). Linkers in the structural biology of protein-protein interactions. *Protein Science*, 22(2), 153–167.
- Riedel, G., Platt, B., & Micheau, J. (2003). Glutamate receptor function in learning and memory. *Behavioural Brain Research*, 140(1–2), 1–47.
- Riva, I., Eibl, C., Volkmer, R., Carbone, A. L., & Plested, A. J. R. (2017). Control of AMPA receptor activity by the extracellular loops of auxiliary proteins. *eLife*, 6, 1–22.
- Rogawski, M. A. (2013). AMPA Receptors as a Molecular Target in Epilepsy Therapy. *Acta Neurologica Scandinavica Supplementum*, (197), 9–18.
- Roll, A., Reich, K., & Boer, A. (2007). Use of fumaric acid esters in psoriasis. *Indian Journal of Dermatology, Venereology and Leprology*, 73(2), 133–7.
- Russo Krauss, I., Merlino, A., Vergara, A., & Sica, F. (2013). An Overview of Biological Macromolecule Crystallisation. *International Journal of Molecular Sciences*, 14(6), 11643–11691.
- Rzepa, H. (n.d.). NMR Spectroscopy. Principles and Application. Available, from <http://www.ch.ic.ac.uk/local/organic/nmr.html>
- Sabers, A., Wolf, P., Møller, A., Rysgaard, K., & Ben-Menachem, E. (2013). A prospective, randomized, multicentre trial for the treatment of refractory status epilepticus; experiences from evaluating the effect of the novel drug candidate, NS1209. *Epilepsy Research*, 106(1–2), 292–295.
- Sakao, K., & Singh, S. V. (2012). D,L-sulforaphane-induced apoptosis in human breast cancer cells is regulated by the adapter protein p66Shc. *Journal of Cellular Biochemistry*, 113(2), 599–610.
- Sakata, H., Niizuma, K., Yoshioka, H., Kim, G. S., Jung, J. E., Katsu, M., Chan, P. H. (2012). Minocycline-preconditioned neural stem cells enhance neuroprotection after ischemic stroke in rats. *The Journal of Neuroscience : The Official Journal of the Society for Neuroscience*, 32(10), 3462–73.
- Salazar, H., Eibl, C., Chebli, M., & Plested, A. (2017). Mechanism of partial agonism in AMPA-type glutamate receptors. *Nature Communications*, 8, 14327.

- Sandberg, M., Patil, J., D'Angelo, B., Weber, S. G., & Mallard, C. (2014). NRF2-regulation in brain health and disease: implication of cerebral inflammation. *Neuropharmacology*, 79, 298–306.
- Sander, T., Hildmann, T., Kretz, R., Furst, R., Sailer, U., Bauer, G., Janz, D. (1997). Allelic association of juvenile absence epilepsy with a GluR5 kainate receptor gene (GRIK1) polymorphism. *American Journal of Medical Genetics - Neuropsychiatric Genetics*, 74(4), 416–421.
- Satoh, M., Saburi, H., Tanaka, T., Matsuura, Y., Naitow, H., Shimozone, R., Kunishima, N. (2015). Multiple binding modes of a small molecule to human Keap1 revealed by X-ray crystallography and molecular dynamics simulation. *FEBS Open Bio*, 5, 557–570.
- Saw, C. L., Huang, M. T., Liu, Y., Khor, T. O., Conney, A. H., & Kong, A. N. (2011). Impact of Nrf2 on UVB-induced skin inflammation/photoprotection and photoprotective effect of sulforaphane. *Molecular Carcinogenesis*, 50(6), 479–486.
- Scharf, S. H., Jaeschke, G., Wettstein, J. G., & Lindemann, L. (2015). Metabotropic glutamate receptor 5 as drug target for Fragile X syndrome. *Current Opinion in Pharmacology*, 20, 124–134.
- Schwenk, J., Harmel, N., Zolles, G., Bildl, W., Kulik, A., Heimrich, B., Klöcker, N. (2009). Functional proteomics identify cornichon proteins as auxiliary subunits of AMPA receptors. *Science (New York, N.Y.)*, 323(5919), 1313–9.
- Schwenk, J., Harmel, N., Brechet, A., Zolles, G., Berkefeld, H., Müller, C. S., Fakler, B. (2012). High-Resolution Proteomics Unravel Architecture and Molecular Diversity of Native AMPA Receptor Complexes. *Neuron*, 74(4), 621–633.
- Serafimoska, Z., & Johansen, T. (2011). Ionotropic Glutamate Receptors (iGluRs): Overview of iGluR2 ligand binding domain in complex with agonists and antagonists. *Macedonia pharmaceutical bulletin*, 57(1,2), 3–16.
- Shanks, N. F., Savas, J. N., Maruo, T., Cais, O., Hirao, A., Oe, S., ... Nakagawa, T. (2012). Differences in AMPA and Kainate Receptor Interactomes Facilitate Identification of AMPA Receptor Auxiliary Subunit GSG1L. *Cell Reports*, 1(6), 590–598.
- Sheardown, M. J., Nielsen, E., Hansen, A. J., Jacobsen, P., & Honor, T. (1990). -6-nitro-7-sulfamoyl-benzo(F)quinoxaline: A Neuroprotectant for Cerebral Ischemia. *Science*, 247(1990), 571–573.
- Shibata, H., Joo, A., Fujii, Y., Tani, A., Makino, C., Hirata, N., Fukumaki, Y. (2001). Association study of polymorphisms in the GluR5 kainate receptor gene (GRIK1) with schizophrenia. *Psychiatric Genetics*, 11(3), 139–44.
- Shiina, A., Kanahara, N., Sasaki, T., Oda, Y., Hashimoto, T., Hasegawa, T., Hashimoto, K. (2015). An Open Study of Sulforaphane-rich Broccoli Sprout Extract in Patients with Schizophrenia. *Clinical Psychopharmacology and Neuroscience*, 13(1), 62–67.
- Shimizu-Sasamata, M., Kawasaki-Yatsugi, S., Okada, M., Sakamoto, S., Yatsugi, S., Togami, J., Murase, K. (1996). YM90K: pharmacological characterization as a selective and potent alpha-amino-3-hydroxy-5-methylisoxazole-4-propionate/kainate receptor antagonist. *The Journal of Pharmacology and Experimental Therapeutics*, 276(1), 84–92.
- Shin, S. M., Yang, J. H., & Ki, S. H. (2013). Role of the Nrf2-are pathway in liver diseases. *Oxidative Medicine and Cellular Longevity*, 2013, 1–9.

- Shinohe, A., Hashimoto, K., Nakamura, K., Tsujii, M., Iwata, Y., Tsuchiya, K. J., Mori, N. (2006). Increased serum levels of glutamate in adult patients with autism. *Progress in Neuro-Psychopharmacology and Biological Psychiatry*, 30(8), 1472–1477.
- Singh, K., Connors, S. L., Macklin, E. A., Smith, K. D., Fahey, J. W., Talalay, P., & Zimmerman, A. W. (2014). Sulforaphane treatment of autism spectrum disorder (ASD). *Proceedings of the National Academy of Sciences*, 111(43), 15550–15555.
- Singh, K., & Zimmerman, A. W. (2016). Sulforaphane Treatment of Young Men with Autism Spectrum Disorder. *CNS & Neurological Disorders Drug Targets*, 15(5), 597–601
- Skradski, S., & White, H. S. (2000). Topiramate blocks kainate-evoked cobalt influx into cultured neurons. *Epilepsia*, 41 (1), S45-7.
- Sleigh, J., Harvey, M., Voss, L., & Denny, B. (2014). Ketamine – More mechanisms of action than just NMDA blockade. *Trends in Anaesthesia and Critical Care*, 4(2–3), 76–81.
- Smith, S. M. (2011). Strategies for the Purification of Membrane Proteins. *Methods in molecular biology (Clifton, N.J.)*, 681, 485–496.
- Smolders, I., Bortolotto, Z. a, Clarke, V. R. J., Warre, R., Khan, G. M., O'Neill, M. J., Michotte, Y. (2002). Antagonists of GLU(K5)-containing kainate receptors prevent pilocarpine-induced limbic seizures. *Nature Neuroscience*, 5(8), 796–804.
- Smyth, M. S., & Martin, J. H. (2000). X Ray Crystallography. *Journal of Clinical Pathology: Molecular Pathology*, 53(1), 8–14.
- Sobolevsky, A. I., Rosconi, M. P., & Gouaux, E. (2009). X-ray structure, symmetry and mechanism of an AMPA-subtype glutamate receptor. *Nature*, 462(7274), 745–56.
- Sobolevsky, A. I. (2015). Structure and gating of tetrameric glutamate receptors. *The Journal of Physiology*, 593(1), 29–38.
- Solly, K., Klein, R., Rudd, M., Holloway, M. K., Johnson, E. N., Henze, D., & Finley, M. F. A. (2015). High-Throughput Screen of GluK1 Receptor Identifies Selective Inhibitors with a Variety of Kinetic Profiles Using Fluorescence and Electrophysiology Assays. *Journal of Biomolecular Screening*, 20(6), 708-19.
- Sommer, B., Keinänen, K., Verdoorn, T. A., Wisden, W., Burnashev, N., Herb, A., Seeburg, P. H. (1990). Flip and flop: a cell-specific functional switch in glutamate-operated channels of the CNS. *Science (New York, N.Y.)*, 249(4976), 1580–5.
- Soto, D., Altafaj, X., Sindreu, C., & Bayés, A. (2014). Glutamate receptor mutations in psychiatric and neurodevelopmental disorders. *Communicative & Integrative Biology*, 7(1), e27887.
- Speranskiy, K., & Kurnikova, M. (2005). On the binding determinants of the glutamate agonist with the glutamate receptor ligand binding domain. *Biochemistry*, 44(34), 11508–11517.
- Sperk, G., Lassmann, H., Baran, H., Kish, S. J., Seitelberger, F., & Hornykiewicz, O. (1983). Kainic acid induced seizures: Neurochemical and histopathological changes. *Neuroscience*, 10(4), 1301–1315.
- Stone, J. M. (2011). Glutamatergic antipsychotic drugs: a new dawn in the treatment of schizophrenia? *Therapeutic Advances in Psychopharmacology*, 1(1), 5–18.

- Stone, T. W. (1995). CNS neurotransmitters and neuromodulators : glutamate. CRC Press. Available from https://books.google.co.uk/books?id=wTBqJh5HhuAC&pg=PA83&lpg=PA83&dq=The+distribution+of+the+AMPA+receptors+subtypes+in+the+mammalian+central+nervous+system&source=bl&ots=xYh219mWp0&sig=QUnylbT83Oy2K-oxWgRsbWgUc-8&hl=en&sa=X&ved=0ahUKEwj_rCjneXUAhXKLVAKH
- Sun, Y., Olson, R., Horning, M., Armstrong, N., Mayer, M., & Gouaux, E. (2002). Mechanism of glutamate receptor desensitization. *Nature*, 417(6886), 245–253.
- Sun, Z., Huang, Z., Zhang, D. D., & Morty, R. E. (2009). Phosphorylation of Nrf2 at Multiple Sites by MAP Kinases Has a Limited Contribution in Modulating the Nrf2- Dependent Antioxidant Response. *PLoS ONE*, 4(8), e6588.
- Sun, L., Li, X., Li, G., Dai, B., & Tan, W. (2017). Actinidia chinensis Planch. Improves the indices of antioxidant and anti-inflammation status of type 2 diabetes mellitus by activating keap1 and Nrf2 via the upregulation of MicroRNA-424. *Oxidative Medicine and Cellular Longevity*, 2017.
- Suter, W., Hartmann, A., Poetter, F., Sagelsdorff, P., Hoffmann, P., & Martus, H.-J. (2002). Genotoxicity assessment of the antiepileptic drug AMP397, an Ames-positive aromatic nitro compound. *Mutation Research/Genetic Toxicology and Environmental Mutagenesis*, 518(2), 181–194.
- Suzuki, T., Motohashi, H., & Yamamoto, M. (2013). Toward clinical application of the Keap1-Nrf2 pathway. *Trends in Pharmacological Sciences*, 34(6), 340–346.
- Swanson, G. T., Gereau, R. W., Green, T., & Heinemann, S. F. (1997). Identification of Amino Acid Residues that Control Functional Behavior in GluR5 and GluR6 Kainate Receptors. *Neuron*, 19(4), 913–926.
- Swanson, G. T., Green, T., & Heinemann, S. F. (1998). Kainate receptors exhibit differential sensitivities to (S)-5-iodowillardiine. *Molecular Pharmacology*, 53(5), 942–949.
- Szabados, T., Gigler, G., Gacsalyi, I., Gyertyan, I., & Gyorgy, L. (2001). Comparison of anticonvulsive and acute neuroprotective activity of three 2, 3-benzodiazepine compounds. *Brain Research Bulletin*, 55(3), 387–391.
- Szczurowska, E., & Mareš, P. (2013). NMDA and AMPA Receptors : Development and Status Epilepticus. *Physiol Res*, 62(Suppl 1), 21–38.
- Szymański, P., Markowicz, M., & Mikiciuk-Olasik, E. (2012). Adaptation of high-throughput screening in drug discovery-toxicological screening tests. *International Journal of Molecular Sciences*, 13(1), 427–452.
- Takahashi, M., Kohara, A., Shishikura, J.-I., Kawasaki-Yatsugi, S., Ni, J. W., Yatsugi, S.-I., Yamaguchi, T. (2002). YM872: a selective, potent and highly water-soluble alpha-amino-3-hydroxy-5-methylisoxazole-4-propionic acid receptor antagonist. *CNS Drug Reviews*, 8(4), 337–52.
- Target Discovery Institute-TDI. Nuffield Department of Medicine. High Throughput Screening. Available online at: <https://www.tdi.ox.ac.uk/high-throughput-screening-2>.
- Tarnawa, I., & Vize, E. S. (1998). 2,3-benzodiazepine AMPA antagonists. *Restorative Neurology and Neuroscience*, 13(1–2), 41–57.

Taylor, G. L. (2010). Introduction to phasing. *Acta Crystallographica. Section D, Biological Crystallography*, 66(Pt 4), 325–38.

The Arc. 2016. Intellectual disability. Accessed on 27/06/2017 [ONLINE] Available at: <https://www.thearc.org/learn-about/intellectual-disability>

Theodore, M., Kawai, Y., Yang, J., Kleshchenko, Y., Reddy, S. P., Villalta, F., & Arinze, I. J. (2008). Multiple nuclear localization signals function in the nuclear import of the transcription factor Nrf2. *Journal of Biological Chemistry*, 283(14), 8984–8994.

Tong, K. I., Padmanabhan, B., Kobayashi, A., Shang, C., Hirotsu, Y., Yokoyama, S., & Yamamoto, M. (2007). Different electrostatic potentials define ETGE and DLG motifs as hinge and latch in oxidative stress response. *Molecular and Cellular Biology*, 27(21), 7511–21.

Traka, M., Gasper, A. V., Smith, J. A., Hawkey, C. J., Bao, Y., & Mithen, R. F. (2005). Transcriptome analysis of human colon Caco-2 cells exposed to sulforaphane. *The Journal of Nutrition*, 135(8), 1865–72.

Traynelis, S. F., Wollmuth, L. P., McBain, C. J., & Menniti, F. (2010). Glutamate Receptor Ion Channels: Structure, Regulation, and Function. *Pharmacological Reviews*, 62(3), 405–496.

Tulane University, Medical Pharmacology, TMedWeb. Accessed on 05/07/2017 [ONLINE]. Available at: http://tmedweb.tulane.edu/pharmwiki/doku.php/overview_of_cns_neurotransmitters

Turski, L., Huth, A., Sheardown, M., McDonald, F., Neuhaus, R., Schneider, H. H., Ottow, E. (1998). ZK200775: a phosphonate quinoxalinedione AMPA antagonist for neuroprotection in stroke and trauma. *Proceedings of the National Academy of Sciences of the United States of America*, 95(18), 10960–10965.

Twele, F., Bankstahl, M., Klein, S., Römermann, K., & Löscher, W. (2015). The AMPA receptor antagonist NBQX exerts anti-seizure but not antiepileptogenic effects in the intrahippocampal kainate mouse model of mesial temporal lobe epilepsy. *Neuropharmacology*, 95, 234–242.

Ullah, M. (2015). Sulforaphane (SFN): An Isothiocyanate in a Cancer Chemoprevention Paradigm. *Medicines*, 2, 141–156.

University of Bristol. NMDA Receptors | Centre for Synaptic Plasticity | University of Bristol. Available from <http://www.bristol.ac.uk/synaptic/receptors/nmdar/>

Unno, M., Shinohara, M., Takayama, K., Tanaka, H., Teruya, K., Doh-ura, K., Ikeda-Saito, M. (2011). Binding and Selectivity of the Marine Toxin Neodysiherbaine A and Its Synthetic Analogues to GluK1 and GluK2 Kainate Receptors. *Journal of Molecular Biology*, 413(3), 667–683.

Uzman, A., Lodish, H., Berk, A., Zipursky, L., & Baltimore, D. (2000). *Molecular Cell Biology* (4th edition) New York, NY, 2000, ISBN 0-7167-3136-3. Biochemistry and Molecular Biology Education, 29, Section 1.2 The Molecules of Life.

Valgeirsson, J., Nielsen, E., Peters, D., Mathiesen, C., Kristensen, A. S., & Madsen, U. (2003). 2-arylureidobenzoic acids: Selective noncompetitive antagonists for the homomeric kainate receptor subtype GluR5. *Journal of Medicinal Chemistry*, 46(26), 5834–5843.

- Valgeirsson, J., Nielsen, E., Peters, D., Mathiesen, C., Kristensen, A. S., & Madsen, U. (2004). Bioisosteric modifications of 2-arylidobenzoic acids: Selective noncompetitive antagonists for the homomeric kainate receptor subtype GluR5. *Journal of Medicinal Chemistry*, 47(27), 6948–6957.
- van Bokhoven, H. (2011). Genetic and Epigenetic Networks in Intellectual Disabilities. *Annual Review of Genetics*, 45(1), 81–104.
- Vance, K. M., Hansen, K. B., & Traynelis, S. F. (2012). GluN1 splice variant control of GluN1/GluN2D NMDA receptors. *The Journal of Physiology*, 590(16), 3857–75.
- Vargas, M. R., Johnson, D. a, Sirkis, D. W., Messing, A., & Johnson, J. a. (2008). Nrf2 activation in astrocytes protects against neurodegeneration in mouse models of familial amyotrophic lateral sclerosis. *The Journal of Neuroscience : The Official Journal of the Society for Neuroscience*, 28(50), 13574–13581.
- Vargas, J. R., Takahashi, D. K., Thomson, K. E., & Wilcox, K. S. (2013). The expression of kainate receptor subunits in hippocampal astrocytes after experimentally induced status epilepticus. *Journal of Neuropathology and Experimental Neurology*, 72(10), 919–32. 6
- Venskutonytė, R., Frydenvang, K., Gajhede, M., Bunch, L., Pickering, D. S., & Kastrup, J. S. (2011). Binding site and interlobe interactions of the ionotropic glutamate receptor GluK3 ligand binding domain revealed by high resolution crystal structure in complex with (S)-glutamate. *Journal of Structural Biology*, 176(3), 307–14.
- Venskutonyte, R., Frydenvang, K., Hald, H., Rabassa, A. C. De, Gajhede, M., Ahring, P. K., & Kastrup, J. S. (2012). Kainate induces various domain closures in AMPA and kainate receptors. *Neurochemistry International*, 61(4), 536–545.
- Veran, J., Kumar, J., Pinheiro, P. S., Athané, A., Mayer, M. L., Perrais, D., & Mulle, C. (2012). Zinc Potentiates GluK3 Glutamate Receptor Function by Stabilizing the Ligand Binding Domain Dimer Interface. *Neuron*, 76(3), 565–578.
- Verdonk, M. L., Cole, J. C., Hartshorn, M. J., Murray, C. W., & Taylor, R. D. (2003). Improved protein-ligand docking using GOLD. *Proteins: Structure, Function, and Bioinformatics*, 52(4), 609–623.
- Vidyasagar, T. R. (1996). Basic information processing and higher cognition: does the mammalian cerebral cortex deal with them at different hierarchical levels? *Clinical and Experimental Pharmacology & Physiology*, 23(10–11), 908–12.
- Volk, L., Chiu, S.-L., Sharma, K., & Huganir, R. L. (2015). Glutamate Synapses in Human Cognitive Disorders. *Annual Review of Neuroscience*, 38(1), 127–149.
- Vriend, J., & Reiter, R. J. (2015). The Keap1-Nrf2-antioxidant response element pathway: a review of its regulation by melatonin and the proteasome. *Molecular and Cellular Endocrinology*, 401, 213–20.
- Vyklický, V., Korinek, M., Smejkalová, T., Balik, A., Krausová, B., Kaniakova, M., Vyklický, L. (2014). Structure, Function, and Pharmacology of NMDA Receptor Channels. *Physiological Research*, 63, 191–203.

- Wang, L., Chen, Y., Sternberg, P., & Cai, J. (2008). Essential roles of the PI3 kinase/Akt pathway in regulating Nrf2-dependent antioxidant functions in the RPE. *Investigative Ophthalmology & Visual Science*, 49(4), 1671–8.
- Wang, X., Zhao, Y., Zhang, X., Badie, H., Zhou, Y., Mu, Y., Xu, H. (2013). Loss of sorting nexin 27 contributes to excitatory synaptic dysfunction by modulating glutamate receptor recycling in Down's syndrome. *Nature Medicine*, 19(4), 473–480.
- Wang, W., Li, S., Wang, H., Li, B., Shao, L., Lai, Y., Cui, T. (2014a). Nrf2 Enhances Myocardial Clearance of Toxic Ubiquitinated Proteins. *Journal of Molecular and Cellular Cardiology*, 72, 305–315.
- Wang, Y., Yang, Y., & Zhe, H. (2014b). Bardoxolone methyl (CDDO-Me) as a therapeutic agent: an update on its pharmacokinetic and pharmacodynamic properties. *Drug Design, Development and Therapy*, 8, 2075–2088.
- Ward, S. E., Harries, M., Aldegheri, L., Austin, N. E., Ballantine, S., Ballini, E., Yusaf, S. P. (2011). Integration of lead Optimization with crystallography for a membrane-bound ion channel target: Discovery of a new class of AMPA receptor positive allosteric modulators. *Journal of Medicinal Chemistry*, 54(1), 78–94.
- Watkins, J. C., & Evans, R. H. (1981). EXCITATORY AMINO ACID TRANSMITTERS. *Annual Review of Pharmacology and Toxicology*, 21, 165–204.
- Weber, H., Borelli, C., Röcken, M., & Schaller, M. (2009). Treatment of Disseminated Granuloma Annulare with Low-dose Fumaric Acid. *Acta Dermato-Venereologica*, 89(3), 295–298.
- Wen Xia, Thorne Gabriell, H. L. (2014). Activation of Nrf2 signaling in HEK293 cells by a first-in-class direct KEAP1-NRF2 Inhibitor. *Journal of Biochemical Molecular Toxicology*, 28(6), 246–255.
- Whiteside, S. P., Port, J. D., Deacon, B. J., & Abramowitz, J. S. (2006). A magnetic resonance spectroscopy investigation of obsessive-compulsive disorder and anxiety. *Psychiatry Research - Neuroimaging*, 146(2), 137–147.
- Whittemore, E. R., Loo, D. T., Watt, J. A., & Cotman, C. W. (1995). A detailed analysis of hydrogen peroxide-induced cell death in primary neuronal culture. *Neuroscience*, 67(4), 921–32.
- Williams, K. (2001). Ifenprodil, a novel NMDA receptor antagonist: site and mechanism of action. *Current Drug Targets*, 2(3), 285–98.
- Winkel, A. F., Engel, C. K., Margerie, D., Kannt, A., Szillat, H., Glombik, H., Schmoll, D. (2015). Characterization of RA839, a noncovalent small molecule binder to Keap1 and selective activator of Nrf2 signaling. *Journal of Biological Chemistry*, 290(47), 28446–28455.
- Wolfgang, L., & Michael A. Rogawski. (2002). "Epilepsy (Ionotropic Glutamate Receptors as Therapeutic Targets)"; by Wolfgang Löscher. California: University of California. Available from https://works.bepress.com/michael_rogawski/25/
- Woo, T.U. W., Shrestha, K., Armstrong, C., Minns, M. M., Walsh, J. P., & Benes, F. M. (2007). Differential alterations of kainate receptor subunits in inhibitory interneurons in the anterior cingulate cortex in schizophrenia and bipolar disorder. *Schizophrenia Research*, 96(1–3), 46–61.
- Wright, A., & Vissel, B. (2012). The essential role of AMPA receptor GluR2 subunit RNA editing in the normal and diseased brain. *Frontiers in Molecular Neuroscience*, 5(April), 1–13.

- Wu, L.-J., Xu, H., Ren, M., & Zhuo, M. (2007). Genetic and pharmacological studies of GluR5 modulation of inhibitory synaptic transmission in the anterior cingulate cortex of adult mice. *Developmental Neurobiology*, 67(2), 146–157.
- Wu, Q. Q., Wang, Y., Senitko, M., Meyer, C., Wigley, W. C., Ferguson, D. A., Lu, C. Y. (2011). Bardoxolone methyl (BARD) ameliorates ischemic AKI and increases expression of protective genes Nrf2, PPAR γ , and HO-1. *American Journal of Physiology. Renal Physiology*, 300(5), F1180–92.
- Wu, K. C., McDonald, P. R., Liu, J., & Klaassen, C. D. (2014). Screening of natural compounds as activators of the keap1-nrf2 pathway. *Planta Medica*, 80(1), 97–104.
- Xu, C., Yuan, X., Pan, Z., Shen, G., Kim, J.-H., Yu, S., Kong, A.-N. T. (2006). Mechanism of action of isothiocyanates: the induction of ARE-regulated genes is associated with activation of ERK and JNK and the phosphorylation and nuclear translocation of Nrf2. *Molecular Cancer Therapeutics*, 5(8), 1918–26.
- Yamada, K., Asai, K., Nagayasu, F., Sato, K., Ijiri, N., Yoshii, N., ... Hirata, K. (2016). Impaired nuclear factor erythroid 2-related factor 2 expression increases apoptosis of airway epithelial cells in patients with chronic obstructive pulmonary disease due to cigarette smoking. *BMC Pulmonary Medicine*, 16(1), 1–4.
- Yamanaka, M., Tian, Z., Darvish-Ghane, S., & Zhuo, M. (2016). Pre-LTP requires extracellular signal-regulated kinase in the ACC. *Molecular Pain*, 12, 1 – 12.
- Yamashita, Y., Ueyama, T., Nishi, T., Yamamoto, Y., Kawakoshi, A., Sunami, S., ... Ichinose, M. (2014). Nrf2-inducing anti-oxidation stress response in the rat liver - New beneficial effect of lansoprazole. *PLoS ONE*, 9(5), 1–12.
- Yelshanskaya, M. V., Li, M., & Sobolevsky, A. I. (2014). Structure of an agonist-bound ionotropic glutamate receptor. *Science*, 345(6200), 1070–1074.
- Yelshanskaya, M. V., Singh, A. K., Sampson, J. M., Narangoda, C., Kurnikova, M., & Sobolevsky, A. I. (2016). Structural Bases of Noncompetitive Inhibition of AMPA-Subtype Ionotropic Glutamate Receptors by Antiepileptic Drugs. *Neuron*, 91(6), 1305–1315.
- Yu, J., Shi, J., Gong, L., Dong, S., Xu, Y., Zhang, Y., Wu, L. (2014). Role of Nrf2/ARE Pathway in Protective Effect of Electroacupuncture against Endotoxic Shock-Induced Acute Lung Injury in Rabbits. *PLOS ONE*, 9(8), e104924.
- Zanotti, G. (2016). Cryo-EM and X-ray Crystallography: Complementary or Alternative Techniques? *Nano World Journal*, 2(2), 22–23.
- Zhang, D. D. (2006). Mechanistic studies of the Nrf2-Keap1 signaling pathway. *Drug Metabolism Reviews*, 38(4), 769–89.
- Zhang, W., Cho, Y., Lolis, E., Howe, J. R., Contractor, A., Swanson, G., Seeburg, P. (2008). Structural and single-channel results indicate that the rates of ligand binding domain closing and opening directly impact AMPA receptor gating. *The Journal of Neuroscience : The Official Journal of the Society for Neuroscience*, 28(4), 932–43.
- Zhang, D. D., Lo, S.-C., Sun, Z., Habib, G. M., Lieberman, M. W., Hannink, M., Chertow, G. M. (2016). Functions of Astrocytes and their Potential as Therapeutic Targets. *Proceedings of the National Academy of Sciences of the United States of America*, 280(6), 338–353.

- Zhang, X.M., & Zhu, J. (2011). Kainic Acid-induced neurotoxicity: targeting glial responses and glia-derived cytokines. *Current Neuropharmacology*, 9(2), 388–98.
- Zhao, J., Moore, A. N., Redell, J. B., & Dash, P. K. (2007a). Enhancing expression of Nrf2-driven genes protects the blood brain barrier after brain injury. *The Journal of Neuroscience : The Official Journal of the Society for Neuroscience*, 27(38), 10240–8.
- Zhao, X., Sun, G., Zhang, J., Strong, R., Dash, P. K., Kan, Y. W., Aronowski, J. (2007b). Transcription factor Nrf2 protects the brain from damage produced by intracerebral hemorrhage. *Stroke; a Journal of Cerebral Circulation*, 38(12), 3280–6.
- Zhou, L. M., Gu, Z. Q., Costa, A. M., Yamada, K. A., Mansson, P. E., Giordano, T., Jones, K. A. (1997). (2S, 4R)-4-methylglutamic acid (SYM 2081): a selective, high-affinity ligand for kainate receptors. *The Journal of Pharmacology and Experimental Therapeutics*, 280(1), 422–7.
- Zhu, S., Stein, R. A., Yoshioka, C., Lee, C. H., Goehring, A., McHaourab, H. S., & Gouaux, E. (2016). Mechanism of NMDA Receptor Inhibition and Activation. *Cell*, 165(3), 704–714.
- Zhuang, C., Narayanapillai, S., Zhang, W., Sham, Y. Y., & Xing, C. (2014). Rapid identification of Keap1-Nrf2 small-molecule inhibitors through structure-based virtual screening and hit-based substructure search. *Journal of Medicinal Chemistry*, 57(3), 1121–1126.
- Zhuo, M. (2017a). Cortical kainate receptors and behavioral anxiety. *Molecular Brain*, 10(1), 1–16.
- Zhuo, M. (2017b). Ionotropic glutamate receptors contribute to pain transmission and chronic pain. *Neuropharmacology*, 112, 228–234.

APPENDIX I

Results generated by Dr. Ben Wahab

1.0 Alignment Report

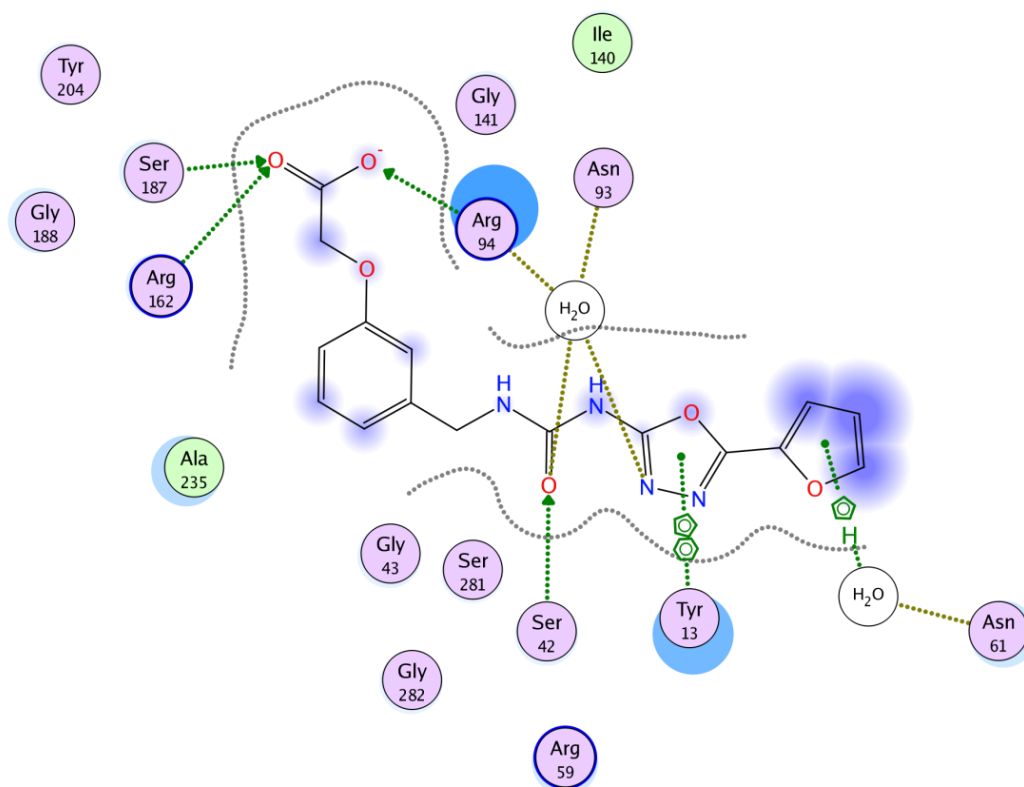
RMSD = 0.451 Å

	1	3	6	11	13	18	23	28	31	34	37	41	44	47	54	57	
1: 1U6D.X	0.00	0.57	0.39	0.13	0.56	0.57	0.37	0.43	0.24	0.44	0.49	0.42	0.33	0.38	0.41	0.44	4.0
3: 1X2J.A	0.57	0.00	0.44	0.56	0.21	0.20	0.44	0.59	0.55	0.56	0.60	0.57	0.52	0.53	0.55	0.56	3.5
6: 1X2R.A	0.39	0.44	0.00	0.39	0.48	0.48	0.25	0.38	0.38	0.38	0.49	0.42	0.35	0.38	0.39	0.39	3.0
11: 1ZGK.A	0.13	0.56	0.39	0.00	0.56	0.57	0.38	0.43	0.26	0.46	0.49	0.42	0.35	0.40	0.42	0.45	2.5
13: 2DYH.A	0.56	0.21	0.48	0.56	0.00	0.20	0.45	0.59	0.54	0.57	0.59	0.55	0.50	0.53	0.54	0.54	2.0
18: 2Z32.A	0.57	0.20	0.48	0.57	0.20	0.00	0.47	0.57	0.56	0.55	0.60	0.56	0.50	0.53	0.55	0.56	1.5
23: 3ADE.A	0.37	0.44	0.25	0.38	0.45	0.47	0.00	0.43	0.37	0.39	0.47	0.43	0.36	0.38	0.39	0.38	1.0
28: 3VNG.A	0.43	0.59	0.38	0.43	0.59	0.57	0.43	0.00	0.45	0.41	0.43	0.44	0.35	0.45	0.32	0.48	0.5
31: 3VNH.A	0.24	0.55	0.38	0.26	0.54	0.56	0.37	0.45	0.00	0.46	0.52	0.42	0.36	0.37	0.41	0.41	0.0
34: 3WDZ.A	0.44	0.56	0.38	0.46	0.57	0.55	0.39	0.41	0.46	0.00	0.53	0.40	0.35	0.43	0.31	0.48	
37: 4IFL.X	0.49	0.60	0.49	0.49	0.59	0.60	0.47	0.43	0.52	0.53	0.00	0.50	0.43	0.50	0.43	0.45	
41: 4IFN.X	0.42	0.57	0.42	0.42	0.55	0.56	0.43	0.44	0.42	0.40	0.50	0.00	0.30	0.46	0.36	0.41	
44: 4IQK.A	0.33	0.52	0.35	0.35	0.50	0.50	0.36	0.35	0.36	0.35	0.43	0.30	0.00	0.38	0.25	0.35	
47: 3WN7.A	0.38	0.53	0.38	0.40	0.53	0.53	0.38	0.45	0.37	0.43	0.50	0.46	0.38	0.00	0.39	0.39	
54: 3ZGD.A	0.41	0.55	0.39	0.42	0.54	0.55	0.39	0.32	0.41	0.31	0.43	0.36	0.25	0.39	0.00	0.41	
57: 4IN4.A	0.44	0.56	0.39	0.45	0.54	0.56	0.38	0.48	0.41	0.48	0.45	0.41	0.35	0.39	0.41	0.00	

Alignment and RMSD generated by MOE.

The lower the RMSD value, the closer the super-position, which reflects close matching 3D positioning of protein residues across multiple structures. An RMSD of under 1.5 Å is said to be a good super-positioning. As some of the structures are *apo*, and some *holo*, the low RMSD represents pockets that are not highly flexible / inducible on contact with ligands.

2.0 Ligand interaction map (from 3VNH crystal structure)



Example of the ligand interaction maps generated using MOE. Residues in green and purple are hydrophobic and hydrophilic respectively. Hydrogen bonding in green dash arrows, and pi-stacking interactions in green dots lines. The grey dash surrounding the ligand represent the surface (edge) of Keap1 protein. Blue colour circles represent solvent contacts.

3.0 Water analysis

Within the pocket, careful analysis gave rise to a number of key waters that were present within at least 50% of the crystal structures OR 75 % of HOLO structures within a ≈ 1 Å cluster size (given below in reference to the 1X2R nomenclature). Waters within *holo* structures indicate possible interaction mediators.

Conserved waters around the binding space:

17, 47, 48, 713, 714, 723, 748, 772, 786, 819, 872, 874, 886, 899, 926

Conserved waters in the bottle neck (under the pocket):

734, 754, 822, 949

4.0 Pharmacophores

ID	Based on	Feature 1	Feature 2	Feature 3	Feature 4	Exclusion volume	Hits
1X2R_1	1X2R	SER363	ASN382	SER602	ASN382(a)	0	923
1X2R_2	1X2R	ARG483 SER508	SER508(a) ARG415	SER602	GLN530	0	757
1X2R_3	1X2R	ARG483 SER508	SER508 ARG415	GLN 530		0	604
1X2R_4	1X2R	GLN530	SER602	GLN530(a)		0	326
1X2R_5	1X2R	SER363	ARG 380	ASN382		1	798
3VNH_1	3VNH	ARG483 SER508	ARG415	SER363		0	359
3VNH_2	3VNH	ARG483 SER508	ARG415	SER363		0	280
3VNH_3	3VNH	ARG483 SER508	ARG415	SER363		1	154
3VNH_4	3VNH	ARG483 SER508	ARG415	SER363	ARG380	1	184
3VNH_5	3VNH	ARG380	ARG415	SER363		1	28
4IFN_1	4IFN	ASN414 ARG380 ARG 415	ASN414(a) ARG380(a)	ARG415(a)	SER602	0	1,366
4IFN_2	4IFN	ASN414 ARG380 ARG 415	ASN414(a) ARG380(a)	ARG415(a)	SER602	1	1,364
4IFN_3	4IFN	ASN414 ARG380 ARG 415	ARG415(a)	SER602	TYR572 (aro)	0	500,000+*
4IFN_4	4IFN	ASN414 ARG380 ARG 415	ASN414(a) ARG380(a)	ARG415(a)	TYR572 (aro)	0	1,314
4IFN_5	4IFN	ASN414 ARG380 ARG 415	ARG415(a)	SER602		0	540
4IN4_1	4IN4	ARG483	ARG483(a)	SER508	SER555	0	21,436*
4IN4_2	4IN4	ARG483		SER508	SER555	1	500,000+*
KEAP1	custom	ARG414	SER363	SER508 ARG483		0	27,138*
KEAP2	custom	SER555	ARG415	SER508 ARG483			43,803*
KEAP3	custom	ARG380 ASN387	SER363	SER508			3
KEAP4	custom	SER363	SER602	SER555			176
KEAP5	custom	SER508 ARG483	GLN530	SER363		0	0

* Considered too non-discriminatory to be of use in the docking phase

(a) Denotes a second interaction feature with the same target as a previous feature in the pharmacophore

(aro) Denotes an aromatic pi stack. The custom interactions are based on observed residues that can be interacting.

APPENDIX II

MORPHEUS[®] HT-96

Mix name	Composition	Catalogue Number (100 & 250mL)
Divalents	0.3M Magnesium chloride hexahydrate; 0.3M Calcium chloride dihydrate	MD2-100(250)-70
Halogens	0.3M Sodium fluoride; 0.3M Sodium bromide; 0.3M Sodium iodide	MD2-100(250)-71
NPS [†]	0.3M Sodium nitrate, 0.3 Sodium phosphate dibasic, 0.3M Ammonium sulfate	MD2-100(250)-72
Alcohols	0.2M 1,6-Hexanediol; 0.2M 1-Butanol; 0.2M 1,2-Propanediol; 0.2M 2-Propanol; 0.2M 1,4-Butanediol; 0.2M 1,3-Propanediol	MD2-100(250)-73
Ethylene glycols	0.3M Diethylene glycol; 0.3M Triethylene-glycol; 0.3M Tetraethylene glycol; 0.3M Pentaethylene glycol	MD2-100(250)-74
Monosaccharides	0.2M D-Glucose; 0.2M D-Mannose; 0.2M D-Galactose; 0.2M L-Fucose; 0.2M D-Xylose; 0.2M N-Acetyl-D-Glucosamine	MD2-100(250)-75
Carboxylic acids	0.2M Sodium formate; 0.2M Ammonium acetate; 0.2M Sodium citrate tribasic dihydrate; 0.2M Sodium potassium tartrate tetrahydrate; 0.2M Sodium oxamate	MD2-100(250)-76
Amino acids	0.2M L-Na-Glutamate; 0.2M Alanine (racemic); 0.2M Glycine; 0.2M Lysine HCl (racemic); 0.2M Serine (racemic)	MD2-100(250)-77

[†]NPS; Nitrate Phosphate Sulfate

Mix name	Conc.	pH @ 20°C	Composition	Catalogue Number (100 & 250mL)
Buffer System 1	1.0M	6.5	Imidazole; MES monohydrate (acid)	MD2-100(250)-100
Buffer System 2	1.0M	7.5	Sodium HEPES; MOPS (acid)	MD2-100(250)-101
Buffer System 3	1.0M	8.5	Tris (base); BICINE	MD2-100(250)-102

Mix name	Old Mix Name	Composition	Catalogue Number (100 & 250mL)
Precipitant Mix 1	P500MME_P20K	40% v/v PEG 500* MME; 20 % w/v PEG 20000	MD2-100(250)-81
Precipitant Mix 2	EDO_P8K	40% v/v Ethylene glycol; 20 % w/v PEG 8000	MD2-100(250)-82
Precipitant Mix 3	GOL_P4K	40% v/v Glycerol; 20% w/v PEG 4000	MD2-100(250)-83
Precipitant Mix 4	MPD_P1K_P3350	25% v/v MPD; 25% PEG 1000; 25% w/v PEG 3350	MD2-100(250)-84

*N.B. The PEG 550 MME that was originally used in this screen has been discontinued and replaced with PEG 500 MME.